Fall 12-13-2011

Chiral Analysis Using Capillary Electrophoresis Coupled to Mass Spectrometry: Development of Novel Modes and Applications Using Molecular Micelles and Surfactant-Bound Monolithic Columns

Jun He

CHIRAL ANALYSIS USING CAPILLARY ELECTROPHORESIS COUPLED TO MASS SPECTROMETRY: DEVELOPMENT OF NOVEL MODES AND APPLICATIONS USING MOLECULAR MICELLES AND SURFACTANT-BOUND MONOLITHIC COLUMNS

by

JUN HE

Under the Direction of Dr. Shahab A. Shamsi

ABSTRACT

Micellar electrokinetic chromatography (MEKC) and capillary electrochromatography (CEC) are two of the major capillary electrophoresis (CE) modes that have been interfaced to mass spectrometry (MS) for sensitive and selective analysis of chiral compounds. This research combines these two modes and expands their applications in chiral CE analysis. Chapter 1 is a review of amino acid based molecular micelles used in MEKC-MS for enantioselective analysis over the past five years. In this chapter, a typical MEKC-MS experiment setup as well as detailed standard operating procedure in synthesis of molecular micelles and running a typical MEKC-MS experiment using the molecular micelles is discussed. Chapter 2 described a multivariate MEKC-MS optimization for the simultaneous analysis of two negatively charged model chiral compounds in negative ion mode with molecular micelles. In this chapter, a central composite design (CCD) is used to first construct a series of experiments to optimize all the important MEKC-MS parameters. Next, response surface methodology (RSM) was used to analyze the interactions between the factors, picking up the best separation and detection conditions, predicting the result of the chiral separation/MS detection, and finally running the actual experiment and comparing

the chromatographic results with the predicted parameters. Chapter 3 demonstrates a similar multivariate MEKC-MS optimization for analysis of a positively charged model chiral compound in a positive ion mode. The same CCD and RSM methods were used to optimize the separations and MS sensitivity. Chapter 4 describes a chiral analysis of four neutral benzoin derivatives (hydrobenzoin, benzoin, benzoin methyl ether, and benzoin ethyl ether) using MEKC coupled to atmospheric pressure photo-ionization mass spectrometry (APPI-MS). The same multivariate experimental design strategy was used to optimize the MEKC as well as APPI-MS parameters. Simultaneous chiral separation of all four benzoin derivatives was achieved with high detection sensitivity compared to UV-detection. Chapter 5 introduces a novel one-pot synthesis scheme for an acryloyl-terminated, carbamate-linked surfactant-bound monolith with leucine head group and different chain lengths. The method promises to open up the discovery of new amino acid based polymeric monoliths for chiral separations and enhanced chemoselectivity for simultaneous chiral separations and enhanced detection in CEC and CEC-MS. In Chapter 6, five amide-linked surfactant-bound monoliths with different chain lengths and head groups (leucine, valine, and phenylalanine) were synthesized and characterized. Enantioseparation of several test compounds was achieved by CEC using the monolithic columns. One of the chiral surfactant, sodium 11-acrylamidoundecanoyl-L-leucinate (SAAUL), was polymerized in aqueous solution under ^{60}Co radiation to form molecular micelle poly-SAAUL. MEKC experiments were carried out with the poly-SAAUL molecular micelle to separate ten cationic chiral compounds. The result was compared with the CEC separation using the AAUL monolithic column. This study is the first comparison of chiral CEC and MEKC with the same surfactant monomer, which has the capability of forming both chiral stationary phase for CEC and chiral pseudophase for MEKC.

INDEX WORDS: Capillary electrochromatography (CEC), Micellar electrokinetic chromatography (MEKC), Chiral separation, Mass spectrometry, Chiral molecular micelles, Chiral monolithic stationary phases, Multivariate design, Atmospheric pressure photoionization

CHIRAL ANALYSIS USING CAPILLARY ELECTROPHORESIS COUPLED TO MASS SPECTROMETRY: DEVELOPMENT OF NOVEL MODES AND APPLICATIONS USING MOLECULAR MICELLES AND SURFACTANT-BOUND MONOLITHIC COLUMNS

by

JUN HE

A Dissertation Submitted in Partial Fulfillment of the Requirements for the Degree of

Doctor of Philosophy

in the College of Arts and Sciences

Georgia State University

2011

CHIRAL ANALYSIS USING CAPILLARY ELECTROPHORESIS COUPLED TO MASS SPECTROMETRY: DEVELOPMENT OF NOVEL MODES AND APPLICATIONS USING MOLECULAR MICELLES AND SURFACTANT-BOUND MONOLITHIC COLUMNS

by

JUN HE

Committee Chair: Dr. Shahab A. Shamsi

Committee: Dr. Binghe Wang

Dr. Gangli Wang

Electronic Version Approved:

Office of Graduate Studies

College of Arts and Sciences

Georgia State University

December 2011

Dedicated to my family

ACKNOWLEDGEMENTS

I would like to sincerely thank my advisor Dr. Shahab A. Shamsi for his thoughtful and patient guidance during my graduate studies at Georgia State University. I would also like to thank my dissertation committee member Drs. Binghe Wang and Gangli Wang for their help in writing this dissertation and throughout my whole graduate projects. Additionally, I am very grateful for the friendship and help from all the colleagues in my research group, namely Drs. Syed A. A. Rizvi, Jie Zhang, Dean Norton, Congying Gu, Xiaochun Wang, William Bragg, Mr. Bin Wang, Francisco Fedullo, Mohsin R. Khan, Hamza Darb, Ms. Yang Lu, Yijin Liu, and Victoria Bianchi. I also owe many thanks to the collaborators in my dissertation projects, especially Dr. Robert Simmons for the help with SEM imaging, Dr. Christopher Jones and Mr. Mike Morrill for the help with the nitrogen adsorption experiments, Dr. Dat Phan and Mr. John Teranova for the help with the APPI-MS instrumentation.

Finally, and most importantly, I would like to thank my wife Mengjuan and my parents. Without their love, encourage, and support, I would never have finished this dissertation.

TABLE OF CONTENTS

LIST OF TABLES

LIST OF FIGURES

Chapter 1

Application of Polymeric Surfactants in Chiral Micellar Electrokinetic Chromatography (CMEKC) and CMEKC Coupled to Mass Spectrometry

The use of amino acid based polymeric surfactants (a.k.a. molecular micelles) in chiral micellar electrokinetic chromatography (CMEKC) has shown to be a successful separation mode for capillary electrophoresis (CE). In this mode, chiral compounds can be enantioseparated with high efficiency, high chiral selectivity and versatility. This chapter describes the state-of-the art studies published in the past five years in CMEKC using polymeric surfactants. Recent trends in compatibility of chiral polymeric surfactants with mass spectrometric (MS) detection in fulfilling mode of CE suggest that this type of chiral selector may be the most promising one for chiral CE-MS applications. The synthesis of new anionic and cationic MS compatible polymeric surfactants and their utility in CMEKC and CMEKC-MS is demonstrated. Examples of how to run a typical CMEKC-MS experiment using univariate and multivariate optimization of CMEKC and MS parameters are discussed.

1.1 Introduction

Chiral separation is one of the most important challenges in chromatographic science. Capillary electrophoresis (CE), as a high efficient and high throughput separation technique, has been widely used for chiral separation since 1985, when the first paper on ligand exchange chiral CE was published [1]. In the years followed, almost all CE modes, such as capillary zone electrophoresis (CZE) [2-4], electrokinetic chromatography (EKC) [5-7], capillary gel electrophoresis [8-11], capillary isoelectric focusing [12, 13], capillary isotachophoresis [14-16], and capillary electrochromatography (CEC) [17-19] have been applied in chiral separation. Among them, electrokinetic chromatography (EKC) with UV detection using charged chiral selectors has been extensively studied due to its high efficiency separation, convenience to operate, and a wide choice of pseudostationary phases. However, the use of low molecular charged chiral selectors (e.g., sulfated cyclodextrins, crown ether, vancomycin as well as unpolymerized chiral micelles) can often mask the mass spectrometric (MS) detection of enantiomeric drugs. This masking of MS signal is particularly crucial when simultaneous separation of parent chiral drugs and their structurally similar chiral metabolites (when present at very low concentrations in human plasma) is desired to be detected at least at low nM levels.

Amino acid based polymeric surfactant (a.k.a. molecular micelles) is one of the newest and most successful pseudostationary phases used in CMEKC-MS [20-30]. The purpose of the current chapter is to provide a brief overview on the basic theories on MEKC using molecular micelles as well as the most recent CMEKC-MS studies in this area. Methods are discussed in detail how to optimize the CMEKC-MS parameters using both univariate and multivariate approaches in ESI-MS and atmospheric pressure photoionization (APPI-MS) with major problems and faults that can occur with the use of these two aforementioned ionization techniques coupled to CE.

1.1.1 Theory of capillary electrophoresis and micellar electrokinetic chromatography using polymeric surfactants

The most basic CE mode is CZE, in which different charged compound separate in a narrow (usually 15 μm to 150 μm i.d.) open tubular fused silica capillary based on their mobility difference under a given electric field. The relationship of the solute velocity and its electrophoretic mobility in CE can be described by the following equation (1).

$$v = \mu_e E \qquad (1)$$

where v is ion velocity, μ_e is electrophoretic mobility, E is electric field. In CE, we can replace v with l/t (l is the effective capillary length, t is the migration time) and E with V/L (V is voltage and L is the total length of the capillary). The equation to calculate μ_e can then be expressed as:

$$\mu_e = \frac{lL}{tV} \qquad (2)$$

The major pushing force of the solute in CE is electroosmotic flow (EOF). In a typical CE setup, aqueous running buffer with neutral to basic pH is used. The interior wall of the glass capillary, under this condition, is negatively charged mainly due to the almost complete deprotonation of the silanol group at the capillary surface. Upon applying an electric field, EOF is originated by the double-layer formed by the adsorbed counterions (cations) on the capillary wall and the excess cations in aqueous mobile phase,

which drives the bulk of the cations, anions, and neutral species to the cathode. One of the features of EOF is its flat flow profile in CE as compared to the parabolic flow in HPLC.

Because CZE only separates charged chiral molecules, all the neutral chiral compounds having the same mobility co-elute with EOF. To overcome this problem, Terabe *et al.* developed MEKC in 1984 [31] and CMEKC in 1989 [5]. In CMEKC, chiral surfactant is added into the running buffer and forms chiral micelles (when the concentration of surfactant is above critical micellar concentration or CMC), which serve as a pseudostationary phase. The neutral compounds are separated based on hydrophobic and hydrogen bonding interactions with the moving micellar phase in CMEKC.

It is now well documented that conventional CMEKC with low molecular weight surfactant forming micelles has several drawbacks. First, the concentration of the chiral surfactant has to be higher than its CMC for micelle formation and for sufficient enantioselectivity. Second, the running buffer containing conventional chiral micelles are not very stable when high concentrations (>25% v/v) organic solvents are used. The solubility issue becomes very important when hydrophobic chiral drugs need to be solubilized and separated only in the presence of high concentration of organic solvents. Third, it is not very practical to use conventional unpolymerized micelles, which fragments into individual monomers when CMEKC is used in combination with ESI-MS.

The basic idea of molecular micelle is to polymerize the chiral surfactant monomers (in the micellar form) by connecting their hydrophobic tails with covalent bounds through free radical polymerization. The micelle obtained is therefore a high molecular weight single molecule. Fig. 1.1 illustrates the separation mechanism of CMEKC with anionic molecular micelle. In this scenario, the capillary wall is negatively charged, thus the bulk solution is positively charged and the EOF is toward cathode. Molecular chiral micelles are multicharged negative polymers in the solution. Their mobility (μ_{psp}) is toward anode and is fairly small due to their size. If μ_{EOF} is bigger than μ_{psp}, the chiral micelles will eventually elute at the time t_{mc}. If μ_{EOF} is smaller than μ_{psp}, the chiral micelles will never elute and t_{mc} is infinite. Very polar neutral chiral analytes with mobility μ_a (triangles in Fig.1.1) interacts only at the micellar surface will be weakly retained and sometimes co-elute with EOF (even sometime elutes before

the EOF). On the contrary, very non-polar chiral compounds with mobility μ_c (squares in the figure) will be adsorbed into the core of the molecular micelle and elute at or near the t_{mc}. The moderately polar chiral analytes with polarities in between with mobility μ_b (diamond in Fig. 1.1) will elute based on the combination of electrostatic, hydrophobic and hydrogen bonding interactions with the molecular micelles and separate accordingly in the middle of micellar eluting window.

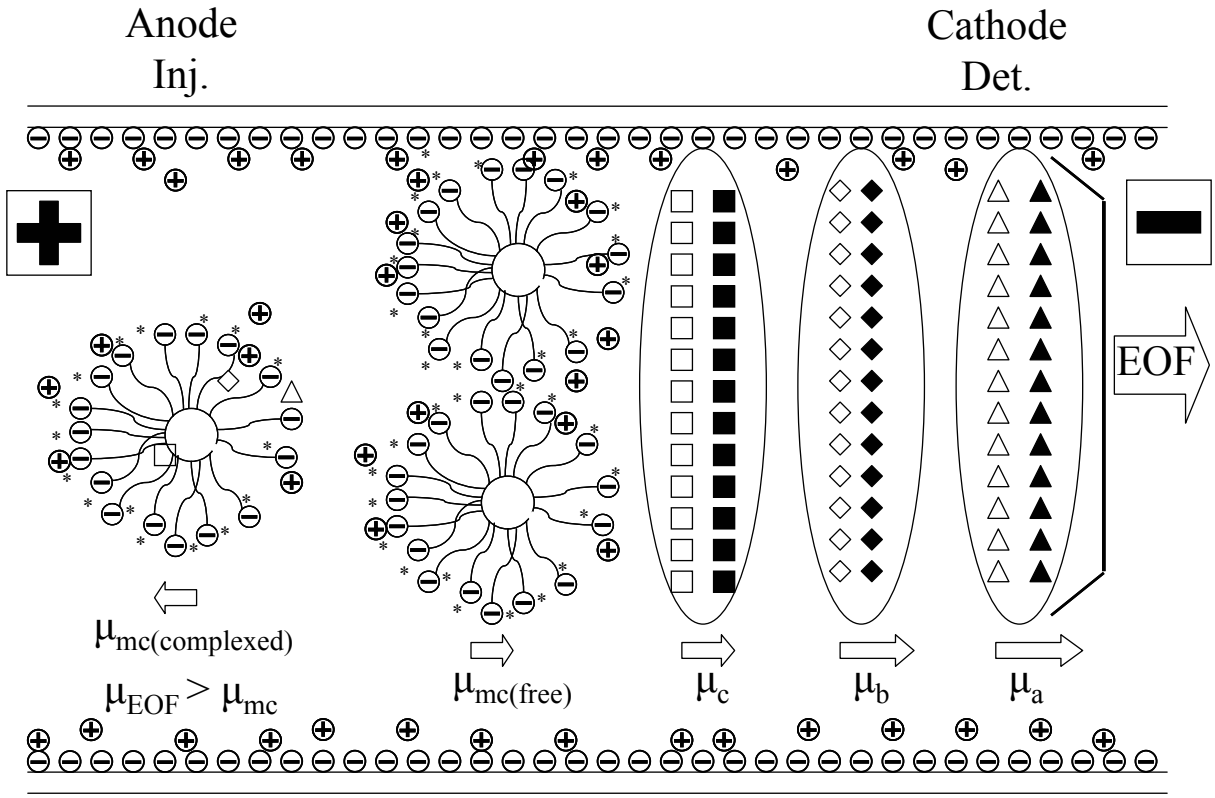

Figure 1.1. Separation mechanism in CMEKC using polymeric surfactants. The open triangles, open diamonds and open squares represent the complexed form of the enantiomer eluting last.

Because CMEKC using polymeric surfactant is fundamentally a type of pseudo-chromatography (without a "real" stationary phase), its theory is very similar to that of traditional chromatography [32, 33]. The capacity factor *k* in CMEKC can be expressed by the following equation (3):

$$k = \frac{(t_R - t_0)}{t_0\left(1 - \frac{t_R}{t_{mc}}\right)} \qquad (3)$$

where t_R is migration time of the solute, t_0 is the migration time of a neutral solute that is not retained by the micelle (dead time marker); t_{mc} is the migration time of the micelle. For micelles with really low mobility, i.e., when t_{mc} approaches infinity, the above equation (3) simplifies to the equation for regular fixed-stationary phase chromatography as follows:

$$k = \frac{(t_R - t_0)}{t_0} \qquad (4)$$

The k can be also expressed with respect to the analyte distribution between micellar phase and aqueous phase:

$$k = K(V_m / V_{aq}) \qquad (5)$$

where K is the distribution coefficient; V_m/V_{aq} is the phase ratio of the chiral micellar phase over aqueous phase [33]. The V_m/V_{aq} ratio can be calculated by:

$$V_m / V_{aq} = \frac{\bar{v}(C_{psp} - CMC)}{1 - \bar{v}(C_{psp} - CMC)} \qquad (6)$$

where $\bar{v}$ is the partial specific volume of the surfactant; C_{psp} is the concentration of pseudostationary phase; CMC is the critical micellar concentration. Because polymeric surfactant's CMC is zero, the above equation can be expressed as [34]:

$$V_m / V_{aq} = \frac{\bar{v} \times C_{psp}}{1 - \bar{v} \times C_{psp}} \qquad (7)$$

$\bar{v}$ is usually a number close to 1 and C_{psp} in CMEKC is a small number. Thus, above equation (7) can be further simplified to the following equation (8):

$$V_m / V_{aq} = \bar{v} \times C_{psp} \qquad (8)$$

The resolution of two enantiomeric peaks in CMEKC can be described as [35, 36]:

$$R_s = \frac{\sqrt{N}}{4}\left(\frac{\alpha-1}{\alpha}\right)\left(\frac{k_2}{1+k_2}\right)\left(\frac{1-t_0/t_{mc}}{1+(t_0/t_{mc})k_1}\right) \qquad (9)$$

This above fundamental equation is used in CMEKC to calculate R_s, where N is the efficiency of the peak; α is the selectivity between the two peaks. For chiral micelles with infinite t_{mc}, the equation (9) can be modified as follows:

$$R_s = \frac{\sqrt{N}}{4}\left(\frac{\alpha-1}{\alpha}\right)\left(\frac{k_2}{1+k_2}\right) \qquad (10)$$

In CMEKC, enantioseparation occurs not only because of the electrophoretic mobility difference between enantiomers, but because of the difference of enantioselective noncovalent interactions between enantiomers and chiral pseudostationary phase [37]. Assume the binding constant between the enantiomers and chiral selectors are K_1 and K_2 respectively, the mobility difference of the enantiomers $\Delta\mu$ can be derived as follows [38]:

$$\Delta\mu = \mu_1 - \mu_2 = \frac{\mu_f + \mu_{C1}K_1[C]}{1+K_1[C]} - \frac{\mu_f + \mu_{C2}K_2[C]}{1+K_2[C]} \qquad (11)$$

where μ_1 and μ_2 are the mobility of the first and second eluting peaks of enantiomer; μ_f and μ_C are mobility of the free and complexed formed of enantiomers, respectively; [C] is the chiral selector concentration.

Palmer and coworkers introduced polymeric sulfated surfactant for separation of hydrophobic achiral compounds using high concentration organic solvent for MEKC-UV [39, 40]. Wang and Warner introduced single amino acid-based acyl chiral polymeric surfactant [7], and then later Shamsi and Warner introduced dipeptide polymeric chiral surfactant [41]. Shamsi was the first to introduce the use of polymeric chiral surfactants for MEKC-MS [20]. Shamsi's group introduced both alkenoxy amino acid based carboxylated and sulfated head group surfactant for MEKC-MS [22, 42]. Recently, Shamsi's group also introduced amino acid based cationic surfactants for chiral separations [23].

1.1.2. Advantages of polymeric surfactants

Polymeric surfactant has three major advantages over conventional surfactant forming micelles when used as pseudostationary phase in MEKC or MEKC-MS: (i) the CMC of polymeric surfactants is zero. This zero CMC simply means one can use the polymeric surfactant in MEKC at very low concentration without sacrificing the chiral selectivity; (ii) molecular micelles are more stable in the presence of organic solvents than their monomeric counterpart due to more rigid molecular scaffold; (iii) because higher molecular weight polymeric surfactants are compatible with MS (especially ESI-MS), they are difficult to ionize in the spray chamber and thus unlikely to interfere with the analyte ions with decrease analyte suppression.

1.1.3. Types of amino acid based polymeric chiral surfactants

Amino acid and dipeptide based polymeric surfactants are one of the most promising pseudostationary phases used in chiral MEKC. The chirality of this type of surfactant polymer originates from the amino acid or dipeptide head groups that cover the surface of the micelle. Based on the charge of the amino acid or dipeptide head groups, it can be categorized to anionic polymeric surfactant and cationic polymeric surfactant, where the former can be further divided into carboxylated amino acid surfactant, carboxylated dipeptide surfactant, and sulfated amino acid surfactant.

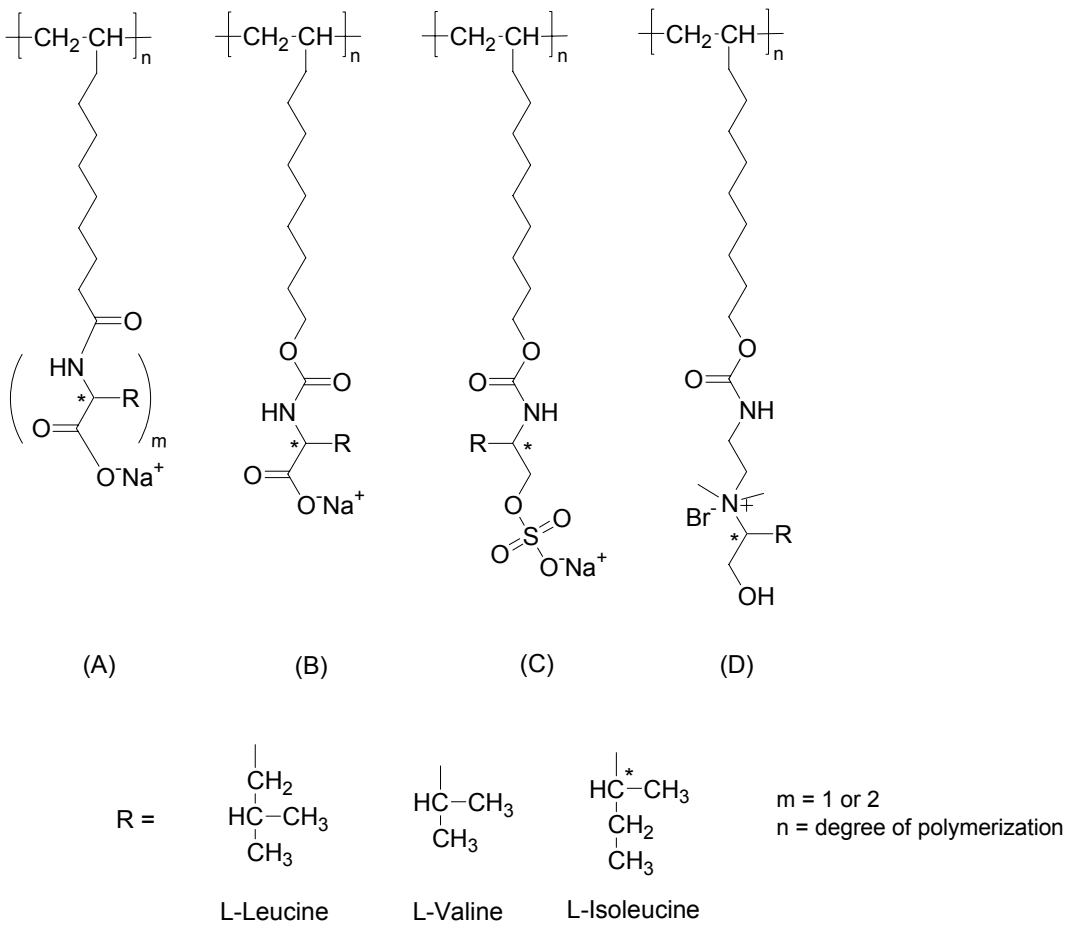

Figure 1.2. Chemical structures of amino acid based polymeric surfactants. (A) amide type amino acid (L-SUA) and dipeptide (L-SUAA) surfactants with a valine, leucine, isoleucine, or leucine-valine head group. (B) carbamate type amino acid surfactants (L-SUCA) with a valine, leucine, or isoleucine head group. (C) sulfated type amino acid surfactants (L-SUCAAS) with a valine, leucine, or isoleucine head group. (D) quaternary ammonium type amino acid surfactants (L-UCAB) with a leucine or pyrrolidine head group.

The structures of different types of polymeric surfactants are illustrated in Fig. 1.2. In this figure, structures (A-C) are anionic surfactants and structure (D) is cationic surfactant. Fig. 1.2A is featured by an amide linker located between the hydrophobic carbon chain and the amino acid or dipeptide head group. Typical example of amide surfactants with single amino acid head group are polysodium *N*-undecenoyl L-leucinate (poly-L-SUL), polysodium *N*-undecenoyl L-valinate (poly-L-SUV), and etc. [7, 33]. Representative amide surfactants with dipeptide head group are polysodium *N*-undecenoyl-L,L-leucylvalinate (poly-L,L-SULV) and polysodium *N*-undecenoyl-L,L-leucylleucinate (poly-L,L-SULL) [43, 44]. Fig. 1.2B is different from the first category by a carbamate linker instead of an amide linker. Typical

surfactants of this kind are polysodium *N*-undecenoxy carbonyl-L-leucinate (poly-L-SUCL) and polysodium *N*-undecenoxy carbonyl-L-isoleucinate (poly-L-SUCIL) [30, 44]. Fig. 1.2C is polymeric sulfated amino acid surfactant. Representative surfactants are polysodium *N*-undecenoyl-L-leucine sulfate (poly-L-SUCLS), *N*-undecenoyl-L-valine sulfate (poly-L-SUCVS) and polysodium *N*-undecenoyl-L-isoleucine sulfate (poly-L-SUCILS) [22]. Fig. 1.2D represents the cationic polymeric surfactant with quaternary ammonium cation and bromide counter ion. Typical surfactants of this type are polyundecenoxycarbonyl-L-pyrrolidinol bromide (poly-L-UCPB) and polyundecenoxycarbonyl-L-leucinol bromide (poly-L-UCLB) [23, 45, 46]. Because L-UCLB and L-UCPB are viscous liquid at room temperature, they are also called ionic-liquid type surfactants. Representative electropherograms of CMEKC separations with these four types of molecular micelles are shown in Fig. 1.3-1.6.

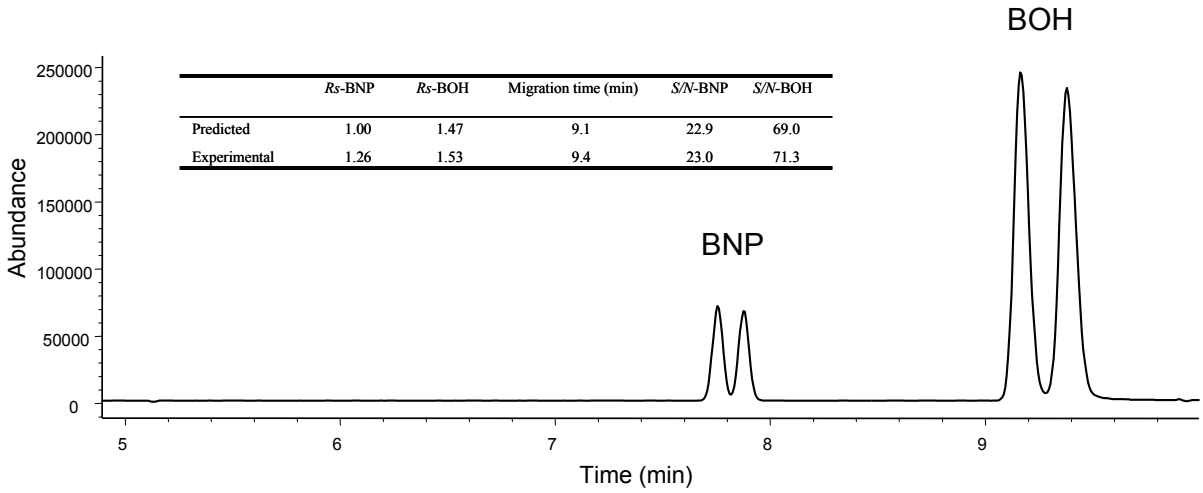

Figure 1.3. Electropherogram of the enantioseparation of (±)1,1′-bi-2-naphthol (BOH) and (±)1,1′-binaphthyl-2,2′-diyl hydrogen phosphate (BNP) using the multivariate optimized MEKC-MS conditions: 60 cm long capillary; 35 mM NH_4OAc buffer, pH 10.8, 27 mM (total) poly-L-SUCL/ poly-L-SULV (1:1, molar ratio), +30 kV; sheath liquid: MeOH/H_2O (80:20, v/v), 5 mM NH_4OAc, pH 8.5, sheath liquid flow rate 5 μL/min; spray chamber: nebulizer pressure 3 psi, DGF 4 L/min, DGT 250 ºC; capillary voltage 3000V, fragmentor 90, gain 3; monitored as group SIM at m/z = 285 and 347.

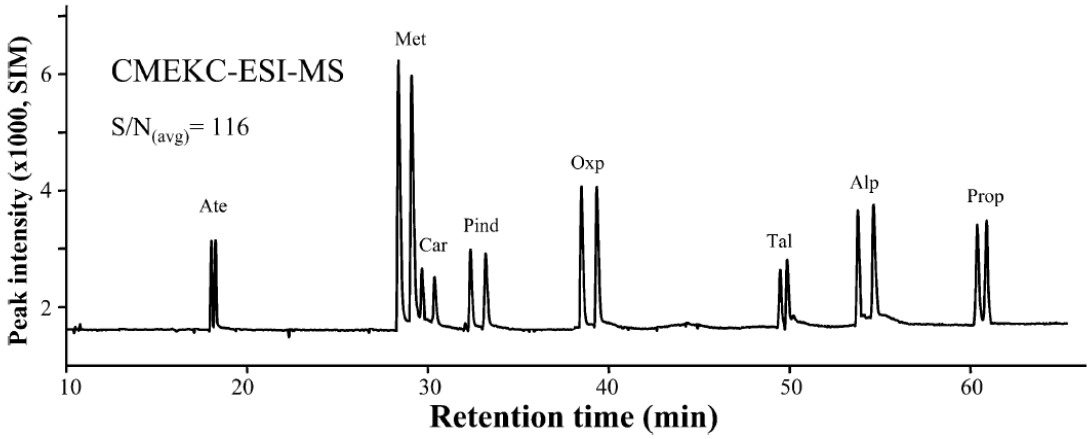

Figure 1.4. Simultaneous MEKC-MS analysis of seven β-blockers. Experimental conditions: 120 cm long capillary; 20 mM each NH_4OAc and TEA buffer, pH 8.8, 25 mM poly-L-SUCL, +30 kV; sheath liquid: MeOH/H_2O (80:20, v/v), 40 mM NH_4OAc, sheath liquid flow rate 5 μL/min; spray chamber: nebulizer pressure 3 psi, DGF 5 L/min, DGT 200 ºC; fragmentor 85V.

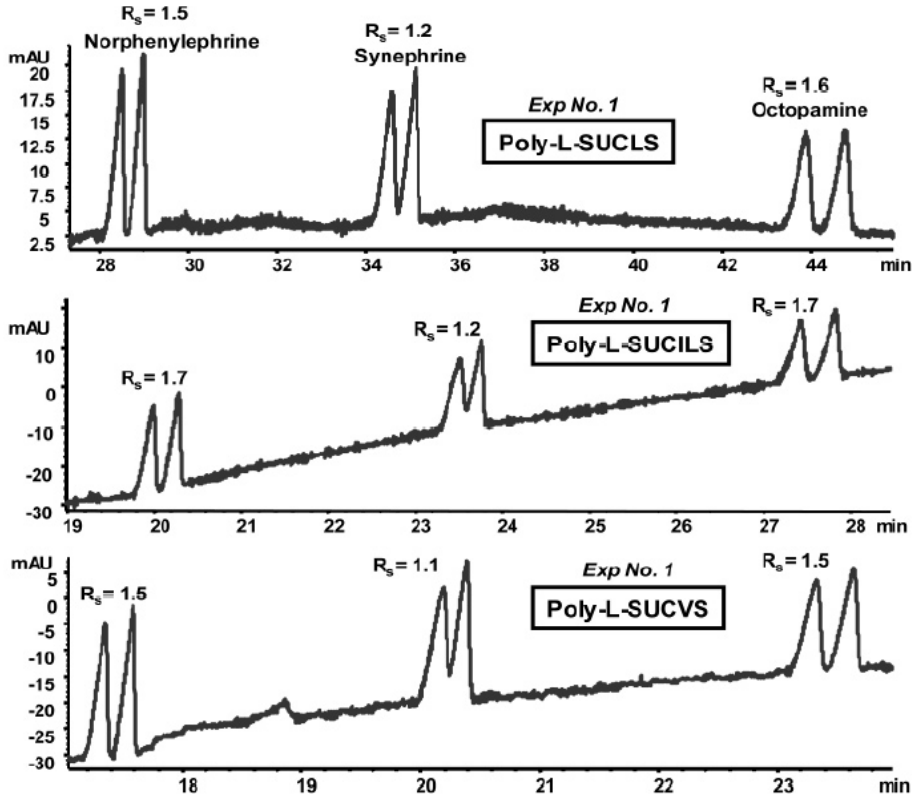

Figure 1.5. MEKC-UV enantioseparation of class II phenylethylamines using a sulfated surfactant at low pH. MEKC conditions: 25 mM TEA/H_3PO_4, pH 2.0, surfactant concentration 50 mM, -20 kV, UV detection at 200 nm.

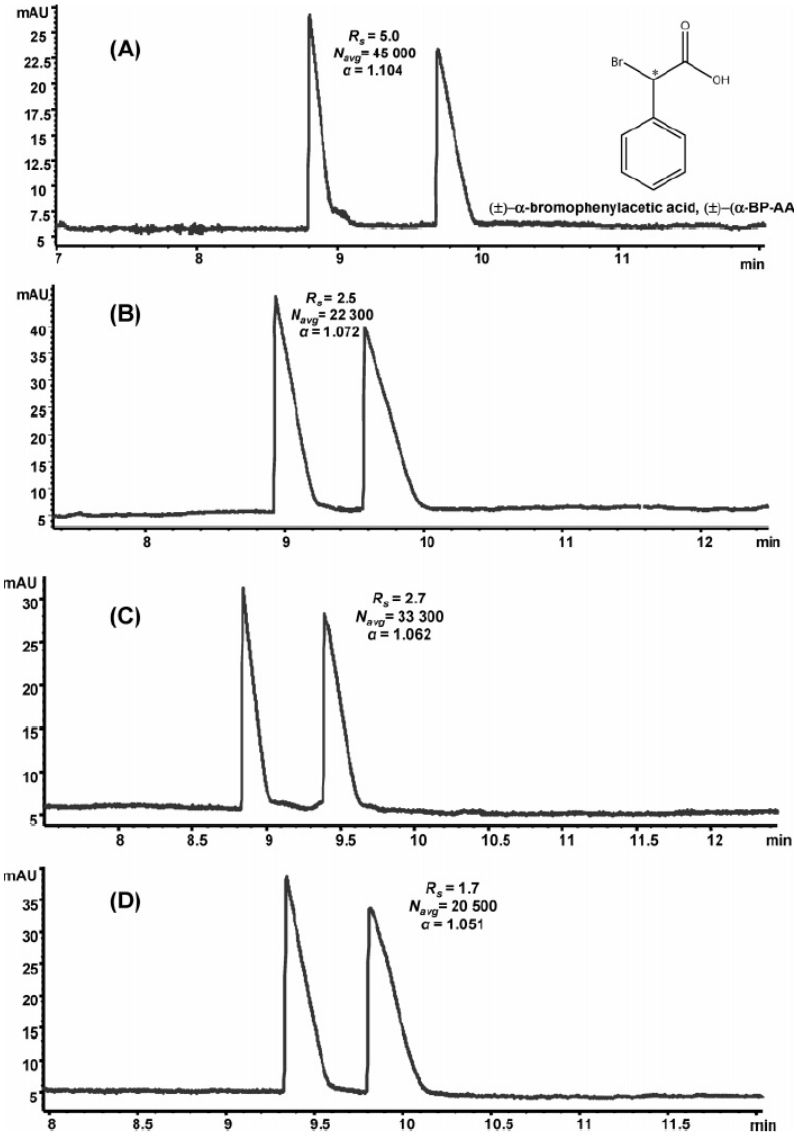

Figure 1.6. Comparison of 25 mM (A) L-UCPB, (B) poly-L-UCPB, (C) 25 mM L-UCLB, and (D) poly-L-UCLB for the enantioseparation of (±)-α-bromophenylacetic acid (2.5 mg/mL in MeOH/H_2O). MEKC conditions: 50 mM NaH_2PO_4/Na_2HPO_4, pH 7.5, pressure injection 50 mbar 5 sec, -20 kV, 20 ^oC, UV detection at 214 nm.

1.1.4. Application of polymeric surfactants in chiral MEKC

Amino acid based polymeric surfactants have been widely used in CMEKC as pseudostationary phase. Table 1.1 summarizes all such applications from 2006. Two groups have been intensively investigating the applications of chiral molecular micelles, Warner's group and Shamsi's group. Warner and co-workers has mainly focused on the studies of chiral interactions between polymeric acyl amino

Table 1.1. Recent applications of polymeric surfactant in chiral MEKC (since 2006)

Analytes	MEKC conditions	Capillary	Detector	Remarks	Refs.
α-bromophenylacetic acid and 2-(2-chlorophenoxy)propanoic acid	50 mM NaH2PO4/Na2HPO4, pH 7.5 25 mM poly-L-UCLB[a] or poly-L-UCPB - 20 kV, 20 ^{o}C	64.5 cm (56.0 cm effective length), 50 μm i.d.	UV-Vis, 214 nm	Amino acid derived cationic surfactant (ionic liquids) was synthesized and characterized. Chiral separation of anionic compounds was achieved and compared to separation using anionic polymeric surfactants.	*(23)*
binaphthyl derivatives and dansyl amino acids	50 mM sodium phosphate (dibasic)/ 25 mM sodium borate buffer, pH 9.0 24 mM poly-L-SULV + 30 kV, 15 ^{o}C	60 cm (52 cm effective length), 50 μm i.d.	UV-Vis, 254 nm	Chiral interactions between analytes and molecular micelle were evaluated by MEKC, steady-state fluorescence, and NMR. The results were compared.	*(47)*
binaphthyl derivatives, benzoin, hydrobenzoin, coumachlor, warfarin, lorazepam, temazepam	100 mM Tris/ 10 mM borate buffer, pH 9.0 1% w/v poly-L-SULV or poly-L-SUILV + 30 kV, 15 ^{o}C	58 cm (50 cm effective length), 50 μm i.d.	UV-Vis, 254 nm	Multivariate optimization of separation parameters was carried out to predict migration time, resolution, and resolution per unit time in MEKC.	*(56)*
phenylethylamines, atenolol, metoprolol, 2-(2-chloro-phenoxy)-propionic acid, benzoin derivatives, PTH amino acids, lorazepam, temazepam, oxazepam	25 mM triethylamine (TEA)/ H_3PO_4, pH 2.0 or 3.0 for CE-UV 15 mM NH_4OAc/ 15 mM TEA, pH 2.0 for CE-MS 20% acetonitrile (CAN) 25 mM poly-L-SUCLS, poly-SUCILS, or poly-L-SUCLVS - 20 kV, 25 ^{o}C	64.5 cm (56.0 cm effective length) for CE-UV, 70 cm for CE-MS, 50 μm i.d.	UV-Vis, 200, 214, 269 nm ESI-MS, NP[b]: 4 psi, DGF[c]: 6 L/min, DGT[d]: 250 ^{o}C Sheath liquid: MeOH/H_2O 80:20 (v:v), 5 mM NH_4OH, 1% (v:v) valeric acid	Polymeric sulfated surfactants were found to provide better enantioselectivity at lower pH. MEKC-ESI-MS method was development to analyze phenylethylamines in human urine sample.	*(22)*
ephedrine alkaloids	15 mM NH_4OAc, pH 6.0 30% (v/v) CAN 35 mM poly-L-SUCL + 30 kV, 20 ^{o}C	120 cm, 50 μm i.d.	ESI-MS NP: 4 psi, DGF: 8 L/min, DGT: 250 ^{o}C Sheath liquid: MeOH/H_2O 80:20 (v:v), 5 mM NH_4OAc, pH 8.5	MEKC conditions for the simultaneous chiral separation of ephedrine alkaloids were optimized and used to analyze ephedra-containing dietary supplements.	*(24, 26)*

phenylethylamines, β-blockers, benzoin derivatives, PTH-amino acids, benzodiazepines	25 mM NH_4OAc/ 25 mM TEA at different pH 20 or 25 mM poly-L-SUCL, poly-L-SUCIL, poly-L-SUCV, poly-L-SUCLS, poly-L-SUCILS, or poly-L-SUCVS + 20 kV, 20 ^oC	64.5 cm (56.0 cm effective length), 50 μm i.d.	UV-Vis, 200, 214 nm	Chiral separations of a wide range of analytes with carboxylate and sulfate polymeric surfactant were compared in MEKC.	*(49)*
warfarin	25 mM NH_4OAc, pH 5.5 25 mM poly-L-SULV + 30 kV, 20 ^oC	120 cm, 50 μm i.d.	ESI-MS NP: 4 psi, DGF: 6 L/min, DGT: 200 ^oC Sheath liquid: MeOH/H_2O 80:20 (v:v), 5 mM NH_4OAc	Chiral MEKC-ESI-MS conditions of warfarin enantiomers were optimized and used for analysis in human plasma	*(25)*
temazepam, benzoin methyl ether, benzoin, coumachlor, aminoglutethmide	50 mM phosphate buffer, pH 7.5 poly-L-SULV at different concentrations + 30 kV, 15 ^oC	57 cm (50 cm effective length), 50 μm i.d.	UV-Vis, 254 nm	Polyelectrolyte multilayer coating was used to enhance the chiral separation of MEKC.	*(48)*
propranolol	10 mM phosphate buffer, pH 7.0 20 % (v/v) ACN molecular imprinted nanoparticle hydrodynamic injection (0.5 mg/mL) 0.5 psi for 10 sec + 16 kV, 25 ^oC	37.0 cm (29.4 cm effective length), 75 μm i.d.	UV-Vis, 214 nm	Molecular imprinted nanoparticle was synthesized by polymerizing a functional sodium N-undecenoyl glycinate surfactant. Chiral separation was achieved by partial filling technique.	*(50)*
fenoprofen, ibuprofen, ketoprofen, suprofen, indoprofen	5 mM NaOAc, 2.63 mM HOAc, pH 5.0 35 mM 2,3,6-tri-O-methyl-β-cyclodextrin (TM-β-CD) 1.5 mM L-UCLB + 30 kV, 16 ^oC	64.5 cm (56.0 cm effective length), 50 μm i.d.	UV-Vis, 214 nm	Binding constants of TM-β-CD, profens, and L-UCLB were calculated.	*(45, 46)*

Binaphthyl derivatives	For 1,1'-bi-2-naphtol (BOH) and 1,1'-binaphthyl-2,2'-diyl hydrogen phosphate (BNP): 35 mM NH_4OAc, pH 10.8 27 mM poly-L-SUCL/poly-SULV (1:1) + 20 kV, 22 ^oC For 1,1'-binaphthyl-2,2'-diamine (BNA): 25 mM NH_4OAc, pH 11.5 20 % (v/v) ACN 40 mM poly-L-SUCL + 15 kV, 20 ^oC	60 cm, 50 µm i.d.	ESI-MS For BOH and BNP: NP: 3 psi, DGF: 4 L/min, DGT: 250 ^oC Sheath liquid: MeOH/H_2O 80:20 (v:v), 5 mM NH_4OAc, pH 8.5 For BNA: NP: 2 psi, DGF: 6 L/min, DGT: 150 ^oC Sheath liquid: MeOH/H_2O 80:20 (v:v), 5 mM NH_4OAc, pH 6.0	MEKC conditions, sheath liquid compositions, and spray chamber parameters were optimized and evaluated by multivariate experimental design.	*(27, 28)*
barbiturates	25 mM NH_4OAc, pH 7.0 39.7 mM poly-L-SUCIL + 25 kV, 20 ^oC	125 cm, 50 µm i.d.	ESI-MS NP: 5 psi, DGF: 4 L/min, DGT: 310 ^oC Sheath liquid: MeOH/H_2O 80:20 (v:v), 5 mM NH_4OH	MEKC, MS, and sheath liquid conditions were optimized by multivariate approach. The final optimum condition was used to analyze barbiturates in human serum	*(30)*
benzoin derivatives	40 mM NH_4OAc, pH 7.0 70 mM mixed molecular micelle (poly-L-SUCL:poly-L,L-SULV molar ratio 85:15) + 25 kV, 20 ^oC	120 cm, 50 µm i.d.	APPI[e]-MS NP: 3 psi, DGF: 5.1 L/min, DGT: 100 ^oC, VT[f]: 176 ^oC Sheath liquid: MeOH/H_2O 50:50 (v:v), 5 mM NH_4OAc, 0.5% (v:v) acetone as dopant	Simultaneous enantioseparation of four benzoin derivatives were achieved with MEKC-APPI-MS. Separation and detection parameters were optimized by multivariate experimental design.	*(29)*

a: Molar concentration of the polymeric surfactant is its equivalent monomer concentration
b: NP: Nebulizer pressure
c: DGF: Drying gas flow rate
d: DGT: Drying gas temperature
e: APPI: atmospheric pressure photoionization
f: VT: vaporizer temperature

acid based surfactants and analytes for MEKC-UV. Besides MEKC, Warner's group has also utilized fluorescence and NMR to study interactions between chiral surfactants and analytes [47]. They are also the first group to develop polyelectrolyte multilayer coating to enhance the chiral separation [48]. Shamsi's group has focused on the development of novel polymeric alkenoxy amino acid based surfactants. As mentioned earlier, they are the first group to develop the application of chiral MEKC with MS. They have also introduced pH independent chiral polymeric sulfated surfactant [22, 49] and chiral ionic liquid [23]. Besides, they have developed several applications for chiral MEKC-MS for simultaneously separating various classes of chiral compounds and pharmaceutical drugs [24-28, 30]. Other than these two groups, Nilsson and Shamsi's group jointly collaborated on developing a molecular imprinted nanoparticle by co-polymerization of surfactant monomer, crosslinker, and template [50]. Enantioseparation was achieved using partial filling techniques with this nanoparticle. The peak shape of the second eluted enantiomer was observed to be symmetrical, which is in contrast to the normal tailing observed with the conventional molecular imprinting acrylate polymers.

1.1.5 Univariate and multivariate experimental design for chiral MEKC-MS

Mass spectrometry is one of the most sensitive detection techniques that can be coupled to MEKC. When using as a detector, MS also provides structural information about the analytes, such as molecular weight and fragmentation pattern. It also has very high selectivity, thus sample purity is less important for MS especially when MS/MS is used. As mentioned earlier, normally, low molecular weight nonvolatile chiral selectors, such as cyclodextrins and unpolymerized micelles, are incompatible with mass spectrometer due to suppressing effect and contamination of the ion source [51, 52]. Partial filling technique has been used to overcome this problem [53, 54]. However, partial filling technique suffers from shorter separation window and lower chiral selectivity due to shorter plug length of chiral pseudostationary phase [51]. With the use of polymeric surfactant, the suppressing effect of surfactant in the running buffer is reduced to minimum because molecular micelles are hard to ionize in the ion source and heavy enough to remain outside the m/z range of the mass analyzer [20, 24, 26].

The traditional way for the optimization of CMEKC-MS parameters is a univariate method. This means, to change one factor at a time while hold other parameters constant, until the best separation and optimum *S/N* is obtained for this single parameter. Next, this parameter is held constant and another parameter is optimized. This process needs to be repeated for all the parameters to find the overall optimum. Thus, when optimizing CMEKC-MS parameters a compromise has to be reached between chiral resolution and sensitivity. For example, CMEKC-MS unlike CMEKC-UV or like any other open tubular columns has a drawback of the suction effect caused by the nebulizer placed at the outlet MS end of the separation capillary. This extra suction force generates laminar flow inside the capillary, which leads to broader peaks deteriorating chiral resolution [20]. This effect is especially important in chiral separation of closely eluting enantiomers. To overcome this problem, lower nebulizer pressure needs to be used [25, 27, 28], which in turn decreases MS abundance.

Another difference between MEKC-UV and MEKC-MS is that the background electrolytes (BGE) used in the running buffer need to be volatile in MEKC-MS. It is well-known that the BGE plays a major role in chiral separation. This limits the type of BGEs to a few choices such as NH_4OAc, NH_4COOH, and NH_4CO_3 for MEKC-MS. Thus, a univariate experimental approach should be first used to optimize the nebulizer pressure and type of background electrolyte.

Current CE-MS interface requires sheath liquid, which is flowed using a HPLC pump through to one of the triple tubes inside the nebulizer body. Thus, sheath liquid not only serves as outlet reservoir for CE but also enhances electrospray and helps grounding the capillary. The sheath liquid parameters need to be optimized in CE-ESI-MS for best *S/N*. These parameters include, type of organic solvent in sheath liquid (usually MeOH or isopropanol), its ratio with H_2O, type of electrolyte and its concentration (both help with the analyte ionization), pH of the sheath liquid, and sheath liquid flow rate. Several studies demonstrated the optimization strategies of sheath liquid in MEKC-ESI-MS [25, 27, 28, 30]. In addition, Rizvi *et al.* found that when separating phenylethylamines at very low pH with sulfated polymeric surfactant in MEKC-ESI-MS, adding 1% valeric acid (in place of acetic acid) as electrolyte in methanol/water sheath

liquid can break the strong ion pair formation between positively charged analytes and negatively charged surfactant, reducing the background noise and leading to 3-fold higher peak intensity and better *S/N*.

The concentration of dopant in the sheath liquid is an important parameter, which needs to be optimized when using APPI ionization mode of CMEKC-MS. Dopants are molecules that help the ionization of analyte in APPI-MS. They have lower ionization energy and thus easier to be ionized by UV beam of the APPI source. Once a dopant molecule is ionized, dopant passes its charge to chiral analyte by electron transfer or proton transfer, with or without the help of solvent molecules. The most commonly used dopants in APPI-MS are acetone and toluene. Several studies have involved the optimization of the dopant concentration in sheath liquid for MEKC-APPI-MS [29, 55].

Other than sheath liquid, spray chamber parameters of the MS also plays an important role in MEKC-MS. The critical factors in spray chamber are electrospray voltage, fragmentor voltage, drying gas flow rate (DGF), drying gas temperature (DGT), and vaporizer temperature (VT, only for APPI-MS). More information regarding the optimization of spray chamber parameters in APPI-MS can be found in references [27, 28, 30].

Note that the univariate method does not cover all the possible combinations of parameter levels and thus does not guarantee a global optimum. Another flaw of this method is that all the factors are considered independent and no interactions between factors are investigated. To overcome these problems, multivariate experimental design was introduced in chiral CE or MEKC. The basic idea of multivariate design is to explore the combinations of all the factors (on different levels) at the same time by running a series of experiments. With the help of statistics, the results of these experiments are fitted to mathematical models. These models are in turn used to analyze the interactions between factors and predict overall optimized conditions.

In a multivariate experimental design, if all the combinations of factorial levels are investigated, it is called a full factorial design. If a subset (usually carefully chosen by statistics to reduce the total experiment number) of these combinations are explored, it is called a fractional factorial design. These two types of design generate linear response surface and are usually used for the screening of the

important factors (among all factors) for further study. A typical linear model (which involves two factors) can be represented as:

$$\hat{y} = b_0 + b_1 x_1 + b_2 x_2 + b_{12} x_1 x_2 \quad (12)$$

where $\hat{y}$ is the response; x_1 and x_2 are factors of interest; b_0, b_1, b_2, and b_{12} are coefficients for the factors. An example of these designs is carried out by Williams and co-workers, who used a full factorial design and multilinear regression model to optimize and predict the separation parameters in MEKC [56].

To explore higher order interactions between factors, more complex designs such as central composite, Doehlert, and Box-Behnken design are necessary [57]. These designs have the ability of generating higher order models such as quadratic model:

$$\hat{y} = b_0 + b_1 x_1 + b_2 x_2 + b_{11} x_1^2 + b_{22} x_2^2 + b_{12} x_1 x_2 \quad (13)$$

Examples of central composite design in chiral MEKC can be found in literature [27, 28, 30]. However, the use of multivariate design in MEKC-MS is more complicated, because not only MEKC parameters, but also sheath liquid conditions and spray chamber parameters need to be optimized. Three sets of multivariate experiments thus need to be carried out to investigate these three aspects separately. The final optimums are then combined to obtain the overall best conditions for MEKC-MS. Examples of multivariate design in CMEKC-MS can be found in literature [27, 28, 30].

1.2 Materials

1.2.1 Chemicals

1. All solvents, such as triply deionized H_2O (18.2 MΩ cm at 25 ^oC), methylene chloride, acetone, isopropanol, ethyl acetate, and n-hexane used are HPLC grade.
2. *N*-hydroxysuccinimide (Sigma-Aldrich, St. Louis, MO, USA)
3. *N,N'*-dicyclohexyl-carbodiimide (Sigma-Aldrich, St. Louis, MO, USA)
4. Undecylenic acid (Sigma-Aldrich, St. Louis, MO, USA)
5. ω-undecylenyl alcohol (Sigma-Aldrich, St. Louis, MO, USA)

6. D- or L- amino acids, such as leucine, valine, and phenylalanine (Sigma-Aldrich, St. Louis, MO, USA)
7. Dipeptides such as leucine-leucine, leucine-valine, valine-valine (Bachem, Torrance, CA, USA)
8. Triphosgene (TCI-America, Portland, OR, USA) (*see* Note 1)
9. D- or L- amino alcohol, such as leucinol, valinol, phenylalaninol, and prolinol (Sigma-Aldrich, St. Louis, MO, USA)
10. Chlorosulfonic acid (Sigma-Aldrich St. Louis, MO, USA) (*see* Note 2)
11. 2-Bromoethylamine hydrobromide (Sigma-Aldrich, St. Louis, MO, USA)

1.2.2 Analyte solutions and CMEKC running buffer

1. Stock solutions of the chiral analytes in the concentration range of 1-2 mg/mL are prepared in acetonitrile or methanol and stored in a freezer at -20 ^{o}C. (*see* Note 3)
2. Dilute the stock solution with equal volumes of triply deionized H_2O to obtain the desired final concentrations of analytes in the range of 0.5-1 mg/mL as working solution on a daily basis. (*see* Note 4)
3. Dilute a 7.5 M ammonium acetate solution (solution for molecular biology, Sigma-Aldrich, St. Louis, MO, USA) with triply deionized water to the desired concentration (usually 5-200 mM). For example, a 10 mM solution is prepared by pipetting 133.3 µL of 7.5 M NH_4OAc solution and making it up to 100 mL with triply deionized water in a volumetric flask.
4. Adjust the pH of the NH_4OAc solution as needed using 14.8 M ammonium hydroxide solution for the pH range of 7 - 12 or with glacial acetic acid for the pH range of 3-7.
5. Dissolve the molecular micelles (typically 10-100 mg) in the 5-10 mL of ammonium acetate buffer to obtain the desired equivalent monomer concentration (EMC), which is defined as the mM concentration of the polymeric surfactant, with the same mass concentration as the corresponding monomer. Note that the pH of the MEKC buffer is reported before the addition of molecular micelles.

1.2. 3 Sheath liquid solution

1. Mix triply deionized water and HPLC grade methanol at various volume fractions in the ratios of 20/80, 30/70, 50/50, 70/30, or 80/20 (v/v).
2. To each of this mixture, add 7.5 M ammonium acetate solution until the final NH_4OAc concentration is obtained (typically in the range of 5-100 mM).
3. Add 1-5% (v/v) concentrated acetic acid or 1-5% (v/v) of concentrated ammonium hydroxide solution to the sheath liquid to promote the ionization of cationic or anionic analytes in the gas phase, respectively.
4. When running MEKC-ESI-MS separation of phenylethylamines at very low pH with sulfated polymeric surfactants, add 1% (v/v) of valeric acid to the sheath liquid containing methanol/water in the ratio of 80/20 (v/v).
5. Add dopants, such as acetone or toluene in the range of 0.5-5% (v/v), to the sheath liquid containing 20-80% methanol/ 80-20% water (v/v) when running MEKC-APPI-MS experiments.

1.2.4 Equipment

1. An Agilent CE instrument interfaced to an Agilent 1100 series single quadrupole mass spectrometer (Agilent Technologies, Palo Alto, CA) can be used for all MEKC-MS experiments. The Agilent 3D-CE/MSD ChemStation software (Rev. A.10.02) is used for instrument control, determination of *Rs*, and *S/N*. The sheath liquid is delivered by an Agilent 1100 series isocratic HPLC pump equipped with a 1:100 splitter. Drying gas (N_2) is delivered as sheath gas to the mass spectrometer.
2. A Barnstead Nanopure II Water System (Dubuque, IA, USA) to obtain the triply deionized water (18.2 MΩcm).
3. A Cobalt 60 panoramic pool irradiator for polymerization of the surfactants (Phoenix Memorial Laboratory, University of Michigan, Ann Arbor, MI).
4. A commercial ultrasonic bath is used for degassing the mobile phase.
5. A commercial pH meter for mobile phase and sheath liquid pH adjustment.

6. Fused silica capillary (50 μm i.d., 360 μm o.d., Polymicro Technologies, Phoenix, AZ).
7. Nylon syringe filters (0.45 μm) for the filtration of the micellar solution. The sheath liquid can be filtered using 0.2 μm polysulfone filter paper in a vacuum flask.
8. 1000 MW cut-off dialysis cellulose ester membrane (Spectra/Por, Rancho Dominguez, CA, USA).
9. Design-Expert (version 7.0.3, Stat-Ease, Inc. Minneapolis, MN) software for the experimental design and data analysis, which includes building the model, generating the response surface plot, validating the model by analysis of variance, and predicting the optimum conditions.

1.3. Methods

1.3.1 Preparation of molecular micelles

The details of the synthetic procedures of various classes of chiral molecular micelles with L- or D-optical configuration one from each class is provided below: one amide type single amino acid or dipeptide molecular micelle (Fig. 2A), one carbamate type amino acid with leucine, valine or isoleucine head groups molecular micelle (Fig. 2B), one pH independent sulfated amino acid head group molecular micelle (Fig. 2C), and one quaternary ammonium molecular micelle (Fig. 2 D).

1.3.1.1 Synthesis of amide type single amino acid (SUA) and dipeptide (SUAA) surfactants with L- or D- configuration and their corresponding molecular micelles

1. Dissolve equimolar amounts (0.1 mol) of *N*-hydroxysuccinimide, *N,N'*-dicyclohexyl-carbodiimide, and undecylenic acid in ethyl acetate and stir overnight (~ 16 h) to yield the *N*-hydoxysuccinimide ester of undecylenic acid (*see* Note 5). Filter the resulting milky solution of ester carefully to remove the by-products (e.g., dicyclohexyl urea) (*see* Note 5). Recrystallize the *N*-hydroxysuccinimide ester of undecylenic acid by dissolving in a minimum volume of hot 2-propanol until a clear solution is obtained. Next, store the clear solution in a freezer overnight followed by filtering of the crystals and washing with chilled 2-propanol.

2. Mix equal molar amounts (0.1 mol) of *N*-hydoxysuccinimide ester of undecylenic acid (synthesized in step 1), $NaHCO_3$, and L- or D-valine, leucine, isoleucine, or leucine-valine in 200 mL of THF and 200 mL of triply deionized water in a round bottom flask and stir overnight.
3. Add 6 N HCl to pH ~1 until formation of a precipitate. Remove the organic content of the solvent mixture under reduced pressure. Filter the precipitate and wash the precipitate with ~ 1000 mL of water, and lyophilize it overnight to yield the acid form of the surfactant (a white waxy solid).
4. Next, weigh out the acid form surfactant and stir in ~ 500 mL of water in a round bottom flask. Add an equimolar amount of $NaHCO_3$ and stir overnight to obtain a clear solution of the salt of the surfactant.
5. Extract the final surfactant salt solution with ~500 mL of ethyl acetate in separatory funnel to remove any organic impurity. Shake and wait until the bottom aqueous layer gets crystal clear. Collect the bottom aqueous layer and lyophilize to yield the solid salt form of the surfactant monomer.
6. Prepare a 100 mM aqueous surfactant solution and place it under ^{60}Co γ-radiation with a total dose of 20 MRad to allow the formation of polymerized surfactant or molecular micelle. The polymerization can be verified by ^{1}H NMR showing the disappearance of vinyl protons around 5-6 ppm.
7. Following polymerization, dialyze the solution to remove any unpolymerized monomers using a 1000 MW cut-off dialysis membrane and then lyophilize the solution to obtain the solid polymeric surfactants, which can be stored at room temperature in a desiccator (*see* Note 6).

1.3.1.2 Synthesis of carbamate single amino acid surfactants (SUCA) with L- or D- optical configuration and their corresponding molecular micelles

1. Dissolve 17 g (0.1 mol) of ω-undecylenyl alcohol and 10 g (0.033 mol) of triphosgene in 200 mL of methylene chloride in a round bottom flask. Add 8 g (0.1 mol) of pyridine dropwise to this solution and stir for 96 h (*see* Note 1).

2. Acidify the resulting solution with 6 N HCl. Extract the solution with water three times with 200 mL water. Collect the methylene chloride layer and dry it over anhydrous Na_2SO_4 (i.e., add ~100-200 g of Na_2SO_4. stir with a glass rod, let the Na_2SO_4 settle and transfer the product from the beaker to round bottom flask). Evaporate methylene chloride under reduced pressure to yield chloroformate of ω-undecylenyl alcohol as a viscous liquid.
3. Mix equal molar (0.02 mol) of the chloroformate prepared in step 2, the amino acid (L- or D-valine, leucine, or isoleucine) and NaOH in 500 mL of water in a round bottom flask and stir for 2 h.
4. Acidify the resulting solution with 6 N HCl to about pH ~1. Extract the solution with methylene chloride three times (500 mL each time). Collect the bottom methylene chloride layer each time. Dry the combined organic phases over anhydrous Na_2SO_4 and evaporate methylene chloride under reduced pressure to yield the acid form of the surfactant as a viscous liquid.
5. Weigh out the acid form of surfactant and convert it to salt form by suspending it in water, adding an equimolar amount of $NaHCO_3$ and stirring for ~16 h.
6. Clean the resulting surfactant salt solution by extracting it with 500 mL of ethyl acetate. The bottom aqueous layer is lyophilized to yield the solid surfactant monomer. The polymerization and dialysis procedure is the same as described above in steps 6 and 7 in section 1.3.1.1 for the amide surfactant.

1.3.1.3 Synthesis of sulfated single amino acid surfactants (L-SUCAAS) with L- or D- configuration and their corresponding molecular micelles

1. Prepare the chloroformate of ω-undecylenyl alcohol as described above in steps 1 and 2 in the synthesis of SUCA (section 1.3.1.2.).
2. Mix equal molar amounts (0.02 mol) of the chloroformate, L-valinol, L-leucinol, or L-isoleucinol, and NaOH in 500 mL of water and stir for 2 h.
3. Acidify the resulting solution with 6 N HCl to about pH ~1. Extract the solution with methylene chloride three times (500 mL each time). Collect the bottom methylene chloride layer. Dry it with

anhydrous Na_2SO_4 and evaporate the organic solvent under reduced pressure to yield a viscous product.

4. Weigh out this product and dissolve it in 500 mL of methylene chloride. Add an equimolar amount of pyridine. Add an equimolar of chlorosulfonic acid dissolved in ~100 mL methylene chloride dropwise and allow the reaction mixture to stir overnight (~16 h) (*see* Note 2).
5. Acidify the resulting solution with 6 N HCl. Wash it with water three times (500 mL each time) in a separatory funnel, collect the bottom methylene chloride layer in a beaker and dry it with anhydrous Na_2SO_4. Evaporate the organic solvent under reduced pressure to obtain the acid form of the L-or D-type SUCAAS as a viscous liquid.
6. The steps for converting the SUCCAS into the salt form and polymerizing them is exactly the same as described above in steps 5 and 6 for the synthesis of SUCA surfactant (section 3.1.2). The dialysis procedure is the same as described above in steps 7 of section 1.3.1.1 for the amide surfactant.

1.3.1.4 Synthesis of quaternary ammonium type amino acid surfactants (L-UCAB) with leucine or pyrrolidine head group, and their corresponding molecular micelles

1. Prepare the chloroformate of ω-undecylenyl alcohol as described above in steps 1 and 2 in the synthesis of SUCA (section 1.3.1.2.).
2. Mix equal molar (0.02 mol) of the chloroformate, 2-bromoethylamine hydrobromide, and 0.02 moles of NaOH in 500 mL of water and stir for 2 h.
3. Acidify the resulting reaction mixture with 6 N HCl. Extract the solution with methylene chloride three times (500 mL each time). Collect the bottom methylene chloride layer each time, combine the layers and dry it with anhydrous Na_2SO_4. Evaporate the organic solvent under reduced pressure to obtain the bromo intermediate as a white solid. Recrystallize the product from hot n-hexane.
4. Add 5 g of L-leucinol (0.043 mol) or L-prolinol (0.05 mol) to a 250 mL round bottom flask immersed in an ice bath (no solvent needed at this step). Add 20 mL of neat 95% formic acid (0.5

mol) very slowly using 100 mL separatory funnel. Wait for 15 min for the reaction to cool down and add 17 mL of formaldehyde solution (37%, 0.23 mol). Reflux this reaction mixture for 12 h. This synthesis procedure is known as Eschweiler-Clark reaction [58].

5. Adjust the pH of the resulting mixture to about pH ~11 using 2 M NaOH and extract the solution with methylene chloride. Wash the methylene chloride layer with ~ 200 mL of water and dry it with anhydrous $NaSO_4$. Evaporate the organic solvent under reduced pressure to yield about 6 g of *N,N*-dimethylleucinol.
6. Dissolve 6.4 g of the bromo intermediate obtained in steps 1 - 3 (0.02 mol) and 2.9 g of *N,N*-dimethylleucinol (0.02 mol) in 250 mL acetone and refluxed the solution for 48 h.
7. Evaporate the acetone in the reaction mixture under reduced pressure to yield the raw product as a viscous liquid. Dissolve the raw product in water and extract it with ethyl acetate to remove organic impurities.
8. Collect the bottom aqueous layer and lyophilize it to yield the monomer of the ionic liquid. The polymerization and dialysis procedure of the cationic liquid surfactant is the same as for the SUCA surfactants (steps 6 and 7 in section 3.1.1 for the amide surfactant).

1.3.2 MEKC experiments

1. Transfer about 200 μL of working analyte solution to a cone shaped sample vial for CE analysis.
2. The surfactant containing buffer is vortexed, filtered trough 0.45 μm nylon syringe filters, and ultrasonicated for 30 min before use. (*see* Note 7)
3. Transfer the running buffer to vials (around 400 μL each vial) for MEKC-MS runs.
4. The MEKC-UV experiment is performed using a 64.5 cm long fused-silica capillary with an effective length of 56.0 cm.
5. When MEKC-MS and MEKC-UV experiments are performed in the tandem mode or high resolution is desired, a fused-silica capillary with a total length of 120 cm is necessary. At 60 cm from the injection end of the capillary, a 3 mm section of polyimide coating is removed to create a UV detection window. However, due to instrument constraints, performing only MEKC-MS

experiments requires at least 50 cm total length. The capillary is inserted into the CE-MS cassette (using the non-metallic UV alignment interface) (*see* Note 8) and installed into the CE instrument.

6. When installing the capillary into the cassette, press the alignment interface against the capillary insertion tool and slide the capillary through the interface until the detection window is aligned with the interface window. Release the interface and place the interface into the interface holder of an empty cassette. Wind the capillary around the reel of the cassette if necessary. Avoid the capillary windings to contact each other. Finally, after closing the cassette cover, ensure the inlet end is the same length as the cassette guiding pins. Once the capillary is installed in the cassette, insert the cassette in the CE instrument.
7. When installing the capillary outlet into the nebulizer, insert the capillary into the nebulizer first; make sure the tip of the capillary is aligned flat with the spray tip. Next, tighten the fitting screw to hold the capillary in position. The distance between the tip of the capillary and the spray tip of the nebulizer can be adjusted by turning the adjustment screw on the nebulizer. For example, turning the screw clockwise makes the capillary retreat inside the nebulizer; turning the screw counterclockwise so that the capillary is sticking out of the nebulizer. (*see* Note 9) Whether the capillary tip should be retreating inside the nebulizer or sticking outside the nebulizer, it needs to be optimized for the CMEKC-MS analysis. The analyst should perform experiments to determine how far inside or outside the capillary should be placed. Typically, for MEKC-ESI-MS experiments, 1-2 turns inside (clockwise) provide a stable current without compromising sensitivity. When running MEKC-APPI-MS, the CE instrument needs to be raised ~6 cm to compensate the height of the spacer used in APPI spray chamber. (*see* Note 10 and 11). The position of the capillary tip inside the nebulizer for APPI-MS also needs to be optimized. One should explore ± 2 turns to find the position that provides the best *S/N* for a given analyte.
8. Routinely rinse the CE electrodes and pre-punchers with 2-propanol and dry both electrodes and pre-punchers. For optimum sensitivity, flush the MS spray chamber with 2-propanol and then

wipe the chamber with a special cloth (*see* Note 12) soaked in 2-propanol before each MEKC-MS experiment.

9. Flush a new capillary sequentially with 1 M NH_4OH at 45°C and deionized water for 40 minutes and 20 minutes, respectively, before use. For MEKC-UV experiments, NH_4OH can be replaced with 1 M NaOH.
10. Flush the capillary with the running buffer containing molecular micelles at various EMC (5-50 mM) for 5 minutes using a pre-conditioning step before each run. After each run, flush the capillary with water for 2 minutes, 1 M NH_4OH for 2 minutes, and water for another 2 minutes as post-conditioning step.
11. Set the capillary temperature and polarity of the voltage based on the nature of analyte.
12. Keep analyte solutions at 15ºC in the sample carousel using a circulating water bath (*see* Note 13 and 14) and inject hydrodynamically at the pressure of 5-10 mbar (*see* Note 15) for various periods of time for MEKC-MS.
13. According to the nature of the analysis, scan mode, selected ion monitoring (SIM), or multiple reaction monitoring (MRM) mode can be chosen for MS detection. To optimize the MS signal of each analytes, parameters such as fragmentor voltage, and collision energy could be determined by direct infusion through CE instrument or using flow injection analysis with the HPLC instrument.
14. A typical ESI-MS spray chamber setting for MEKC-ESI-MS experiment is: nebulizer pressure, 3-4 psi (*see* Note 16); drying gas flow rate: 5 L/min; drying gas temperature, 200ºC; capillary voltage + 3000 V; gain setting, 3. These parameters should be further optimized for best *S/N* of the analyte.
15. A typical APPI-MS spray chamber setting for MEKC-APPI-MS experiment is: nebulizer pressure, 3-4 psi; drying gas flow rate: 5 L/min; drying gas temperature, 200 ºC; Vaporizer temperature, 200 ºC; capillary voltage + 2000 V; gain setting, 3. These parameters should be further optimized for best *S/N* of the analyte.

16. An example of sheath liquid used in MEKC-ESI-MS is typically 80/20 MeOH/H_2O (v/v) with 5 mM NH_4OAc (pH 6.8) at a flow rate of 5 μL/min for high pH, and acetic acid or valeric acid (1%, v/v) at low pH.
17. An example of sheath liquid used in APPI-MS is typically 80/20 MeOH/H_2O (v/v) with 5 mM NH_4OAc (pH 6.8) at a flow rate of 7.5 μL/min with 0.5-5% (v/v) dopant (acetone or toluene).
18. An example of the MEKC conditions and instrument settings for a typical CMEKC-MS experiments for the enantioseparation of (±) 1,1′-bi-2-naphthol (BOH) and (±) 1,1′-binaphthyl-2,2′-diyl hydrogen phosphate (BNP) as shown in Fig. 3 are given below:

    (a) Cut a 60 cm long fused silica capillary with square endings. (*see* Note 17). Conditioned the capillary with 1 M NH_4OH (40 min at 45 ^oC) and H_2O (20 min at 20 ^oC) before use.

    (b) Preparation of the running buffer: 35 mM NH_4OAc buffer, pH 10.8, 27 mM (total) poly-L-SUCL/ poly-L-SULV (1:1, molar ratio). Filter the running buffer with a 0.45 μm nylon syringe filter and sonicate it for 30 min.

    (c) Preparation of the analyte solution: Dissolve the solid (±) BOH and (±) BNP in MeOH to make 1 mg/mL stock solution. Mix 50 μL of each stock solution and dilute the mixture with 100 μL H_2O to make a 0.25 mg/mL working analyte solution.

    CE instrument settings: +30 kV, 20 ^oC. Injection size: 5 mbar, 3 sec. Pre-conditioning: 5 min with running buffer. Post-conditioning: H_2O (1 min), 1 M NH_4OH (2 min) and H_2O (2 min).

    MS instrument settings: Negative ion SIM mode, 285 for (±) BOH and 347 for (±) BNP. Fragmentor voltage, 90V; capillary voltage, 3000V; gain setting, 3 nebulizer pressure, 3 psi; DGF, 4 L/min; DGT, 250 ºC.

    Sheath liquid settings: MeOH/H_2O (80:20, v/v), 5 mM NH_4OAc, pH 8.5, sheath liquid flow rate 5 μL/min.

1.3.3 Optimization of the MEKC-MS procedures and conditions

1. Type of the BGE needs to be determined first. Because only volatile electrolytes are compatible with MS, the choices are limited to ammonium acetate, ammonium carbonate, or triethylammonium acetate, in the pH range of 5.0-10.0, whereas ammonium formate is used in the pH range of 2.0-4.5.
2. The concentration and pH of the BGE are critical for a successful chiral separation. Their values need to be determined by experiments on an individual basis.
3. An organic modifier, usually methanol or acetonitrile, sometimes helps chiral separation. Up to 50% of acetonitrile and 60% methanol can be used with molecular micelles to improve enantioseparations.
4. CE parameters, such as voltage and capillary temperature, should be optimized for each chiral analyte.
5. Direct infusion is usually used to determine some of the MS parameters before online CE-MS experiments. These parameters are m/z of the analytes, fragmentor voltage, drying gas flow rate, drying gas temperature, capillary voltage, and collision energy (only for MRM detection).
6. The result of direct infusion experiment does not always reflect the *S/N* of the online experiment. Thus, online MEKC-MS experiments are usually required to further optimize MS parameters.
7. Sheath liquid parameters such as composition, pH, and flow rate are also optimized by direct infusion and online experiments. If APPI-MS is used, the concentration of dopant needs to be determined as well.
8. Multivariate design is a powerful tool in optimizing MEKC-MS parameters, especially when the interactions of each parameter are of interest, the reproducibility of response in a random fashion provide valuable information on system ruggedness. However, multivariate design sometimes requires more runs, and thus more time and material, than its univariate counterpart. The reproducibility between runs also needs to be good to guarantee the fitness of the model. The inset in Fig. 1.3 shows the comparison of the experimental value vs. the predicted values for the

CMEKC-MS of (±) BOH and (±) BNP. The experimental multivariate design is performed in several steps as summarized below:

(a) First, preliminary experiments need to be performed to determine the range of full factorial or fractional factorial design experiments for all the MEKC parameters. From the response generated from each experiment, linear models are then built up and the significances of all the parameters are determined by statistical analysis (*F*-test).

(b) Higher order designs such as central composite, Doehlert, and Box-Behnken design are used to further investigate the interactions between all the significant factors found above. The level for each factor is determined by univariate approach or using full factorial or fractional factorial design. These levels are then plugged into the Design-Expert software. The software will generate combinations of all levels of each factor in a random order.

Run all the experiments and input the response into the software. The software will generate models to fit the experimental data. These models are then validated by analysis of variance and the most fitted model will be selected for further data analysis such as the building of the response surface plots and the prediction of the optimum conditions.

From the most fitted model, response surface plots with any two interacting factors are generated. By investigating these plots the interactions between factors can be revealed.

This process also needs to be performed for the optimization of sheath liquid as well as MS spray chamber conditions.

1.4 Notes

1. Triphosgene is toxic and severely irritating to eyes and skin. It decomposes (on heating and reactions with any nucleophile) to phosgene which is a highly toxic gas. Therefore, triphosgene has to be handled only in a chemical fume hood with extreme care and proper protection. Even the glassware used for the reactions of triphosgene and the resulting chloroformate needs to be cleaned in the fume hood. Triphosgene needs to be stored in a cool, dry place.

2. Chlorosulfonic acid is an extremely corrosive liquid. It should be handled only in fume hood with proper protection.
3. When making the sample stock solution, if the analyte is not soluble in acetonitrile or methanol, a drop of HCl or NaOH can be added to basic and acidic chiral compound, respectively to increase the solubility.
4. Similar to HPLC, changing the solvent used to dissolve the analytes could have an effect on the efficiency and resolution of the peaks. Therefore, if the chiral resolution is not satisfactory, try using a different solvent system (e.g., acetonitrile or methanol in combination with water at various ratios) to dissolve the analytes. This promotes stacking, which in turn improves efficiency and resolution.
5. Ester preparation requires that all reagents including glassware should be very dry. This is essential to obtain a pure dry ester. The filtration process should be done very slowly to ensure removal of the water soluble byproducts.
6. Almost all the molecular micelles are hygroscopic. Store them in desiccator for improved run time reproducibility and longer shelf life.
7. A running buffer containing molecular micelles needs to be degassed very well to avoid formation of air bubbles during MEKC-MS runs. Also, the running buffer needs to be freshly made every time and filtered through a 0.45 μm filter.
8. Metal alignment interface (typically sold for CE-UV) detection should not be used for CE-MS to prevent arcing. Only non-metallic interface especially designed for CE-MS should be used.
9. The position of the capillary in the nebulizer is sometimes important. Our experience is that if the capillary tip is a little inside the nebulizer (around 2 turns clockwise), the current is easier to be stabilized for the MEKC-MS runs. However, with capillary inside the nebulizer, the MS signal tends to be noisier. Online experiments need to be carried out to find the best compromise between current stability and *S/N* of the analytes.

10. When running MEKC-MS (both ESI-MS and APPI-MS) the inlet of the capillary (located inside the CE instrument) needs to be leveled with the outlet end (at the tip of the nebulizer) to avoid siphoning effect. Thus, adjusting the height of the CE instrument is sometimes necessary. When running MEKC-ESI-MS, the CE instrument can be placed at the same level as the MS instrument. However, when running MEKC-APPI-MS, the CE instrument needs to sit on a stand of 6 cm above the level of the MS instrument.
11. When running CE-APPI-MS on Agilent CE system, the nebulizer needs to be grounded due to the plastic spacer between nebulizer and spray chamber.
12. The cleaning cloth used to clean the MS spray chamber should be lint-free (Agilent part number 05980-60051). If the spray shield is too dirty, an abrasive paper (8000 grit, Agilent part number 8660-0852) can be used to remove the stain.
13. When using volatile running buffer, lower sample tray temperature and new caps of the buffer vials are necessary to keep the buffer from evaporating.
14. Sample tray temperature of the instrument can be important to prevent volatile buffers (e.g., ammonium acetate) evaporation. However, some analytes are less soluble at lower temperature and may precipitate out, which causes irreproducible elution time and peak area. Hence, the carousel temperature needs to be determined based on the solubility of each analyte at any specific temperature.
15. The injection pressure should be kept at low settings (5 - 10 mbar) because of the extra suction created by the nebulizer to prevent peak coalescence of the closely eluting enantiomers. To increase sensitivity, injection time can be increased.
16. Nebulizer pressure is critical in chiral MEKC-MS as suction caused by higher nebulizer pressure deteriorate efficiency as well as chiral resolution of the enantiomer peaks. However, there is usually a lower limit to nebulizer pressure (3 psi for Agilent MS instrument). Sometimes lower nebulizer pressure (<3 psi) even causes current break down. Nevertheless, the analyst should use lowest possible nebulizer pressure to get better chiral resolution without sacrificing *S/N*.

17. Both ends of the capillary need to be perfectly square cut when running MEKC-MS. Jagged edges of the capillary can cause noisy baseline and poor peak shape in MS as well as uneven spray in the source resulting in current breakdown. One procedure is to cut a small wedge through the polyimide coating of the capillary with the sharper edge of a cutter first and then pull one end steadily of the capillary with pliers while holding the other end with hand until the capillary breaks.

References

[1] Gassmann, E.; Kuo, J. E.; Zare, R. N. *Science* 1985, *230* (4727), 813-4.

[2] Fanali, S. *J. Chromatogr. A* 1989, *474* (2), 441-446.

[3] Nielen, M. W. F. *Anal. Chem.* 1993, *65* (7), 885-893.

[4] Zhu, W.; Vigh, G. *Electrophoresis* 2001, *22* (7), 1394-1398.

[5] Terabe, S.; Shibata, M.; Miyashita, Y. *J. Chromatogr. A* 1989, *480*, 403-411.

[6] Nishi, H.; Fukuyama, T.; Terabe, S. *J. Chromatogr. A* 1991, *553*, 503-516.

[7] Wang, J.; Warner, I. M. *Anal. Chem.* 1994, *66* (21), 3773-3776.

[8] Guttman, A.; Paulus, A.; Cohen, A. S.; Grinberg, N.; Karger, B. L. *J. Chromatogr. A* 1988, *448*, 41-53.

[9] Dowling, V. A.; Charles, J. A. M.; Nwakpuda, E.; McGown, L. B. *Anal. Chem.* 2004, *76* (15), 4558-4563.

[10] De, B. T.; Bijma, R.; Ensing, K. *J. Pharm. Biomed. Anal.* 1999, *19* (3-4), 529-537.

[11] Lin, J. M.; Nakagama, T.; Uchiyama, K.; Hobo, T. *Chromatographia* 1996, *43* (11/12), 585-591.

[12] Glukhovskiy, P.; Vigh, G. *Anal. Chem.* 1999, *71* (17), 3814-3820.

[13] Spanik, I.; Lim, P.; Vigh, G. *J. Chromatogr. A* 2002, *960* (1-2), 241-246.

[14] Hoffmann, P.; Wagner, H.; Weber, G.; Lanz, M.; Caslavska, J.; Thormann, W. *Anal. Chem.* 1999, *71* (9), 1840-1850.

[15] Kaniansky, D.; Šimuničova, E.; Ölvecká, E.; Ferancová, A. *Electrophoresis* 1999, *20* (13), 2786-2793.

[16] Snopek, J.; Jelínek, I.; Smolková-Keulemansová, E. *J. Chromatogr. A* 1988, *438*, 211-218.

[17] Mayer, S.; Schurig, V. *J. High Res. Chromatog* 1992, *15* (2), 129-131.

[18] Otsuka, K.; Mikami, C.; Terabe, S. *J. Chromatogr. A* 2000, *887* (1-2), 457-463.

[19] Zheng, J.; Norton, D.; Shamsi, S. A. *Anal. Chem.* 2006, *78* (4), 1323-1330.

[20] Shamsi, S. A. *Anal. Chem.* 2001, *73* (21), 5103-5108.

[21] Akbay, C.; Rizvi, S. A. A.; Shamsi, S. A. *Anal. Chem.* 2005, *77* (6), 1672-1683.

[22] Rizvi, S. A. A.; Zheng, J.; Apkarian, R. P.; Dublin, S. N.; Shamsi, S. A. *Anal. Chem.* 2006, *79* (3), 879-898.

[23] Rizvi, S. A. A.; Shamsi, S. A. *Anal. Chem.* 2006, *78* (19), 7061-7069.

[24] Hou, J.; Zheng, J.; Rizvi, S. A. A.; Shamsi, S. A. *Electrophoresis* 2007, *28* (9), 1352-1363.

[25] Hou, J.; Zheng, J.; Shamsi, S. A. *J. Chromatogr. A* 2007, *1159* (1-2), 208-216.

[26] Hou, J.; Zheng, J.; Shamsi, S. A. *Electrophoresis* 2007, *28* (9), 1426-1434.

[27] He, J.; Shamsi, S. A. *J. Chromatogr. A* 2009, *1216* (5), 845-856.

[28] He, J.; Shamsi, S. A. *J. Sep. Sci.* 2009, *32* (11), 1916-1926.

[29] He, J.; Shamsi, S. A. *Electrophoresis* 2011, *32* (10), 1164-1175.

[30] Wang, B.; He, J.; Shamsi, S. A. *J. Chromatogr. Sci.* 2010, *48* (7), 572-583.

[31] Terabe, S.; Otsuka, K.; Ichikawa, K.; Tsuchiya, A.; Ando, T. *Anal. Chem.* 1984, *56* (1), 111-113.

[32] Palmer, C. P.; Terabe, S. *Anal. Chem.* 1997, *69* (10), 1852-1860.

[33] Akbay, C.; Gill, N. L.; Agbaria, R. A.; Warner, I. M. *Electrophoresis* 2003, *24* (24), 4209-4220.

[34] Akbay, C.; Shamsi, S. A. *Electrophoresis* 2004, *25* (4-5), 622-634.

[35] Ahuja, E. S.; Foley, J. P. *Anal. Chem.* 1995, *67* (14), 2315-2324.

[36] Terabe, S.; Otsuka, K.; Ando, T. *Anal. Chem.* 1985, *57* (4), 834-841.

[37] Chankvetadze, B. *J. Chromatogr. A* 2007, *1168* (1-2), 45-70.

[38] Wren, S. A. C.; Rowe, R. C. *J. Chromatogr. A* 1992, *603* (1-2), 235-241.

[39] Palmer, C. P.; Khaled, M. Y.; McNair, H. M. *J. High Res. Chromatog* 1992, *15* (11), 756-762.

[40] Palmer, C. P.; McNair, H. M. *J. Microcolumn Sep.* 1992, *4* (6), 509-514.

[41] Shamsi, S. A.; Macossay, J.; Warner, I. M. *Anal. Chem.* 1997, *69* (15), 2980-2987.

[42] Rizvi, S. A. A.; Shamsi, S. A. *Electrophoresis* 2003, *24* (15), 2514-2526.

[43] Billiot, E.; Macossay, J.; Thibodeaux, S.; Shamsi, S. A.; Warner, I. M. *Anal. Chem.* 1998, *70* (7), 1375-1381.

[44] Shamsi, S. A.; Valle, B. C.; Billiot, F.; Warner, I. M. *Anal. Chem.* 2003, *75* (3), 379-387.

[45] Wang, B.; He, J.; Bianchi, V.; Shamsi, S. A. *Electrophoresis* 2009, *30* (16), 2812-2819.

[46] Wang, B.; He, J.; Bianchi, V.; Shamsi, S. A. *Electrophoresis* 2009, *30* (16), 2820-2828.

[47] Valle, B. C.; Morris, K. F.; Fletcher, K. A.; Fernand, V.; Sword, D. M.; Eldridge, S.; Larive, C. K.; Warner, I. M. *Langmuir* 2006, *23* (2), 425-435.

[48] Luces, C. A.; Warner, I. M. *Electrophoresis* 2010, *31* (6), 1036-1043.

[49] Rizvi, S. A. A.; Shamsi, S. A. *Electrophoresis* 2007, *28* (11), 1762-1778.

[50] Priego-Capote, F.; Ye, L.; Shakil, S.; Shamsi, S. A.; Nilsson, S. *Anal. Chem.* 2008, *80* (8), 2881-2887.

[51] Shamsi, S. A. *Electrophoresis* 2002, *23* (22-23), 4036-4051.

[52] Lamoree, M. H.; Sprang, A. F. H.; Tjaden, U. R.; van der Greef, J. *J. Chromatogr. A* 1996, *742* (1-2), 235-242.

[53] Jäverfalk, E. M.; Amini, A.; Westerlund, D.; Andrén, P. E. *J. Mass Spectrom.* 1998, *33* (2), 183-186.

[54] Tanaka, Y.; Otsuka, K.; Terabe, S. *J. Chromatogr. A* 2000, *875* (1-2), 323-330.

[55] Schappler, J.; Guillarme, D.; Prat, J.; Veuthey, J.-L.; Rudaz, S. *Electrophoresis* 2007, *28* (17), 3078-3087.

[56] Williams, A. A.; Fakayode, S. O.; Huang, X.; Warner, I. M. *Electrophoresis* 2006, *27* (21), 4127-4140.

[57] Ferreira, S. L. C.; Bruns, R. E.; da Silva, E. G. P.; dos Santos, W. N. L.; Quintella, C. M.; David, J. M.; de Andrade, J. B.; Breitkreitz, M. C.; Jardim, I. C. S. F.; Neto, B. B. *J. Chromatogr. A* 2007, *1158* (1-2), 2-14.

[58] Clarke, H. T.; Gillespie, H. B.; Weisshaus, S. Z. *J. Am. Chem. Soc.* 1933, *55* (11), 4571-4587.

Chapter 2

Multivariate Approach for the Enantioselective Analysis in Micellar Electrokinetic Chromatography- Mass Spectrometry: I. Simultaneous Optimization of Binaphthyl Derivatives in Negative Ion Mode

A mixture of two molecular micelles polysodium *N*-undecenoxy carbonyl-L-leucinate, (poly-L-SUCL) and polysodium *N*-undecanoyl leucylvalinate, (poly-L-SULV) was utilized in micellar electrokinetic chromatography-electrospray ionization-mass spectrometry (MEKC-ESI-MS) to simultaneously separate and detect enantiomers of binaphthyl derivatives. Separation parameters such as background buffer composition, voltage, temperature, and nebulizer pressure were optimized using a multivariate central composite design (CCD). Baseline enantioseparation for both analytes was achieved. The CCD was also used in the optimization of sheath liquid and spray chamber parameters to achieve optimum ESI-MS response. The results demonstrate that CCD is a powerful tool for the optimization of MEKC-MS parameters and the response surface model analysis can provide in-depth statistical understandings of the significant factors required to achieve maximum enantioresolution and ESI-MS sensitivity.

2.1 Introduction

The binaphthyl derivatives such as 1,1′-bi-2-naphthol (BOH) and 1,1′-binaphthyl-2,2′-diyl hydrogen phosphate (BNP) are very important chiral ligands for asymmetric catalysis [1,2]. They are also used to evaluate the enantioselectivity of chiral stationary phase (CSP) and chiral selectors in chromatography and capillary electrophoresis (CE), respectively [3-5]. In the last several years, surfactants bearing amino acid or small peptide head groups have been developed for the micellar electrokinetic chromatography (MEKC) separation of binaphthyl derivatives. The chiral pseudo-stationary phases (PSPs) include sodium *N*-[4-n-dodecyloxy-benzoyl]-L-leucinate (SDLL), sodium *N*-[4-n-dodecyloxybenzoyl]-L-isoleucinate (SDLIL), polysodium *N*-undeccanoly-L,L-leucylvalinate (poly-L,L-SULV), polysodium *N*-undecanoyl-L-isoleucylvalinate (poly-L-SUILV), polysodium *N*-undecenoxy carbonyl-L-leucinate (poly-L-SUCL), and polysodium *N*-undecenoxy carbonyl-L-isoleucinate (poly-L-SUCIL) [6-8]. However, all of the aforementioned chiral PSPs have been used in MEKC with UV detection, which has comparably less sensitivity and specificity. In several of our recent papers [9-14], we have shown that the problems encountered with the electrospray stability and the poor signal-to-noise (*S/N*) ratio associated with the conventional unpolymerized micelle in MEKC-MS can be overcome with

the hyphenation of microemulsion electrokinetic chromatography to atmospheric pressure photoionization mass spectrometry (MEEKC-APPI-MS) [15, 16] or by using molecular micelles (also known as polymeric surfactants) as pseudo-stationary phase. Molecular micelles, when used in MEKC-MS, are difficult to ionize, providing a much improved *S/N* in electrospray ionization-mass spectrometry (ESI-MS). Other important features of using molecular micelles in MEKC-MS include zero critical micelle concentration (CMC) [17] as well as compatibility with the use of higher concentration of organic solvents [18] and volatile buffers [9]. Thus, the molecular micelles have a great potential to be used as a MS compatible PSP in routine hyphenation of CE to MS.

Our previous work on univariate approach, which focuses on only one factor at a time is mainly used to optimize the separation and detection parameters in MEKC-MS [9, 10, 13]. However, univariate approach does not guarantee a global optimum and often results in poor predictions. On the other hand, the multivariate optimization using design of experiments (DOE) provides simultaneous and much more efficient way of identifying experimental factors in MEKC-MS. Several papers have reported the use of experimental design for CZE-MS [19, 20] and MEKC-MS [9] optimization of achiral compounds. However, to our knowledge, not much work involving multivariate optimization of chiral MEKC-MS method has been published [9]. Thus, with the aim of providing additional data on the potential of MEKC-MS, simultaneous enantioseparation and ESI-MS detection of two binaphthyl derivatives using a multivariate approach is developed.

We present herein, the application of central composite design (CCD) to evaluate the importance of selected MEKC-MS parameters in a simultaneous analysis of two chiral compounds [(e.g.) (±) BOH and (±) BNP] in the negative ion mode. The use of CCD allowed us to determine the optimal conditions for resolution, analysis time and *S/N* in MEKC-MS using a mixture of two molecular micelles containing one single amino acid based polymeric surfactant, i.e., polysodium *N*-undecenoxy carbonyl-L-leucinate (poly-L-SUCL) and one dipeptide polymeric surfactant (polysodium *N*-undecanoyl-L,L-leucylvalinate (poly-L,L-SULV).

2.2 Materials and methods

2.22.1 Chemicals and reagents

Both (±) BOH and (±) BNP as racemic mixtures were obtained from Aldrich (Milwaukee, WI). Standard solution of 7.5 M ammonium acetate (NH_4OAc) was purchased from Sigma-Aldrich (St. Louis, MO). Methanol (MeOH, HPLC grade), acetonitrile (ACN, HPLC grade), and acetic acid (glacial) were obtained from Caledon Laboratories Ltd. (Georgetown, ON, Canada). Ammonium hydroxide (NH_4OH, 28%-30% ammonia solution) was purchased from EM Science (Gibbstown, NJ). Deionized water (18 MΩ-cm) was purified by a Barnstead Nanopure II Water System (Dubuque, IA). Chemicals used to synthesize L-SUCL, such as ω-undecylenyl alcohol, pyridine, triphosgene, L-leucine, dichloromethane, sodium bicarbonate, sodium hydroxide, hydrochloric acid, and ethyl acetate were purchased from Sigma-Aldrich (St. Louis, MO). Chemicals used to synthesize L,L-SULV such as undecylenic acid, *N*-hydroxysuccinimide, and *N,N'*-dicyclohexylcarbodiimide were also obtained from Sigma-Aldrich (St. Louis, MO). Tetrahydrofuran was obtained from Caledon Laboratories Ltd (Georgetown, ON, Canada). Isopropanol was purchased from Fisher Scientific (Fair Lawn, NJ). Leucine-valine and leucine was obtained from Bachem California Inc (Torrance, CA). All the chemicals have the purity of 98% or higher if not stated otherwise and were used as received.

2.2.2 Synthesis of poly-L-SUCL and poly-L-SULV

The surfactant monomers of L-SUCL and L,L-SULV were synthesized using the procedure developed by Rizvi et al. [21] and Wang et al. [17], respectively. The monomers were polymerized using a total dose of 20 Mrad of ^{60}Co radiation by Phoenix Memorial Laboratory (University of Michigan, Ann Arbor, MI).

2.2.3 Preparation of running buffer and analyte solutions

The background electrolyte (BGE) used in the running buffer was NH_4OAc at different concentrations. The pH of the buffer was adjusted as needed by NH_4OH or acetic acid. The buffer was then filtered by 0.45 μm PTFE syringe filter (Fisher Scientific, Pittsburgh, PA) and ultrasonicated for 15

min. Next, different amount of poly-L-SUCL and poly-L-SULV surfactant were added into the buffer. The molar concentration of the polymeric surfactants was calculated using the molecular weight of their respective monomers (referred to as equivalent monomer concentration, EMC). The final polymer surfactant containing running buffer was vortexed and ultrasonicated for another 15-20 min before use. Standard stock solutions of (±) BOH (1 mg/mL) and (±) BNP (1 mg/mL) were prepared in MeOH. Working solution containing a mixture of (±) BOH and (±) BNP were prepared by diluting the mixed standard stock solution with equal volume of H_2O to obtain the desired final concentration of 0.25 mg/mL of each binaphthyl compound.

2.2.4 MEKC-ESI-MS instrumentation

The MEKC-ESI-MS experiments were performed on an Agilent capillary electrophoresis system (Palo Alto, CA) interfaced to an Agilent 1100 series quadrupole mass spectrometer (Palo Alto, CA). Sheath liquid was delivered by an Agilent 1100 series HPLC pump with a 1:100 splitter. The Agilent 3D-CE/MSD ChemStation software (Rev. A.08.04) was used to control the instrument and analyze the raw data. The fused silica capillaries (50 μm i.d., 360 μm o.d.) with a total length of 60 cm (Polymicro Technologies, Phoenix, AZ) was used for the MEKC-MS experiments. New capillary was flushed with 1 M NH_4OH for 40 min followed by deionized water for 15 min before usage. Before each run, the capillary was rinsed with actual running buffer for 5 min as pre-conditioning. After each run, the capillary was flushed with water (1 min), NH_4OH (2 min) and water (2 min) as post-conditioning protocol. Positive voltage (varied according to experimental design) was applied for all the CE runs. Analytes were kept at 15 ºC temperature in the auto sampler and injected hydro-dynamically at the pressure of 5 mbar for 3 sec. Sheath liquid containing various proportions (20-50 v/v) of MeOH/H_2O and 5-40 mM NH_4OAc was delivered by an Agilent isocratic pump at 5 μL/min for all the experiments. MS detection was carried out in selected ion monitoring (SIM) mode for deprotonated molecular ion $[M-H]^-$. The following m/z was monitored as group SIM: 285 for (±) BOH and 347 for (±) BNP. Other MSD parameters were set as follows: fragmentor voltage, 90V; capillary voltage, 3000V; gain setting, 3.

2.2.5 Experimental design and data analysis

Experimental design and response surface methodology (RSM) data analysis were performed on Design-Expert (version 7.0.3, Stat-Ease, Inc. Minneapolis, MN) software. Six factors were chosen for the MEKC optimization: F_1: buffer pH, F_2: total concentration of polymeric surfactants ([poly-L-SUCL] + [poly-L,L-SULV]), F_3: concentration of NH_4OAc, F_4: voltage, F_5: temperature, F_6: nebulizer pressure. Three levels were set for each of the factors. The detailed values for each level are shown in Table 1, rows 1-6. Enantiomeric resolution and analysis time (measured as the migration time (t_m) of the last peak) were used as response (Table 2.2) for MEKC optimization. Central composite design (CCD) was used to design the experiment, which covers all the combinations of factors and provides most information about factorial interactions. Though this type of design requires more runs, we considered the 86 runs generated by the software to be necessary to obtain true and practical global optima. All the data obtained from the actual experiments were input into the Design-Expert software. After which the data was fit into quadratic model for the analysis of resolution and 2 factor interaction (2FI) model for the analysis time. Models were chosen based on F-test and lack of fit test. Critical factors were then screened out by analysis of variance (ANOVA). The 3-D surface plots were created by the software to show the interactions between significant factors. Finally, the optimum combination of all variables was generated by the software. To achieve a good trade-off between resolution and analysis time, maximum resolution for both analytes and minimum analysis time were set as experimental goals. The optimization of MS detection was performed by varying the sheath liquid composition and spray chamber parameters, respectively using the same methodology. Detailed designs of sheath liquid and spray chamber parameters are shown in Table 2.1, rows 7-12. Average peak area and signal to noise ratio (*S/N*) of the two enantiomers for both (±) BOH and (±) BNP are used as response (Table 2.2).

Table 2.1. Level of factors in the CCD used for the optimization of separation parameters, sheath liquid parameters, and spay chamber parameters in MEKC-MS

MEKC parameters						
Level	F_1: pH	F_2: [Surfactant] (mM)	F_3: [NH_4OAc] (mM)	F_4: Voltage (kV)	F_5: Temp. (ºC)	F_6: Neb. Pres. (psi)
-1	10.00	15.0	15.0	10	16.0	3
0	10.75	22.5	25.0	15	20.5	4
+1	11.50	30.0	35.0	20	25.0	5

Sheath liquid parameters				Spay chamber parameters		
Level	F_1: %MeOH (v/v)	F_2: pH	F_3: [NH_4OAc] (mM)	Level	F_1: DGF[a] (L/min)	F_2: DGT[b] (ºC)
-1	20	6.00	5.0	-1	4.0	150
0	50	7.25	22.5	0	5.0	200
+1	80	8.50	40.0	+1	6.0	250

[a] DGF: drying gas flow rate
[b] DGT: drying gas temperature

2.3 Results and discussion

Simultaneous separation and MS detection of binaphthyl derivatives (± BOH and ± BNP) were optimized by selecting the most important parameters of MEKC-ESI-MS in terms of resolution, analysis time, peak area, and *S/N* ratio. The first set of multivariate experiments was related to optimization of MEKC parameters (buffer pH, NH_4OAc concentration, EMC of polymeric surfactant, voltage, temperature, and nebulizer pressure). The second set of multivariate experiments was conducted by varying the sheath liquid parameters (MeOH/H_2O ratio, NH_4OAc concentration, pH). Finally, the spray chamber conditions (drying gas flow rate and drying gas temperature) were studied to achieve the highest possible sensitivity under optimum resolution.

2.3.1 Preliminary experiments

A sequential preliminary study was carried out before the multivariate DOE experiment. In this study, all the factors that could influence enantiomeric resolution and migration time of the two binaphthyl derivatives were optimized individually. There are two purposes for this study. First, to determine which factors are the most important ones for the enantioseparation. Second, to decide the range of all the factors to be further explored in CCD experiment. The buffer pH, NH_4OAc concentration,

surfactant concentration, ratio of the two types of polymeric surfactant in the mixed-micelle, voltage, temperature, organic modifier, and nebulizer pressure were chosen in this study. A fairly wide range for each factor was explored. The best enantioseparation condition was determined as follows: pH, 11.5; voltage, 15 kV; total surfactant (poly-L-SUCL and poly-L-SULV) concentration, 25 mM EMC; NH_4OAc concentration, 25 mM; temperature, 20 ºC; nebulizer pressure, 4 psi. Organic solvents (MeOH and ACN) was found to be ineffective to enantioselectivity. Thus, it was excluded from the multivariate experiments. The preliminary study suggested that poly-L-SUCL gives better separation for (±) BOH, but poly-L-SULV is better for (±) BNP. As a result, a mixture of both polymeric surfactants was utilized and set at 1:1 molar ratio for the multivariate experiments.

2.3.2 Multivariate approach

The six-factor, three-level full-factorial CCD to optimize MEKC parameters is summarized in Table 2.1(rows 1-6). To determine the three levels for each factor, we placed some of the aforementioned sequentially optimized values in the middle level i.e., level 0, and then a reasonable value was created both at the high and low levels (level +1 and -1). The effect of buffer pH, from 10.5-11.5 was investigated. The pH higher than 11.5 was not studied because it is difficult to adjust the pH of NH_4OAc buffer over pH 11.5. Buffer pH lower than 10.0 was not investigated because this pH range was found not good for the resolution of both analytes in preliminary studies. The concentration range of polymeric surfactant was also determined by the preliminary studies. Concentration lower than 15 mM EMC usually does not provide enough enantioresolution; while higher concentration (i.e., higher than 30 mM EMC) causes suppression of MS signal. The concentration of NH_4OAc used as BGE in the running buffer ranged from 15 mM to 35 mM. When the concentration of NH_4OAc was too low, the buffer strength and pH was not well maintained and the current was also unstable. On the other hand, too high of NH_4OAc concentration suppressed the MS signal. A voltage range of 10-20 kV was chosen to compromise between analysis time and Joule heating. For temperature, the lowest stable temperature our CE instrument could reach is 16 ºC, so we set the range from 16-25 ºC. As for the nebulizer pressure, it is found that the nebulizer pressure higher than 5 psi gives significant suction on the capillary, which

deteriorated enantiomeric resolution. On the other hand, nebulizer pressure lower than 2 psi causes current breakdown during MEKC run. Therefore, we chose nebulizer pressure over the 2-4 psi range.

The CCD design layout, which includes the combinations of all the factors at different levels in randomized order as well as the experimental and predicted responses are listed in Table 2.2. Chiral resolution for both enantiomers and the analysis time (i.e., t_m of the last eluting peak) were considered as quality responses. Among all 86 runs, 10 of them (experiment 6, 8, 9, 18, 42, 43, 47, 68, 78, 83) are repetitive runs of center points (meaning that all factors are at the mean values). The pure error from these replicates are compared with the excess design points (α= 1.565) in the F-test and lack of fit test in the ANOVA to screen out the most critical factors and evaluate the model [22]. As shown in Table 2.2, the experimental resolution varies from 0 to 1.24 for (±) BNP, 0.05 to 1.89 for (±) BOH, and t_m from 5.52 to 20.31 min. Fig. 2.2.1 shows two of the representative electropherograms obtained from the CCD experiments (i.e., experiments 58 and 35). The experiment 58 represents one of the worst results among all the experiments because it showed almost no chiral and achiral separation at all. However, experiment 35 demonstrates one of the best separations for both enantiomers.

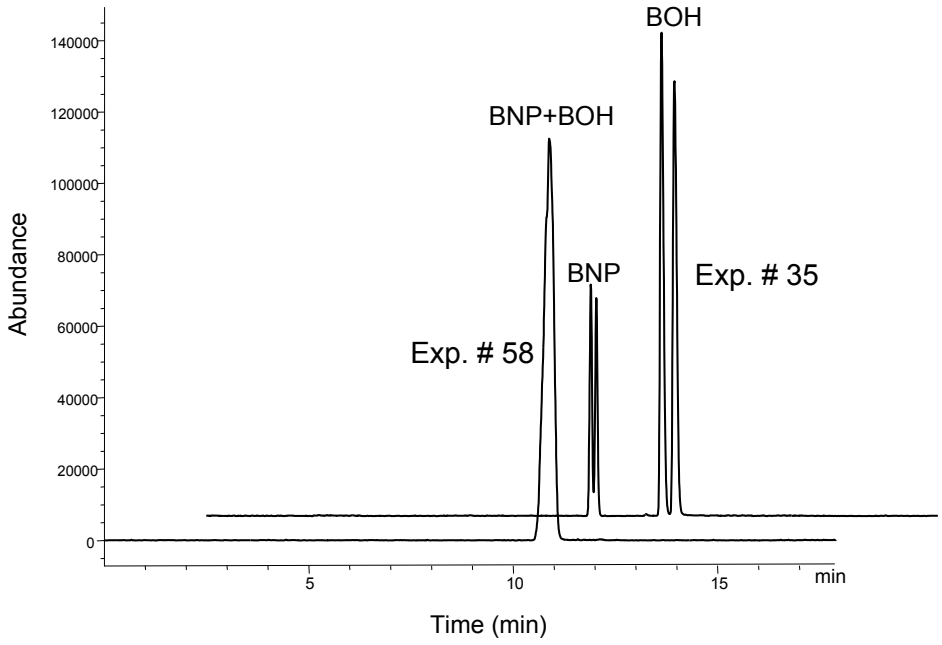

Figure 2.1. Comparison of the electropherograms of two selected runs obtained in experiment 35 and 58 of the MEKC condition optimization. Experimental conditions: 60 cm × 50 μm id fused silica capillary; poly-L-SUCL/ poly-L,L-SULV (1:1); injection: 5 mbar, 3 sec; sheath liquid: MeOH/H_2O (50:50, v/v), 5 mM NH_4OAc, delivered at a flow rate of 5 μL/min; spray chamber parameters: drying gas flow rate 5 L/min; drying gas temperature 200 ºC; capillary voltage 3000V; fragmentor 90, gain 3; monitored as group SIM at m/z = 285 and 347. CE separation conditions are shown in Table 2.2 (row 35 and 58).

The regression coefficients shown in Table 2.3 represent all of the terms in the predictive multifactor models calculated by the Design-Expert software. For quadratic regression model, the fitted equation is in the form of:

$$\hat{y} = b_0 + b_1F_1 + b_2F_2 + b_3F_3 + \cdots + b_{12}F_1F_2 + b_{13}F_1F_3 + b_{23}F_2F_3 + \cdots B_{11}F_1^{\,2} + B_{22}F_2^{\,2} + B_{33}F_3^{\,2} + \cdots \quad (1)$$

For 2FI model, the equation is:

$$\hat{y} = b_0 + b_1F_1 + b_2F_2 + b_3F_3 + \cdots + b_{12}F_1F_2 + b_{13}F_1F_3 + b_{23}F_2F_3 + \cdots \quad (2)$$

Where ŷ is the predicted experimental response; F_1, F_2, F_3…are the factors of interest; b_0 is the intercept coefficient; b_1, b_2, b_3, b_{12}, b_{13}, b_{23}, B_{11}, B_{22}, B_{33}…are the coefficients of all the terms in the model [23]. All the coefficients of the equations as well as their probability of having effect on the response (i.e., Prob>*F*) are summarized in Table 2.3. Positive coefficient value means the corresponding factor is directly proportional to the response, i.e., the bigger the factor, the bigger the response. Negative value means the factor is inversely proportional to the response, i.e., the bigger the factor, the smaller the response. Enantiomeric resolution for both (±) BNP and (±) BOH as well as t_m of the last eluting peak of the MEKC runs are considered as response in this table. If the Prob>*F* value for each single term is higher than 0.05, it indicates that the coefficient is not significantly different from zero. As a result, the corresponding factor is regarded as a non-critical factor. The absolute value of the coefficient exhibit the relative contribution of each term to the response, the bigger the value is, the higher impact it will have to the response. The coefficients of the second-order terms will not be discussed in the following sections because of their lack of chemical denotations.

The results of the ANOVA for all three response models used in MEKC optimization are tabulated in Table 2.3 (the last four rows of the table). R^2, adjusted R^2, predicted R^2, and *P*-lack of fit are all tests of the goodness of fit for the models. R^2 close to 1, the difference between adjusted R^2 and predicted R^2 being within 0.2, or *P*-lack of fit value bigger than 0.05 indicates a well fitted model. For the quadratic model of (±) BNP resolution, the *P*-Lack of Fit value is smaller than 0.05, but the R^2, adjusted R^2, and predicted R^2 are all in acceptable range. Therefore, the model is still considered valid. For the quadratic model of (±) BOH resolution, the difference between adjusted R^2 and predicted R^2 is bigger than 0.2, but the R^2 value is still in acceptable range and more importantly, the *P*-Lack of Fit value is much bigger than 0.05. This suggests the model still fits well. For the 2FI model of migration time, all the R^2 values are perfectly within the acceptable range and *P*-Lack of Fit value is also much bigger than 0.05, which indicates the model fit the experimental data very well. Thus, all three models in the optimization of MEKC parameters are tested fitted to the experimental data and are good enough to be used to identify the significant factors and predict optimum experimental conditions.

Table 2.2. Resolution and migration time data gathered from the CCD experiment for the optimizaion of separation parameters

Exp. #	Experimental parameters						Experimental/ Model predicted responses					
	pH	[Surfactant] (mM)	[NH_4OAc] (mM)	Voltage (kV)	Temp. (ºC)	Neb. Pres. (psi)	Resolution BNP		Resolution BOH		Migration time[c] (min)	
1	11.50	15.0	15.0	20	16.0	3	0.45	0.64	0.70	1.06	6.5	6.8
2	11.50	30.0	15.0	20	16.0	5	0.46	0.52	0.99	0.90	6.9	6.8
3	10.00	30.0	35.0	10	16.0	3	1.24	1.11	0.49	0.54	19.3	18.5
4	11.50	15.0	15.0	10	16.0	3	0.66	0.46	1.11	0.78	12.7	11.8
5	11.50	30.0	35.0	10	25.0	5	0.02	0.11	0.22	0.50	13.9	13.6
6	10.75	22.5	25.0	15	20.5	4	0.82	0.73	1.26	1.11	11.5	10.4
7	11.50	15.0	35.0	20	25.0	3	0.63	0.50	1.61	1.27	8.7	8.3
8	10.75	22.5	25.0	15	20.5	4	0.90	0.73	1.25	1.11	12.1	10.4
9	10.75	22.5	25.0	15	20.5	4	0.89	0.73	1.44	1.11	11.0	10.4
10	11.50	30.0	15.0	20	25.0	3	0.76	0.78	1.22	1.24	7.5	6.9
11	11.50	30.0	15.0	20	25.0	5	0.75	0.45	1.58	0.93	6.9	6.4
12	10.00	30.0	15.0	10	25.0	5	0.75	0.46	0.52	0.40	13.9	11.3
13	11.50	15.0	35.0	20	25.0	5	0.28	0.12	0.65	0.43	7.8	7.0
14	10.00	30.0	35.0	10	25.0	3	1.22	1.15	0.66	0.62	20.3	17.8
15	10.00	30.0	35.0	10	16.0	5	0.69	0.55	0.31	0.39	16.1	15.4
16	11.50	30.0	35.0	10	16.0	5	0.08	0.03	0.62	0.48	14.6	14.2
17	10.00	30.0	35.0	20	16.0	5	0.76	0.51	0.57	0.37	8.6	8.1
18	10.75	22.5	25.0	15	20.5	4	0.80	0.73	1.26	1.11	10.3	10.4
19	10.00	30.0	35.0	20	16.0	3	1.12	1.08	0.78	0.67	9.8	9.8
20	10.00	15.0	15.0	20	25.0	3	0.32	0.19	1.02	0.79	7.1	6.8
21	10.75	22.5	40.7	15	20.5	4	0.77	0.78	1.23	1.24	11.5	12.1
22	10.75	22.5	9.4	15	20.5	4	0.67	0.73	1.22	1.21	8.7	8.7
23	10.00	30.0	35.0	10	25.0	5	0.67	0.61	1.16	0.38	12.1	14.5
24	10.00	15.0	15.0	20	25.0	5	0.20	-0.02	0.25	0.28	5.7	5.9
25	11.50	30.0	15.0	10	25.0	3	0.68	0.62	1.15	0.89	12.1	12.5
26	10.75	10.8	25.0	15	20.5	4	0.32	0.41	1.22	0.96	8.4	9.4
27	10.00	15.0	15.0	10	25.0	5	0.01	0.18	0.36	0.26	9.6	9.6
28	10.00	30.0	15.0	20	16.0	5	0.36	0.48	0.39	0.41	6.8	7.2
29	10.00	15.0	35.0	10	16.0	3	0.68	0.80	0.65	0.87	15.1	16.2
30	10.00	30.0	15.0	20	25.0	3	0.74	0.68	0.73	0.59	7.7	7.4
31	11.50	15.0	35.0	10	25.0	5	0.07	-0.02	0.06	0.13	12.3	11.9
32	11.50	30.0	15.0	10	16.0	3	0.93	0.65	0.89	0.85	13.1	13.3
33	10.75	22.5	25.0	23	20.5	4	0.67	0.53	1.42	1.12	6.8	5.7
34	10.00	15.0	15.0	10	25.0	3	0.55	0.38	0.71	0.63	12.1	11.9
35	10.75	22.5	25.0	15	20.5	2	1.21	1.08	1.89	1.54	11.5	12.1
36	11.50	30.0	15.0	20	16.0	3	0.87	0.88	1.00	1.12	7.1	7.0
37	11.92	22.5	25.0	15	20.5	4	0.29	0.33	0.58	0.56	10.9	9.8
38	10.00	15.0	35.0	10	25.0	3	0.66	0.73	0.69	0.90	15.3	15.6
39	10.00	15.0	35.0	10	25.0	5	0.36	0.34	0.34	0.32	12.3	12.3
40	11.50	15.0	35.0	10	25.0	3	0.36	0.34	0.84	0.84	14.4	14.6
41	10.00	15.0	35.0	10	16.0	5	0.42	0.39	0.37	0.38	13.8	13.2
42	10.75	22.5	25.0	15	20.5	4	0.75	0.73	1.21	1.11	10.4	10.4
43	10.75	22.5	25.0	15	20.5	4	0.81	0.73	0.91	1.11	10.6	10.4

44	10.00	15.0	35.0	20	25.0	5	0.10	0.18	0.27	0.41	7.5	6.9
45	10.00	15.0	15.0	20	16.0	5	0.11	0.25	0.11	0.33	6.7	6.5
46	11.50	15.0	15.0	10	16.0	5	0.26	0.26	0.52	0.37	10.4	10.3
47	10.75	22.5	25.0	15	20.5	4	0.71	0.73	0.70	1.11	10.9	10.4
48	11.50	30.0	15.0	10	16.0	5	0.34	0.30	0.70	0.77	12.2	11.7
49	11.50	15.0	35.0	10	16.0	3	0.36	0.33	0.84	0.78	15.5	14.8
50	11.50	15.0	15.0	20	25.0	5	0.11	0.25	0.41	0.49	5.5	6.3
51	11.50	15.0	15.0	10	25.0	5	0.22	0.15	0.33	0.26	9.3	9.4
52	11.50	30.0	35.0	20	25.0	5	0.30	0.30	0.64	0.79	7.5	7.5
53	10.75	22.5	25.0	15	27.5	4	0.65	0.68	0.88	0.83	10.0	10.0
54	11.50	15.0	15.0	10	25.0	3	0.22	0.32	0.61	0.77	11.0	11.2
55	11.50	15.0	15.0	20	25.0	3	0.17	0.44	0.61	1.13	6.1	6.7
56	10.00	15.0	35.0	20	16.0	5	0.26	0.30	0.43	0.38	7.4	7.1
57	10.00	30.0	15.0	10	25.0	3	0.66	0.81	0.16	0.44	12.3	13.7
58	11.50	15.0	35.0	10	16.0	5	0.00	-0.05	0.05	0.16	11.0	12.4
59	11.50	15.0	35.0	20	16.0	5	0.00	0.15	0.38	0.37	6.7	6.9
60	11.50	30.0	15.0	10	25.0	5	0.02	0.30	0.38	0.72	9.9	10.7
61	10.00	30.0	15.0	10	16.0	5	0.47	0.56	0.52	0.49	11.3	12.6
62	10.00	15.0	15.0	10	16.0	3	0.53	0.60	0.56	0.68	12.7	12.9
63	11.50	30.0	35.0	10	16.0	3	0.02	0.50	0.90	0.76	16.1	16.7
64	10.00	30.0	15.0	20	16.0	3	0.81	0.86	0.56	0.50	8.2	7.9
65	10.00	30.0	15.0	10	16.0	3	0.83	0.93	0.36	0.44	14.2	14.8
66	10.00	15.0	15.0	10	16.0	5	0.51	0.38	0.51	0.40	11.1	10.8
67	11.50	15.0	15.0	20	16.0	5	0.70	0.43	0.56	0.51	5.8	6.6
68	10.75	22.5	25.0	15	20.5	4	0.68	0.73	0.99	1.11	9.6	10.4
69	11.50	30.0	35.0	20	16.0	3	0.94	0.77	0.89	1.10	8.0	8.6
70	10.00	30.0	15.0	20	25.0	5	0.28	0.31	0.13	0.41	6.1	6.5
71	10.00	30.0	35.0	20	25.0	5	0.33	0.50	0.15	0.46	7.2	7.8
72	10.75	34.2	25.0	15	20.5	4	0.82	0.80	0.78	1.05	10.1	11.3
73	11.50	30.0	35.0	20	16.0	5	0.10	0.22	0.70	0.67	7.5	7.5
74	10.75	22.5	25.0	15	20.5	6	0.16	0.33	0.40	0.75	8.4	8.7
75	10.00	15.0	15.0	20	16.0	3	0.56	0.48	0.92	0.75	7.8	7.2
76	10.00	15.0	35.0	20	25.0	3	0.54	0.58	1.01	1.12	8.0	8.7
77	10.75	22.5	25.0	15	16.0	4	0.65	0.77	0.84	0.97	10.4	10.6
78	10.75	22.5	25.0	15	20.5	4	0.64	0.73	1.00	1.11	9.4	10.4
79	9.58	22.5	25.0	15	20.5	4	0.57	0.60	0.20	0.22	10.1	10.9
80	11.50	30.0	35.0	20	25.0	3	0.76	0.82	1.25	1.30	8.3	8.9
81	11.50	15.0	35.0	20	16.0	3	0.54	0.55	0.96	1.13	8.1	8.0
82	10.00	30.0	35.0	20	25.0	3	0.85	1.05	0.64	0.84	9.8	9.7
83	10.75	22.5	25.0	15	20.5	4	0.73	0.73	1.10	1.11	10.3	10.4
84	10.75	22.5	25.0	7	20.5	4	0.27	0.47	0.54	0.84	16.1	15.1
85	11.50	30.0	35.0	10	25.0	3	0.86	0.62	0.92	0.88	16.0	16.3
86	10.00	15.0	35.0	20	16.0	3	0.83	0.72	1.10	1.00	8.6	8.7

[c] Migration time of the last peak

2.3.2.1 Evaluation of MEKC parameters on enantioseparation

The enantiomeric resolution for both analytes was evaluated. At least eight terms (F_1, F_2, F_6, F_1F_3, F_1F_4, F_3F_6, F_1^2, and F_4^2) are critical to (±) BNP; and six terms (F_1, F_4, F_6, F_1F_2, F_2F_6, and F_1^2) are significant to (±) BOH (Table 2.3). The buffer pH (F_1) and the nebulizer pressure (F_6) are both significant at the level of 0.05 for both (±) BNP and (±) BOH. Judging from the absolute values of each coefficient, it appears that nebulizer pressure has the most significant effect on the enantiomeric resolution, and as expected, the lower the nebulizer pressure, the high the resolution value. This is because that lower nebulizer pressure provides smaller suction force at the outlet end of the capillary, thus reduces the laminar flow, which in turn decreases the efficiency [24, 25]. Polymeric surfactant concentration (F_2) is significant to (±) BNP, and higher concentration of polymeric surfactant gives higher resolution. However, the resolution of (±) BOH is less sensitive to F_2 factor. This may be due to the fact that the range of surfactant concentration studied in this CCD experiment is outside the range where the enantiomeric resolution of (±) BOH is occurring. It is well documented that the chiral resolution is highly dependent on the concentration of polymeric surfactant [26]. Similar phenomenon was also observed in our preliminary studies, which showed that even very low concentration of poly-L-SUCL can provide baseline enantioseparation for (±) BOH and the enantiomeric resolution does not change much at higher surfactant concentrations. The running MEKC voltage (F_4) is significant to (±) BOH and higher voltage produces higher resolution. This might be due to the fact that high voltage generally results in higher efficiency. However, voltage influence on resolution is less noticeable on (±) BNP, probably because the shorter elution time of (±) BNP offsets the effect that the voltage has on efficiency.

The NH_4OAc concentration (F_3) and capillary temperature (F_5) are not significant to the enantioseparation of either analytes in Table 2.3. The insignificance of NH_4OAc concentration may be attributed to the fact that (±) BNP and (±) BOH are completely ionized as negatively charged species in the studied pH range. The electrostatic attractive interactions between the analytes and molecular micelles are relatively weak. Thus, the total ionic strength of the NH_4OAc buffer in the studied range has essentially no role in the MEKC process. Finally, with regard to temperature, usually lower temperature

gives better separation due to less peak broadening caused by Joule heating. Nevertheless, this parameter was poorly controlled during the whole experiment, because almost half the capillary length is actually outside the CE-MS instrument. This explains why temperature does not significantly affect enantiomeric separation.

Table 2.3. Regression coefficient of the coded factors and analysis of variance for the response surface models of chiral resolution (quadratic model) and migration time (2FI model) for the optimization of MEKC factors

Term	Resolution-BNP		Resolution -BOH		Migration time time[d]	
	Coefficient	Prob>*F* [e]	Coefficient	Prob>*F*	Coefficient	Prob>*F*
Intercept (b_0)	0.74		1.1		10.38	
F_1: pH	-0.085	< 0.0010	0.11	0.0010	-0.34	0.0022
F_2: [surfactant]	0.13	< 0.0010	0.028	0.38	0.60	< 0.0010
F_3: [NH_4OAc]	0.013	0.53	0.0087	0.78	1.10	< 0.0010
F_4: Voltage	0.019	0.37	0.088	0.0066	-2.9	< 0.0010
F_5: Temperature	-0.036	0.090	0.016	0.61	-0.24	0.029
F_6: Neb. Pres.	-0.19	< 0.0010	-0.20	< 0.0010	-0.86	< 0.0010
F_1 F_2	-0.035	0.10	0.078	0.020	-0.11	0.33
F_1 F_3	-0.083	< 0.0010	-0.048	0.15	-0.074	0.51
F_1 F_4	0.075	< 0.0010	0.052	0.12	0.14	0.20
F_1 F_5	0.022	0.30	0.0079	0.81	0.088	0.43
F_1 F_6	0.0061	0.78	-0.033	0.32	0.14	0.22
F_2 F_3	-0.0041	0.85	-0.021	0.51	0.10	0.37
F_2 F_4	0.012	0.57	-0.0032	0.92	-0.30	0.0098
F_2 F_5	0.027	0.22	0.013	0.69	-0.017	0.88
F_2 F_6	-0.038	0.080	0.083	0.013	-0.020	0.86
F_3 F_4	0.0094	0.66	0.017	0.60	-0.45	< 0.0010
F_3 F_5	0.037	0.089	0.020	0.55	0.093	0.41
F_3 F_6	-0.047	0.032	-0.051	0.12	-0.23	0.039
F_4 F_5	-0.017	0.43	0.022	0.50	0.14	0.20
F_4 F_6	-0.0032	0.88	-0.035	0.29	0.35	0.0027
F_5 F_6	0.0055	0.80	-0.021	0.51	-0.054	0.63
F_1^2	-0.11	0.020	-0.29	< 0.0010		
F_2^2	-0.053	0.26	-0.044	0.53		
F_3^2	0.0085	0.85	0.047	0.51		
F_4^2	-0.091	0.045	-0.050	0.46		
F_5^2	-0.00065	0.99	-0.12	0.15		
F_6^2	-0.0068	0.82	0.0094	0.84		
R^2	0.79		0.70		0.94	
Adjusted R^2 [f]	0.69		0.56		0.92	
Predicted R^2 [g]	0.51		0.95		0.89	
P-Lack of Fit	0.011		0.25		0.36	

[d] Migration time of the last peak.
[e] Probability of the null hypothesis being true (the factor has no significant effect on the response) based on the F-test for comparing model variance with residual variance. Any term with $P < 0.05$ is considered significant, and call for rejection of null hypothesis.

[f] Coefficient of determination adjusted for the number of terms in the model.
[g] A measure of the amount of variation around the mean explained by the model, Coefficient of determination is based on the predicted residuals from the model

In addition to the first order terms, three cross terms (F_1F_3, F_1F_4, F_3F_6) are found to be significant to the resolution of (±) BNP, and two (F_1F_2, F_2F_6) are found to be significant to (±) BOH. The significance of the cross terms indicates that the interactions between the corresponding factors are not negligible. For example, NH_4OAc concentration (F_3), as a single term, is not significant to the resolution of (±) BNP. However, it is significant as a cooperative factor when combined with buffer pH (F_1) and nebulizer pressure (F_6). Similarly, voltage (F_4) is not significant as a single term, but the combination of this factor with buffer pH (F_1) is significant. For the resolution of (±) BOH, polymeric surfactant concentration (F_2) is not significant as discussed above, while the product of this factor with buffer pH (F_1) and nebulizer pressure (F_6) are significant. Besides the cross terms, some of the squared terms are also significant to the responses (F_1^2, and F_4^2 is significant to the resolution of (±) BNP, F_1^2 is significant to (±) BNP). The significance of the squared terms suggests the curvature of the corresponding terms in the response surface plot.

Fig. 2.2 and Fig. 2.3 show the response surface plots of enantiomeric resolution vs. any two of the three critical factors for (±) BNP and (±) BOH, respectively. When the enantioresolution of (±) BNP is plotted vs. nebulizer pressure and pH, while all the other parameters are maintained at their mean levels the surface plot shows a steady downtrend slope along the nebulizer pressure axis (from 3 psi to 5 psi, Figure 2.2A). This indicates an inversely proportional relationship between the resolution and nebulizer pressure as discussed earlier. Across the pH axis, the plot shows a moderate curvature, with the top of the curvature at around pH 10.5. Thus, the highest point of this plot is a combination of nebulizer pressure 3 psi and pH 10.4. Fig. 2.2B shows the three dimensional graph representing the relationship of surfactant concentration and pH in the running buffer. A downtrend of the response surface can be seen when the EMC of surfactant decrease from 30 mM to 15 mM. Again, pH shows a stronger degree of curvature with the maximum resolution of (±) BNP at around 10.5 indicating pH is a crucial factor to the robustness of the method. The curvature of the whole plot turns to become flatter at the top region ([surfactant] at 30

mM EMC and pH around 10.5). This region appears to be the response optimal and the most robust zone. Fig. 2.2C represents the interaction between nebulizer pressure and polymeric surfactant concentration. The shape of the plot is planar. A strong incline in resolution of (±) BNP can be observed from highest nebulizer pressure and lowest polymeric surfactant concentration to lowest nebulizer pressure and highest polymeric surfactant concentration. Thus, the influence of EMC of polymeric surfactant on the resolution was only significant at a low nebulizer pressure. This trend once again proves the inverse and direct correlations of nebulizer pressure and polymeric surfactant concentration, respectively to the resolution of (±) BNP. To summarize, the use of 30 mM EMC of polymeric surfactant, pH 10.5 and nebulizer pressure of 3 psi is enough for achieving the maximum resolution of (±) BNP.

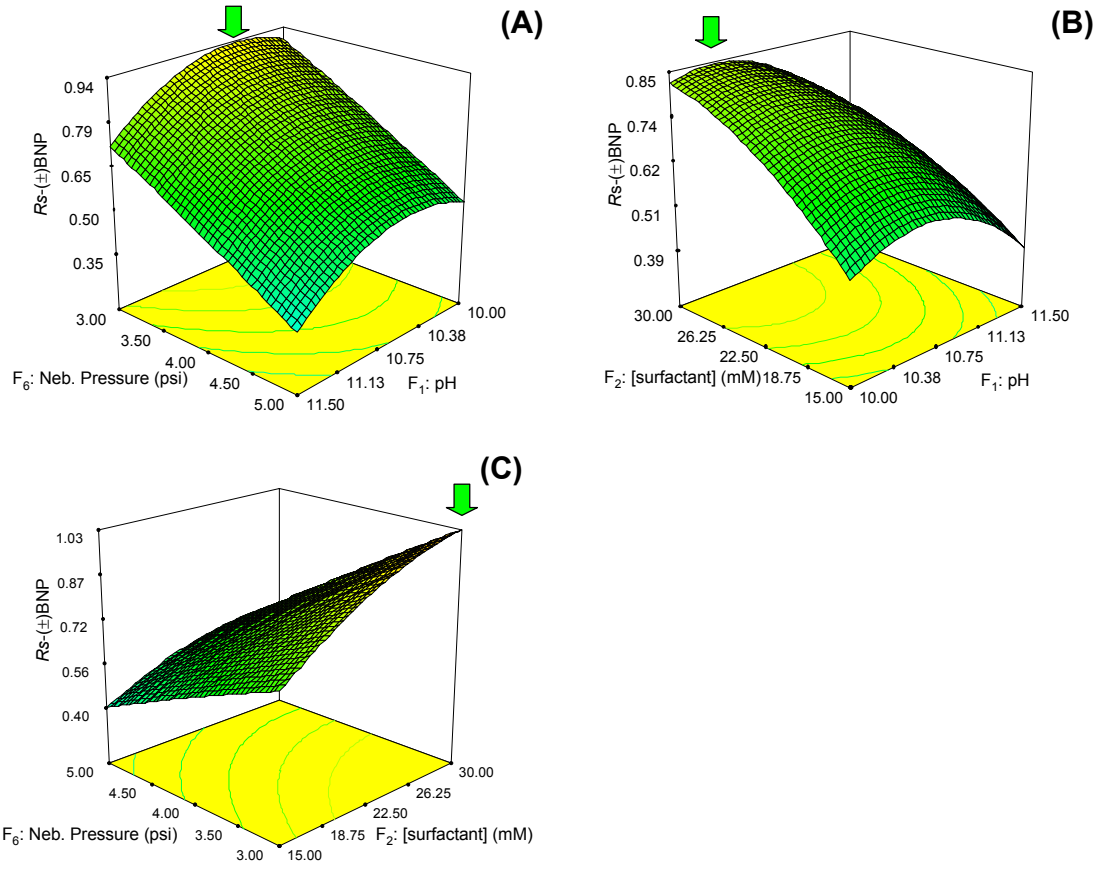

Figure 2.2. Response surface graphs for the enantiomeric resolution of (±)BNP involving the three most significant factors in separation optimization using CCD. Factor which is not analyzed in each plot is held at its mean value (i.e. level 0 in Table 2.1). Sheath liquid and spray chamber parameters are the same as those in Figure 2.1.

Fig. 2.3 shows another three surface plots with the enantioresolution of (±) BOH as response. Fig. 2.3A exhibits a very similar plot shape as shown in Fig. 2.2A (Note the pH axes are reversed between the two figures). In contrast to Figure 2.2A, the resolution of (±) BOH shown in Fig 2.3A increases only very slightly with the decreasing nebulizer pressure, but shows an upward sloping curvature along the pH axis. However, only this time the highest point of the curvature is around pH 10.9 Fig. 2.3B shows the relationship between voltage and pH. The surface plot again illustrates a curvature along pH axis and a moderate uptrend along voltage axis. The highest and flattest zone for the resolution of (±) BOH is when voltage is between 15-20 kV while pH is around 10.9. Note that the degree of the curvature along the pH axis is very signficant in this plot. This suggests a very critical role the pH plays in the enantioseparation process. Fig. 2.3C shows the resolution response surface of (±) BOH versus nebulizer pressure and voltage obtained when the other factors are held constant at their mean values. As can be observed, *Rs* of (±) BOH increased as the main factors (nebulizer pressure decreased and voltage) increased. As a result, the optimum *Rs* of (±) BOH in this plot can be obtained at a voltage 20 kV and a nebulizer pressure of 3 psi.

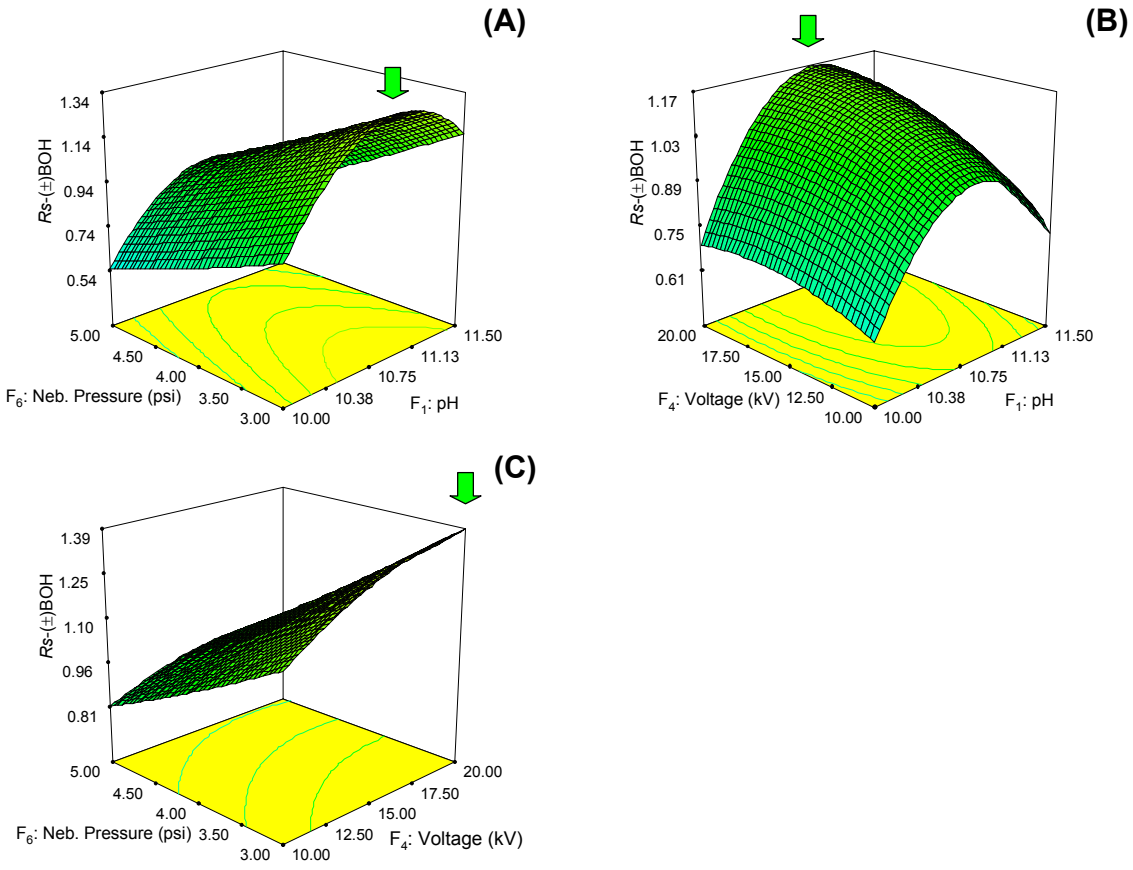

Figure 2.3. Response surface graphs for the enantiomeric resolution of (±)BOH involving the three most significant factors in separation optimization using CCD. Factor which is not analyzed in each plot is held at its mean value (i.e. level 0 in Table 2.1). Sheath liquid and spray chamber parameters are the same as those in Figure 2.1.

2.3.2.2 Evaluation of MEKC parameters on migration time

In addition to chiral *Rs*, analysis time (i.e., migration time of the last eluting enantiomer) was also studied as a possible response. As shown in Table 2.3, nine terms (F_1-F_6, F_2F_4, F_3F_4, and F_4F_6) are significant to the response. Among them, column temperature has the minimum effect as compared to other factors (i.e., Prob>*F* value is 0.029, which is the biggest among all the significant terms). This is probably because capillary temperature is not very well controlled in CE-MS as mentioned earlier. The buffer pH has an inverse effect on migration time. This is not surprising because higher pH of running buffer leads to faster electroosmotic flow (EOF), and thus shortens the run time. On the other hand, higher

polymeric surfactant concentration will retain the analytes more in the micellar phase. This trend is observed because both type of polymeric surfactants are negatively charged over the entire pH range studied and have the tendency to migrate opposite to the direction of the EOF, increasing the run time. With regard to the BGE concentration, running time was elongated by higher NH_4OAc concentration. This trend can be attributed to the fact that the high ionic strength introduced by high BGE concentration decreases electric double layer thickness and consequently the ζ potential declines, which decreases the EOF [9, 27]. Not surprisingly, the voltage is inversely proportional to the run time and has the biggest effect among all of the six factors. Finally, the nebulizer pressure also has a substantial effect on the migration time. As mentioned earlier, this could be due to the fact that higher nebulizer pressure produces higher negative pressure at the outlet end of the capillary and shortens the run time. In addition to the first order terms, three cross terms are found significant to the migration time (F_2F_4, F_3F_4, and F_4F_6), which indicates the importance of the interactive effects between the corresponding factors. Voltage (F_4), as the most significant single factor, also has the most interactions with other factors. The products of this factor with polymeric surfactant concentration (F_2), NH_4OAc concentration (F_3), and nebulizer pressure (F_6) are critical to the total migration time.

2.3.2.3 Evaluation of sheath liquid parameters

The composition of methanol (MeOH), pH, and NH_4OAc concentration were chosen as the three important factors for the sheath liquid optimization. The settings of the factors for sheath liquid optimization were determined from our earlier MEKC-MS studies [9]. A total of three factors were studied at three levels (Table 2.1, rows 7-12, columns 2-4), which resulted in experimental matrix consisting of 20 experiments (Table 2.4) with 6 replicate runs (labeled as experiment 3, 5, 7, 11, 12, and 18 in Table 2.4). The average peak area and *S/N* were chosen as experimental responses. Good repeatability is shown from the experimental responses for most of the replicate runs. The %RSD for the average peak area is 11.2% for (±) BNP and 10.6 for (±) BOH. When using *S/N* as response, the %RSD is 18.9% for (±) BNP and 11.9 for (±) BOH. This indicates that the errors of the experiment are acceptable.

Table 2.4. ANOVA table for models used in the optimization of MEKC, sheath liquid, and spray chamber parameters

Responses	Source	Sum of squares	Degrees of freedom	Mean square	*F*-ratio	Prob>*F*
		MEKC factors				
Resolution-BNP	Model	6.40	27	0.24	8.12	<0.0001
	Residual (error)	1.69	58	0.029		
	Corrected total	8.09	85			
Resolution-BOH	Model	9.07	27	0.34	4.97	<0.0001
	Residual (error)	3.92	58	0.068		
	Corrected total	12.98	85			
Migration time	Model	804.96	21	38.33	48.31	<0.0001
	Residual (error)	50.78	64	0.79		
	Corrected total	855.73	85			
		Sheath liquid parameters				
Peak area-BNP	Model	3.03×10^{10}	9	3.38×10^{9}	2.84	0.0597
	Residual (error)	1.19×10^{10}	10	1.19×10^{9}		
	Corrected total	4.22×10^{10}	19			
Peak area-BOH	Model	2.42×10^{11}	9	2.69×10^{10}	5.48	0.0069
	Residual (error)	4.90×10^{10}	10	4.90×10^{9}		
	Corrected total	2.91×10^{11}	19			
S/N-BNP	Model	5.46×10^{4}	9	6.07×10^{3}	2.91	0.0557
	Residual (error)	2.09×10^{4}	10	2.09×10^{3}		
	Corrected total	7.55×10^{4}	19			
S/N-BOH	Model	1.41×10^{6}	9	1.57×10^{5}	3.80	0.0245
	Residual (error)	4.13×10^{5}	10	4.13×10^{4}		
	Corrected total	1.82×10^{6}	19			
		Spray chamber parameters				
Peak area-BNP	Model	9.41×10^{8}	3	3.14×10^{8}	0.76	0.5423
	Residual (error)	3.70×10^{9}	9	4.11×10^{8}		
	Corrected total	4.64×10^{12}	12			
Peak area-BOH	Model	1.25×10^{10}	2	6.23×10^{9}	1.63	0.2443
	Residual (error)	3.83×10^{10}	10	3.83×10^{9}		
	Corrected total	5.08×10^{10}	12			
S/N-BNP	Model	47.69	5	9.54	1.62	0.2709
	Residual (error)	41.22	7	5.89		
	Corrected total	88.91	12			
S/N-BOH	Model	7.71×10^{2}	5	1.54×10^{2}	3.74	0.0575
	Residual (error)	2.89×10^{2}	7	41.25		
	Corrected total	1.06×10^{3}	12			

Table 2.5, rows 1-13 shows the coefficients of the quadratic models using both peak area and *S/N* of the two analytes as the responses. The NH_4OAc concentration was observed to be significant for both analytes when using peak area as response. This factor is inversely proportional to the response because NH_4OAc suppresses the ESI-MS signal at high concentration. The percentage of MeOH has a significant effect on peak area of (±) BOH only. However, both (±) BOH and (±) BNP provided higher *S/N* using higher percentage of MeOH in sheath liquid. Figure 2.4 (A) and (B) show the electropherograms of experiment 9 and 2 giving the worst and best *S/N* respectively. Note that the ammonium acetate concentration remains constant in both experiments. However, a high level of noise is observed in experiment 9 while an almost noise free baseline remains in experiment 2. The peak heights and *S/N* ratios of racemic mixtures of (±) BNP and (±) BOH are also clearly different.

Sheath liquid flow rate was not included in our optimization study. However, a recent research [28] showed that this factor could also be important to the MS response and even the nebulizer suction effect.

Table 2.5. Peak areas and *S/N* ratios from the CCD experiment for the optimization of sheath liquid parameters and spay chamber parameters

Sheath liquid parameters							
Exp. #	Experimental parameters			Experimental response			
	MeOH%	pH	[NH_4OAc]	Avg. Peak area		(S/N)$_{avg}$	
	(v/v)		(mM)	BNP	BOH	BNP	BOH
1	20	8.50	40.0	14427	99432	21	113
2	50	5.15	22.5	49152	290824	206	960
3	50	7.25	22.5	40602	241814	115	559
4	50	7.25	51.9	29718	223362	115	706
5	50	7.25	22.5	39097	232124	99	492
6	20	6.00	40.0	9252	67256	16	93
7	50	7.25	22.5	45068	298748	106	562
8	100	7.25	22.5	15281	222053	23	273
9	0	7.25	22.5	3478	10883	7	18
10	20	6.00	5.0	63326	177618	90	196
11	50	7.25	22.5	42950	275642	100	506
12	50	7.25	22.5	48909	272059	133	594
13	50	9.35	22.5	49445	296241	132	623
14	50	7.25	0.0	208453	242844	125	127
15	80	8.50	40.0	37082	307778	165	1092
16	20	8.50	5.0	59459	159065	93	211
17	80	6.00	5.0	11830	492208	178	596
18	50	7.25	22.5	52173	302398	156	678
19	80	6.00	40.0	38757	327795	139	913
20	80	8.50	5.0	139984	540163	247	749

Spay chamber parameters						
Exp. #	Experimental parameters		Experimental response			
	DGF	DGT	Avg. Peak area		(S/N)$_{avg}$	
	(L/min)	(ºC)	BNP	BOH	BNP	BOH
1	6.4	200	111512	400420	30	95
2	5.0	200	133235	427354	30	83
3	3.6	200	87505	293752	27	84
4	5.0	200	109555	366425	25	71
5	5.0	200	71654	269713	25	83
6	5.0	200	76124	276415	22	70
7	5.0	129	71120	226286	27	74
8	6.0	150	73594	246687	27	72
9	4.0	150	76428	325822	26	96
10	5.0	200	83234	276337	24	70
11	5.0	271	105381	377627	23	70
12	6.0	250	78936	283556	29	83
13	4.0	250	103499	388948	23	71

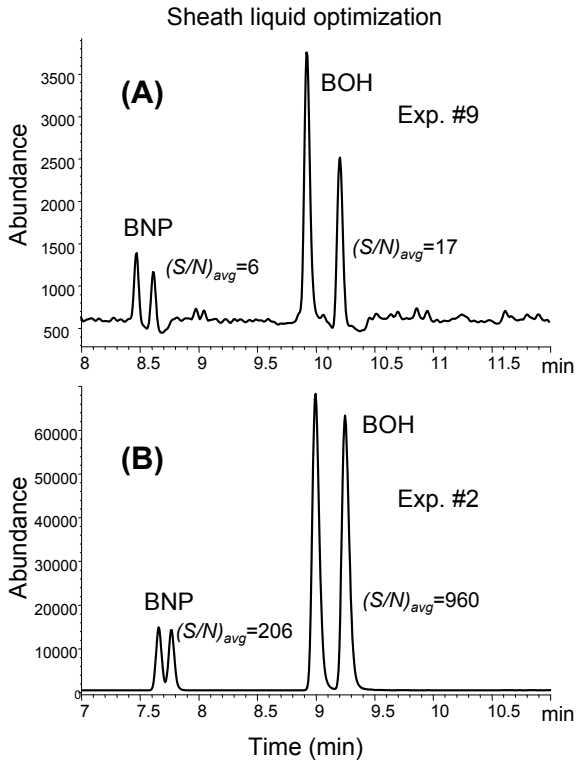

Figure 2.4. Comparison of S/N of MEKC-MS runs from the CCD experiments for the optimization of sheath liquid composition. Detailed sheath liquid and spray chamber conditions can be found in Table 2.4 (rows 9 & 2).

2.3.2.4 Spray chamber parameter optimization

Two factors, drying gas flow rate (DGF) and drying gas temperature (DGT), are included in the evaluation of spray chamber parameter at these levels using a CCD with 2^3 runs and five central points. The lower half of Table 2.4 shows the experimental matrix with thirteen runs generated by the software. Again, the repeatability of replicate runs (labeled as experiment 2, 4, 5, 6, and 10) is acceptable. The %RSD for the average *S/N* is 11.7% for (±) BNP and 9.2% for (±) BOH. The RSM model generated by the software indicates that neither factor has any significant influence on peak area or *S/N* of binaphthyl derivatives at the level of 0.05 (see Table 2.5, rows 14-20) under the selected experimental range.

Therefore, further optimization of drying gas temperature and drying gas flow rate was not performed and they were fixed at 250 ºC and 4 L/min, respectively.

2.3.2.5 ANOVA

The original ANOVA data (sum of squares, degree of freedom, mean square, *F*-ratio, and Prob>*F* value) for all the models used in MEKC, sheath liquid, and spray chamber experiment are listed in Table 2.6. In this ANOVA table, model sum of square and residual (error) sum of square for all the models were calculated first. The sum of square values were then divided by degree of freedom to get corresponding mean square values. In the end, *F*-ratio is calculated by model mean square divided by mean residual square. If these two mean squares are close to each other, i.e. *F*-ratio is close to 1, it suggests that the null hypothesis (none of the factors has significant effect on the response) is true. In addition, the Prob>*F* value (probability of the null hypothesis being true) should be bigger than 0.05. On the other hand, if Prob>*F* is equal or smaller than 0.05, at least one of the terms in the model is considered significant to the response. A close examination of Table 2.6 reveals that all three models used for the optimization of MEKC factors are significant (have at least one significant factor). All four models used in the sheath liquid study are either significant or very closed to significant (with the Prob>*F* value slightly bigger than 0.05). However, none of the models used for the spray chamber study is significant (except for the *S/N* of (±) BOH which is close to significant).

Table 2.6. Regression coefficient of the coded factors and analysis of variance for the response surface models of average peak area and *S/N* for the optimization of sheath liquid and spray chamber parameters.

Term	Peak area-BNP		Peak area-BOH		*S/N*-BNP		*S/N*-BOH	
	Coefficient	Prob>*F*	Coefficient	Prob>*F*	Coefficient	Prob>*F*	Coefficient	Prob>*F*
Sheath liquid parameters								
Intercept (b_o)	50157		261600		115.08		548.27	
F_1: %MeOH	7398	0.45	111300	0.00020	39.36	0.0097	231.88	0.0018
F_2: pH	9393	0.34	3710	0.85	-1.51	0.91	-14.65	0.80
F_3: [NH_4OAc]	-38087	0.0034	-51430	0.029	-24.65	0.092	108.84	0.094
F_1 F_2	15646	0.23	1789	0.94	10.81	0.52	37.14	0.62
F_1 F_3	2891	0.82	-28350	0.28	2.94	0.86	107.51	0.17
F_2 F_3	-15098	0.24	-2155	0.93	-5.14	0.76	3.74	0.96
F_1^2	-17514	0.082	-42167	0.045	-33.17	0.020	-132.74	0.032
F_2^2	-3401	0.71	20435	0.29	21.29	0.11	95.67	0.10
F_3^2	23716	0.050	13276	0.55	10.81	0.46	-35.48	0.58
R^2	0.72		0.83		0.72		0.77	
Adjusted R^2	0.47		0.68		0.48		0.57	
Predicted R^2	-0.90		-0.13		-0.96		-0.66	
P-Lack of Fit	<0.0010		0.010		0.024		0.0035	
Spray chamber parameters								
Intercept (b_0)	90906		3.1990×10^5		25.12		75.2	
F_1: DGF	819.32	0.91	-4209.4	0.85	1.41	0.14	0.310	0.89
F_2: DGT	10108	0.17	39253	0.10	-0.810	0.38	-2.60	0.29
F_1 F_2					1.33	0.31	8.88	0.028
F_1^2					1.61	0.12	7.14	0.022
F_2^2					-0.240	0.80	-1.64	0.52
R^2	0.18		0.25		0.54		0.73	
Adjusted R^2	0.013		0.095		0.21		0.53	
Predicted R^2	-0.19		-0.26		0.076		0.017	
P-Lack of Fit	0.92		0.72		0.95		0.56	

2.3.3 Final optimum conditions

In the MEKC optimization study, three models were generated to represent the *Rs* of (±) BNP, the *Rs* of (±) BOH, and migration time, respectively (see Table 2.3). Highest resolution for the two analytes and a shortest possible total analysis run time were set as criteria in the optimization. A desirability function calculated as the geometric mean of all transformed responses was generated in the form of:

$$D = (d_1 \times d_2 \times \ldots \times d_n)^{\frac{1}{n}} = \left(\prod_{i=1}^{n} d_i \right)^{\frac{1}{n}} \quad (3)$$

where d_i is the response (i.e. two resolutions and migration time in MEKC) to be optimized, n is the number (in our case, 3)of responses in the design. D is the desirability that ranges from 0 (the least

desirable) to 1 (the most desirable). The goal of the optimization is to find the maximum of the desirability function based on the given criteria. The whole process was conducted by the DOE software and the best conditions (a combination of factors with the highest possible D value) for MEKC separation was obtained as the optimum. Similar strategy was also used to predict the best conditions for sheath liquid and spray chamber, each has two models (the S/Ns for the two analytes). Therefore, the final overall optimum conditions are a combination of the three optimums from the three parts of the study (MEKC, sheath liquid, and spray chamber optimizations).

Finally, the aforementioned optimized prediction was validated experimentally by 20 replicate runs at the following optimum conditions (one of the representative electropherograms is shown in Figure 2.5). The best MEKC parameters are determined as following: F_1 (buffer pH): 10.8, F_2 (total concentration of polymeric surfactants): 27 mM EMC, F_3 (concentration of NH_4OAc): 35 mM, F_4 (voltage): +20 kV, F_5 (temperature): 22 ºC, F_6 (nebulizer pressure): 3 psi. Sheath liquid conditions are: MeOH/H_2O (80:20, v/v), 5 mM NH_4OAc, pH 8.5. Spray chamber: drying gas flow rate: 4 L/min; drying gas temperature: 250 ºC. The average enantiomeric resolutions are 1.26 and 1.53 for (±) BNP and (±) BOH, respectively which are are 26% and 4% different from the predicted values. The average migration time is 9.4 min which is 3% higher than the predicted value. The *S/N* ratios are also very close to the predicted values for both analytes as shown in the inset table of Figure 2.5. These results obtained from the response surface models are better than what we got from the sequential optimization experiment (data not shown).

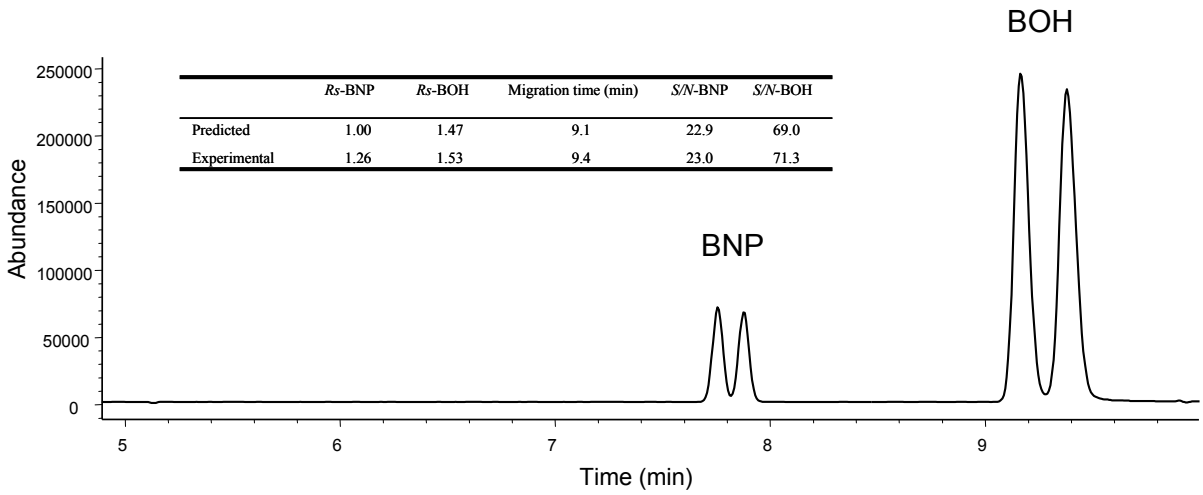

Figure 2.5. Experimental electropherogram of (±)BNP and (±)BOH under the final optimized MEKC-MS conditions: 35 mM NH_4OAc buffer, pH 10.8, 27 mM poly-L-SUCL/ ploy-L-SULV (1:1); sheath liquid: MeOH/H_2O (80:20, v/v), 5 mM NH_4OAc, pH 8.5, sheath liquid flow rate 5 μL/min; spray chamber: nebulizer pressure 3 psi, DGF 4 L/min, DGT 250 ºC. Other MEKC-MS conditions are the same as those in Figure 2.1.

2.4 Concluding remarks

This paper demonstrates the successful simultaneous optimization of two binaphthyl derivatives [(±) BOH and (±) BNP] by MEKC-ESI-MS methodology using a mixture of poly-L-SUCL and poly-L-SULV. Six-factor three level CCD experiments were carried out to optimize the MEKC conditions. Data of resolution and analysis time were fitted into models and coefficients of the each term were evaluated. Results showed that nebulizer pressure and pH are the two most significant factors to the enantioresolution of both (±) BNP and (±) BOH. Besides these two factors, polymeric surfactant concentration is significant to the enantioresolution of (±) BNP and voltage is significant to that of (±) BOH. As to analysis time, all six factors were determined to be significant. After the screening of the significant factors, the separation condition with best enantioseparation and shortest analysis time was determined from the model.

Similar strategies were applied to optimize the sheath liquid composition to get the highest *S/N* for both analytes. Three factors were examined and MeOH/H_2O ratio is found significant to the *S/N* of both analytes. Two factors (DGF and DGT) of the ESI spray chamber were optimized as well. None of

them were found significant within the range studied. The final optimized condition (including the optimum MEKC, sheath liquid, and spray chamber parameters) predicted from the desirability function was tested. The experimental data were in agreement to the predicted results. In this study, CCD experimental design was found to be an effective tool to analyze and optimize the parameters for MEKC-ESI-MS experiment. In our forthcoming studies, we will perform similar multivariate approach to optimize enantioseparation of other binaphthyl compounds in the positive ion mode.

References

[1] Korostylev, A.; Tararov, V. I. ; Fischer, C.; Monsees, A.; Börner, A.; *J. Org. Chem.* **2004**, 69 3220-3221.

[2] McCarthy, M.; Guiry, P. J. *Tetrahedron* **2001**, 57, 3809-3844.

[3] Bielejewska, A.; Duszczyk, K.; Kwaterczak, A.; Sybilska, D. *J. Chromatogr. A* **2002**, 997, 225-237.

[4] Nakamura, H.; Sano, A.; Sumii, H. *Anal. Sci.* **1998**, *14*, 375-378.

[5] Kamande, M. W.; Zhu, X.; Kapnissi-Christodoulou, C.; Warner, I. M. *Anal. Chem.* **2004**, 76, 6681-6692.

[6] Mohanty, A.; Dey, J. *J. Chromatogr. A* **2005**, *1070*, 185-192.

[7] Williams, A. A.; Fakayode, S. O.; Huang, X.; Warner, I. M. *Electrophoresis* **2006**, *27*, 4127-4140.

[8] Rizvi, S. A. A.; Simons, D. N.; Shamsi, S. A. *Electrophoresis* **2004**, *25*, 712-722.

[9] Hou, J.; Zheng, J.; Rizvi, S. A. A.; Shamsi, S. A. *Electrophoresis* **2007**, *28*, 1352-1363.

[10] Rizvi, S. A. A.; Zheng, J.; Apkarian, R. P.; Dublin, S. N.; Shamsi, S. A. *Anal. Chem.* **2007**, *79*, 879-898.

[11] Rizvi, S. A. A.; Shamsi, S. A. *Anal. Chem*. **2006**, *78*, 7061-7069.

[12] Hou, J.; Rizvi, S. A. A.; Zheng, J.; Shamsi, S. A. *Electrophoresis* **2006**, *27*, 1263-1275.

[13] Hou, J.; Rizvi, S. A. A.; Zheng, J.; Shamsi, S. A. *Electrophoresis* **2007**, *28*, 1426-1434.

[14] Shamsi, S. A. *Anal. Chem.* **2001**, *73*, 5103-5108.

[15] Himmelsbach, M.; Haunschmidt, M.; Buchberger, W.; Klampfl, C. W. *J. Chromatogr. A* **2007**, *1159*, 58-62.

[16] Schappler, J.; Guillarme, D.; Rudaz, S.; Veuthey, J. *Electrophoresis* **2008**, *29*, 11-19.

[17] Wang, J.; Warner, I. M. *Anal. Chem.* **1994**, *66*, 3773-3776.

[18] Agnew-Heard, K. A.; Peña, M. S.; Shamsi, S. A.; Warner, I. M. *Anal. Chem.* **1997**, *69*, 958-964.

[19] Hernández-Borges, J.; Rodríguez-Delgado, M. Á.; García-Montelongo, F. J.; Cifuentes, A. *Electrophoresis* **2004**, *25*, 2065-2076.

[20] Lara, F. J. ; García-Campaña, A. M.; Alés-Barrero, F.; Bosque-Sendra, J. M.; García-Ayuso, L. E. *Anal. Chem.* **2006**, *78*, 7665-7673.

[21] Rizvi, S. A. A.; Shamsi, S. A. *Electrophoresis* **2003**, *24*, 2514-2526.

[22] Anderson, M. J.; Whitcomb, P. J. DOE Simplified Practical Tools for Effective Experimentation, 2nd ed. Productivity Press, New York, **2007**, p. 152.

[23] Rudaz, S.; Cherkaoui, S.; Gauvrit, J.; Lantéri, P.; Veuthey, J. *Electrophoresis* **2001**, *22*, 3316-3326.

[24] Hou, J.; Zheng, J.; Shamsi, S. A. *J. Chromatogr. A* **2007**, *1159*, 208-216.

[25] Axén,J.; Axelsson, B.; Jörntén-Karlsson, M.; Petersson, P.; Sjöberg, P. J. R. *Electrophoresis* **2007**, *28*, 3207-3213.

[26] Billiot, E.; Macossay, J.; Thibodeaux, S.; Shamsi, S. A.; Warner, I. M., *Anal. Chem.* **1998**, *70*, 1375-1381.

[27] Cikalo, M. G.; Bartle, K. D.; Myers, P. *J. Chromatogr. A* **1999**, *836*, 35-51.

[28] Mokaddem, M.; Gareil, P.; Belgaied, J.; Varenne, A. *Electrophoresis* **2008**, *29*, 1957-1964.

Chapter 3

Multivariate Approach for the Enantioselective Analysis in Micellar Electrokinetic Chromatography- Mass Spectrometry: II. Optimization of 1,1'-Binaphthyl-2,2'-diamine in Positive Ion Mode

Enantiomeric separation and detection of 1,1'-binaphthyl-2,2'-diamine (BNA) has been successfully optimized by micellar electrokinetic chromatography coupled to electrospray ionization mass spectrometry (MEKC-ESI-MS) using a polymeric surfactant polysodium *N*-undecenoxycarbonyl-L-leucinate (poly-L-SUCL) as a pseudostationary phase. In the first step, MEKC conditions were optimized by a five-factor three-level central composite design (CCD) of experiment. All five MEKC factors (buffer pH, percentage of acetonitrile in the running buffer, concentration of surfactant, concentration of NH_4OAc, and voltage) were found significant to the responses (measured as the chiral resolution and analysis time). The interactions between MEKC factors were further evaluated using a quadratic model equation which allowed the generation of 3-D response surface image to reach the optimum conditions. To obtain the best signal to noise (*S/N*) ratio, sheath liquid composition and spray chamber parameters were successfully optimized using the same strategy. Baseline enantiomeric resolution in less than 20 min and optimum mass spectrometry signal of BNA enantiomers (*S/N* = 45 at 0.4 mg/mL) were ultimately achieved at the optimized conditions. The adequacy of the model was validated by experimental runs at the optimal predicted conditions. The predicted results were found to be in good agreement with the experimental data.

3.1 Introduction

Although the second dimension offered by the MS detection is very attractive choice to obtain molecular mass (m/z) and structural information of co-eluting analytes in HPLC or CE, separation is very critical for optical isomers with identical m/z. Micellar electrokinetic chromatography (MEKC) coupled to electrospray ionization mass spectrometry (ESI-MS) using molecular micelle has been increasingly used for chiral analysis since its first report in 2001 [1]. Molecular micelles (also known as polymeric surfactants) are typically formed via covalent bonds of the vinyl terminated surfactant monomers. Some of the properties of molecular micelles include zero critical micelle concentration, structural rigidity, and less competitive interactions between surfactant and other chiral selectors (e.g., cyclodextrins) in the running buffer [2, 3]. In addition, molecular micelles are very difficult to ionize under normal ESI-MS conditions, which makes them compatible with MS detection. Such capabilities of molecular micelles

consequently enhance the signal-to-noise ratio (*S/N*) and electrospray stability [2, 4-8] in MEKC-MS. Another practical advantage of molecular micelles includes compatibility with higher concentration of organic solvents in the running buffer [3, 9]. These aforementioned features of molecular micelle make MEKC-ESI-MS an effective hyphenation methodology for analysis of both chiral and achiral compounds. Several chiral molecular micelles derived from amino acids or small peptides head groups have been utilized in a univariate approach to optimize separation of various classes of enantiomers and employed in MEKC over the past decade [10-13]. However, the detector used in majority of chiral MEKC studies is a UV detector, which is inherently less sensitive than ESI-MS.

The multivariate statistical experimental designs may provide important benefits in the development of chiral MEKC-MS methods because they are considered superior to sequential design due to their ability to simultaneously screen all critical variables and determine their interactions with a relatively smaller number of experiments. In addition, they also provides a better global optimum condition [14]. The most commonly used multivariate method is a factorial design, which is useful in screening out the critical factors that could affect both separation and detection. However, the interactions among the various separation parameters or detection parameters are neglected in a factorial design. If these interactions are not negligible, more complex design (such as central composite, Box-Behnken, D-optimal, etc) should be used[14, 15]. Central composite design (CCD) is one of the most normally used higher order designs, which provides data for the fitting of a linear polynomial model to a set of data. The most critical points of this design are: (a) the combinations of the extreme values for all the factors within their ranges (often coded as -1 and +1 level); (b) axial points that are outside the original factor ranges (often coded as - α and +α level); (c) center point which inludes all factors at their mean values (coded as 0 level and are usually run multiple times to conduct lack of fit test). Quadratic response surface models are usually constructed from the CCD, based on which maximum or minimum values can be predicted [15-18]. The response in the case of chiral MEKC-MS can be resolution of the peak pair, migration times and signal-to-noise (*S/N*) of the two enantiomers.

As a further extension to our earlier works on the analysis of chiral compound using MEKC-MS, we present here the first report for the chiral MEKC separation and ESI-MS detection of 1,1'-binaphthyl-2,2'-diamine (BNA). The BNA is one of the 2,2'-substituted 1,1'-binaphthyl derivatives that have been extensively used as asymmetric ligands in the synthesis of chiral catalysts [19, 20]. Due to their highly stable chiral configuration, binaphthyl derivatives are also widely used as model test compound in chiral recognition [21, 22] as well as chiral separation [23-26]. A polymeric chiral surfactant polysodium *N*-undecenoxy carbonyl-L-leucinate (poly-L-SUCL) was chosen as a pseudostationary phase. A five-factor (acetonitrile (ACN) concentration, background electrolyte (BGE) concentration, poly-L-SUCL concentration, buffer pH, and voltage) full factorial CCD was carried out to obtain the actual (experimental) responses. The experimental MEKC responses for chiral resolution and migration time were compared to the predicted responses. Next, three factors (% methanol (MeOH), pH, and ammonium acetate (NH_4OAc) concentration) were considered in the sheath liquid condition optimization to predict the best possible *S/N* for the MS detection. The drying gas temperature (DGT) and drying gas flow rate (DGF) were studied using the same multivariate approach to evaluate the significance of spray chamber parameters. Finally, the adequacy of the developed MEKC-MS method was validated by experimental runs at the predicted conditions.

3.2 Materials and methods

3.2.1 Chemicals and reagents

The analyte (±) BNA was obtained from Aldrich (Milwaukee, WI). Both MeOH and ACN (HPLC grade), glacial acetic acid (99.7+% ACS reagent) were obtained from Caledon Laboratories Ltd (Georgetown, ON, Canada). A 7.5 M NH_4OAc aqueous solution was purchased from Sigma-Aldrich (St. Louis, MO). Ammonium hydroxide (NH_4OH, 28%-30% ammonia solution) was purchased from EM Science (Gibbstown, NJ). Triply deionized water (18.2 MΩcm) was generated in the laboratory using Barnstead Nanopure II Water System (Dubuque, IA). Chemicals used to synthesize L-SUCL such as ω-undecylenyl alcohol, pyridine, triphosgene, L-leucine, dichloromethane, sodium bicarbonate, sodium

hydroxide, hydrochloric acid, and ethyl acetate were purchased from Sigma-Aldrich (St. Louis, MO). All the chemicals have the purity of 98% or higher if not stated otherwise and were used as received.

3.2.2 Synthesis of poly-L-SUCL

The surfactant monomer of L-SUCL was synthesized using the procedure developed by Rizvi *et al.* [27]. The monomers were polymerized using a total dose of 20 Mrad of ^{60}Co radiation by Phoenix Memorial Laboratory (University of Michigan, Ann Arbor, MI).

3.2.3 Preparation of running buffer and analyte solutions

The BGE was NH_4OAc, which was prepared at different concentrations with different percentage of ACN. The pH of the NH_4OAc BGE was adjusted as needed by NH_4OH (1 M) or acetic acid (1 M). ACN was then added to this buffer to obtain the desired final NH_4OAc concentration. The buffer was then filtered by 0.45 μm PTFE syringe filter (Fisher Scientific, Pittsburgh, PA) and ultrasonicated for 15 min. Next, poly-L-SUCL surfactant was added into the buffer. The molar concentration of poly-L-SUCL was calculated using the molecular weight of its monomer and is expressed as equivalent monomer concentration (EMC). The final running buffer was vortexed and ultrasonicated for another 15-20 min before usage. Stock analyte solution of (±) BNA (1 mg/mL) was prepared in ACN and stored at 4 ºC. The working analyte solution was prepared by diluting the standard stock solution with deionized water to a final concentration of 0.40 mg/mL.

3.2.4 MEKC-ESI-MS instrumentation

An Agilent capillary electrophoresis system (3D-CE system, Palo Alto, CA) interfaced to an Agilent 1100 series quadrupole mass spectrometer (Palo Alto, CA) was used to carry out the MEKC-ESI-MS experiments. The sheath liquid was delivered using an Agilent 1100 series HPLC pump with a 1:100 splitter. The raw data was collected and analyzed by the Agilent 3D-CE/MSD ChemStation software (Rev. A.08.04). A 60 cm long fused silica capillary (50 μm i.d., 360 μm o.d., purchased from Polymicro Technologies, Phoenix, AZ) was used for the MEKC-MS experiments.

3.2.5 MEKC-ESI-MS conditions

A new capillary was flushed with 1 M NH_4OH for 40 min followed by deionized water for 15 min before usage. Prior to each run, the capillary was rinsed with actual running buffer for 5 min. After each run, the capillary was flushed with deionized water for 1 min, 1 M NH_4OH for 2 min, and deionized water for 2 min, respectively, as post-conditioning protocol. The column cassette temperature was set to 20ºC. Positive voltage was applied for all the CE runs (voltage varied according to experimental design) keeping the sprayer on ground potential. Analytes were kept at 15ºC temperature in the autosampler and injected hydrodynamically at the pressure of 5 mbar for 3 sec. The sheath liquid delivered at 5 μL/min was MeOH/H_2O in different ratios containing various concentration of NH_4OAc and pH. ESI-MS detection was carried out in the selected ion monitoring (SIM) mode for protonated molecular ion of BNA $[M+H]^+$ (m/z = 285). Other MS parameters were set as follows: nebulizer pressure, 2 psi; fragmentor voltage, 90 V; capillary voltage, +3 kV; gain setting, 3.

3.2.6 Experimental design and data analysis

The Design-Expert (version 7.0.3, Stat-Ease, Inc. Minneapolis, MN) software was employed to perform the experimental design and response surface methodology (RSM) data analysis. Five factors were chosen for the MEKC optimization: buffer pH (F_1), ACN percentage in running buffer (F_2), concentration of polymeric surfactant (F_3), concentration of NH_4OAc (F_4), and voltage (F_5). Three factors were chosen for sheath liquid optimization: MeOH percentage (F_1), pH (F_2), and NH_4OAc concentration (F_3). Two factors were chosen in spray chamber parameter optimization: DGF (F_1) and DGT (F_2). Three levels were set for each of the factors. The detailed values for each level are shown in Table 3.1. For the full factorial CCD, the α value, which is defined as the distance from the center of the design space to a star point, used in MEKC optimization was 2.38. For sheath liquid and spray chamber optimization, this value was 1.68 and 1.41, respectively. Nebulizer pressure was not studied in the MEKC optimization because its influence to enantiomeric resolution is very clear. That is, the higher the nebulizer pressure, the bigger the suction effect the nebulizer creates at the outlet end of the capillary, which increase the laminar flow in the capillary and consequently deteriorate the resolution and decrease the run time [28].

Therefore, throughout all the experiments, we simply kept the nebulizer pressure at 2 psi, which is the lowest level that could maintain a stable current. As to capillary cassette temperature, we found in the previous study that this factor is difficult to control in our instrument because about half of the capillary needs to be exposed to room temperature when interfacing to ESI chamber.

Table 3.1. Level of factors in the CCD used for the optimization of separation parameters, sheath liquid parameters, and spray chamber parameters in MEKC-MS of BNA

MEKC parameters					
Level	F_1: pH	F_2: %ACN	F_3: [poly-L-SUCL] (mM)	F_4: [NH_4OAc] (mM)	F_5: Voltage (kV)
-1	10.00	25	30.0	15.0	15
0	10.50	30	35.0	20.0	20
+1	11.00	35	40.0	25.0	25

Sheath liquid parameters			
Level	F_1: %MeOH (v/v)	F_2: pH	F_3: [NH_4OAc] (mM)
-1	20	6.00	5.0
0	50	7.25	22.5
+1	80	8.50	40.0

Spray chamber parameters		
Level	F_1: DGF[a] (L/min)	F_2: DGT[b] (ºC)
-1	4.0	150
0	5.0	200
+1	6.0	250

[a] DGF: drying gas flow rate
[b] DGT: drying gas temperature

Table 3.2 shows the detailed design and response (enantiomeric resolution and migration time measured as the elution time of the last peak) for all 50 runs generated by the CCD. The full factorial CCD covers all the combinations of factors at their ±1 levels and by comparing the errors of the repetitive center points with those of the ±α level, the significance of each factor is determined. Data of the experimental responses were input into the Design-Expert software and were fitted into different models for further analysis and optimization. Quadratic model was chosen for both responses of the MEKC optimization and linear and two-factor interaction (2FI) model were chosen for sheath liquid and spray chamber optimization. Models were then validated by the process of analysis of variance (ANOVA). The interactions between all significant factors were demonstrated by the 3-D RSM surface plots generated by the software. Finally, the optimum combination of all variables was calculated from the model. To guarantee baseline separation, maximum enantiomeric resolution was set as the only goal for the MEKC

condition optimization experiment. In sheath liquid composition and spray chamber parameters study, maximizing the *S/N* was chosen as the goal of the optimization.

Table 3.2. Resolution and migration time data gathered from the CCD experiment and model predicted responses of BNA enatiomers

Exp. #	Experimental parameters					Experimental/ Model predicted responses			
	pH	%ACN	[poly-L-SUCL] (mM)	[NH_4OAc] (mM)	Voltage (kV)	Resolution		Migration time[c] (min)	
1	11.00	35	40.0	25.0	25	0.36	0.42	7.8	8.6
2	10.50	30	35.0	20.0	20	0.89	0.85	10.0	10.3
3	10.00	25	30.0	15.0	25	0.66	0.59	7.1	7.5
4	11.00	35	40.0	15.0	25	0.44	0.40	7.3	7.8
5	10.00	25	30.0	25.0	25	0.81	0.78	7.8	8.0
6	10.00	35	40.0	25.0	25	0.51	0.35	7.4	8.4
7	11.00	35	40.0	15.0	15	0.72	0.72	13.1	13.8
8	11.69	30	35.0	20.0	20	0.89	0.89	10.3	10.6
9	10.50	30	35.0	20.0	20	0.97	0.85	10.0	10.3
10	10.50	30	35.0	20.0	20	0.96	0.85	10.2	10.3
11	11.00	35	30.0	15.0	25	0.36	0.26	6.9	7.3
12	11.00	35	30.0	25.0	25	0.05	0.19	6.6	7.6
13	11.00	25	30.0	25.0	15	1.36	1.23	14.9	15.1
14	11.00	25	30.0	25.0	25	0.89	0.82	7.8	8.3
15	10.00	25	30.0	15.0	15	1.19	1.05	12.5	13.0
16	10.00	35	30.0	25.0	15	0.48	0.47	11.6	12.6
17	10.50	30	35.0	20.0	20	0.84	0.85	9.5	10.3
18	10.50	30	35.0	20.0	30	0.33	0.23	5.5	7.3
19	10.50	30	35.0	20.0	20	0.73	0.85	9.0	10.3
20	11.00	25	40.0	25.0	25	0.98	0.96	8.7	8.8
21	11.00	35	40.0	25.0	15	0.69	0.73	14.6	15.2
22	10.00	35	40.0	15.0	25	0.12	0.23	6.9	7.3
23	10.00	35	30.0	25.0	25	0.11	0.13	6.8	7.4
24	10.50	30	35.0	31.9	20	0.80	0.84	10.8	11.0
25	10.00	35	40.0	25.0	15	0.74	0.69	14.8	14.5
26	10.50	30	35.0	20.0	20	0.81	0.85	10.1	10.3
27	11.00	25	30.0	15.0	15	1.03	1.16	13.7	14.2
28	10.50	30	35.0	20.0	20	0.84	0.85	10.2	10.3
29	9.31	30	35.0	20.0	20	0.62	0.67	8.4	9.0
30	10.50	30	35.0	20.0	8	0.86	0.97	22.6	21.9
31	11.00	25	40.0	25.0	15	1.42	1.38	15.4	16.5
32	10.50	30	35.0	8.1	20	0.61	0.61	8.0	8.7
33	10.00	25	40.0	15.0	15	1.16	1.09	13.7	14.0
34	10.00	35	40.0	15.0	15	0.60	0.58	11.5	12.7
35	10.00	25	30.0	25.0	15	1.19	1.22	13.3	14.2
36	11.00	35	30.0	25.0	15	0.59	0.50	12.7	13.4
37	10.00	35	30.0	15.0	15	0.49	0.45	11.0	11.2
38	10.50	42	35.0	20.0	20	0.04	-0.04	8.7	9.6

39	10.50	30	23.1	20.0	20	0.63	0.64	8.6	8.8
40	11.00	35	30.0	15.0	15	0.59	0.58	11.7	12.4
41	10.50	18	35.0	20.0	20	1.20	1.32	11.9	12.0
42	11.00	25	40.0	15.0	15	1.35	1.22	14.9	15.1
43	10.00	25	40.0	15.0	25	0.66	0.64	7.3	7.6
44	10.00	35	30.0	15.0	25	0.03	0.10	5.8	6.7
45	11.00	25	40.0	15.0	25	0.79	0.80	7.6	8.2
46	10.00	25	40.0	25.0	25	0.88	0.91	7.7	8.6
47	10.50	30	46.9	20.0	20	0.93	0.96	10.4	11.1
48	11.00	25	30.0	15.0	25	0.69	0.74	7.1	8.2
49	10.50	30	35.0	20.0	20	0.77	0.85	9.4	10.3
50	10.00	25	40.0	25.0	15	1.38	1.35	15.3	15.7

[c] Migration time of the last peak of BNA.

3.3 Results and discussion

To achieve the optimum MEKC-ESI-MS separation (best enantioseparation and highest *S/N* for the analyte) three sets of experiments were carried out. First, the multivariate CCD optimization of MEKC condition including five factors (buffer pH, ACN percentage in running buffer, concentration of surfactant, concentration of NH_4OAc, and voltage) were chosen and tested at these levels in a CCD design. The second set of experiments involved the optimization of sheath liquid parameters. Three factors were considered: MeOH/H_2O ratio, NH_4OAc concentration, and pH. The third set of experiments was carried out to optimize the spray chamber condition, which includes drying gas flow rate and drying gas temperature.

3.3.1 Preliminary experiments

Before using the multivariate CCD experiment for the optimization of MEKC conditions, a series of preliminary sequential studies on all the factors that could affect the MEKC separation were performed to determine the most important factors which need to be further optimized using multivariate experiments. In addition, their range (i.e. the levels) required for later experiments was also determined. A fairly wide range was explored for the following factors: the buffer pH, NH_4OAc concentration, surfactant concentration, voltage, temperature, organic modifier (MeOH and ACN), and nebulizer pressure. In contrast to our previous studies on negatively charged binaphthyl derivatives (i.e. 1,1′-bi-2-naphthol (BOH) and 1,1′-binaphthyl-2,2′-diyl-hydrogen-phosphate (BNP)) [29], the use of ACN was found

to be very effective for enantioselectivity of positively charged BNA. The optimum conditions determined by univariate approach for enantioseparation of BNA were as follows: pH 10.5, 35 mM poly-L-SUCL, 20 mM NH_4OAc, 20% (v/v) ACN, voltage +20 kV, and nebulizer pressure 2 psi. A brief preliminary study was also carried out to evaluate and determine the range of sheath liquid (%MeOH: 20-80% (v/v), pH: 6.00-8.50, and [NH_4OAc]: 5-40 mM) and spray chamber (drying gas flow rate: 4-6 L/min and drying gas temperature: 150-250 ºC) conditions.

3.3.2 Multivariate approach

Table 3.1 shows the detailed design levels for all five factors to be studied in MEKC optimization. Level 0 of each factor was determined based on the optimum value from the preliminary study. Next, a reasonable value was created both at the high and low levels (level +1 and -1). The detailed justifications for the selected range can be found in our recent MEKC-MS studies on (±) BNP and (±) BOH [29].

The design matrix including both experimental and model predicted responses of the CCD for MEKC optimization are presented in Table 3.2. Chiral resolution for (±) BNA and the retention time of the last eluting peak were considered as quality responses. A total of 50 experiments were carried out according to the CCD, 8 of which (experiment 2, 9, 10, 17, 19, 26, 28, and 49) are repetitive runs with all the factors at their mean values. The errors of these repetitive runs were compared with the excess design points by *F*-test to determine the significance of the critical factors [14] (data not shown). As shown in Table 3.2, enantiomeric resolution varies from 0.03 to 1.42 and analysis time from 5.8 to 22.6 min.

Shown in Table 3.3 are all the coefficients for the terms of the predicted multifactor models calculated by the Design-Expert software. These coefficients represent the influence of the corresponding factor to the final response. For example, positive coefficient means the factor is directly proportional to the response and vice versa. Enantiomeric resolution and analysis time (i.e. retention of the last eluted enantiomer) are both considered as response in this table. The probabilities of each term having no effect on the response (i.e., Prob>*F*) are also summarized in Table 3.3. A coefficient is not considered significantly different to zero if its Prob>*F* value is bigger than 0.05, and the corresponding factor is

regarded as non-critical. Other results of ANOVA such as R^2, adjusted R^2, predicted R^2 and Q^2 are tabulated in Table 3.3 (the last four rows). These values are all close to 1, suggesting a very good fitness for both models.

Table 3.3. Regression coefficient of the coded factors and analysis of variance for the response surface models of chiral resolution and migration time (quadratic model) for the optimization of MEKC factors for BNA

Term	Resolution		Migration time[c]	
	Coefficient	Prob>*F* [d]	Coefficient	Prob>*F*
Intercept	0.86		9.7	
F_1: pH	0.046	0.049	0.34	0.0001
F_2: ACN%	-0.28	< 0.0001	-0.60	< 0.0001
F_3: [surfactant]	0.070	< 0.0001	0.48	< 0.0001
F_4: [NH_4OAc]	0.046	0.0046	0.50	< 0.0001
F_5: Voltage	-0.19	< 0.0001	-3.2	< 0.0001
$F_1 F_2$	0.0044	0.80	-0.018	0.84
$F_1 F_3$	0.0031	0.86	-0.021	0.82
$F_1 F_4$	-0.025	0.16	-0.089	0.33
$F_1 F_5$	0.0072	0.68	-0.14	0.14
$F_2 F_3$	0.021	0.24	0.12	0.18
$F_2 F_4$	-0.038	0.041	0.033	0.71
$F_2 F_5$	0.026	0.15	0.22	0.019
$F_3 F_4$	0.022	0.22	0.12	0.18
$F_3 F_5$	0.00063	0.97	-0.23	0.018
$F_4 F_5$	0.0034	0.85	-0.17	0.065
F_1^2	-0.013	0.32	-0.085	0.22
F_2^2	-0.038	0.0082	0.085	0.22
F_3^2	-0.0089	0.51	-0.056	0.42
F_4^2	-0.023	0.10	-0.078	0.26
F_5^2	-0.059	0.0005	0.78	< 0.0001
R^2	0.95		0.99	
Adjusted R^2 [e]	0.92		0.98	
Predicted R^2 [f]	0.84		0.95	
Q^2	0.95		0.96	

[c] Migration time of the last peak.
[d] Probability of the null hypothesis being true (the factor has no significant effect on the response) based on the F-test for comparing model variance with residual variance. Any term with $P < 0.05$ is considered significant, and call for rejection of null hypothesis.
[e] Coefficient of determination adjusted for the number of terms in the model.
[f] A measure of the amount of variation around the mean explained by the model, coefficient of determination is based on the predicted residuals from the model.

3.3.2.1 Model validation

Models obtained from the CCD experiment were further validated by ANOVA as shown in Table 3.4. Each model was first tested by lack of fit using the ANOVA results shown in the fourth and ninth row of Table 3.4. The *F* value for lack of fit test was calculated by the mean square of lack of fit divided by the mean square of pure error. As shown in Table 3.4, the *F* values are 1.4 and 1.5 for chiral resolution and migration time, respectively. Both are smaller than the tabulated value at the 95% confidence level. The probability of the null hypothesis being true (i.e., the difference between lack of fit and pure error is caused by random error) is 0.33 and 0.31 for both responses. Thus, we can not reject the null hypothesis and there is no evidence of lack of fit at 95% level for both models. Further tests for the significance of the models were carried out by calculating the model *F* value as shown in the second and seventh row of Table 3.4. The *F* values were calculated as the mean square of the model divided by the mean square of residual. The results are 30 and 100, respectively, and the Prob>*F* values are <0.0001 for both models, which indicate that there is at least one significant factor for each model.

Table 3.4. ANOVA table for models used in the optimization of MEKC parameters

Responses	Source	Sum of squares	Degrees of freedom	Mean square	*F*-ratio	Prob>*F*
Resolution	Model	5.7	20	2.9×10^{-1}	30	<0.0001
	Residual	2.8×10^{-1}	29	9.7×10^{-3}		
	Lack of fit	2.3×10^{-1}	22	1.0×10^{-2}	1.4	0.33
	Pure error	5.2×10^{-2}	7	7.4×10^{-3}		
	Corrected total	6.0	49			
Migration time	Model	5.3×10^{2}	20	27	1.0×10^{2}	<0.0001
	Residual	7.6	29	2.6×10^{-1}		
	Lack of fit	6.2	22	2.8×10^{-1}	1.5	0.31
	Pure error	1.3	7	1.9×10^{-1}		
	Corrected total	5.3×10^{2}	49			

3.3.2.2 Evaluation of MEKC parameters on enantioseparation and migration time

As is shown in Table 3.3, eight terms in the quadratic model for the chiral resolution are significant at the level of 0.05 (F_1-F_5, F_2F_4 and F_5^2) with Prob>*F* values less than 0.05. Interestingly, only %ACN when combined with voltage has some interactive effect (Prob>*F* = 0.041). Among them, buffer pH (F_1), surfactant concentration (F_3), and BGE concentration (F_4) are directly related to the response due

to positive coefficients. The coefficient of surfactant concentration is the highest, which means this factor has the biggest effect on the response. This suggests that high concentration of surfactant provides more chiral binding sites and thus enhance the chiral interaction between the analyte and molecular micelles. Voltage (F_5) and the %ACN (F_2) are inversely related to the resolution in this model due to negative coefficients. Higher voltage decreases the retention time and does not give the analyte enough time to interact with the polymeric surfactant. The addition of ACN might change the micellar structure and intervene the interaction between the micelle and the analyte [30, 31]. This might be able to explain its negative effect on the resolution.

Figure 3.1 shows how the response of resolution changes in accordance with any two factors and the relationship between them. Fig. 3.1 (A) is a three dimensional view of response surface plot which shows the impact of the combination of pH and %ACN. The plot indicates that pH is positively correlated to the response (i.e. resolution), while %ACN is inversely correlated. This comparison suggests that the %ACN has a bigger effect as the slope of the surface plot along the %ACN axis is bigger than that of pH axis. The best resolution is obtained when both factors are at their extremes (i.e., the highest for pH and the lowest for %ACN). Fig. 3.1 (B) shows the combination of [NH_4OAc] and pH. The surface plot goes from the point where both factors are at their lowest value (pH 10.00 and 15.00 mM NH_4OAc, respectively) to its maximum when both factors are at their highest value (pH 11.00 and 25.00 mM NH_4OAc, respectively). Note that the plot is pretty steep at lower pH and lower NH_4OAc concentration, which means that the response is very sensitive to the change of the two factors in this region. However, the top region of the plot is fairly flat, indicating a comparably robust zone at the combination of higher pH and higher NH_4OAc concentration. The plot shown in Fig. 3.1 (C) is a fairly planar plot almost goes straight up from the corner of low [poly-L-SUCL] and low pH to the corner of high [poly-L-SUCL] and high pH. This plot is in accordance with the direct relationship of the response and the two factors. In addition, the slope of the surface is bigger along [poly-L-SUCL] axis than pH axis, suggesting that the effect of surfactant concentration is bigger than that of pH. In Fig. 3.1 (D), pH still shows the same trend

as shown in Fig. 3.1 (A) while voltage has a bigger (yet negative) effect to the response. The highest resolution in this plot occurs at the combination of the highest pH and lowest voltage.

The interaction of ACN when combined with either poly-L-SUCL, NH_4OAc or voltage allowed the generation of response surface images shown in Figs. 1 (E-G). Fig. 3.1 (E) displays the relationship between [poly-L-SUCL] and %ACN. At the combination of the highest [poly-L-SUCL] and lowest %ACN, the plot reaches its peak. In this figure, %ACN shows bigger effect than [poly-SUCL] because the plot is steeper along the %ACN axis. This is not surprising since the absolute value of coefficient for %ACN is bigger than that of [poly-SUCL] (0.28 vs. 0.070 as shown in Table 3.3) in the model. Fig. 3.1 (F) shows a similar resolution trend for the interactive effects between [NH_4OAc] and %ACN as Fig. 3.1 (E). The highest resolution is reached at the highest [NH_4OAc] and lowest %ACN. The effect of %ACN is again much bigger than that of [NH_4OAc]. In Fig. 3.1 (G), the plot suggests that the two interactive factors (voltage and %ACN) are inversely correlated to the response and the maximum resolution is achieve at the minimums of the two factors.

Figs. 3.1 (H-I) illustrates the interaction between voltage vs. [NH_4OAc] or [poly-L-SUCL]. As suggested in the plot, voltage is inversely related to the response while [NH_4OAc] or [poly-L-SUCL] is positively related. Again, voltage has a much bigger effect (similar to the plot shown in Fig. 3.1D) because the slope is much steeper along the voltage axis. Finally, Fig. 3.1 (J) shows the relationship of the two positive factors: [NH_4OAc] and [poly-L-SUCL]. As indicated in the plot, both factors have very comparable effect and provide the highest response at their highest values.

The coefficients of the migration time listed in Table 3.3 shows that 8 terms (F_1-F_5, F_3F_5, F_2F_5, and F_5^2) in the quadratic model are significant to the response. The factors such as buffer pH (F_1), surfactant concentration (F_3), and NH_4OAc concentration (F_4) have positive coefficients suggesting increasing migration time upon increasing any of these factors. On the other hand, voltage (F_5) and %ACN (F_2) are inversely related to the migration time as evident by the negative coefficients. Higher concentration of surfactant retains the analyte more in the micellar phase and hence would increase the elution time. Increasing NH_4OAc concentration causes higher ionic strength of the running buffer as well

as thinner electric double layer, consequently decreasing the EOF [8, 32]. In particular, note that the voltage has the biggest effect on the migration time among all factors (i.e., has the highest absolute value of coefficient).

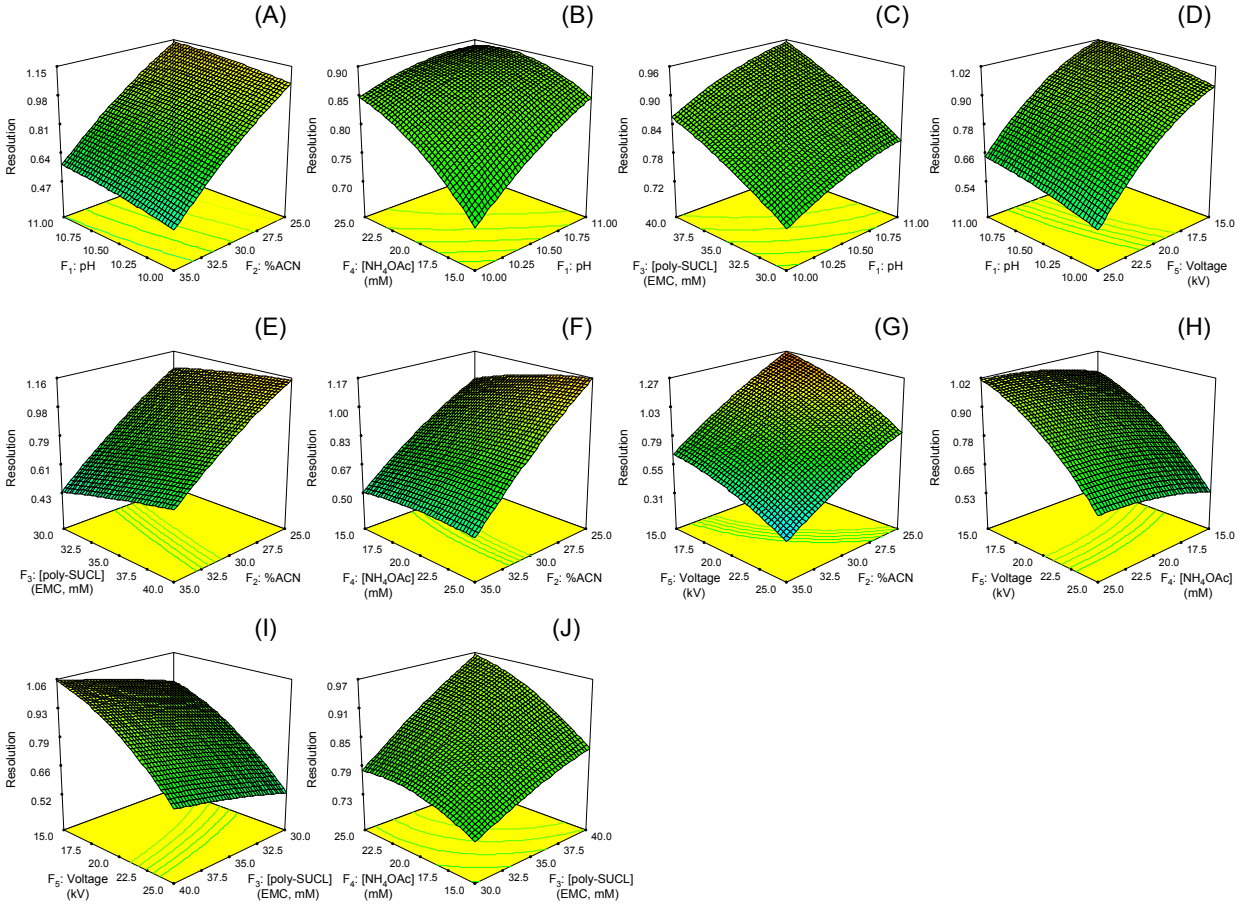

Figure 3.1. Response surface graphs for the enantiomeric resolution of (±) BNA involving all significant factors in separation optimization using CCD experiment. Factors which are not analyzed in the plots are held at their mean values (i.e. level 0 in Table 3.1). Experimental conditions: 60 cm × 50 μm id fused silica capillary; analytes: 0.4 mg/mL BNA in ACN/H_2O (40:60, v/v); injection: 5 mbar, 3 seconds; sheath liquid: MeOH/H_2O (50:50, v/v), 5 mM NH_4OAc, flow rate: 5 μL/min; ESI-MS parameters: nebulizer pressure: 2 psi; drying gas flow rate: 5 L/min; drying gas temperature: 200 ºC; capillary voltage: 3000 V. m/z = 285; fragmentor: 90; gain: 3. MEKC separation conditions are shown in Table 3.2.

3.3.2.3 Evaluation of sheath liquid parameters on *S/N* and peak area

MeOH percentage, pH, and NH_4OAc concentration were chosen as the three factors for the sheath liquid optimization (Table 3.1). Sheath liquid flow rate was not examined in this study because several of our previous studies have shown that there is only a very narrow range (e.g., 4-6 μL/min)

where this parameter is significant. Hence, in most cases 5 μL/min provided effective ionization. Therefore, a total of three factors were studied at three levels, which resulted in experimental matrix consisting of 20 experiments (Table 3.5) with 6 replicate runs (labeled as experiment 3, 5, 7, 11, 12, and 18). The range of all the selected factors was justified based on our earlier MEKC-ESI-MS study [9]. Peak area and *S/N* were chosen as responses in this study. Acceptable repeatability was obtained for the replicate runs. The %RSD values for the peak area was 27% and 31% for peak area and *S/N*, respectively. From Table 3.5, we can see that some of the experiments at extreme sheath liquids conditions were not successful due to current breakdowns. These conditions include very low percentage of MeOH (experiment 9), very low NH_4OAc concentration (experiment 14), or a combination of both (experiment 10 and 16). Figure 3.2 (A-B) shows the runs which gave the worst (experiment 6) and best (experiment 19) *S/N*, respectively at the MEKC conditions of pH: 11.5, 20% ACN, [NH_4OAc]: 25 mM, [poly-L-SUCL]: 40 mM, and voltage: +15 kV. ANOVA was again used to further validate the models. The ANOVA data suggest no evidence of lack of fit for both models (data not shown). The top half of Table 3.6 shows the regression coefficients for the sheath liquid factors. A close examination of Prob>*F* shows that concentration of NH_4OAc in the sheath liquid had significant single effects on both *S/N* and peak area with Prob>F values of 0.017 and 0.0010, respectively. However, this factor is inversely related to the peak area and *S/N* mainly because NH_4OAc in sheath liquid suppresses the ESI-MS signal at high concentrations. Interestingly, % (v/v) MeOH in the studied range did not have a significant single effect (Prob>*F* = 0.33) on *S/N* but was significant (Prob>*F* = 0.015) as an interactive effect when combined with NH_4OAc.

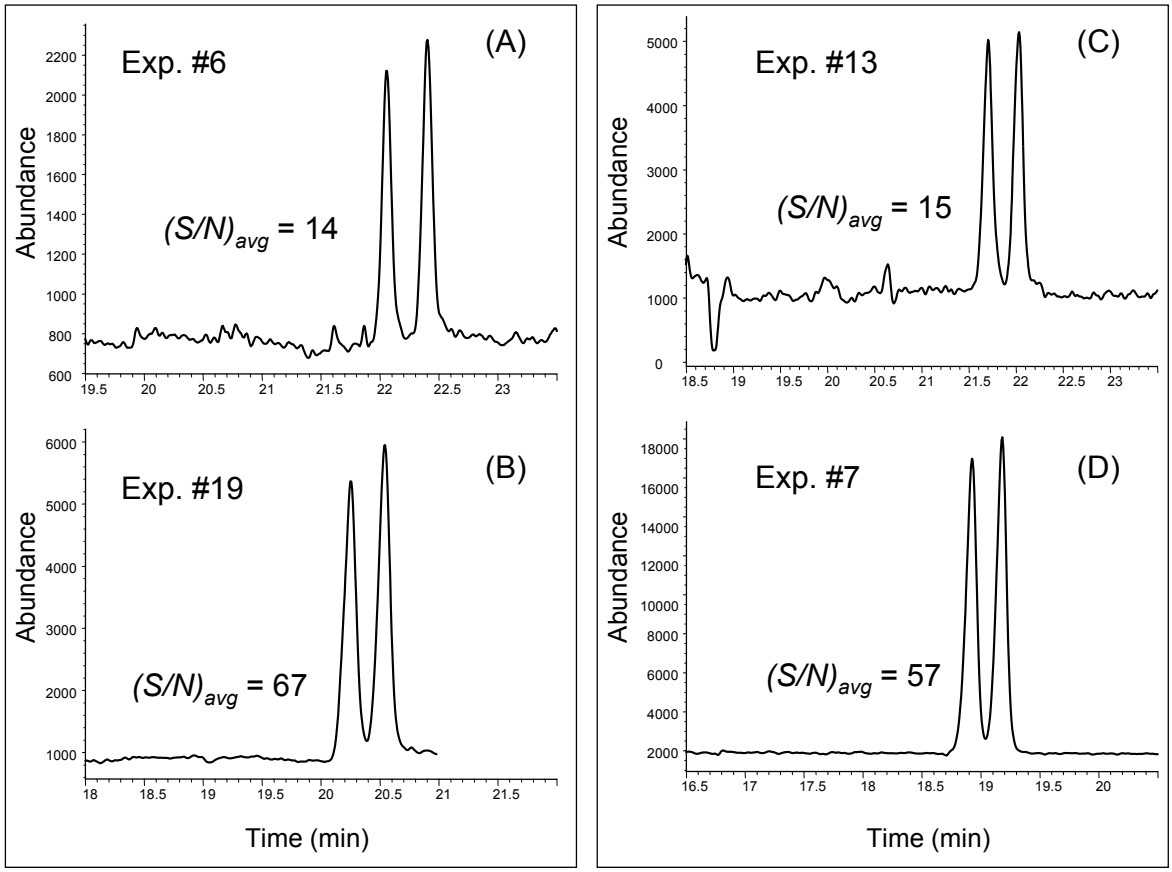

Figure 3.2. Selected electropherograms of MEKC-MS runs from the CCD experiments for the optimization of sheath liquid composition (A-B) and spray chamber parameters (C-D). Experimental conditions for (A-B) are: 60 cm × 50 μm id fused silica capillary; 25 mM NH_4OAc in 20% ACN (v/v) buffer, pH 11.5; 40 mM poly-L-SUCL; CE voltage +15 kV, column temperature 20 ºC; analytes: 0.4 mg/mL BNA in ACN/H_2O (40:60, v/v); injection 5 mbar, 3 sec; sheath liquid flow rate: 5 μL/min; Spray chamber parameters are same as those in Fig.3.1. Detailed sheath liquid conditions can be found in Table 3.5 (experiment 6 and 19 of the sheath liquid parameters). Separation conditions for (C-D) are the same to that of (A-B) except that the sheath liquid conditions are: MeOH/H_2O (80:20, v/v), 5 mM NH_4OAc, pH 6.0, delivered at a flow rate of 5 μL/min. Detailed spray chamber conditions can be found in Table 3.5 (experiment 13 and 7 of the spray chamber parameters).

Table 3.5. Peak areas and *S/N* ratios from the CCD experiment for the optimization of sheath liquid parameters and spray chamber parameters

Sheath liquid parameters						
	Experimental parameters			Experimental response		
Exp. #	%MeOH (v/v)	pH	[NH_4OAc] (mM)	Avg. Peak area	Avg. *S/N*	
1	20	8.50	40.0	19110	25	
2	50	5.15	22.5	40192	54	
3	50	7.25	22.5	32941	46	
4	50	7.25	51.9	17091	16	
5	50	7.25	22.5	19571	26	
6	20	6.00	40.0	9384	14	
7	50	7.25	22.5	39556	54	
8	100	7.25	22.5	29854	41	
9	0	7.25	22.5	N/A	N/A	*
10	20	6.00	5.0	N/A	N/A	*
11	50	7.25	22.5	45218	54	
12	50	7.25	22.5	45938	75	
13	50	9.35	22.5	40716	30	
14	50	7.25	0.0	N/A	N/A	*
15	80	8.50	40.0	25253	28	
16	20	8.50	5.0	N/A	N/A	*
17	80	6.00	5.0	89457	53	
18	50	7.25	22.5	44909	50	
19	80	6.00	40.0	35907	67	
20	80	8.50	5.0	67074	23	

Spray chamber parameters				
	Experimental parameters		Experimental response	
Exp. #	Drying gas flow rate (L/min)	Drying gas temperature (ºC)	Avg. Peak area	Avg. *S/N*
1	6.4	200	61319	48
2	5.0	200	70044	47
3	3.6	200	73744	54
4	5.0	200	46001	43
5	5.0	200	77827	48
6	5.0	200	96153	54
7	5.0	129	101409	57
8	6.0	150	77195	45
9	4.0	150	53219	29
10	5.0	200	57994	49
11	5.0	271	39219	21
12	6.0	250	41356	23
13	4.0	250	29377	15

* Data unavailable due to current break down.

3.3.2.4 Spray chamber parameter optimization on *S/N* and peak area

Two factors, DGF and DGT, were included in the evaluation of spray chamber parameter study using a three level CCD with eight runs and five central points (experiment 2, 4, 5, 6, and 10), which result in a total 13 runs. Peak area and *S/N* are again chosen as responses. The detailed design and results are shown in the bottom half of Table 3.5. The %RSD for all the replicate runs was 27% for peak area and 8.2% for *S/N*. These %RSD values indicate acceptable experimental errors. Figure 3.2 (C-D) shows the electropherograms of the runs which gave the worst (experiment 13) and best (experiment 7) *S/N*, respectively. The two models for both peak area and *S/N* are also validated by ANOVA, which suggests that the model for peak area shows no sign of lack of fit but the model for *S/N* does. Finally, judging from Table 3.6, we can see that DGT is a significant factor and inversely related to both peak area and *S/N* with the Prob>F values of 0.013 and 0.027, respectively. This could be due to the possibility of BNA being less stable at higher temperature, consequently decomposing in the spray chamber.

Table 3.6. Regression coefficient of the coded factors and analysis of variance for the response surface models of average peak area and *S/N* for the optimization of sheath liquid and spray chamber parameters.

Term	Peak area		*S/N*	
	Coefficient	Prob>*F*	Coefficient	Prob>*F*
Sheath liquid parameters				
Intercept	4.1×10^4		49	
F_1: %MeOH	5.4×10^3	0.26	-5.9	0.33
F_2: pH	-1.9×10^3	0.29	-6.2	0.16
F_3: [NH_4OAc]	-2.0×10^4	0.0010	-17	0.017
F_1 F_2			-12	0.071
F_1 F_3			20	0.015
F_2 F_3			-1.3	0.83
R^2	0.71		0.72	
Adjusted R^2	0.63		0.53	
Predicted R^2	0.43		0.53	
Spray chamber parameters				
Intercept	6.3×10^4		41	
F_1: DGF	2.3×10^3	0.71	2.0	0.65
F_2: DGT	-1.8×10^4	0.013	-11	0.027
R^2	0.48		0.41	
Adjusted R^2	0.38		0.29	
Predicted R^2	0.16		-0.16	

3.3.3 Final optimum conditions

The optimum MEKC separation condition was determined by calculating the maximum values of the responses and the corresponding variables in the model generated from the CCD. To guarantee baseline chiral separation, highest resolution for (±) BNA was chosen as the only optimization criterion. The best MEKC conditions determined by the model were as follows: F_1 (buffer pH): 11.5, F_2 (%ACN): 20%, F_3 (concentration of surfactants): 40 mM, F_4 (concentration of NH_4OAc): 25 mM, F_5 (voltage): +15 kV. Compared to the optimum conditions obtained from the univariate approach discussed in section 3.1, the buffer pH, concentration of surfactant and concentration of NH_4OAc from multivariate experiment are all higher (11.5 vs. 10.5, 40 mM vs. 35 mM, and 25 mM vs. 20 mM, respectively); while voltage is lower (+15 kV vs. +20 kV). However, %ACN remains the same (20%v/v). Similar strategies were also applied to optimize the best sheath liquid conditions and spray chamber conditions. For both optimizations, highest *S/N* was chosen as the criterion. The optimum sheath liquid conditions were determined as: MeOH/H_2O (80:20, v/v), 5 mM NH_4OAc, pH 6.0. The optimum spray chamber conditions are determined to be: drying gas flow rate: 6 L/min; drying gas temperature: 150 ºC. Electropherograms of MEKC-MS under the final optimum MEKC-MS conditions is shown in Figure 3.3. The enantioresolution of BNA is 1.61. The average *S/N* of both enantiomers is 45. As shown in the inset of Fig. 3.3, the experimental values are close to what were predicted by the response surface models and are better than what were obtained from the preliminary sequential experiment (data not shown). Under the optimized MEKC-MS condition, the experimental and model predicted had a percent discrepancy difference of only 3.3%, 12%, and 12% for resolution, analysis time and *S/N*, respectively.

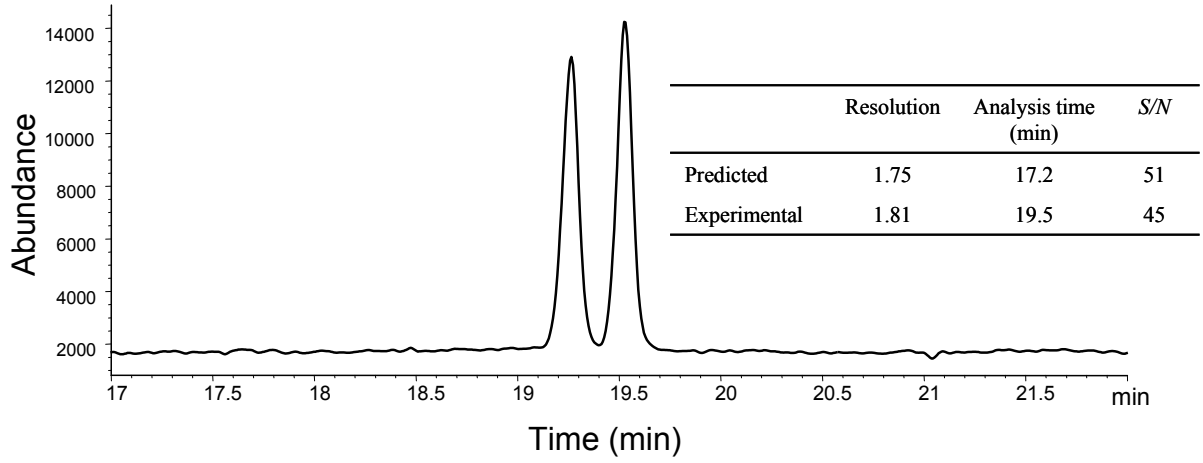

	Resolution	Analysis time (min)	*S/N*
Predicted	1.75	17.2	51
Experimental	1.81	19.5	45

Figure 3.3. Experimental electropherograms of MEKC-MS enantioseparation of (±) BNA under final optimized conditions: 60 cm × 50 μm id fused silica capillary; 25 mM NH_4OAc in 20% ACN (v/v) buffer, pH 11.5; 40 mM poly-L-SUCL; +15 kV, 20 ºC; analytes: 0.4 mg/mL BNA in ACN/H_2O (40:60, v/v); injection size: 5 mbar, 3 seconds; sheath liquid: MeOH/H_2O (80:20, v/v), 5 mM NH_4OAc, pH 6.0, flow rate: 5 μL/min; ESI-MS parameters: nebulizer pressure: 2 psi; drying gas flow rate: 6 L/min; drying gas temperature: 150 ºC; capillary voltage: 3000 V. m/z = 285; fragmentor: 90; gain: 3.

3.4 Concluding remarks

The enantiomers of (±) BNA was separated and detected by MEKC-ESI-MS using a polymeric surfactant poly-L-SUCL in a positive ion mode. A three-level five-factor full factorial CCD experiment was employed to optimize the MEKC separation parameters. Response surface models were built base on the CCD experiment and all factors were analyzed and optimized. It was found from the experiment that all five factors of MEKC are significant to both chiral resolution and analysis time of (±) BNA. The most significant factors that affect chiral resolution were identified as %ACN and voltage (both have negative effect to the resolution); while the most significant factor that affect the run time is voltage (inversely correlated to run time). Their relationship and interactions were further explored by the response surface plots generated from the model. Using maximum enantioresolution as criterion, all the factors were optimized by the models created in the analysis and the response also predicted. Actual running data of the optimum condition agreed with the predicted value and provided baseline resolution for (±) BNA. Sheath liquid composition and spray chamber conditions were also optimized using the same

methodology. Models for the peak area and the *S/N* for the ESI-MS signal was established and NH_4OAc concentration and drying gas temperature were found significant in these studies and were both inversely related to the *S/N* of the analyte. Running under the optimized MEKC-MS condition, the final experimental results matched adequately with the predicted value (Fig. 3.3 inset). This study not only provides an optimized MEKC-ESI-MS method for the chiral analysis of (±) BNA, but also suggests that multivariate experimental design methods such as CCD are effective tools for optimization of chiral separation and detection in MEKC-ESI-MS.

References

[1] Shamsi, S. A., *Anal. Chem*. **2001**, *73*, 5103-5108.

[2] Valle, B. C., Billiot, F. H., Shamsi, S. A., Zhu, X., Powe, A. M., Warner, I. M., *Electrophoresis* **2004**, *25*, 743-752.

[3] Palmer, C. P., *J. Sep. Sci.* **2008**, *31*, 783-793.

[4] Palmer, C. P., Terabe, S., *Anal. Chem*. **1997**, *69*, 1852-1860.

[5] Rizvi, S. A. A., Zheng, J., Shamsi, S. A., *Electrophoresis* **2007**, *28*, 1762-1778.

[6] Akbay, C., Rizvi, S. A. A., Shamsi, S. A., *Anal. Chem*. **2005**, *77*, 1672-1683.

[7] Shamsi, S. A., Miller, B. E., *Electrophoresis* **2004**, *25*, 3927-3961.

[8] Shamsi, S. A., *Electrophoresis* **2002**, *23*, 4036-4051.

[9] Hou, J., Zheng, J., Rizvi, S. A. A., Shamsi, S. A., *Electrophoresis* **2007**, *28*, 1352-1363.

[10] Mohanty, A., Dey, J., *J. Chromatogr. A* **2005**, *1070*, 185-192.

[11] Williams, A. A., Fakayode, S. O., Huang, X., Warner, I., *Electrophoresis* **2006**, *27*, 4127-4140.

[12] Rizvi, S. A. A., Simons, D. N., Shamsi, S. A., *Electrophoresis* **2004**, *25*, 712-722.

[13] Rizvi, S. A. A., Shamsi, S. A., *Electrophoresis* **2005**, *26*, 4172-4186.

[14] Anderson, M. J., Whitcomb, P. J., *DOE Simplified Practical Tools for Effective Experimentation*, *2nd ed.,* Productivity Press, New York **2007**.

[15] Ferreira, S. L. C., Bruns, R. E., da Silva, E. G. P., dos Santos, W. N. L., Quintella, C. M., David, J. M., de Andrade, J. B., Breitkreitz, M. C., Jardim, I. C. S. F., Neto, B. B., *J. Chromatogr. A* **2007**, *1158*, 2-14.

[16] Anderson, M. J., Whitcomb, P. J., *RSM Simplified: Optimizing Processes Using Response Surface Methods for Design of Experiments,* Productivity Press, New York **2005**.

[17] Schappler, J., Guillarme, D., Prat, J., Veuthey, J-L., Rudaz, S., *Electrophoresis* **2007**, *28*, 3078-3087.

[18] Varesio, E., Gauvrit, J-Y. Longeray, R., Lantéri, P., Veuthey, J-L., *Electrophoresis* **1997**, *18*, 931-937.

[19] Wan, K. T., Davis, M. E., *Nature* **1994**, *370*, 449-450.

[20] Setnička, V., Urbanová, M., Bouř, P., Král, V., Volka, K., *J. Phys. Chem. A* **2001**, *105*, 8931-8938.

[21] Pu, L., *Chem. Rev.* **1998**, *98*, 2405-2494.

[22] Billiot, F. H., McCarroll, M. C., Billiot, E. J. , Warner, I. M., *Electrophoresis* **2004**, *25*, 753-757.

[23] Kano, K., Minami, K., Horiguchi, K., Ishimura, T., Kodera, M., *J. Chromatogr. A* **1995**, *694*, 307-313.

[24] Nakamura, H., Sano, A., Sumii, H., Anal. Sci. **1998**, 14, 375-378.

[25] Pais, L. S., Loureiro, J. M., Rodrigues, A. E., *Chem. Eng. Sci*. **1997**, *52*, 245-257.

[26] Yarabe, H. H., Rugutt, J. K. McCarroll, M. E., Warner, I. M., *Electrophoresis* **2000**, *21*, 2025-2032.

[27] Rizvi, S. A. A., Shamsi, S. A., *Electrophoresis* **2003**, *24*, 2514-2526.

[28] Hou, J., Zheng, J., Shamsi, S. A., *J. Chromatogr. A* **2007**, *1159*, 208-216.

[29] He, J., Shamsi, S. A., *J. Chromatogr. A* **2009**, 1216, 845-856.

[30] Thorsteinsdóttir, M., Ringbom, C., Westerlund, D., Andersson, G., Kaufmann P., *J. Chromatogr. A* **1999**, *831*, 293-309.

[31] Mikaeli, S., Thorsén, G., Karlberg, B., *J. Chromatogr. A* **2001**, *907*, 267-277.

[32] Cikalo, M. G., Bartle, K. D., Myers, P., *J. Chromatogr. A* **1999**, *836*, 35-51.

Chapter 4

Chiral Micellar Electrokinetic Chromatography -Atmospheric Pressure Photoionization Mass Spectrometry of Benzoin Derivatives Using Mixed Molecular Micelles

In the present work we report, for the first time, the successful on-line coupling of chiral micellar electrokinetic chromatography (CMEKC) to atmospheric pressure photo-ionization mass spectrometry (APPI-MS). Four structurally similar neutral test solutes (e.g., benzoin derivatives) were successfully ionized by APPI-MS. The mass spectra in the positive ion mode showed that the protonated molecular ions of benzoins are not the most abundant fragment ions. Simultaneous enantioseparation by CMEKC and on-line APPI-MS detection of four photoinitiators: hydrobenzoin (HBNZ), benzoin (BNZ), benzoin methyl ether (BME), benzoin ethyl ether (BEE), were achieved using an optimized molar ratio of mixed molecular micelle of two polymeric chiral surfactants (polysodium *N*-undecenoxy carbonyl-L-leucinate and polysodium *N*-undecenoyl-L,L-leucylvalinate). The CMEKC conditions, such as voltage, chiral polymeric surfactant concentration, buffer pH, and BGE concentration, were optimized using a multivariate central composite design (CCD). The sheath liquid composition (involving % v/v methanol, dopant concentration, electrolyte additive concentration, and flow rate) and spray chamber parameters (drying gas flow rate, drying gas temperature, and vaporizer temperature) were also optimized with CCD. Models built based on the CCD results and response surface method was used to analyze the interactions between factors and their effects on the responses. The final overall optimum conditions for CMEKC-APPI-MS were also predicted and found in agreement with the experimentally optimized parameters.

4.1 Introduction

Enantiomeric separation and detection of chiral compounds with electrokinetic chromatography (EKC)-mass spectrometry (MS) is one of the challenging areas in the use of hyphenated technology for chiral analysis. Although a wide array of low molecular weight chiral selector(s) (e.g., cyclodextrins, macrocyclic antibiotics, unpolymerized chiral micelles), are available, the use of the aforementioned chiral selectors is very difficult when UV detection is replaced with electrospray ionization (ESI)-MS. This is mainly due to the use of charged chiral selector, which when present in the running buffer at concentrations ≥10 mM often interferes with the ionization of the analytes. Moreover, the conventional charged surfactant also coats on the surface of the ionization source, and suppresses the MS signal in a few runs. To overcome this problem, polymeric chiral surfactant (also known as chiral molecular

micelle) was introduced for the first time by our research group in 2001 for micellar electrokinetic chromatography (MEKC)-ESI-MS [1]. The molecular micelles are typically in the high molecular mass range (15,000-20,000 Daltons), and are very hard to ionize in the ESI spray chamber, hence providing a much more stable baseline and cleaner electropherograms with significantly lower background noise. Other advantages of the molecular micelle include zero critical micelle concentration and compatibility of organic solvents [1-3]. Hence, several reports have identified the use of polymeric chiral surfactants in chiral MEKC-ESI-MS applications over the last decade [1-5]. Recently, both MEKC [6] and microemulsion electrokinetic chromatography (MEEKC) [7] were coupled to atmospheric pressure photoionization APPI-MS using conventional SDS micelles for achiral separations of neutral achiral compounds. However, to the best of our knowledge, no studies describing the separation of neutral or even charged chiral compounds using any chiral selector in EKC or MEKC equipped with APPI-MS can be found in the literature. This is surprising in light of the obvious benefits of APPI-MS over atmospheric pressure chemical ionization (APCI-MS) or ESI-MS for several classes of non-polar chiral compounds.

The APPI is one of the latest "soft ionization" modes of mass spectrometry. As mentioned earlier, APPI-MS is especially suitable for the analysis of highly non-polar or neutral compounds, which cannot be ionized by ESI or less efficiently by APCI. It is reported to be a more universal, rugged and sensitive ionization technique than APCI due to its higher tolerance to non-polar (e.g., hexane-based) mobile phase and low flow rates in HPLC-MS applications [8-10].

The feasibility of coupling CE to APPI-MS was first reported by Nilsson *et al.* [11]. In a short time, several works involving CE-APPI-MS have been reported [6, 12-16]. Mol and coworkers studied the setup and performance of CE-APPI-MS using non-volatile background electrolyte and an ion-trap mass spectrometer [6]. In the same work [6], this research group also reported a MEKC-APPI-MS of two neutral compounds using a running buffer of 20 mM SDS, 10 mM sodium phosphate and 20% acetonitrile. Zheng *et al.* [12] separated positional isomers of methylated benzo [α] pyrene with capillary electrochromatography using C-18 column followed by APPI-MS. The detection limits of three most carcinogenic MBAP isomers were reported in the range of 2.5-5.0 mg/mL. Schappler and coworkers

successfully separated three basic compounds with CE-APPI-MS and optimized the APPI conditions with multivariate experimental designs [13]. The same research group also separated a series of pharmaceutical drugs (β-blockers, central stimulants, and diuretics) with MEEKC-APPI-MS using a microemulsion system containing SDS, butanol, and *n*-octane [14]. Hommerson *et al.* compared ESI and APPI for coupling to MEKC using SDS running buffer and APPI was found to provide better LOD [15]. They also tested drug impurity with different ionization sources (including ESI, APCI, APPI and dopant assisted APPI) for CE-MS [16]. However, as mentioned earlier, despite all the recent CE-APPI-MS applications of achiral compounds, no chiral selectors or chiral pseudostationary phases for MEKC-APPI-MS analysis is reported in the literature.

In this work, four chiral photoinitiators, hydrobenzoin (HBNZ), benzoin (BNZ), benzoin methyl ether (BME), and benzoin ethyl ether (BEE), were simultaneously enantioseparated with MEKC using a mixture of two chiral molecular micelles polysodium *N*-undecenoxy carbonyl-L-leucinate (poly-L-SUCL) and poly-sodium *N*-undecenoyl-L,L-leucylvalinate (poly-L,L-SULV). Chiral benzoins are important structural units of many useful biological compounds. These compounds are considered as versatile building blocks in a lot of asymmetric synthesis. For example, enzymatic synthesis of chiral benzoins in high enantiomeric excess from racemic benzoyl benzene is reported [17]. One real life application of benzoin suggests that benzoin is a drug intermediate used in cancer treatment [18]. Hence, they are often used as model compounds to test the selectivity of the enantioselective analysis method in separation science [19-21]. The use of the two molecular micelles has provided good chiral resolutions and selectivities for the benzoin derivatives in previous MEKC-UV studies [3, 19]. However, when MEKC is coupled to APPI-MS, the MEKC-UV conditions need to be reoptimized to compensate the use of volatile background electrolyte and the suction effect of nebulizing gas on the separation performance. These two are very important factors, which can have significant influence on the choice of buffer pH, surfactant concentration, as well as the separation voltage. Therefore, a series of factors that involved in the MEKC enantioseparation were first examined by sequential optimization experiments, using a univariate

approach. Next, to guarantee an overall optimum condition and to understand the interactions between the various separation factors and the APPI-MS parameters, multivariate optimization or design of experiment (DOE) needs to be performed.

Central composite design (CCD) as one of the effective secondary DOE method was chosen because CCD allows the deduction of quadratic models and the resulting response surface method (RSM) analysis can be used to analyze the interactions between related factors [4, 22]. Besides MEKC conditions, sheath liquid composition and spray chamber conditions were also optimized using the same method.

4.2 Material and methods

4.2.1 Chemicals

The analytes *R, R* and *S, S* (±) hydrobenzoin (HBNZ), *R,S* benzoin (±) (BNZ), benzoin methyl ether (±) BME, as well as benzoin ethyl ether (±) BEE were purchased from Sigma-Aldrich (St. Louis, MO). Acetonitrile (ACN, HPLC grade) was purchased from Fisher Scientific (Fair Lawn, NJ). Acetic acid, methanol (Meow, HPLC grade) and aqueous solution of 7.5 M ammonium acetate (NH_4OAc) were purchased from Sigma-Aldrich (St. Louis, MO). Ammonium hydroxide (NH_4OH, 28%-30% ammonia solution) was purchased from EM Science (Gibbstown, NJ). Deionized water (18 MΩcm) was purified by a Barnstead Nanopure II Water System (Dubuque, IA). Chemicals (*N*-hydroxysuccinimide, *N,N'*-dicyclohexylcarbodiimide, undecylenic acid, isopropanol, ethyl acetate, and sodium bicarbonate) used to synthesize dipeptide surfactants were obtained from Sigma-Aldrich (St. Louis, MO). Sodium hydroxide (50%, w/w) was obtained from Fisher Scientific (Fair Lawn, NJ). Hydrochloric acid and tetrahydrofuran were purchased from Caledon Laboratories Ltd (Georgetown, Ont., Canada). Chemicals such as ω-undecylenyl alcohol, pyridine, dichloromethane, and L-leucine used to synthesize the surfactant monomer were purchased from Sigma-Aldrich (St. Louis, MO). Triphosgene was purchased from TCI-America (Portland, OR). Leucine-valine dipeptide was obtained from Bachem California Inc (Torrance, CA). Sodium sulfate anhydrous was purchased from EMD Chemicals (Gibbstown, NJ). All the chemicals have

the purity of 98% or higher and were used as received without further purification unless specifically noted. The surfactant monomers of sodium *N*-undecenoyl-L, L-leucylvalinate (L, L-SULV) and sodium *N*-undecenoyl–, L-leucinate (L-SUCL) were synthesized following the procedures described in references [23-25]. The monomers were polymerized by Phoenix Memorial Laboratory (University of Michigan, Ann Arbor, MI) using a total dose of 20 M red of ^{60}Co γ-radiation.

4.2.2 Sample and running buffer preparation

Stock solutions of the analytes *R, R* and *S, S* (±) HBNZ, *R, S* (±) BNZ, (±) BME, and (±) BEE were prepared at the concentration of 8.0 mg/mL in ACN. Working standard of the analyte solution was prepared by mixing 20 all of each stock solution and then diluting the mixture with 80 all of H_2O to obtain the desired final concentration of 1.0 mg/mL for each benzoin derivative. The CE running buffer was prepared by diluting the 7.5 M NH_4OAc solution to the desired concentration. The pH of the NH_4OAc BGE was adjusted as needed with 1 M NH_4OH. Next, poly-L-SUCL and poly-L,L-SULV were dissolved in the NH_4OAc buffer to obtain the desired equivalent molar concentration, which is defined as the concentration of the polymeric surfactant that has the same weight as the monomer. The surfactant containing buffer was then vortexed, filtered by 0.45 μm PTFE syringe filter (Fisher Scientific, Pittsburgh, PA), and ultrasonicated for 15-20 min before use.

4.2.3 MEKC-APPI-MS instrumentation

All MEKC-APPI-MS experiments were performed on an Agilent CE (Agilent Technologies, Palo Alto, CA) interfaced to an Agilent 1100 series single quadrupole mass spectrometer (Agilent Technologies, Palo Alto, CA). The Agilent 3D-CE/MSD ChemStation software (Rev. A.10.02) was used for instrument control and data analysis. Sheath liquid was delivered by an Agilent 1100 series isocratic HPLC pump equipped with a 1:100 splitter. The MEKC separation was performed on a 120 cm long fused silica capillary (50 μm i.d., 360 μm o.d., Polymicro Technologies, Phoenix, AZ). At 60 cm from the injection end of the capillary, a 3 mm section of polyimide coating was burned off with a home-made electronic burner to create a UV detection window. New capillary was sequentially flushed with 1 M NH_4OH and

triply deionized water for 40 minutes and 20 minutes, respectively before use. The capillary was flushed with the running buffer for 5 minutes using a pre-conditioning step before each run. After each run, the capillary was flushed with water for 2 minutes, 1 M NH_4OH for 2 minutes, and water for another 2 minutes as post-conditioning. The capillary temperature was set at 20 ^oC; positive voltage (anode at the inlet end and cathode at the MS end) was applied for all the experiments. Analytes were kept at 15 ºC in the auto sampler and injected hydrodynamically at the pressure of 10 mbar for 10 sec.

The nebulizer was mounted on a 36 mm plastic spacer, which was placed between the nebulizer and the APPI spray chamber. The nebulizer was grounded by a wire to maintain the steady current. The APPI lamp was a krypton UV lamp (emits photons at 10.0 and 10.6 eV) developed by Syagen Technology, Inc. (Tustin, CA). The following conditions were used for preliminary APPI-MS detection: nebulizer pressure, 5 psi; capillary voltage + 2000 V; fragmentor voltage, 90V; gain setting, 3. Other APPI-MS conditions were varied according to the experimental design. The positive ion mode was selected in which the ions were group SIM at m/z = 197 for HBNZ for its detection as $[M+H-H_2O]^+$, whereas the most abundant ion $[M+H–H_2O]^+$, $[M+H-CH_3OH]^+$, and $[M+H-C_2H_5OH]^+$ were observed for BNZ, BME, and BEE, respectively at m/z 195.

4.2.4 Experimental design and data processing

Experimental design and data analysis for the optimization of MEKC as well as APPI-MS parameters were performed on Design-Expert (version 7.0.3, Stat-Ease, Inc. Minneapolis, MN) software. Four factors (separation voltage, pH, surfactant concentration and NH_4OAC concentration) were chosen for MEKC optimization using CCD. All CCDs were generated using default settings. Experiments were carried out. The results of the experiments were then input into the software and the fitted models generated. The models were validated by analysis of variance (ANOVA), and the response surface plots were created by the software.

4.3 Results and discussion

4.3.1 Preliminary experiments

The preliminary experiments on the APPI-MS conditions (including both direct infusion experiments and on-line CMEKC-MS experiments) were carried out to determine the MS spray chamber parameters, which are most significant for better detectability of all four benzoins. These experiments were followed by a set of univariate experiments to determine the range and significance of CMEKC conditions of all four benzoin derivatives. Because a make-up solution delivered at the tip of the nebulizer provides sheath liquid, the parameter of sheath liquids (flow rate and composition) is carefully optimized to promote efficient ionization of the benzoin derivatives.

4.3.1.1 Direct Infusion spectra and fragmentation pathway

Direct infusion experiments for the benzoins in both positive and negative ion modes showed that positive ion mode is more sensitive than negative mode. The full scan positive ion MS spectra for all four benzoin derivatives are shown in Fig. 4.1 at variable fragmentor voltages by direct infusion without dopant. However, with or without dopant, the fragmentation pattern in the mass spectrum remained the same for all four benzoins. The main ions (in water/-methanol/5mM ammonium acetate sheath liquid) for HBNZ and BNZ were the $[M+H-H_2O]^+$ ions at m/z 197 and 195, but the protonated molecular ion $[M+H]^+$ at m/z 213 is only observed for BNZ. Similarly for BME and BEE, the highest abundant ion is observed at m/z 195, which corresponds to $[M+H-CH_3OH]^+$ and $[M+H-C_2H_5OH]^+$, respectively. In addition, $[M+H]^+$is observed for both BME and BEE. Direct infusion experiments with and without dopant (i.e., acetone) were also conducted. Adding acetone in the sheath liquid increased the APPI-MS intensity of HBNZ and BNZ (insets of Fig. 4.1). In contrast, sensitivity of BME and BEE was not affected significantly (data not shown). This suggests that the proton affinity (PA) for HBNZ and BNZ is greater than that of the solvent (MeOH) as well as the dopant (acetone). Thus, proton transfer reaction could have been facilitated by both the solvent clusters (Sn) as well as the dopant. On the other hand, the PA of the benzoin ethers (i.e., BME and BEE) must be lower than dopant, but higher than solvent. Thus, the proton transfer to BME and BEE can be still be obtained by the proton transfer reaction between Sn

(i.e., the use of 50/50% methanol/water) present in the sheath liquid and the benzoin ethers (M) [S_nH^+ + M → MH^+ + nS] [24].

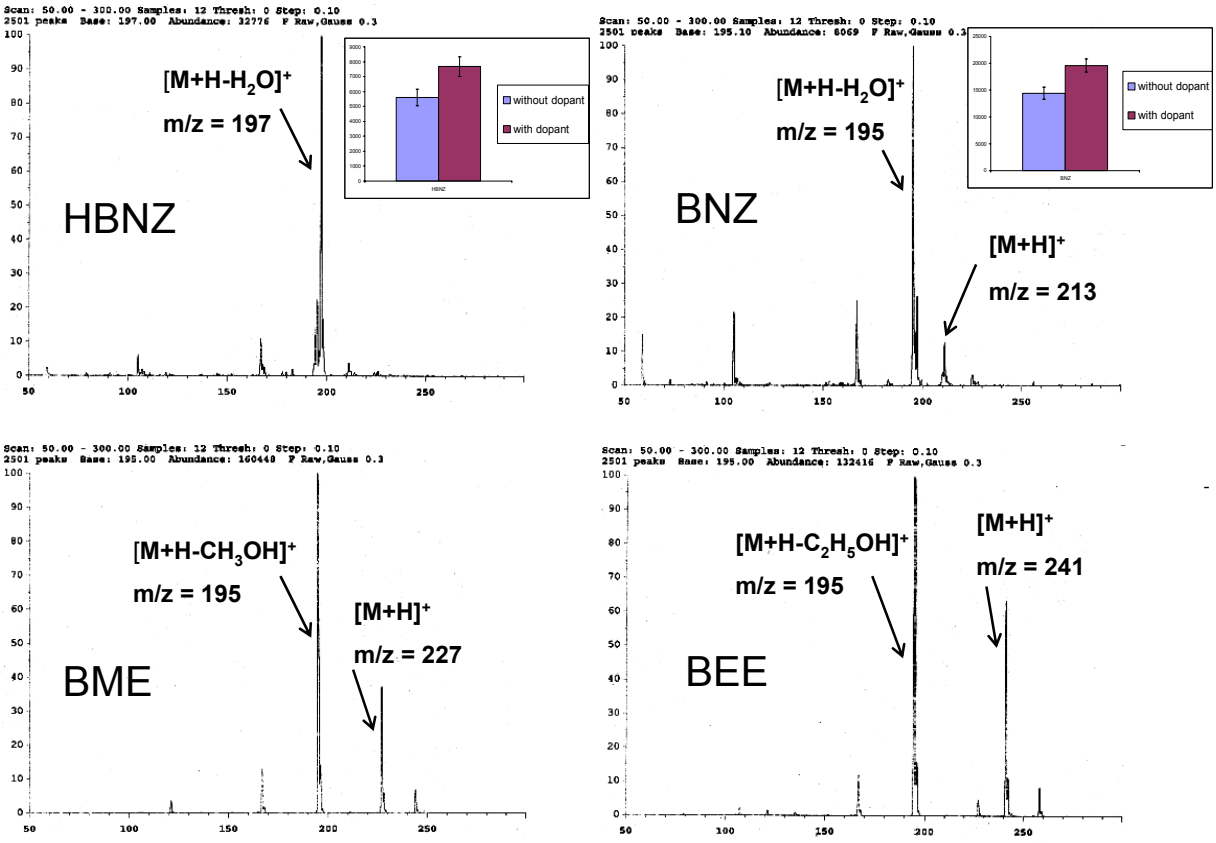

Figure 4.1. APPI-MS spectra of the four benzoin compounds. The inset plots of HBNZ and BNZ shows the signal intensity with and without 0.5% acetone. The error bar in each plot represents 3 standard deviations.

The chemical structure the four benzoin derivatives are provided in Fig. 4.2. Note that HBZN is a diol with two chiral centers. Among its three possible isomers, only *(1R, 2R)* and *(1S, 2S)* forms are enantiomers, which are available commercially, whereas the *(1R, 2S)* form is the *meso* isomer and is excluded from the experiment. The BZN is a hydroxy ketone with two phenyl groups. BME and BEE are the methyl and ethyl ether of benzoin, respectively. Consistent with Fig. 4.1, the fragmentation pathway proposed in Figure 4.2 should consists of protonated molecular ions of HBZN and BZ, which are significantly less stable and eventually lose water molecules to form fragment ions $[M+H-H_20]^+$ at m/z

195 and 197, respectively. Similarly, BME and BEE, after forming relatively low abundance $[M+H]^+$ ions, losses CH_3OH and C_2H_5OH, respectively to form $[M+H-CH_3OH]$ and $[M+H-C_2H_5OH]$ species at m/z =195. Eventually, only two ions at *m/z* 195 and 197 were chosen in group SIM for the on-line MEKC-APPI-MS for the four benzoin compounds.

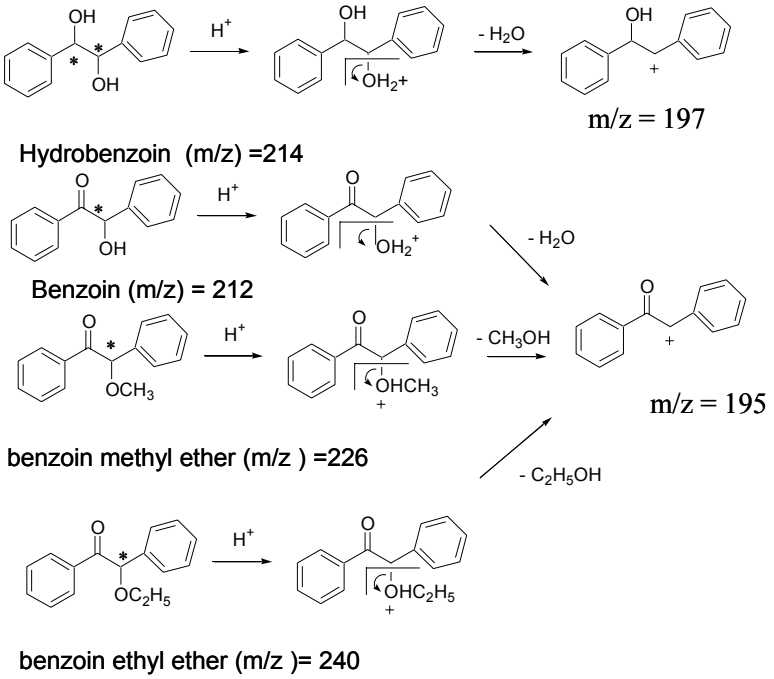

Figure 4.2. Proposed ionization and fragmentation mechanism of four benzoin derivatives in APPI-MS.

4.3.1.2 Determination of the APPI-MS conditions

An online MEKC-APPI-MS study was carried out to determine the optimum fragmentor voltage for all four benzoins. The results shown in Fig. 4.3 illustrates that for all four derivatives, 80 V is the best fragmentor voltage in terms of peak area and *S/N*. MS capillary voltage and nebulizer pressure were also explored; 2000 V and 5 psi were determined respectively to be the best to provide the optimum *S/N* (data not shown). Other importance factors to be investigated in the extensive multivariate optimization are vaporizer temperature, drying gas flow rate, and drying gas temperature. The DOE levels for these parameters were determined by univariate experiments and listed in [supplementary section, Table A7].

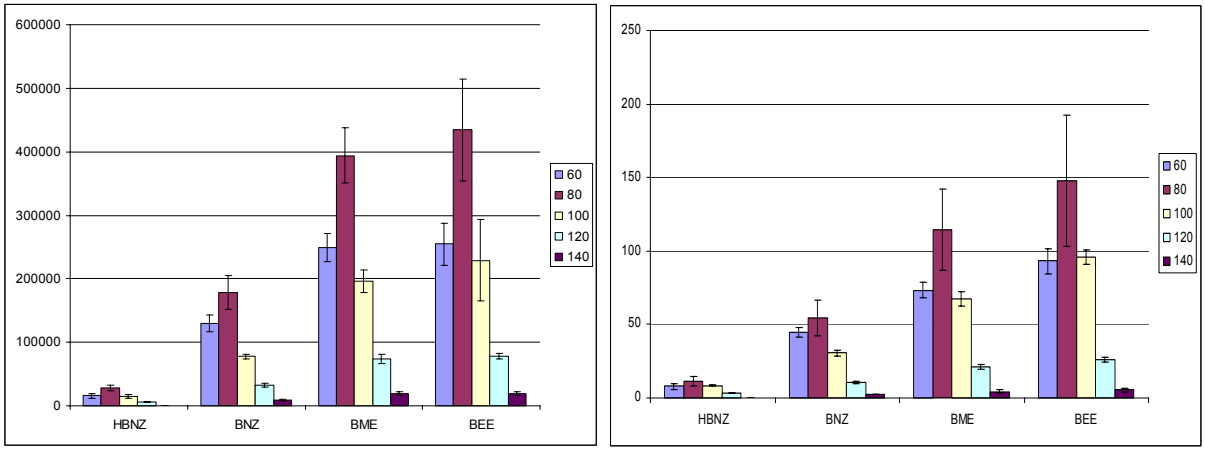

Figure 4.3. The bar plots showing the results of the online MEKC-APPI-MS fragmentor study. The error bar in each plot represents 3(s) standard deviations. Experimental conditions: 120 cm × 50 μm i.d. fused silica capillary; 40 mM NH_4OAc, pH 10.0, with 70 mM mixed micelle of (poly-L,L-SULV and mM poly-L-SUCL 85:15, molar ratio); +25 kV, 20 ºC; analyte: 1 mg/mL benzoin derivatives in 50/50 MeOH/H_2O, injected at 5 mbar, 10 sec; spray chamber parameters: drying gas flow rate 5 L/min; nebulizer pressure 5 psi; drying gas temperature 150 ºC; vaporizer temperature 150 ºC; capillary voltage 2000V; fragmentor voltage varied from 60-140 V, gain 3; SIM at m/z = 195, 197; sheath liquid: 5 mM NH_4OAc in 50/50 MeOH/H_2O, 0.5% Acetone; flow rate 7.5 μL/min.

4.3.1.3 CMEKC parameters

A series of sequential online CMEKC-APPI-MS experiments were performed to obtain the reasonable ranges for all the CMEKC parameters for multivariate studies. The first factor explored is the type of polymeric surfactant. Two most commonly versatile polymeric surfactants [i.e., alkenoxy-based single amino acid (poly-L-SUCL) and acyl-based dipeptide (poly-L, L-SULV)], were mixed in various proportions to test the synergistic effect for the simultaneous enantioseparation of all four benzoins. Using poly-L-SUCL alone was only very effective for the chiral separation of (±) HBNZ and to some extent (±) BNZ (Figure 4.4A). However, using poly-L,L-SULV, (±) BNZ, (±) BME, and (±) BEE, provided significantly higher chiral resolution (Figure 4.4F) compared to poly-L-SUCL. We hypothesize that the difference in chiral selectivity between the two molecular micelles might be due to the presence of carbamate group in poly-L-SUCL, which tends to form hydrogen bond with the hydroxyl group in HBNZ assisting chiral recognition. On the other hand, the amide bond in poly-L,L-SULV does not have this structural effect. To achieve a simultaneous enantioseparation of all four benzoins, a mixture of poly-

L-SUCL and poly-L,L-SULV was investigated at different ratios via an online CMEKC-APPI-MS experiment (Figure 4.4B-E). The resulting electropherograms shows that with the increasing molar concentrations of poly-L,L-SULV, the chiral resolution for HBNZ decreases, while the chiral resolution for BNZ, BME, and BEE increases. As a compromise, a ratio of 15:85 (poly-L-SUCL: poly-L,L-SULV molar ratio) was chosen as the optimum mixed molecular micelle ratio.

CMEKC conditions to be further explored in multivariate experiments are background electrolyte (BGE, in our case NH_4OAc) concentration, buffer pH, voltage, and polymeric surfactant concentration. Their levels are shown in Table A1.

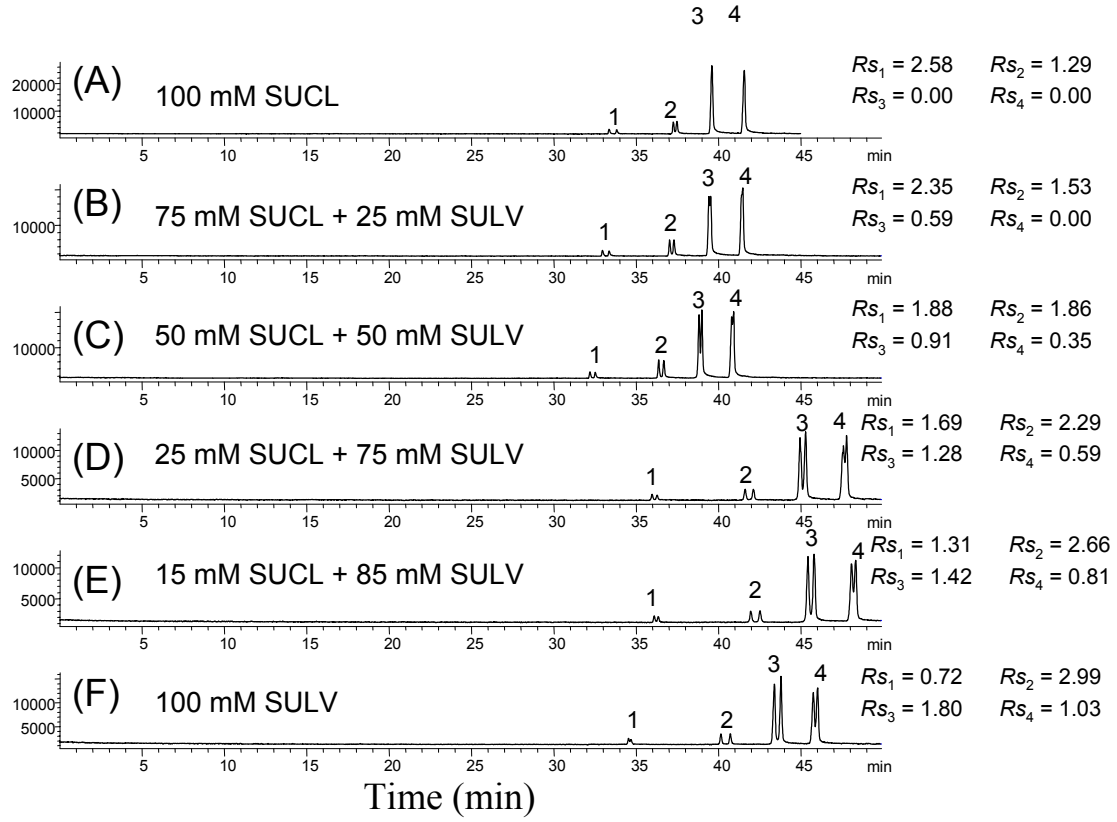

Figure 4.4. The CMEKC-APPI-MS electropherograms showing the effect of the mixed-micelle (poly-L-SUCL and poly-L,L-SULV) A-F ratio on the simultaneous enantioseparation of benzoin derivatives. Separation condition: 120 cm × 50 μm i.d. fused silica capillary; 25 mM NH_4OAc, pH 8.0, with 100 mM poly-SULV and poly-SUCL at different ratio; +25 kV, 20 ºC; analyte: 1 mg/mL benzoin derivatives in 50/50 ACN/H_2O, injected at 5 mbar, 10 sec; spray chamber parameters: drying gas flow rate 5 L/min; nebulizer pressure 5 psi; drying gas temperature 150 ºC; vaporizer temperature 150 ºC; capillary voltage 2000V; fragmentor 80, gain 3; SIM at m/z = 195, 197; sheath liquid: 5 mM NH_4OAc in 50/50 MeOH/H_2O, 0.5% Acetone; flow rate 7.5 μL/min.

4.3.1.4 Determination of the sheath liquid conditions

Sheath liquid helps to ground the outlet end of the capillary and provide enhanced liquid flow to form a steady sprayer cone [1, 12, 28]. In CE-APPI-MS, sheath liquid is even more important due to the requirement of adding dopant to the analytes to obtain enhanced signal [9, 13]. A series of sequential experiments were performed to determine the ranges for the following parameter: sheath liquid composition, dopant type, dopant concentration, sheath liquid flow rate, pH of the sheath liquid, and electrolyte concentration in the sheath liquid. After the preliminary experiments (data not shown), the dopant type was determined to be acetone. Levels of other parameters are listed in Table A4.

4.3.2 Multivariate optimization experiments

Three sets of CCD experiments were performed to determine the optimum conditions for MEKC parameters, sheath liquid composition, and spray chamber parameters. Full factorial CCD was chosen as the design method due to its ability to evaluate the interactions between all factors with fairly less experiments [20, 27]. The factors used in these CCD experiments (Table A1, A4 and A7) as well as their levels were chosen based on the preliminary experiments aforementioned. The factors and their levels were input into the Design-Expert software and a series of runs at different level combinations were generated in random order. According to the rule of CCD, these runs include the combination of all factors at their + and – levels and several repetitive runs at their mean value (0 level, also called center point in CCD). Each factor was also tested at the value outside the +/- levels when other factors were held at 0 level. These runs are called axial or star points in CCD [20]. All the runs generated by CCD were performed and the results were input into the software as responses. Models that represent the relations between factors and responses were then fitted by least squares. These models were then evaluated by ANOVA, and RSM plots generated from the models were used to examine the interactions between factors and their effects to responses. Detailed description on CCD method can be found in literature [13, 20] and our earlier work [5, 27].

4.3.2.1 Optimization of MEKC parameters

Four factors (voltage, buffer pH, total surfactant concentration, and NH_4OAc concentration) were evaluated for the optimization of MEKC parameters. Their levels are listed in Table A1 (Supplementary Information). A total of 30 runs were generated by CCD. Detailed conditions for all the runs and their responses (ratio of chiral resolution/elution time of the last eluting enantiomer and total migration time) are shown in Table A2 (Supplemental Information). Rs/t_R is chosen as the response because it represents the best resolution in the least analysis time and has better repeatability in the CCD experiments. Run # 4, 11, 14, 17, 23, and 24 are repetitive runs. The %RSD for the four responses (Rs/t_R) of the four compounds of these repetitive runs are 10% for HBNZ, 5.0% for BNZ, 9.3% for BME, 6.1% for BEE), and 1.1% for total run time (i.e.,t_R), respectively. Thus, the RSD for Rs/t_R in the range of 5-10% is acceptable, and t_R seems relatively small illustrating overall good to excellent repeatability for the CCD experiments.

Once the responses were input into the Design-Expert software, they were fit into different models (mean, linear, 2FI, quadratic, and cubic). These models were then compared by F-test. The most non-aliased model was eventually selected. The regression coefficients for all the factors in the eventually fitted models are shown in Table 4.1. The Prob>F values is the probability of corresponding factors having no effect on the response) are also listed. The factor is considered as significant effect on the response if the Prob>F value is smaller than 0.05. As indicated in Table 4.1, linear models were chosen for Rs/t_R of HBNZ, BME, and BEE; whereas quadratic models were chosen for Rs/t_R and t_R of BNZ.

Table 4.1. Regression coefficient of the coded factors and analysis of variance for the response surface models of Rs/t_R and analysis time for the optimization of MEKC factors

Term	Rs/t_R-HBNZ		Rs/t_R-BNZ		Rs/t_R-BME		Rs/t_R-BEE		t_R[a]	
	Coefficient	Prob>F[b]	Coefficient	Prob>F	Coefficient	Prob>F	Coefficient	Prob>F	Coefficient	Prob>F
Intercept	0.018		0.049		0.033		0.017		44	
F_1 Voltage	0.0036	< **0.01**	0.011	**< 0.01**	0.0082	**< 0.01**	0.0044	**< 0.01**	-14	**< 0.01**
F_2 pH	0.0013	**0.010**	0.0016	**0.053**	0.00026	0.70	0.00044	0.37	2.1	**< 0.01**
F_3 [Surf.]	0.0010	**0.036**	-0.00076	0.32	-0.00055	0.42	0.000095	0.84	3.9	**< 0.01**
F_4 [NH_4OAc]	0.00032	0.50	0.00063	0.41	0.000055	0.94	-0.00037	0.44	4.2	**< 0.01**
F_1 F_2			0.0012	0.21					-0.65	0.36
F_1 F_3			0.0012	0.22					-1.4	0.064
F_1 F_4			0.0022	**0.029**					-1.5	**0.043**
F_2 F_3			0.0010	0.28					0.98	0.18
F_2 F_4			-0.0018	0.071					0.12	0.87
F_3 F_4			0.0011	0.25					1.8	**0.023**
F_1^2			-0.0015	**0.042**					3.9	**< 0.01**
F_2^2			0.0012	0.12					1.7	**< 0.01**
F_3^2			-0.0012	0.12					-0.065	0.90
F_4^2			-0.00068	0.34					0.69	0.21
R^2	0.75		0.94		0.85		0.77		0.98	
Adjusted R^2[c]	0.71		0.89		0.83		0.74		0.97	
Predicted R^2[d]	0.63		0.71		0.79		0.65		0.90	

[a] Migration time of the last peak.
[b] Probability of the null hypothesis being true (the factor has no significant effect on the response) based on the F-test for comparing model variance with residual variance. Any term with $P < 0.05$ is considered significant, and call for rejection of null hypothesis.
[c] Coefficient of determination adjusted for the number of terms in the model.
[d] A measure of the amount of variation around the mean explained by the model, coefficient of determination is based on the predicted residuals from the model.

As shown in Table 4.1, three factors (voltage, buffer pH, and surfactant concentration) and two factors (voltage and and buffer pH) were found significant for Rs/t_R of HBNZ and BNZ, respectively. Their coefficients are all positive, meaning that they are all positively correlated to the response. As expected in a univariate experiments, voltage has a positive effect on the Rs/t_R value because higher voltage usually produces higher peak efficiency and thus improves the chiral resolution. The buffer pH also shows a positive effect. This is because higher pH causes higher ionization of the surfactant. The effect of pH is significant, since its Prob>F value is very close to or less than 0.05. Surprisingly, the concentration of polymeric surfactant is only significant to the Rs/t_R for HBNZ but not for the remaining three benzoin derivatives. Perhaps, the more polymeric chiral surfactant in the running buffer, the better chiral separation is for the analyte with low retention (e.g., HBNZ), but not for highly retained benzoin

compounds (BME and BEE). For BNZ, another significant term is the product of voltage and NH_4OAc concentration (i.e.,$F_1 \times F_4$). This means that the interaction of these two terms is also significant. The square of the voltage (i.e., F_1^2) value for BNZ is significant as well, which means the effect of voltage on the Rs/t_R is not linear (i.e., not directly proportional). However, the products of other factors are not significant for the remaining three benzoin compounds.

Figure 4.5 (A) illustrates the RSM plots for the interaction between voltage and pH and their combined effect on the Rs/t_R of BNZ. It can be observed in this plot that voltage has a much bigger effect than pH since the slope is much steeper along the voltage axis. The Rs/t_R value is lower at a voltage 15 kV than 25 kV indicating a positive correlation between voltage and response. The plot along pH axis is almost flat when voltage is held at 15 kV. However, at 25 kV, it shows a positive trend, which makes the combination of 25 kV and pH 10.0 the highest point on the plot. Similar trend of RSM plots between voltage and [NH_4OAc] is shown in Fig. 4.5 (B). The highest Rs/t_R value in this plot is when voltage is at 25 kV and [NH_4OAc] is 40 mM. The models for Rs/t_R of BME and BEE are very similar to BNZ. Both models are linear model but in both models, the only significant factor is voltage. It is also positively related to the response as the case of HBNZ.

A quadratic model was selected for the total MEKC analysis time (t_R) by *F*-test. All of the first order terms are found significant in this model as indicated in Table 4.1, last column. The coefficient for voltage is negative. This means that higher voltage produces shorter run time. The coefficients for all the other three factors are positive, which suggests a positive correlation between these factors and the total run time. For pH, as mentioned above, increasing the buffer pH from 8.0-10.0 requires titration of NH_4OAC with NH_4OH increasing ionic strength. This is in agreement with the theory that higher BGE causes thinner electric double layer and lower the ζ potential, which consequently causes lower EOF and longer migration time [28-30]. Similarly, surfactant at higher concentration will retain the analytes more because the molecular micelle is a negatively charged and is moving in direction opposite to EOF causing longer elution time. Higher [NH_4OAc] also causes longer t_R due to increase in ionic strength as discussed above. In addition, note that the absolute value of the coefficient for voltage is the most positive among

all the factors (see Table 4.1 row2 vs. rows 3-5). This means that voltage has the biggest influence on migration time.

Fig. 4.5C shows the RSM interaction plots of the two most significant factors (e.g., voltage and polymeric surfactant concentration with higher coefficients) on the t_R. The patterns of the other interaction factors (Table.A1) are similar to the one shown in Fig. 4.5 (C). Note that the surface plot is strongly tilted along the voltage axis. This indicates a significant influence of voltage on t_R. In addition, note that t_R increases when voltage decreases. This suggests an inverse correlation between voltage and migration time as mentioned above. The slope of the plot increases slowly along the surfactant concentration axis form 50-70 mM suggesting a positive correlation between total mixed micelle concentration and total run time. The highest point on this plot is at the combination of voltage 15 kV and a total polymeric surfactant concentration of 70 mM (poly-L-SUCL:poly-L,L-SULV molar ratio 85:15). The R^2, adjusted R^2, predicted R^2 values for each model are tabulated in last few rows of Table 4.1. These values are all close to 1, suggesting a good fit for all models. Table A3 shows the ANOVA results for all the models. In this table, the Prob>F values for all the models are smaller than 0.05. This means that all models are significant, i.e., at least one factor in the model has significant effect on the response. Detailed explanation on how ANOVA are performed can be found in the literature and our earlier work [5, 20, 27].

After the models were validated by ANOVA, a criterion of highest Rs/t_R values for all analytes was input into the DOE software to obtain the optimum values for all factors. The final optimum condition for MEKC was determined to be: voltage 25 kV, buffer pH 10.0, total concentration of polymeric surfactants: 70 mM, concentration of NH_4OAc: 40 mM. Using the aforementioned optimized conditions, the following online optimizations were performed for sheath liquid composition and spray chamber parameters.

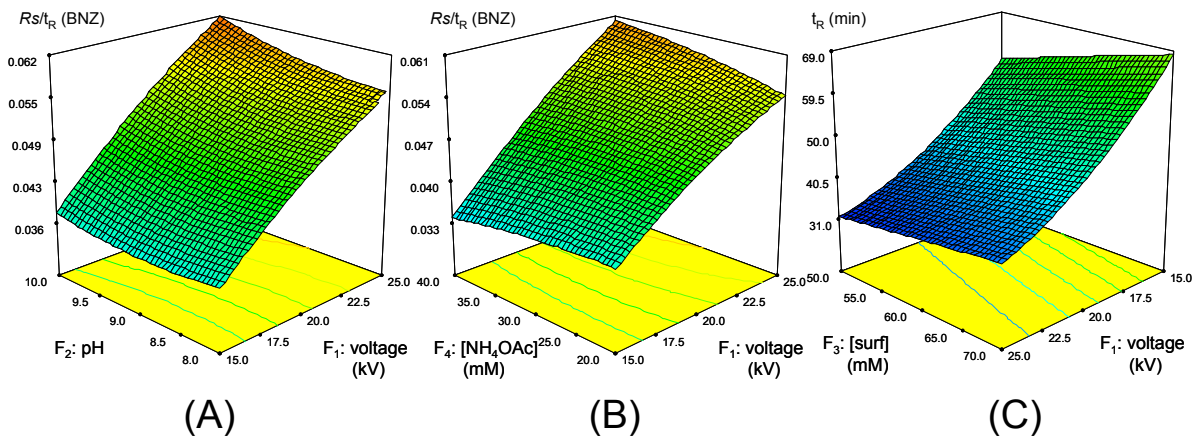

Figure 4.5. Response surface plots for the Rs/t_R of benzoin (A and B) and total retention time (C) in MEKC separation optimization using CCD experiment. Factors which are not analyzed in the plots are held at their mean values (i.e. level 0 in Table A1).

4.3.2.2 Optimization of sheath liquid compositions

Four factors (percentage of MeOH, NH_4OAc concentration, percentage of acetone, and sheath liquid flow rate) were chosen in the CCD optimization of sheath liquid composition (Table A4, Supporting Information). A total of 30 runs were generated by CCD and response are tabulated in Table A5 (Supporting Information). Peak area of each analyte was chosen as the response instead of *S/N*. This is because that peak area was less sensitive to the change of retention time and thus introduces less error than *S/N*.

The regression coefficients for all the sheath liquid parameters are shown in Table 4.2. The models for the peak areas of HBNZ and BNZ are linear; while the models for BME and BEE are constant. For the peak area of HBNZ, two factors, % volume fraction of MeOH and sheath liquid flow rate are found significant (i.e., Prob>*F* value < 0.05). For example, judging from their coefficients %MeOH is positively correlated to the peak area, while flow rate is inversely related. For the peak area of BNZ, %MeOH and sheath liquid flow rate are also the only two significant factors, and they are also positively and negatively related to the response, respectively. For the peak areas of BME and BEE, the model is a

constant. This means in the factor range we explored for the sheath liquid, the peak areas of the two analytes remains unchanged. Therefore, none of the factors are significant for these two compounds.

Table 4.2. Regression coefficient of the coded factors and analysis of variance for the response surface models of peak area for the optimization of sheath liquid

Term	Peak area-HBNZ		Peak area-BNZ		Peak area-BME		Peak area-BEE	
	Coeff	Prob>*F*	Coeff	Prob>*F*	Coeff	Prob>*F*	Coeff	Prob>*F*
Intercept	2.9×10^4		1.7×10^5		5.4×10^5		5.7×10^5	
F_1(MeOH)%(v/v)	5.2×10^3	**0.016**	2.9×10^4	**0.015**				
F_2 [NH_4OAc]	1.0×10^3	0.57	1.3×10^4	0.12				
F_3 Acetone%	-1.7×10^3	0.35	-1.4×10^4	0.19				
F_4 Flow rate	-3.8×10^3	**0.045**	-2.3×10^4	**0.035**				
R^2	0.34		0.40		0.00		0.00	
Adjusted R^2	0.23		0.30		0.00		0.00	
Predicted R^2	0.022		0.09		-0.073		-0.073	

Table A6 shows the ANOVA results of the four models for the optimization of the sheath liquid. The models for the peak area of HBNZ and BNZ are found to be significant. Because the model for BME and BEE is constant, there are no Prob>*F* values for them. The final optimum sheath liquid composition was eventually determined to get the highest peak area for all analytes as follows: 50% MeOH, 5 mM NH_4OAc concentration, 0.5% acetone, sheath liquid flow rate 10 μL/min.

4.3.2.3 Optimization of spray chamber parameters

After optimizing the MEKC and sheath liquid conditions, the optimization of spray chamber parameters were performed. Three parameters, drying gas flow rate (DGF), drying gas temperature (DGT), and vaporizer temperature (VT), were chosen for the CCD. Their levels are listed in Table A7 (Supporting Information). Detailed experimental conditions and responses are shown in Table A8 (Supporting Information). Peak area is again chosen as the response for this experiment. Among the 20 experiments carried out, experiment # 13 was not successful due to current break down. This may be because high vaporizer temperature in this experiment causes significant drying at the capillary outlet resulting in poor grounding.

The regression coefficients for all the peak areas of the four analytes for the optimization of spray chamber parameters are listed in Table 4.3. All four models for the benzoin derivatives are quadratic. For the peak area of HBNZ, all the factors (except DGF) are found to be significant (i.e., Prob>*F* value < 0.05). On the other hand, in case of BNZ and BME two factors and one factor, respectively, whereas for BEE none of the factors were significant. Their R^2 values are all in acceptable range as shown in the bottom row of this table.

Table 4.3. Regression coefficient of the coded factors and analysis of variance for the response surface models of peak area for the optimization of spray chamber parameters

Term	Peak area -HBNZ		Peak area -BNZ		Peak area -BME		Peak area -BEE	
	Coeff	Prob>*F*	Coeff	Prob>*F*	Coeff	Prob>*F*	Coeff	Prob>*F*
Intercept	4.2×10^4		2.3×10^5		5.1×10^5		5.7×10^5	
F_1 DGF	3.6×10^3	0.23	-8.9×10^3	0.60	-7.0×10^4	0.073	-7.7×10^4	0.056
F_2 DGT	-7.5×10^3	**0.025**	-2.1×10^4	0.24	-5.1×10^4	0.18	-5.4×10^4	0.16
F_3 VT	2.2×10^4	**0.001**	-3.4×10^4	0.14	-5.7×10^3	0.90	-3.0×10^4	0.51
F_1 F_2	-8.3×10^3	**0.048**	-7.6×10^3	0.73	-1.3×10^4	0.79	-2.9×10^3	0.95
F_1 F_3	1.1×10^4	**0.011**	9.2×10^3	0.68	5.2×10^4	0.28	7.4×10^4	0.14
F_2 F_3	-9.8×10^3	**0.024**	-1.1×10^4	0.62	-2.3×10^4	0.62	-2.8×10^4	0.55
F_1^2	-1.0×10^4	**0.006**	-5.2×10^4	**0.012**	-5.6×10^4	0.14	-6.5×10^4	0.098
F_2^2	2.2×10^3	0.45	5.7×10^3	0.74	1.2×10^4	0.73	1.7×10^4	0.65
F_3^2	3.8×10^3	0.31	-5.2×10^4	**0.037**	-1.2×10^5	0.24	-1.1×10^5	**0.040**
R^2	0.91		0.74		0.68		0.69	
Adjusted R^2	0.81		0.49		0.37		0.39	
Predicted R^2	0.24		-0.41		-0.63		-0.56	

Fig. 4.6 illustrates the interactions of all three factors and their combined effect on the peak area of HBNZ. Fig. 4.6 (A) is a saddle shaped surface. Along the DGF axis, the peak area grows higher when DGF increases from 4.0 to 6.0 L/min with a convex curvature. Along the DGT axis, on the other hand, the peak area gets higher when DGT decreases form 200 to 100 ^oC with a concave curvature. The maximum peak area found in this plot is at DGF at 5.5 L/min and DGT at 100 ^oC. Fig. 4.6 (B) shows the relation between DGF and VT. The surface plot shows that peak area gets higher with an increasing DGF and VT. This provided the highest point at DGF of 6.0 L/min and VT at 200 ^oC. Fig. 4.6 (C) illustrates the interaction between DGT and VT. Along the VT axis, the peak area is continuously increased when VT increases from 100 to 200 ^oC. This shows a positive correlation between VT and peak area. Along the

DGT axis, the surface plot is almost flat at VT 100 °C, but shows strong negative correlation at VT 200 °C. Therefore, the maximum value of peak area in this plot can be found at VT 200 °C and DGT 100 °C.

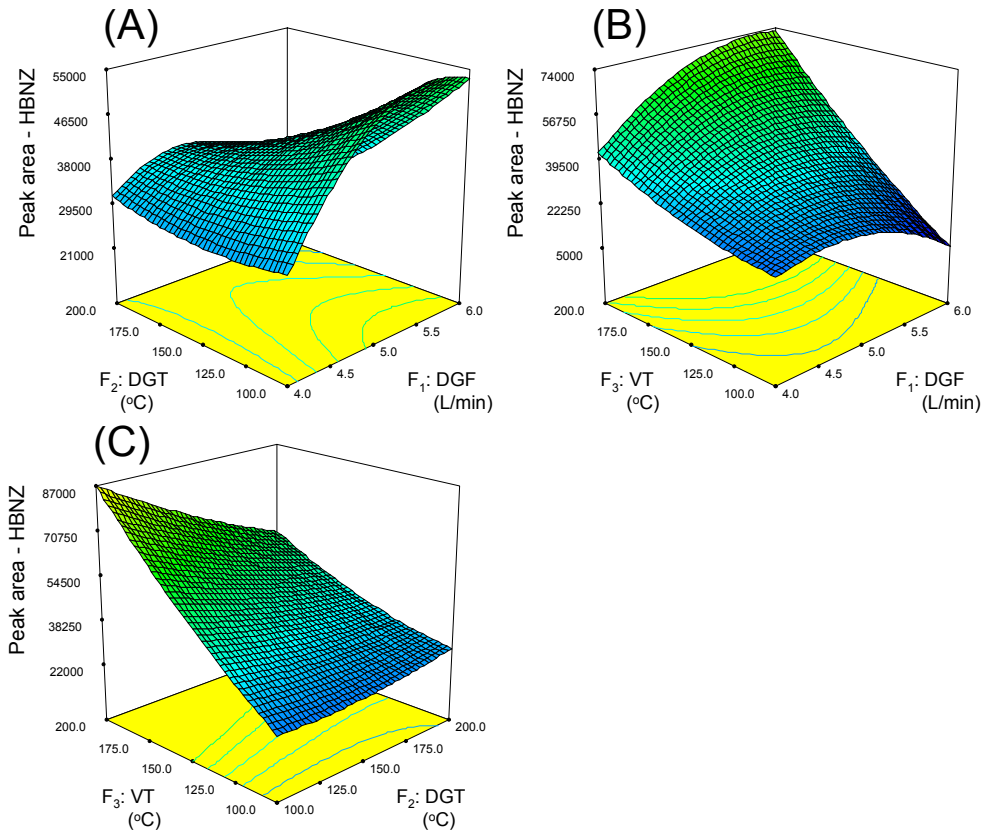

Figure 4.6. Response surface graphs for hydrobenzoin in spray chamber condition optimization using CCD experiment. Factors which are not analyzed in the plots are held at their mean values (i.e. level 0 in Table A7).

Fig. 4.7A shows the RSM plots for the peak area of BME. Note that the shapes of the RSM plots for the interaction factors for BME shows a different shape than the one observed for HBNZ in Fig. 4.6A. The highest point of this plot is at DGF 4.5 L/min and DGT 100 °C. Fig. 4.7 (B) shows a dome shaped surface plot with a highest point at DGF 4.5 L/min and VT 145 °C, which is again significantly different from HBNZ. Another saddle shaped surface plot is shown in Fig. 4.7 (C). A convex curvature can be observed along the VT axis with a highest point at 155 °C. A slight concave but upward trend can be found along the DGT axis when DGT is decreasing from 200 to 100 °C. Therefore, the overall highest

point in this plot is at DGT 100 ^{o}C and VT 155 ^{o}C. The RSM plots for BNZ and BEE are very similar to those of BME (data not shown).

ANOVA data for models used in the optimization of spray chamber parameters is shown in Table A9 (Supplementary Information). It can be found that the model for the peak area of HBNZ is significant. For BNZ, it is almost significant. On the other hand, for BME and BEE, the models are not significant. The overall optimum spray chamber parameters determined for the simultaneous analysis of all four benzoin derivative by the models are: DGF at 5.0 L/min, DGT at 100 ^{o}C, and VT at 176 ^{o}C.

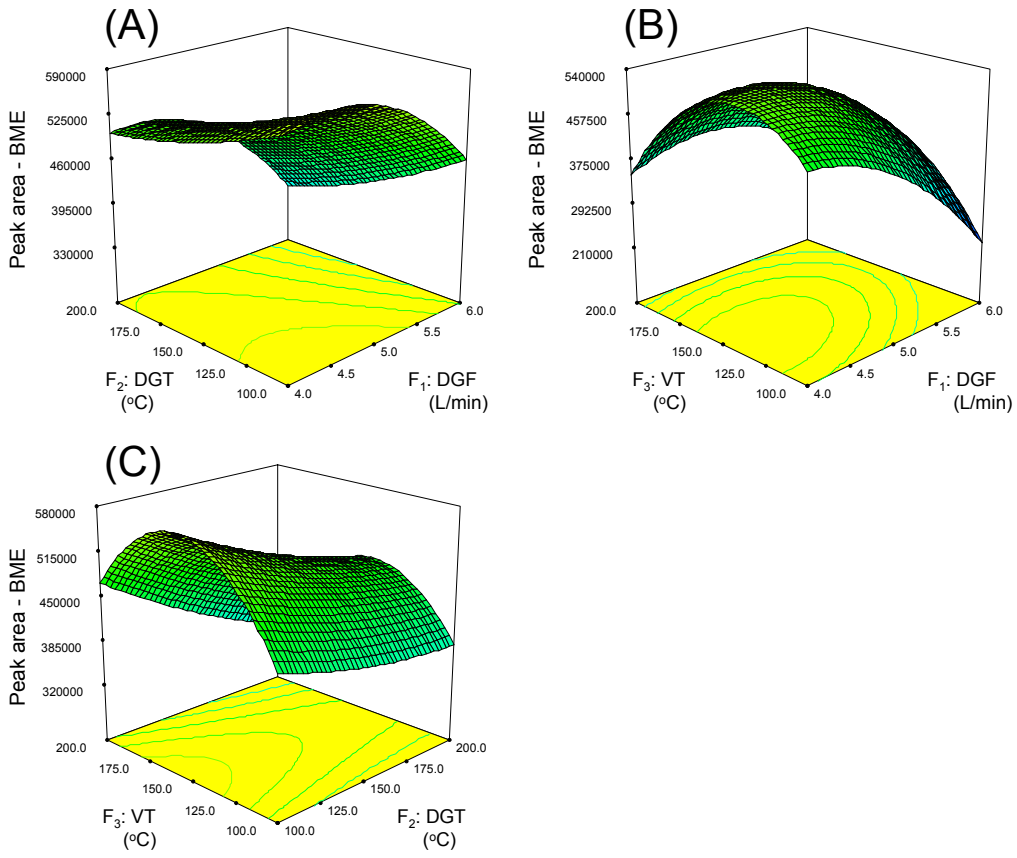

Figure 4.7. Response surface graphs for benzoin methyl ether in spray chamber condition optimization using CCD experiment. Factors which are not analyzed in the plots are held at their mean values (i.e. level 0 in Table A7).

4.3.2.4 Overall optimum condition for MEKC-APPI-MS

The final overall optimum conditions for the chiral MEKC-APPI-MS of benzoin derivatives are the combinations of the optimized conditions aforementioned. The best conditions are: For MEKC: voltage 25 kV, buffer pH 10.0, total concentration of polymeric surfactant: 70 mM (poly-L-SUCL:poly-L,L-SULV molar ratio 85:15), concentration of NH_4OAc: 40 mM. For sheath liquid: MeOH%: 50%, NH_4OAc concentration: 5.0 mM, acetone 0.5 %:(v/v), flow rate: 10 mL/min. For spray chamber: DGF: 5.1 L/min, DGT: 100 ^oC, and VT: 176 ^oC. Experiment at the aforementioned optimized conditions was performed and the results were compared with the values predicted by the model. The comparison is listed in Table 4.4. As shown in this table, the % errors between experimental and predicted values for all the responses for Rs/t_R for HBNZ and BNZ are all reasonably small, whereas for the peak area of BME and BEE have significantly high error. This shows an overall good fit for all the models, and thus an acceptable predictability for shorter retained benzoin compounds but not for longer retained benzoin compounds.

Table 4.4. Comparison of the model predicted values vs. the experimental values

	HBNZ		BNZ		BME		BEE		t_R (min)
	Rs/t_R	Peak area	Rs/t_R	Peak area	Rs/t_R	Peak area	Rs/t_R	Peak area	
Predicted	0.025	70514	0.064	267999	0.041	546381	0.021	603177	46.0
Experimental	0.024	53170	0.052	347734	0.036	902995	0.023	1193080	47.5
% error	4.0	25	19	30	12	65	9.5	98	3.3

Compared to the typical APPI-MS conditions used in ref. 6 (VT: 300 ^oC, DGT: 150 ^oC, DGF: 3 L/min, nebulizer pressure: 25 psi, sheath liquid flow rate: 15 mL/min) and ref 13 (VT: 330 ^oC, DGT: 250 ^oC, DGF: 1 L/min, nebulizer pressure: 10 psi, sheath liquid flow rate: 50 mL/min, capillary voltage: +800 V), the conditions we used are mild with lower temperatures (for both VT and DGT) due to the thermal instability of our analytes. In addition, the nebulizer pressure reported in this work is also significantly lower due to nature of chiral MEKC runs, which requires lower nebulizer pressure to separate two closely eluting optical isomers of each benzoin. Hence, the APPI-MS ionization conditions are both analytes dependent and CE modes used for separation.

4.3.2.5 Comparison of MEKC-UV-MS and MEKC-APPI-MS

Because all the experiments in this study were all tandem UV-MS runs, the resolution and *S/N* between UV and MS were also compared. As shown in Figure 4.8, MEKC-APPI-MS gives much higher sensitivities (1.2-11.0 folds) than MEKC-UV for the analysis of all four benzoin derivatives. In addition, the chiral resolution of the last three benzoin derivatives were also higher for BNZ, BME and BEE but not for HBNZ. However, this high resolution in MEKC-APPI-MS was obtained at the expense of longer retention time.

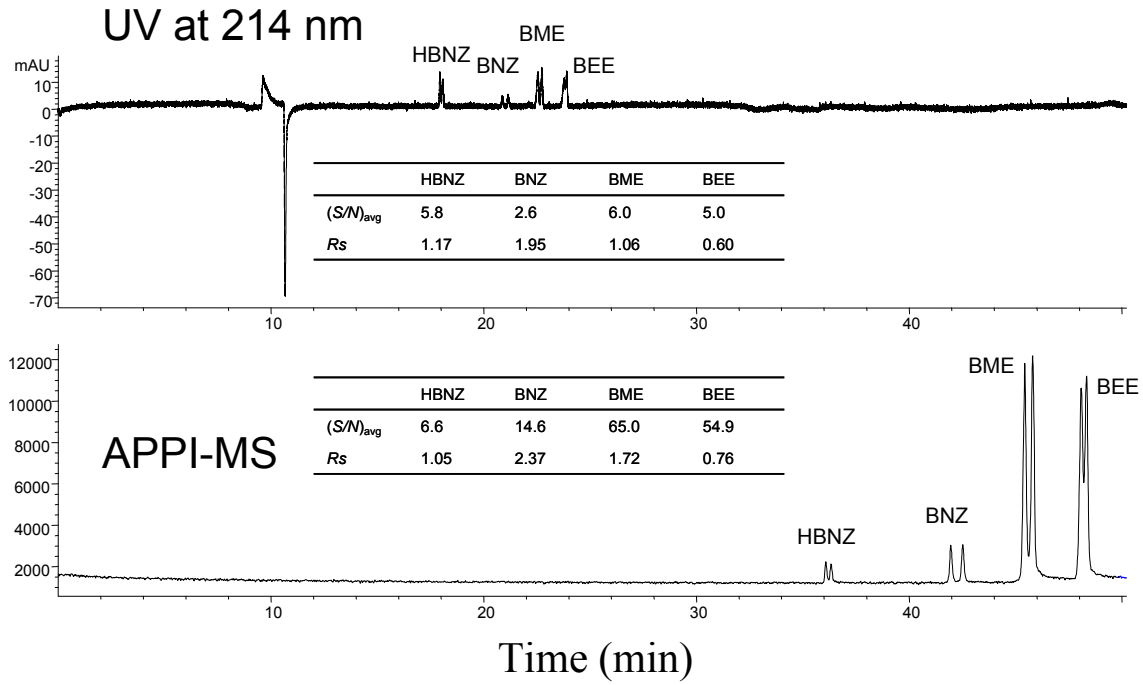

Figure 4.8. Representative electropherograms showing the comparison of CMEKC-UV vs. CMEKC-APPI-MS. Experimental conditions: 120 cm × 50 μm i.d. fused silica capillary; 55 mM NH_4OAc, pH 8.0, with 50 mM poly-L,L-SULV, 15 mM poly-L-SUCL; +25 kV, 20 ºC; analyte: 1 mg/mL benzoin derivatives in 50/50 MeOH/H_2O, injected at 5 mbar, 10 sec; spray chamber parameters: drying gas flow rate 5 L/min; nebulizer pressure 5 psi; drying gas temperature 150 ºC; vaporizer temperature 150 ºC; capillary voltage 2000V; fragmentor 80 V, gain 3; SIM at m/z = 195, 197; UV absorbance at 214 nm; sheath liquid: 5 mM NH_4OAc in 50/50 MeOH/H_2O, 0.5% Acetone; flow rate 7.5 μL/min.

4.4 Concluding remarks

A mixed molecular micelle of poly-L-SUCL and poly-L,L-SULV was useful as the chiral pseudostationary phase for the simultaneous separation and high throughput optimization of all four benzoin compounds in MEKC-APPI-MS. A univariate approach was used to optimize the MEKC conditions, the sheath liquid composition, and the spray chamber parameters. Next, three set of full factorial CCD experiments were carried out separately after obtaining information on the optimization range from the univariate experiments. From the multivariate experiments, models were generated and RSM plots were created to evaluate the relationship between the MEKC-APPI-MS parameters and their effects on the responses. The final optimum conditions were also calculated from the models and runs were performed under these conditions. By comparing the experimental and theoretical data from these runs, a good fitness of the models can be seen for shorter retained benzoin compounds. In addition, significantly higher *S/N* and higher resolution can be obtained with MEKC-APPI-MS compared to MEKC-UV method.

Therefore, in this study we successfully demonstrated that molecular micelles can be used in APPI-MS and has potential to produce excellent sensitivity for select chiral molecules. In particular, when trying to separate non-polar, non-ionic chiral compounds the use of molecular micelles open up the possibility of performing APPI-MS with high sensitivity compared to APCI-MS or ESI-MS.

References

[1] Shamsi, S. A., *Anal. Chem.* **2001**, *73*, 5103-5108.

[2] Palmer, C. P., Terabe, S., *Anal. Chem.* **1997**, *69*, 1852-1860.

[3] Shamsi, S. A., Valle, B. C., Billiot, F., Warner, I. M., *Anal. Chem.* **2003**, *75*, 379-387.

[4] Hou, J., Zheng, J., Rizvi, S. A. A., Shamsi, S. A., *Electrophoresis* **2007**, *28*, 1352-1363.

[5] He, J., Shamsi, S. A., *J. Sep. Sci.* **2009**, *32*, 1916-1926.

[6] Mol, R., de Jong, G. J., Somsen, G. W., *Electrophoresis* **2005**, *26*, 146-154.

[7] Himmelsbach, M., Haunschmidt, M., Buchberger, W., Klampfl, C. W., *Anal. Chem.* **2007**, *79*, 1564-1568.

[8] Robb, D. B., Covey, T. R., Bruins, A. P., *Anal. Chem.* **2000**, *72*, 3653-3659.

[9] Cai, S.-S., Hanold, K. A., Syage, J. A., *Anal. Chem.* **2007**, *79*, 2491-2498.

[10] Cai, Y., Kingery, D., McConnell, O., *Rapid Commun. Mass Spectrom.* **2005**, *19*, 1717-1724.

[11] Nilsson, S. L., Andersson, C., Sjöberg, P. J. R., Bylund, D., Petersson, P., Jörntén-Karlsson, M., Markides, K. E., *Rapid Commun. Mass Spectrom.* **2003**, *17*, 2267-2272.

[12] Zheng, J., Shamsi, S. A., *Anal. Chem.* **2006**, *78*, 6921-6927.

[13] Schappler, J., Guillarme, D., Prat, J., Veuthey, J.-L., Rudaz, S., *Electrophoresis* **2007**, *28*, 3078-3087.

[14] Schappler, J., Guillarme, D., Rudaz, S., Veuthey, J.-L., *Electrophoresis* **2008**, *29*, 11-19.

[15] Hommerson, P., Khan, A. M., de Jong, G. J., Somsen, G. W., *J. Chromatogr. A* **2008**, *1204*, 197-203.

[16] Hommerson, P., Khan, A. M., Bristow, T., Harrison, M. W., de Jong, G. J., Somsen, G. W., *Rapid Commun. Mass Spectrom.* **2009**, *23*, 2878-2884.

[17] Celibi, N., Yildiz, N., Demir, A., Calimli, A. *J.of Supercritical fluids*. **2007**, *41,* 386-390.

[18] Olceroglu, A. Y., Calik, P., Yilmaz, L. *Desalination,* **2000**, 206, 464-465].

[19] Mwongela, S., Akbay, C., Zhu, X., Collins, S., Warner, I. M., *Electrophoresis* **2003**, *24*, 2940-2947.

[20] Tarus, J., Agbaria, R. A., Morris, K., Billiot, F. H., Williams, A. A., Chatman, T., Warner, I. M., *Electrophoresis* **2003**, *24*, 2499-2507.

[21] Otsuka, K., Mikami, C., Terabe, S., *J. Chromatogr. A* **2000**, *887*, 457-463.

[22] Ferreira, S. L. C., Bruns, R. E., da Silva, E. G. P., dos Santos, W. N. L., Quintella, C. M., David, J. M., de Andrade, J. B., Breitkreitz, M. C., Jardim, I. C. S. F., Neto, B. B., *J. Chromatogr. A* **2007**, *1158*, 2-14.

[23] Wang, J., Warner, I. M., *Anal. Chem.* **1994**, *66*, 3773-3776.

[24] Ding, W., Fritz, J. S., *J. Chromatogr. A* **1999**, *831*, 311-320.

[25] Rizvi, S. A. A., Shamsi, S. A., *Electrophoresis* **2003**, *24*, 2514-2526.

[26] Kauppila, T. J., Kuuranne, T., Meurer, E. C., Eberlin, M. N., Kotiaho, T., Kostiainen, R., *Anal. Chem.* **2002**, *74*, 5470-5479.

[27] He, J., Shamsi, S. A., *J. Chromatogr. A* **2009**, *1216*, 845-856.

[28] Schwer, C., Kenndler, E., *Anal.l Chem.* **1991**, *63*, 1801-1807.

[29] Basso, E., Marotta, E., Seraglia, R., Tubaro, M.; Traldi, P., *J. Mass Spectrom.* **2003**, *38*, 1113-1115.

[30] Rizvi, S. A. A., Simons, D. N., Shamsi, S. A., *Electrophoresis* **2004**, *25*, 712-722.

Chapter 5

Amino Acid Bound Surfactants: A New Synthetic Family of Polymeric Monoliths Open Up Possibilities for Chiral Separations in Capillary Electrochromatography

By combining a conventional crosslinker and polymerization techniques, a new one-pot, synthesis method for the generation of novel class of polymerizable amino acid surfactants containing acryloyl amide tail, carbamate linker and leucine head group of different chain length is realized. The method promises to open up the discovery of new amino-acid based polymeric monoliths for chiral separations and illustrate the possibility of enhanced chemoselectivity for simultaneous enantioseparations in capillary electrochromatography (CEC). The potential of coupling this surfactant bound monolithic column for CEC with mass spectrometry detection is demonstrated.

5.1 Introduction

Amino acid based surfactant synthesized from various amino acid head groups, hydrocarbon tails, amino acid linkers and optical configurations are a uniquely tunable family of functional synthetic chiral materials.[1-3] They are generally designed to contain terminal double bond to constitute covalently stabilized molecular micelles when dissolved and polymerized in aqueous solutions. With 15 years of work, the palette of useable acyl and alkenoxy based chiral molecular micelles has grown in breadth nuance, and their number of applications for chiral separations in micellar electrokinetic chromatography (MEKC) and MEKC coupled to mass spectrometry (MS) has increased. Still the number of research groups tinkering with these amino acid based surfactant polymers is relatively small. The spectrum of new synthetic form of chiral materials must broaden if amino acid based polymers are to fulfill their considerable potential in separation science.

Unlike the success of chiral molecular micelles, design and discovery of new amino-acid based chiral surfactants which can form chiral nanoparticles and chiral polymeric monoliths to be used in capillary electrophoresis separations until now has been challenging. However, this is about to change. Priego-Capote and colleagues reported an elegant approach to achieve chiral nanoparticles in which miniemulsion polymerization was performed for the synthesis of molecularly imprinted MIP nanoparticles.[4] Using amino acid surfactant, sodium *N*-undecenoyl glycinate (SUG) as functional monomer they developed MIP-NPs with relatively narrow range of particle size (30-150 nm). The long standing challenge of peak tailing of later eluting enantiomers was eliminated and nanoparticles provided

fast separation with symmetrical peaks shapes of later eluting enantiomer of propranolol. Obtaining chiral monoliths in which amino acid surfactants are bound to achiral monolithic backbones provide an exciting opportunity to study chiral recognition on a column surface. Although several class of chiral materials (cyclodextrins, vancomycin, alkaloids, cellulose)[5-11] have been polymerized to generate polymer-based monolithic columns for capillary electrophoresis, design and discovery of new families of polymeric monolithic columns derived from new synthetic chiral monomers is warranted.

In the present study, the discovery of a novel synthetic chiral polymeric monolith derived from acryloylamide tail, carbamate linker and amino acid head group is demonstrated for chiral separations in capillary electrochromatography (CEC). Three polymerizable leucine based carbamate chiral surfactants with 8, 10, and 12 carbon alkyl chain (namely sodium 8-acrylamidooctenoxy carbonyl-L-leucinate (SAAOCL), sodium 10-acrylamido-decenoxy carbonyl-L-leucinate (SAADCL), and sodium 12-acrylamidododecenoxy carbonyl-L-leucinate (SAADoCL)) were synthesized (Scheme 5.1). With the polymeri- zable acrylamide tail group, the acid form of the surfactants was conveniently copolymerized with ethylene glycol dimethacrylate (EDMA) in a ternary porogenic solvent system to form a chiral monolith. The obtained mixed-mode anionic monolithic columns were characterized and evaluated for enantioseparation of several cationic drugs in CEC. To the best of our knowledge, this is the first study, which has described the use of chiral surfactant bound monolithic materials for CEC. It is anticipated that the successful application of surfactant-bound monolithic material as chiral CEC columns could substantially reduce the cost of using particle-based chiral HPLC columns in pharmaceutical laboratories for analytical-scale chiral separations. Furthermore, for the application of CE-MS, the use of moving chiral pseudophase (in the micellar form) in the CE running buffer is challenging because of signal suppression by chiral micelles in ESI-MS. Therefore, the use of surfactant bound monolithic column could provide us with a unique opportunity to develop CEC-MS method for sensitive detection of chiral compounds.

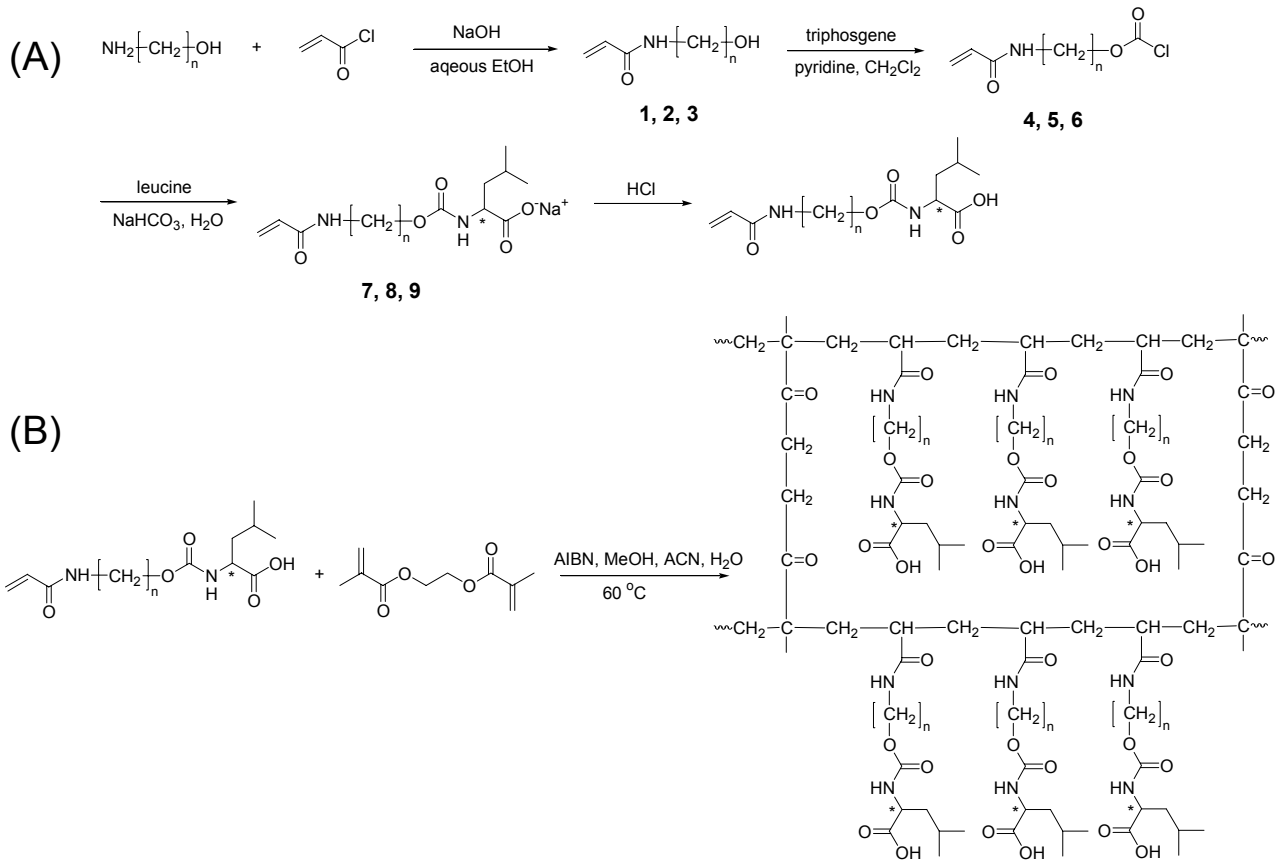

Scheme 5.1. Synthesis of polymerizable monoliths: poly-(AAOCL-*co*-EDMA), poly-(AADCL-*co*-EDMA), or poly-(AADoCL-*co*-EDMA) monoliths with n = 8, 10, or 12.

5.2 Experimental Section

5.2.1 Chemicals and Materials.

2,2′-azobis(2-methylpropionitrile) (AIBN), 3-(trimethoxy-silyl)propyl methacrylate (γ-MAPS), glycidyl methacrylate (GMA), β-cyclodextrin (β-CD), 2-acrylamido-2-methyl-1-propanesulphonic acid (AMPS) and acryloyl chloride were purchased from Sigma-Aldrich (St. Louis, MO). 10-amino-1-decanol, 8-amino-1-octanol, 12-amino-1-dodecanol, and triphosgene were obtained from TCI-America (Portland, OR). Ethylene glycol dimethacrylate (EDMA) purchased from Sigma-Aldrich was distilled to remove inhibitor before its usage. The HPLC grade acetonitrile (ACN), methanol (MeOH), triethylamine (TEA) and 7.5 M ammonium acetate (NH_4OAc) aqueous solution, dimethyl sulfoxide (DMSO), benzene, toluene, ethylbenzene, propylbenzene, butylbenzene, (±) propranolol, (±) atenolol, (±) metoprolol, (±)

alprenolol, (±) pindolol, (±) pseudoephedrine, (±) ephedrine, (±) synephrine, (±) norephedrine, (±) norepinephrine, (±) isoproterenol, and (±) *N*-methyl ephedrine were purchased from Sigma-Aldrich (St. Louis, MO). Other chemicals used for the synthesis of surfactant monomer, such as pyridine, anhydrous Na_2SO_4, L-leucine, dichloromethane, sodium bicarbonate, sodium hydroxide, hydrochloric acid, and ethyl acetate were also purchased from Sigma-Aldrich. Ethanol (HPLC grade) was purchased from Fisher Scientific (Fair Lawn, NJ). Triply deionized water (18.2 MΩcm) was generated in the laboratory using Barnstead Nanopure II Water System (Dubuque, IA). All the chemicals have the purity of 98% or higher and were used as received without further purification unless specifically noted.

5.2.2 Synthesis of Surfactants

The synthesis of acrylamido alkoxy carbonyl-L-leucinate (SAACL) surfactants with three different chain lengths is shown in Scheme 5.1. First, 4.4g, 5.1g, or 6.0g (0.03 moles) each of 8-amino-1-octanol, 10-amino-1-decanol, or 12-amino-1-dodecanol, respectively were dissolved in 125 mL of ethanol and 18 mL of triply deionized H_2O in a 500 mL round bottom flask. Next, 7.2 g (0.09 mol) of 50% wt/wt NaOH solution was added carefully (not dropwise) to the stirring solution of each alcohol followed by dropwise addition of 4.0 mL (0.05 moles) of neat acryloyl chloride. Each of the above solution was stirred at 10 ^oC for 3 h (in ice bath). The reaction mixture of each solution was acidified with 6 M HCl to pH ~2, the excess acryloyl chloride and the residual solvent was rotoevaporated to yield dry white solid products **1-3.** Next, 100 mL of triply deionized water was added to wash the precipitates (8-, 10- and 12-acrylamidoalkanol), which were collected after filtration, followed by recrystallization using aqueous ethanol. Recrystallization with aqueous ethanol was generally performed by first adding 50 mL of hot ethanol followed by addition of ~10 mL of triply deionized water and refrigerating the clear solution at 4^oC overnight. Next day, the frozen solid product was washed and filtered with 20 mL of water under vacuum.

The synthesis of chloroformate of the acrylamidoalkanol was similar to the one used in the snynthesi of alkenoxy amino acid-based chiral surfactants reported previously by our group and others.[2, 12] Briefly, about 0.60, 0.70 and 0.77 g (0.003 mol) of 8-, 10-and 12 acrylamidoalkanol and 0.3 g (0.001 mol)

of triphosgene were dissolved in 200 mL of dichloromethane in a 500 mL round bottom flask. To each of this solution, 0.25 g (0.003 mol) of pyridine (dissolved in 50 mL of dichloromethane) was added dropwise. Each of the reaction mixture was stirred for 96 h at room temperatue, acidified with 6 M HCl to pH ~2 and washed with triply deionized H_2O in an extraction funnel three times. Each time, 200 mL of triply deionized H_2O was used. After each extraction, the top aqueous layer was discarded. The bottom dichloromethane layer was collected, dried by anhydrous Na_2SO_4, and rotoevaporated to yield 0.71g, 0.79g, and 0.85 g (0.0027 mol) of chlorformate derivative of 8-, 10- and 12-acrylamidoalkanol **(4-6).** To each of the synthesized chloroformate, 100 mL of triply deionized water was added containing equimolar (i.e., 0.027 mol) of L-leucine and NaOH. The reaction solution was stirred vigorously for 2 h, after which, it was acidified to pH ~1 by 6 M HCl and extracted three times with 200 mL aliquots of dichloromethane. The final bottom dichloromethane layer was then dried by anhydrous Na_2SO_4 and rotoevaporated. The resulting acid form of 8-acrylamidooctenoxy carbonyl-L-leucinate (AAOCL),10-acrylamidodecenoxy carbonyl-L-leucinate(AADCL), or 12-acrylamidododecenoxy carbonyl-L-leucinate (AADoCL) was dried, weighed and dissolved in equimolar amount of $NaHCO_3$ in ~200 mL triply deionized water to form the corresponding sodium salt of each surfactant. The salt solution was extracted once by ethyl acetate to remove the organic impurities. The bottom aqueous layer was collected and lyophilized to obtain SAAOCL, SAADCL, or SAADoCL **(7-9).**

The lyophilized salt form of each aforementioned surfactant was characterized by ESI-MS, elemental analysis, and NMR. The NMR spectra were recorded on a Bruker 400 MHz instrument. All NMR samples were dissolved in D_2O. Electrospray ionization (ESI) mass spectrometry (MS) analysis was performed on an Agilent 1100 series single quadrupole mass spectrometer. For ESI-MS analysis each of the surfactant was dissolved in 50/50 (v/v) MeOH/H_2O and direct infusion was performed using a CE nebulizer. The elemental analysis (Table B1), mass spectra (Figure B1-B6), and ^1H NMR spectra (Figure B7-B9) for each surfactant are attached in appendix. Before each surfactant can be polymerized into monolith, it was transformed to acid form to yield AAOCL, AADCL, or AADoCL. For example, 0.5 g of surfactant salt was first dissolved in ~100 mL of H_2O. The solution was then acidified by 6 M HCl to

pH ~1, followed by extractions with three aliquots of 300 mL ethyl acetate. The final top ethyl acetate layers were collected, dried by anhydrous Na_2SO_4, and rotoevaporated to yield the acid forms (viscous liquid) of the surfactant with various chain lengths.

5.2.3 Preparation of Monolithic Columns

A 40 cm long fused silica capillary (360 μm o.d., 100 μm i.d., Polymicro Technologies, Phoenix, AZ) was flushed under vacuum with acetone and 1 M NaOH for 15 min each. The capillary was filled with 1 M NaOH, both ends were sealed with two rubber septa and heated at 100 ^oC for 2 h in a GC oven. Next, the capillary was flushed with triply deionized water, 1 M HCl, triply deionized H_2O, and acetone for 15 minutes each under vacuum. A solution of γ-MAPS (30%, v/v in acetone) was then filled through the capillary under vacuum. The filled capillary was once again sealed with rubber septa and kept at 50 ^oC for 14 h in a GC oven. Next, the unreacted γ-MAPS solution was removed by flushing the capillary under vacuum using acetone for 30 min. The vinylized capillary was eventually dried by nitrogen for 3 h at 70 ^oC in a GC oven.

The polymerization process of monolithic columns is similar to that described in our previous publication.[13] A typical procedure for making AAOCL, AADCL, or AADoCL monolithic columns is described as follows. First, 15 mg of AAOCL, AADCL, or AADoCL and 0.5 mg of AIBN were dissolved in a mixture containing various compositions (% wt/wt) of dimethyl ether, ACN, MeOH, and H_2O as porogens (see Table B2 for representative calculations). To each of the porogen mixture, 14.3 μL of EDMA was added. The final polymerization solution was ultrasonicated for 30 min and filled into the pretreated capillary using a hand held syringe. Typically, in the preparation of CEC-UV column, 30 cm out of 40 cm of the pretreated capillary was filled. The column was then sealed with rubber septum and was kept at 60 ^oC to polymerize. After 20 h of polymerization, the column was flushed with ACN for ~2 h to remove the unreacted monomers. The on-column detection window was then burned in the empty segment of the capillary adjacent to the packed monolithic bed and 8.5 cm to the outlet end of the capillary for CEC-UV experiment. The column was eventually cut to obtain a total length of 33.5 cm with

a monolithic portion of 25 cm (from the inlet end). The monolithic capillary was conditioned for 24 h with running buffer before use.

For CEC-MS experiment, a capillary of 60 cm long (150 μm i.d.) was first vinylized using the same procedure discussed above. A polymerization mixture with AADCL as monomer (prepared as described above) was then filled into the capillary. A section of ~35 cm from one end of the capillary was usually filled. The two ends of the capillary were then sealed with rubber septa. Next, the whole column was kept in a GC oven (60 ^{o}C) for 20 h. After polymerization, the column was cut to 55 cm long (with 30 cm monolithic bed), flushed with ACN for 2 h, followed by flushing with mobile phase for 24 h before CEC-MS experiment.

5.2.4 Morphology and Surface Area Measurements

A Hitachi X-650 (Hitachi, Japan) scanning electron microscope (SEM) was used to characterize the microscopic morphology of the monolithic columns. The SEM was operated at 7.5 kV; the filament current was set at 40 mA. Monolithic columns samples were cut to 2 mm in length and stuck on an aluminum stub by double-sided carbon tape. The samples were then sputter-coated with gold/palladium alloy with a SPI sputter (SPI supplies Division of Structure Probe, West Chester, PA) for 1 min.

The surface area of the monolithic samples was obtained by nitrogen adsorption experiments. Samples for the nitrogen adsorption experiments were prepared in 1.5 mL plastic centrifuge tubes in parallel with the monolithic columns. The monolith was crushed into powder; further cleaned with Soxhlet extraction (MeOH as solvent) for 24 hours and dried at 70 ^{o}C for 24 hours under vacuum. The surface area was calculated via a multi-point BET method applied to nitrogen physisorption data obtained on a Micromeritics Tristar 3020 instrument (Micromeritics Instrument, Norcross, GA). All samples were first heated under vacuum at 70 ^{o}C for 24 hours to remove physisorbed water before being analyzed. The 59 point adsorption/desorption isotherm was then obtained at liquid nitrogen temperatures.

5.2.5 CEC Instrumentation

An Agilent CE system (Agilent Technologies, Palo Alto, CA), which is equipped with an auto sampler, 0-30 kV power supply, and a diode-array UV detector was used to carry out all the CEC experiment. Agilent 3D-CE ChemStation software (Rev. A. 08.04) was used for data acquisition and analysis. A series III isocratic HPLC pump (Lab Alliance, State College, PA) was used to flush and condition the column. An Ultra-Plus II micro-HPLC system (Micro-Tech Scientific Inc., Fontana, CA) was used for the measurement of porosity and permeability.

5.2.6 CEC conditions

Various parameters were used to optimize the CEC conditions for the monolithic surfactant-bound columns as following: voltage was varied in the range of 5-15 kV; high pressure of 6 bar was applied at both ends of the column; column temperature was 20 ^{o}C. The mobile phase, containing a mixture of 50% – 70% ACN and 30%-50% aqueous buffer containing 5 mM NH_4OAc, 0.3% -0.7% TEA (pH 5.0); UV detection wavelength, 200 nm for all the analytes. A typical aqueous buffer with 5 mM NH_4OAc, 0.5% TEA (pH 5.0) was made by dissolving 66.7 μL of 7.5 M NH_4OAc solution into ~80 mL triply deionized water. To this solution, 0.5 mL of TEA was added. The solution was adjusted to pH 5.0 with acetic acid and transferred to a 100 mL volumetric flask to be diluted with triply deionized water to the final volume of 100 mL. The final mobile phase was prepared by mixing the aqueous solution and ACN to the desired ratio. For example, in the final mobile phase of a typical mixture of 70% ACN and 30% aqueous buffer (containing 5 mM NH_4OAc and 0.5% TEA), the final concentration of NH_4OAc is 1.5 mM; the final concentration of TEA is 0.15%. Before a monolithic column was used in CEC runs, voltage conditioning was performed to equilibrate the column at an increment of +2 kV, +5 kV, +7 kV, and +10 kV. Analyte stock solutions were prepared at 8 mg/mL by dissolving solid analyte into pure ACN. Working analyte solutions were prepared at 1 mg/mL by diluting the analyte stock solution into the mobile phase. Injections were performed electrokinetically at 3 kV, 2 sec.

5.2.7 Calculations

Resolution (*Rs*), efficiency (*N*), and selectivity (α) were calculated by the Chemstation software. Resolution was calculated using the following equation:

$$Rs = \frac{1.18 \times (t_{R2} - t_{R1})}{W_{(1/2)1} + W_{(1/2)2}} \qquad (1)$$

where t_{R1} and t_{R2} are the retention times of the first and second eluting peaks. $W_{(1/2)1}$ *and* $W_{(1/2)2}$ are the peak widths at half height for first and second eluting enantiomer.

Capacity factor (*k'*) was calculated by the following equation:

$$k' = \frac{t_R - t_m}{t_m} \qquad (2)$$

where t_R and t_m are the retention times of the analyte and the dead time marker, respectively.

The porosity of the monolithic columns was calculated by the flow method.[13, 14] The porosity experiment was carried out on a micro-HPLC system, in which the volumetric flow rate V (m^3/s) was measured by weighing the mobile phase eluted out of the column in a certain amount of time. (see appendix for sample calculation). The linear velocity of the mobile phase u (m/s) was measured by taking a ratio of column length with an untrained dead time marker (DMSO). The porosity was calculated by the following equation:

$$\varepsilon_T = \frac{V}{\pi r^2 u} \times 100\% \qquad (3)$$

where ε_T is the total porosity of the column; r (m) is the inner radius of the column.

The specific permeability of the monolithic column was calculated by:

$$K^0 = \frac{u \eta L \varepsilon_T}{\Delta p} \qquad (4)$$

where η (Pa s) is the dynamic viscosity of the mobile phase; L (m) is the effective length of the column; Δp (Pa) is the pressure drop across the column.

5.3 Results and Discussion

5.3.1 Optimization of the Polymerization Mixture

As mentioned earlier, the major advantage of our procedure is the simple preparation of the chiral monolithic column by directly crosslinking the chiral surfactant monomer with a conventional crosslinker with no charged achiral co-monomer. This is essential to improve the chiral recognition. The composition of the polymerization mixture is critical to the physical and chromatographic properties of the monolith. Thus, the percentage of the monomers, crosslinkers, and porogens were carefully optimized to yield the best monolithic CSPs for the chiral CEC. Preliminary experiment revealed that the best composition of the monomer and crosslinker was 15% (wt/wt) of each (data not shown). Different porogenic solvents such as ACN, MeOH, propanol, butanol, butanediol, decanol, dimethyl ether, and triply deionized were investigated as possible porogens in various proportions. Four possible combinations of polymerization mixture with various ratios (% wt/wt) of dimethyl ether, ACN, MeOH and triply deionized water using 0.5% AIBN as initiator were tested as summarized in Table B2. Column #1 was chosen over #2 due to better CEC chiral separations, whereas column #3 and #4 were not homogeneous). A ternary porogen mixture of ACN and MeOH with small portion (i.e., 5% wt/wt) of H_2O provided homogenous monolithic columns with improved chiral selectivity. The final optimum compositions of the polymerization mixtures for the three monolithic columns of different chain lengths at 15% wt/wt of each surfactant monomer are shown in Table 5.1.

Table 5.1. Composition of the reaction mixtures used in the preparation of the optimized surfactant-bound monolithic columns

Column	Monomers (wt%)		Porogen (wt%)			Initiator (wt%)
	Surfactant	EDMA	ACN	MeOH	H_2O	AIBN
AAOCL	15	15	45	20	5	0.5
AADCL	15	15	45	20	5	0.5
AADoCL	15	15	45	20	5	0.5

5.3.2 Characterization of the Monolithic Columns.

(1) Morphology of the Monolithic Columns

The SEM images of the three monolithic columns are shown in Figure B1. From the three sets of SEM micrographs, one can easily conclude that the monolithic material was successfully formed in the capillary. The material is homogeneous and micropores are evenly distributed. However, for the three different monolithic columns with various chain lengths, no significant difference in SEM morphology was observed.

(2) Porosity, Permeability, and Surface Area of the Monolithic Columns

The porosity and specific permeability values are tabulated in Table 5.2. Interestingly, it was found that the porosities of AAOCL and AADoCL columns with a chain length of eight and twelve carbon atoms, respectively are close to each other (0.852 and 0.863, respectively). These porosity values are slightly higher than the porosity (0.658) of AADCL column with ten carbon atoms (Table 5.2). This means that the AAOCL and AADoCL columns are more porous than the AADCL column for the mobile phase transport.

Table 5.2. Physical characteristics of monolithic columns: ε_T total porosity, K^o specific permeabililty, r surface area

Monolithic columns	Determined with flow method		Determined with BET
	ε_T	K^o (m^2)	r (m^2/g)
AAOCL	0.852	1.04×10^{-15}	25
AADCL	0.658	3.32×10^{-16}	16
AADoCL	0.863	6.55×10^{-16}	38

The overlaid plots of the back pressure vs. the volumetric flow rate observed on the three monolithic columns are shown in Figure 5.1. It is clear that at any given flow rate, AADCL column provided the highest back pressure. On the other hand, AADoCL column and AAOCL columns provided very similar back pressure which is consistent with the porosity data listed in Table 5.2. In addition, the linearity of all three plots is very good, which means the mechanical stability of all three monolithic columns is excellent. The specific permeability of the three monolithic columns follows the order: AAOCL>AADCL~AADoCL. Note that the permeability values of the three surfactant-bound chiral monolithic columns are significantly smaller (10^{-15}-10^{-16} m^2) compared to the achiral surfactant-bound columns, which were developed in our previous studies (~10^{-14} m^2).[13]

The surface area data for all three monolithic columns are also listed in Table 5.2. AADoCL column has the highest surface area (38.2 m^2/g), followed by AAOCL (24.7 m^2/g) and AADCL (16.2 m^2/g) columns. According to the experimental results obtained by Gu *et al.,* the BET surface area of the achiral surfactant-bound columns is in the range of 6-30 m^2/g,[13] which is comparable to the values of the BET surface area of chiral columns mentioned above.

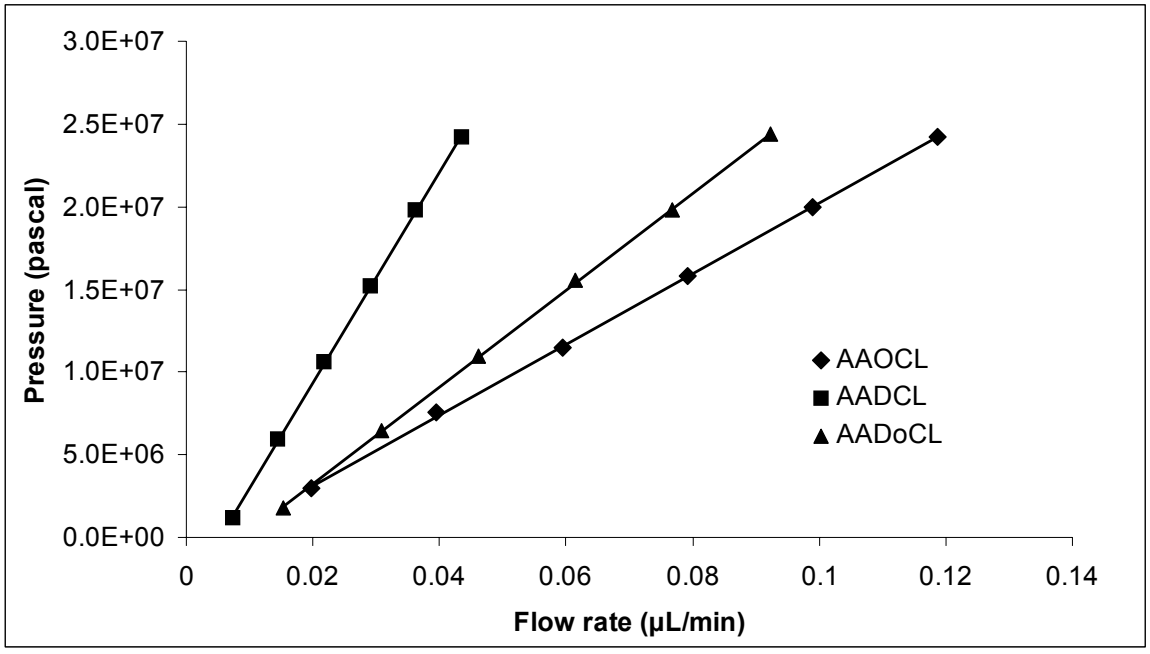

Figure 5.1. Plots of the applied pressure against the volumetric flow rate of ACN in micro-HPLC experiment. Mobile phase: pure ACN.

5.3.3 Mobile phase optimization

With a long C_8-C_{12} hydrophobic alkyl chains and the polar anionic head group, the surfactant-bound monolithic columns are considered to mimic a mixed mode-reverse phase cation exchange CSP. The CEC experiments using AADCL column and a model chiral cationic analyte, such as pseudoephedrine [(±)-PEP] were carried out to examine the effect of mobile phase parameters.

(1) Effect of Percent Triethylamine

The % TEA in the mobile phase contains a mixture of ACN and aqueous buffer at a fixed concentration of 5 mM NH_4OAc. Representative electrochromatograms of CEC experiments using AADCL column at 0.1%, 0.3%, 0.5%, and 1.0% TEA (v/v) are overlaid in Figure 5.2. It can be seen form the inset of the figure that when volume fraction of TEA increases from 0.1% to 1.0%, the retention time decreases from ~28 min to ~22 min. This suggests that at higher % (v/v) of TEA, more mobile phase triethyl ammonium cations compete with (±)-PEP for the cation-exchange sites on the CSP causing faster elution. From the inset of Figure 2, one can observe that the chiral *Rs* of (±)-PEP first increases from 0.1%(v/v) TEA to 0.5% (v/v) TEA (due to significant increase in N_{avg}), and then the *Rs* values were very similar from 0.5%(v/v) TEA to 1.0% (v/v) TEA. However, high volume of TEA counterions (e.g., ≥1.0%) in the mobile phase might compete with the PEP for the ion-pairing sites with the anionic head group of AADCL deteriorating chiral resolution. Thus, 0.5% (v/v) was chosen as the optimum TEA concentration.

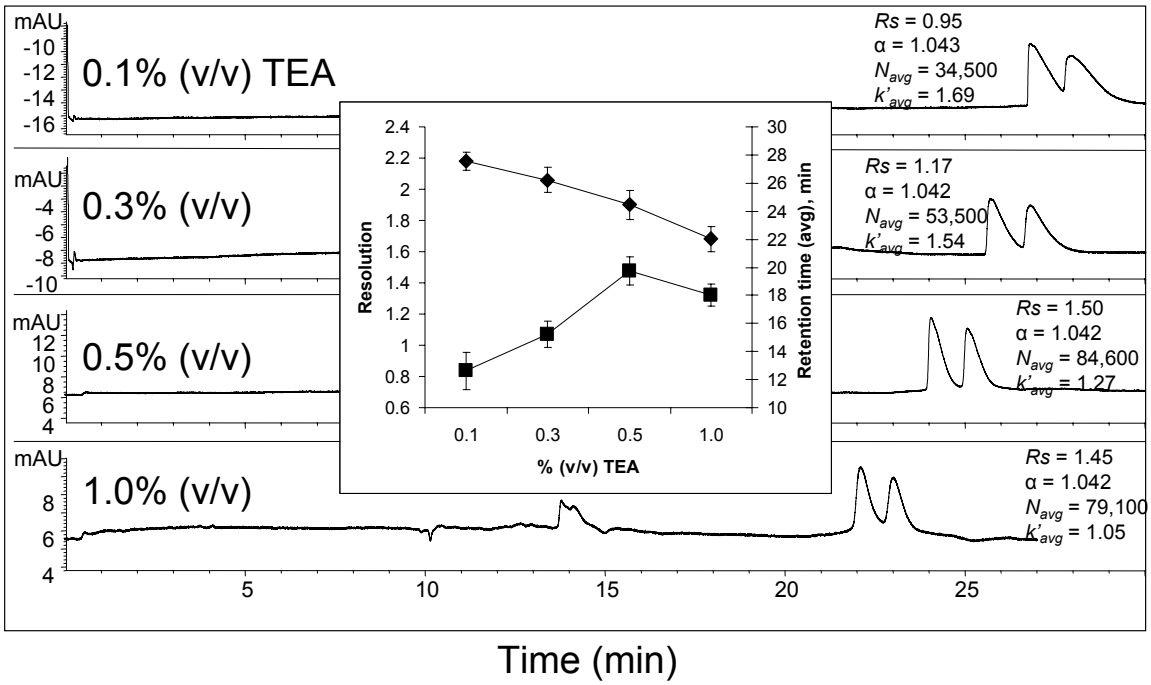

Figure 5.2. Chiral CEC separation of (±)-pseudoephedrine (PEP) at different volume fraction of TEA. CEC conditions: AADCL column, 33.5 cm total length, with 25 cm monolithic bed length, 8.5 cm open bed from the outlet end to the detection window. Voltage, +10 kV; high pressure, 6 bar applied at both ends of the column; column temperature, 20 ^{o}C. Mobile phase is a mixture of 70% ACN and 30% aqueous buffer containing 5 mM NH_4OAc, 0.1-1.0% TEA (pH 5.0); UV detection wavelength, 200 nm. Analyte, (±)-PEP (1 mg/mL) dissolved in mobile phase; injection, 3 kV for 2 s. The inset of the Figure is the plot of retention time (-♦-) and chiral resolution (-■-) against the change % (v/v) of TEA in the mobile phase.

(2) Effect of pH

Mobile phase pH was varied from 4.0-5.5. It was found that the increase in mobile phase pH from 4.0 to 5.0, cause an increase in both retention time and chiral resolution (see Figure B11). However, the current was unstable when running the monolithic columns at mobile phase pH ≥ 5.5 (data not shown). As a result, pH 5.0 was chosen as the optimum pH for the chiral CEC separations.

(3) Effect of Acetonitrile

The % (v/v) ACN was varied from 60% (v/v) ACN to 80% (v/v) ACN to optimize the chiral separation of (±)-PEP. Lower than 60% (v/v) ACN was not studied due to high current and low chiral resolution. It was found in the CEC separation (Figure 5.3) that lowering the % ACN [e.g., < 60 % (v/v) ACN] causes shorter retention time, smaller *k'*, lower chiral resolution, efficiency, and selectivity. On the other hand, when the % ACN was higher than 80% (v/v), the retention time was longer than 50 min and

the chiral resolution deteriorated. This increase of retention at ≥ 80% (v/v) ACN is probably related to relatively lower affinity and solubility of (±)-PEP. Because (±)-PEP is much more soluble in H_2O than in ACN, when the percentage of ACN increases in the mobile phase, the (±)-PEP tends to retain longer in the stationary phase. To examine the effect of % ACN on EOF, DMSO was also injected at 60% (v/v), 70% (v/v), and 80% (v/v). It was observed in the experiments that at 60% (v/v) ACN, the retention time of DMSO is the longest (~18 min). At 70% (v/v) and 80% (v/v), the retention times of DMSO are very similar (~15 min) and shorter than 60% (v/v) (Data not shown). As a compromise between chiral resolution and analysis time, 70% (v/v) was eventually chosen as a desirable volume percentage of ACN in the mobile phase.

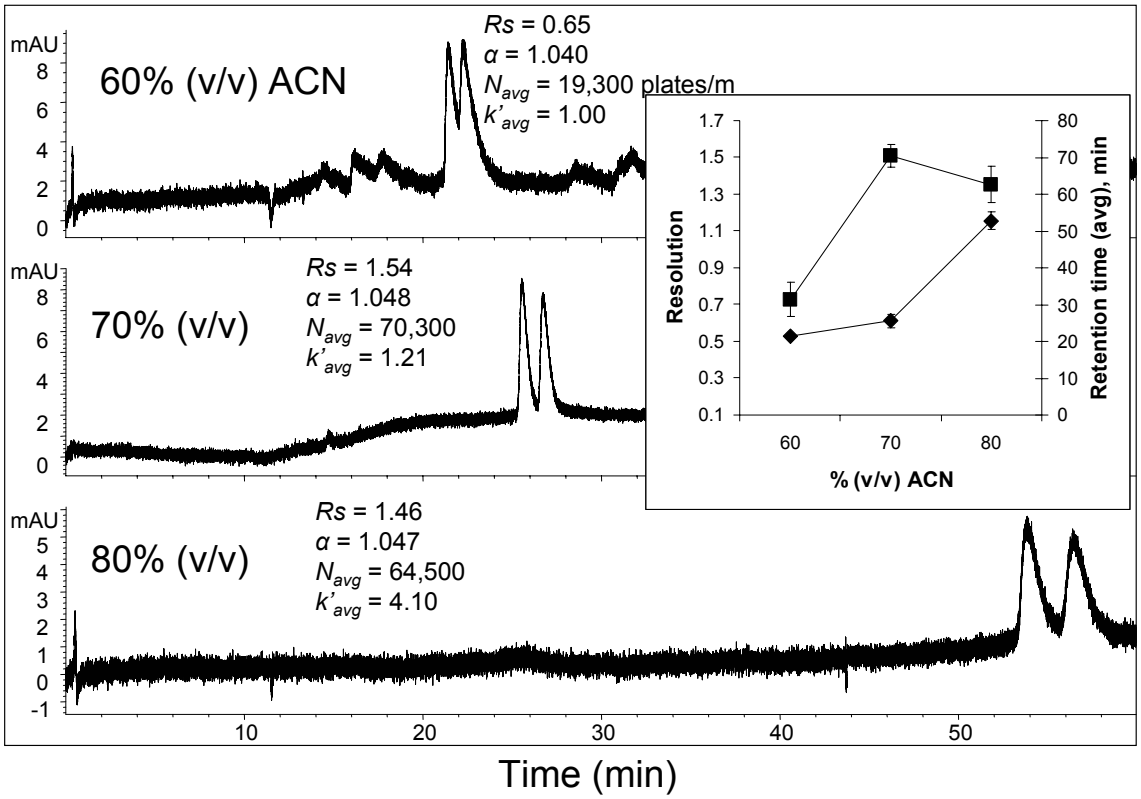

Figure 5.3. Effect of volume fraction of ACN in the mobile phase on chiral CEC separation of (±)-PEP. CEC conditions: AADCL column, 33.5 cm total long, with 25 cm monolithic bed length, 8.5 cm open bed from the outlet end to the detection window. Voltage, +10 kV; high pressure, 6 bar applied at both ends of the column; column temperature, 20 ^{o}C. Mobile phase contain various mobile mixtures in the range of 60-80% (v/v) ACN and 40-20% (v/v) aqueous buffer containing 5 mM NH_4OAc, 0.5% (v/v)TEA (pH 5.0); UV detection wavelength, 200 nm. Analyte, (±)-PEP (1 mg/mL) dissolved in mobile phase; injection, 3 kV for 2 s. The inset of the figure is the plot of retention time (-♦-) and chiral resolution (-■-) as a function of % (v/v) ACN in the mobile phase.

(4) Effect of CEC Voltage

The effect of CEC voltage on chiral resolution and retention time is illustrated in Figure 5.4. As expected, when voltage increases from +5 kV to +15 kV, the retention time decreases accordingly; while the chiral resolution first increases and then decreases significantly. At +15 kV, the run time might be too short for the analyte to interact with the CSP and separate sufficiently. In addition, higher voltage causes higher joule heating and deteriorates efficiency of the enantiomers of PSP. Therefore, +10 kV is considered the optimum voltage to yield the best enantioresolution.

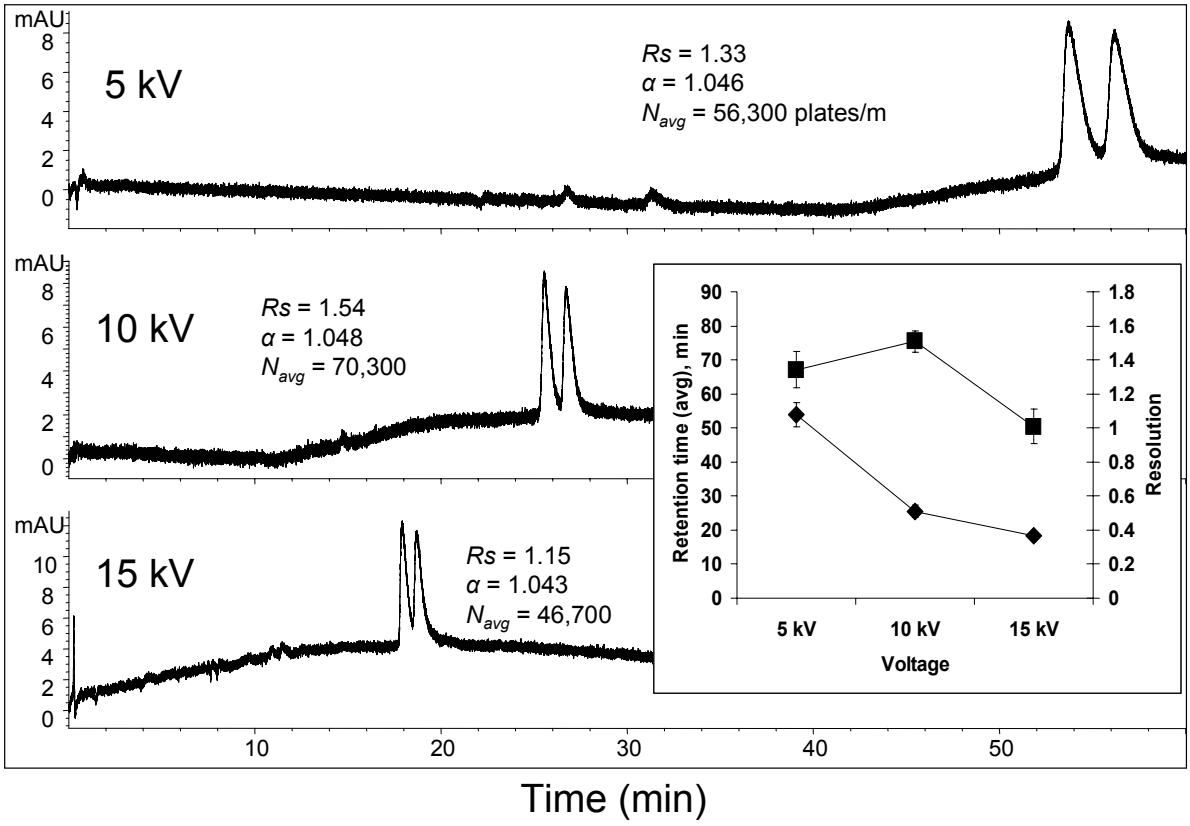

Figure 5.4. Chiral CEC separation of (±)-PEP at different voltage. CEC conditions are same as Figure 5.3 except the mobile phase is a mixture of 70%(v/v) of ACN and 30% (v/v) of aqueous buffer containing 5 mM NH_4OAc, 0.5% (v/v) TEA (pH 5.0) The inset of the figure is the plot of retention time (-♦-) and chiral resolution (-■-) against the change of CEC voltage.

5.3.4. Effect of Surfactant Chain Length

The effect of surfactant chain length was first examined by achiral CEC separation of five neutral test solutes (benzene, toluene, ethylbenzene, propylbenzene, and butylbenzene) with AAOCL, AADCL,

and AADoCL monolithic columns. Methylene selectivity of all three columns was calculated using the equation $\alpha_{CH2} = k'_{n+1}/k'_{n}$,[15] where n and n+1 are the carbon numbers of the adjacent alkylbenezenes. The average methylene selectivity numbers for all five alkylbenzenes were expressed as the slope of a plot of $\ln k'_n$ vs. n,[16, 17] as shown in the inset plot of Figure 5.5. The methylene selectivity of the columns is in the order of: AADoCL > AADCL > AAOCL. Additionally, the overlaid electrochromatograms in Figure 5.5 suggest that the increase of surfactant chain length from C_8-C_{12} increases the retention time and k' of all five alkylbenzenes (i.e., benzene, toluene, ethylbenzene, propylbenzene and butylbenzene). This clearly shows a strong hydrophobic interaction between the neutral alkylbenzenes with all three CSPs. With longer chain length of surfactant-bound CSP, the hydrophobic interaction gets stronger and thus causes longer retention. In addition, AADCL and AADoCL columns provide an overall better achiral resolution than AAOCL column.

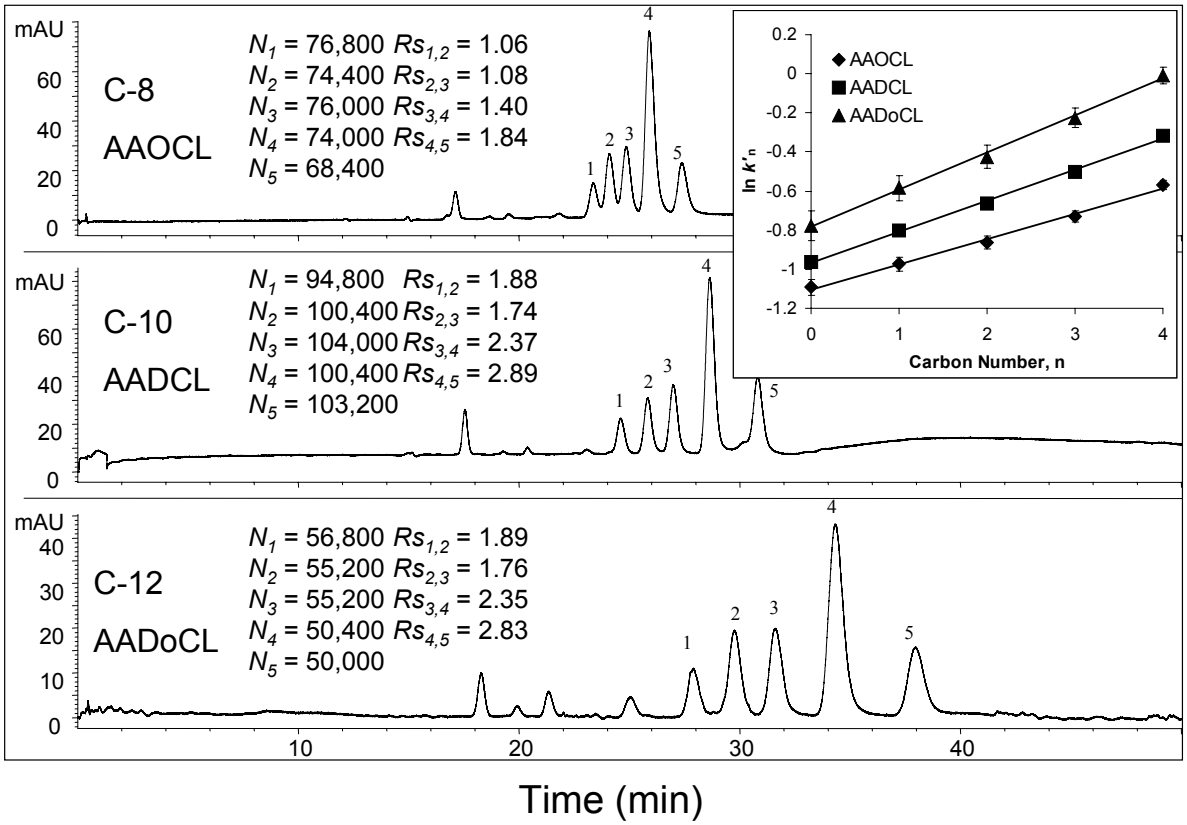

Figure 5.5. Effect of monomer chain length of monolithic columns on achiral CEC separation of 5 alkylbenzenes. The CEC conditions are same as optimized in Figure 5.2, Figure 5.3, and Figure 5.4. The inset of the figure is the methylene selectivity of the AAOCL, AADCL, and AADoCL columns expressed as the plots of $\ln k'_n$ vs. carbon number n.

Next, AAOCL, AADCL, and AADoCL columns were tested for chiral separations of (±)-PEP. Figure 5.6 compares the CEC enantioseparations of (±)-PEP by the three monolithic columns. The inset of Figure 5.6 shows a linear increase in retention time of (±)-PEP with increasing surfactant chain length from C_8-C_{12} monolithic stationary phase. However, the chiral *Rs* of (±)-PEP with C_{10} and C_{12} columns are significantly higher compared to C_8 column. The *Rs* and α values of several positively charged chiral compounds are listed in Table 5.3. The trend in this Table 5.3 suggests that overall the AADCL (i.e., C_{10}) surfactant-bound column provides the best chiral selectivity and resolution for most compounds (except for pseudoephedrine for which C_{12} column gives slightly higher resolution). In contrast, the AAOCL (i.e., C-8 column) provided the worst chiral *Rs* and α. Furthermore, note that AADCL surfactant-bound column usually have highest *k*', which is consistent with the trend found in the permeability study, where AADCL column has significantly lower permeability than AAOCL column. Although, AADoCL has similar permeability than AADCL column, but the former has longer hydrocarbon, which may be not the best chain length for optimum chiral separations. The result of this study suggests that there is delicate balance between the hydrocarbon chain of the surfactant monomer and the column permeability in the chiral recognition process between the separated enantiomer and the CSP.

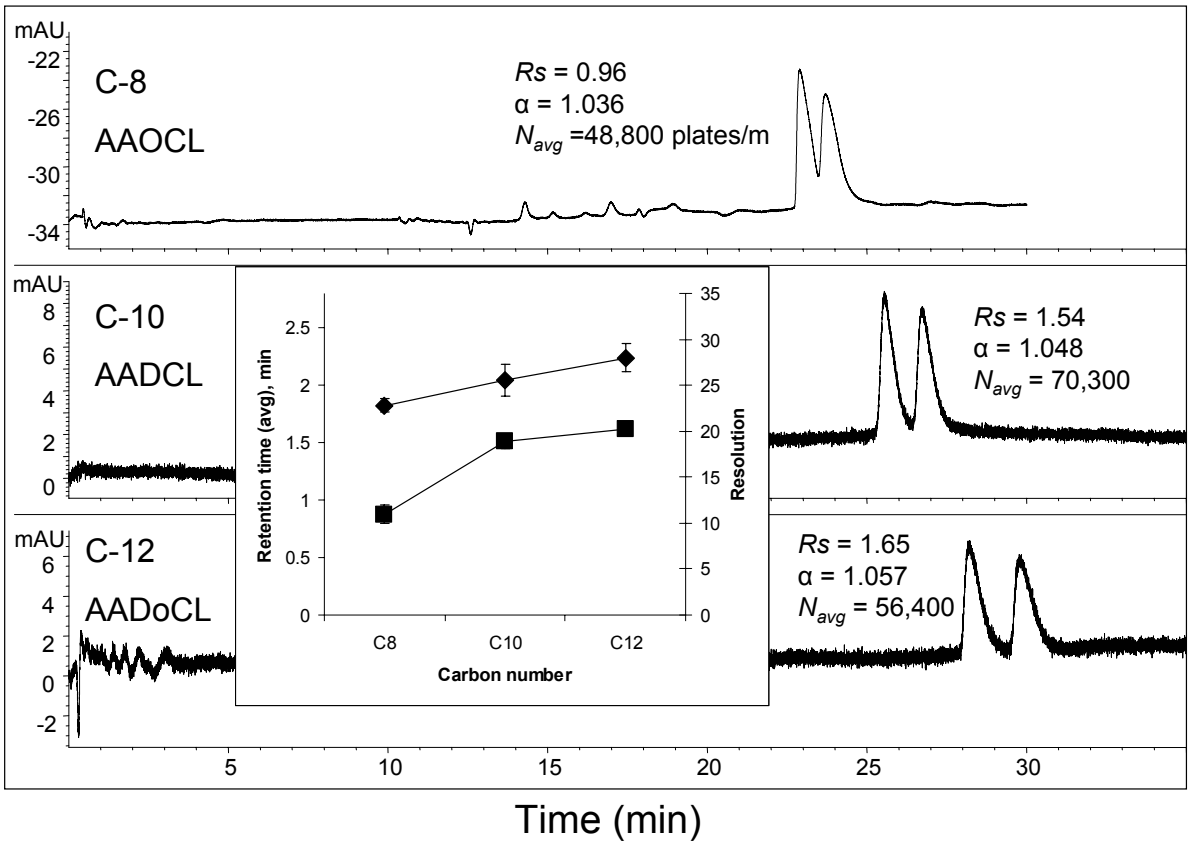

Figure 5.6. Effect of monomer chain length of monolithic columns on chiral CEC separation of (±)-PEP. The CEC conditions are same as optimized in Figure 5.2 and Figure 5.3. The inset of the figure is the plot of retention time (-♦-) and chiral resolution (-■-) as a function of alkyl chain length of the surfactant-bound monolithic column.

Table 5.3. Chiral resolution *Rs*, and selectivity *α* for the test compounds on the three monolithic columns

Compounds	AAOCL		AADCL		AADoCL	
	Rs (sd)	*α* (sd)	*Rs* (sd)	*α* (sd)	*Rs* (sd)	*α* (sd)
Pseudoephedrine	0.64 (0.02)	1.038 (0.001)	1.51 (0.06)	1.049 (0.003)	1.62 (0.05)	1.055 (0.002)
Ephedrine	0.51 (0.06)	1.024 (0.003)	0.94 (0.02)	1.031 (0.001)	0.57 (0.15)	1.037 (0.004)
N-Methylephedrine	0.42 (0.12)	1.018 (0.004)	0.64 (0.12)	1.009 (0.029)	0.65 (0.04)	1.033 (0.003)
Norepinephrine	0.54 (0.04)	1.029 (0.003)	0.82 (0.20)	1.033 (0.004)	0.54 (0.02)	1.025 (0.002)
Synephrine	0.67 (0.16)	1.036 (0.003)	1.02 (0.28)	1.041 (0.002)	0.75 (0.18)	1.034 (0.004)
Norphenylephrine	0.45 (0.07)	1.026 (0.003)	0.90 (0.26)	1.037 (0.002)	0.84 (0.17)	1.037 (0.004)
Alprenolol	0.38 (0.11)	1.018 (0.004)	0.86 (0.09)	1.033 (0.002)	0.70 (0.23)	1.034 (0.006)
Atenolol	0.12 (0.02)	1.005 (0.005)	0.52 (0.03)	1.016 (0.001)	0.36 (0.10)	1.013 (0.005)
Metoprolol	0.24 (0.03)	1.011 (0.003)	0.92 (0.08)	1.028 (0.003)	0.60 (0.09)	1.019 (0.014)
Oxprenolol	0.21 (0.08)	1.008 (0.003)	0.54 (0.01)	1.021 (0.001)	0.55 (0.03)	1.024 (0.002)
Pindolol	0.39 (0.10)	1.018 (0.005)	0.64 (0.02)	1.035 (0.003)	0.52 (0.03)	1.031 (0.003)

5.3.5 Comparison of GMA-β-CD versus AADCL Based Monolithic Columns

Next, we compared the simultaneous separation of both enantiomers of (±)-PSP with its diastereomers [i.e., (±)-ephedrine (EP)] using β-CD based monolithic column. Although close to baseline separation of (±)-PEP enantiomers is possible using GMA-β-CD-*co*-EDMA-*co*-AMPS column (Figure 5.7A), no enantioseparation is noted for its diastereomers of (±)-EP. On the other hand, Figure 5.7B show electrochromatogram with simultaneous enantioseparations of both (±)-PEP and (±)-EP using AADCL-*co*-EDMA monolithic column. Thus, the use synthetically design chiral surfactant bound (e.g.,L-AADCL) column not only shows reversal of enantiomeric order (evident from reversal in peak height of the enantiomers) but also shows wider chiral window allowing improved discrimination of chemoselectivity compared to the GMA-β-CD bound chiral monoliths column. This enhanced

chemoselectivity and wide elution window of the amino acid based chiral monoliths open up the possibilty of investigating various amino acid and dipeptide chiral surfactant as possible chiral monomers.

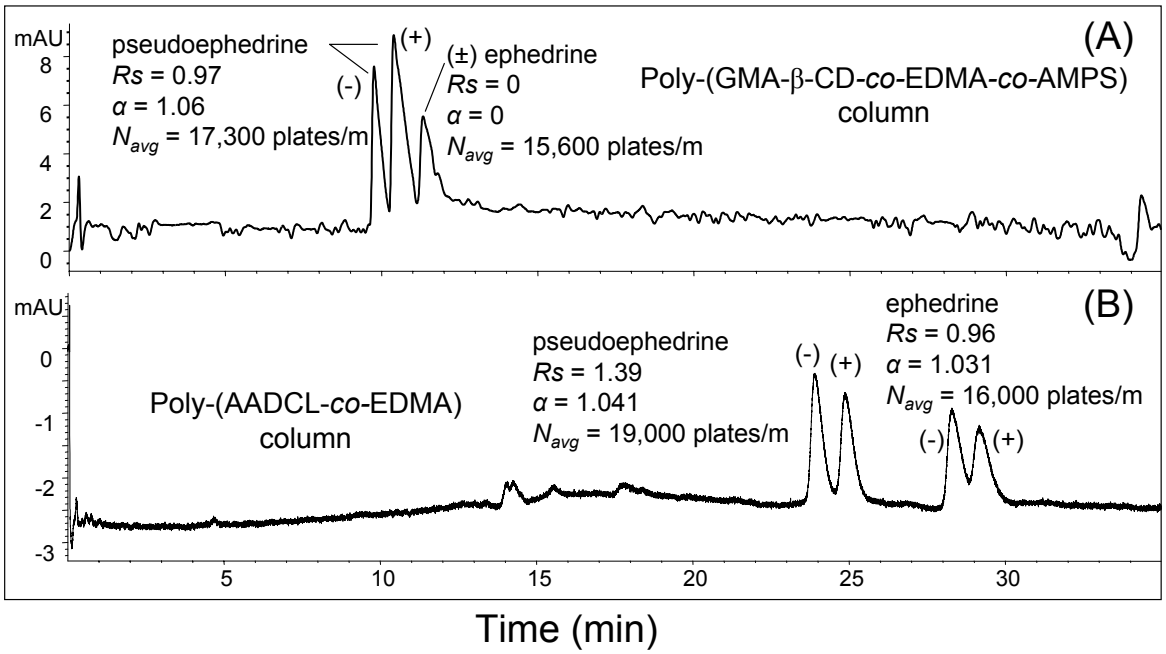

Figure 5.7. Comparison between poly-(GMA-β-CD-*co*-EDMA-*co*-AMPS) column and poly-(AADCL-*co*-EDMA) column for simultaneous enantioseparation of (±)-PEP and (±)-EP enantiomers. The CEC column dimensions for the poly-(GMA-β-CD-*co*-EDMA-*co*-AMPS) columns are the same as described in Figure 3. The mobile phase was a mixture of 50% ACN and 50% aqueous buffer containing 5 mM NH_4OAc, 0.3% (v/v) TEA (pH 4.0). Analyte, (±)-PEP and (±)-EP (1 mg/mL) dissolved in 50/50 ACN/H_2O (v/v); injection, 5 kV for 3 s. The CEC conditions for the AADCL column are same as optimized in Figure 3-5.

5.3.6 CEC-MS Capability

The final portion of this work was to show the potential of surfactant-bound monolith column for it compatibility in CEC-MS mode. As an example, the CEC-MS separations and MS detection for (±)-PEP enantiomers was achieved using AADCL column (Figure B12). However, fused silica capillaries with an inner diameter of 100 μm commonly used in open-tubular chiral CEC-UV poses significant challenge when monolithic columns are coupled to MS. Therefore, due to lower permeability and significantly back pressure of chiral monoliths, the CEC-MS experiments are generally hampered by the limited low flow rates and low inlet pressure, which result in longer conditioning time before installing in the CE-MS instrument. Two modifications to the system were necessary to counteract this problem.

First, a 150 µm i.d. capillary was used to increase the flow rate. Second, for these experiments it was necessary to place the segment of the capillary containing monolith in the outlet CE side of the capillary cassette, and the open segment of the capillary at the inlet end of the CE instrument. This combination of open segment and monolithic segment at the inlet and outlet end, respectively was necessary to achieve faster separation on the monolithic phase via CEC-MS. Note that in CEC-MS, the outlet portion of the capillary is inserted through the nebulizer and is directly sprayed into in the mass spectrometer. Although this set-up led to some band broadening, the enantiomeric resolution was still achieved. There was some loss in the *Rs* value of the (±)-PEP, this was offset by improvement in the *S/N*. The (±)-PEP had an almost 1.5 fold increase in *S/N* (S/N ~ 39) in CEC-MS as compared to a *S/N* of ~27 in CEC-UV. Thus, to counteract the extra dead volume created by the empty segment of the AADCL monolithic bed, it is important to carefully evaluate a range of negatively charged chiral surfactant monomers with various linkers, head group and chain lengths to find the best chiral monomer, crosslinker and porogen combination to develop a monolithic chiral columns with high porosity and high permeability allowing easy operation in CEC-MS.

5.3.7 Column-to-Column and Operator-to-Operator Repeatability

The column-to-column repeatability study was carried out by preparing three different batches of chiral AADCL column using three different batches of polymerization mixtures. A test mixture of separation of (±)-PEP was injected 15 times for three consecutive days on three different columns. The statistical results are tabulated in Table 5.4. The %RSD values for the intraday repeatability of efficiency, retention time, and chiral resolution range from 6.7-21.5, 2.9-11.1, and 2.0-9.9, respectively. Representative electropherograms of intercolumn repeatability study shown in Figure 5.8 illustrates that the preparation of monolithic column is stable and robust.

The operator-to-operator repeatability studies for the preparation of AADCL monolithic columns was carried out using the chiral (±)-PEP prepared by another researcher in our laboratory. The statistical results are also listed in last low of Table 5.4. The %RSD values for the efficiency, retention time and

chiral resolution of (±)-PEP between the two operators are 18.5, 11.3, and 8.7, respectively, indicating acceptable repeatability between operators.

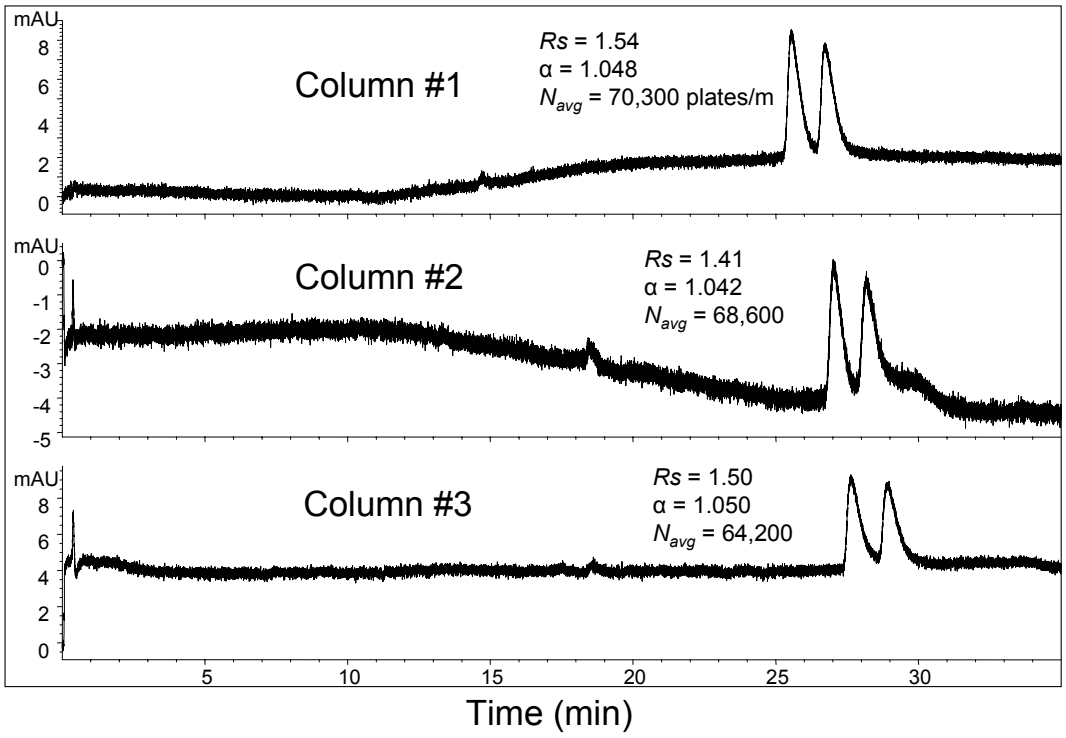

Figure 5.8. Representative electropherograms of intracolumn repeatability using AADCL column. CEC conditions are the same as described in Figure 5.4.

Table 5.4. Intracolumn and intercolumn repeatability of the monolithic columns between two operators comparing average retention time (t_{Ravg}), chiral resolution (Rs) and efficiency (N_{avg}) (±)-PEP using the AADCL monolithic columns

Batch No.	N(avg), m^{-1} (%RSD)	t_R (avg), min (%RSD)	Rs (%RSD)
Intracolumn Operator 1			
Column1(n=15)	5.9×10^4 (21.5)	27.4 (11.1)	1.37 (9.9)
Column 2 (n=15)	8.3×10^4 (12.1)	25.2 (4.9)	1.49 (4.3)
Column 3(n =15)	7.3×10^4 (16.2)	23.8 (2.9)	1.53 (7.5)
Intercolumn(n=45)	7.2×10^4 (21.0)	25.5 (9.5)	1.46 (8.6)
Intracolumn Operator 2			
Column1(n =15)	5.9×10^4 (11.4)	22.4 (4.5)	1.26 (2.7)
Column2(n =15)	6.6×10^4 (12.3)	21.7 (5.1)	1.33 (3.4)
Column3(n=15)	7.4×10^4 (6.7)	24.7 (4.7)	1.39 (2.0)
Intercolumn(n=45)	6.6×10^4 (13.9)	22.4 (8.9)	1.33 (4.8)
Operator-to-Operator Repeatability			
Intercolumn (n=90)	6.9×10^4 (18.5)	23.9 (11.3)	1.40 (8.7)

5.4 Conclusions

Three novel chiral surfactant-bound monolithic columns (poly-(AAOCL-*co*-EDMA), poly-(AADCL-*co*-EDMA), and poly-(AADoCL-*co*-EDMA)) were successfully synthesized and characterized. Baseline separation of model test analyte (±)-PEP was been achieved by AADCL and AADoCL columns. The CEC conditions to deliver the best chiral selectivity of (±)-PEP were found to be: 70% ACN, 0.5% TEA%, pH, 5.0; at +10 kV. Several other cationic chiral compounds were tested with all three columns. Overall, 10-carbon chain AADCL CSP provides the overall best enantioselectivity. This phenomenon suggests that the length of the surfactant's alkyl chain plays a critical role in the chiral recognition process of this type of monolithic CSPs. This is probably due to the hydrophobic interaction between the alkyl chain of the surfactant and the analyte. In addition, the long alkyl chain of the surfactant monomer when polymerized as a monolithic column provided a unique feature of achiral selectivity. For example simultaneous separation of (±)-PEP and (±)-EP enantiomers clearly suggest enhanced chemoselectivity. On the other hand, β-CD based chiral monolithic column was unable to provide such chemoselectivity. This study not only provides a useful mixed-mode hydrophobic/anionic CSP for the separation of cationic chiral compounds, but also a CSP which could be optimized in terms of optical configuration (L or D) amino acid order, linker as well as head group to understand the role these synthetic class of monomers may play when investigating chiral recognition on solid surface compare to solution phase used in MEKC. In addition, the preliminary data on CEC-MS of (±)-PEP with AADCL column suggest great potential of hyphenating this type of monolithic column to MS. Once CEC studies are optimized we should be in a position to compared simultaneous enantioseparation of various pharmaceutical drugs and its structurally similar chiral metabolites with molecular micelles of the same surfactants in MEKC. Such comparisons will help us compare whether the solution phase molecular micelles or solid phase chiral surfactant forming both molecular micelles and monoliths.

References

[1] Wang, J.; Warner, I. M. *Anal. Chem.* **1994,** *66* (21), 3773-3776.

[2] Rizvi, S. A. A.; Shamsi, S. A. *Electrophoresis* **2003,** *24* (15), 2514-2526.

[3] Shamsi, S. A.; Valle, B. C.; Billiot, F.; Warner, I. M. *Anal. Chem.* **2003,** *75* (3), 379-387.

[4] Priego-Capote, F.; Ye, L.; Shakil, S.; Shamsi, S. A.; Nilsson, S. *Anal. Chem.* **2008,** *80* (8), 2881-2887.

[5] Messina, A.; Moroni, S.; Flieger, M.; Sinibaldi, M.; Ursini, O. *Electrophoresis* **2009,** *30* (16), 2890-2896.

[6] Guerrouache, M.; Millot, M.-C.; Carbonnier, B. *Macromol. Rapid Commun.* **2009,** *30* (2), 109-113.

[7] Tian, Y.; Zhong, C.; Fu, E.; Zeng, Z. *J. Chromatogr. A* **2009,** *1216* (6), 1000-1007.

[8] Kornyšova, O.; Jarmalavičienė, R.; Maruška, A. *Electrophoresis* **2004,** *25* (16), 2825-2829.

[9] Dong, X.; Dong, J.; Ou, J.; Zhu, Y.; Zou, H. *Electrophoresis* **2007,** *28* (15), 2606-2612.

[10] Dong, X.; Wu, R.; Dong, J.; Wu, M.; Zhu, Y.; Zou, H. *Electrophoresis* **2008,** *29* (4), 919-927.

[11] Dong, X.; Wu, R. a.; Dong, J.; Wu, M.; Zhu, Y.; Zou, H. *J. Chromatogr. B* **2008,** *875* (1), 317-322.

[12] Ding, W.; Fritz, J. S. *J. Chromatogr. A* **1999,** *831* (2), 311-320.

[13] Gu, C.; He, J.; Jia, J.; Fang, N.; Shamsi, S. A. *Electrophoresis* **2009,** *30* (22), 3814-3827.

[14] Gusev, I.; Huang, X.; Horváth, C. *J. Chromatogr. A* **1999,** *855* (1), 273-290.

[15] Gurdale, K.; Lesellier, E.; Tchapla, A. *Anal. Chem.* **1999,** *71* (11), 2164-2170.

[16] Gilpin, R.; Jaroniec, M.; Lin, S. *Chromatographia* **1990,** *30* (7), 393-399.

[17] Layne, J. *J. Chromatogr. A* **2002,** *957* (2), 149-164.

Chapter 6

Development of Surfactant-Bound Chiral Monoliths for Capillary Electrochromatography and Its Comparison to the Use of Molecular Micelles in Micellar Electrokinetic Chromatography

Capillary electrochromatography (CEC) and micellar electrokinetic chromatography (MEKC) are two of the major capillary electrophoresis (CE) modes, which have been extensively used in the analysis of chiral compounds. In CEC, chiral selectors are coated or chemically bonded on the stationary phase to form a chiral stationary phase (CSP); while in MEKC, chiral surfactant is used as pseudostationary phase. One important question, which is addressed in this study, is the following. Will MEKC using psuedostationary and CEC using a true stationary phase provide similar enantioselectivity when used with the same chiral selector in capillary electrophoresis? To address this question, five amino-acid amide based chiral surfactants with different chain lengths and head groups (sodium 8-acrylamidooctanoyl-L-leucinate (SAAOL), sodium 11-acrylamidoundecanoyl-L-leucinate (SAAUL), sodium 12-acrylamidododecanoyl-L-leucinate (SAADoL), 11-acrylamidoundecanoyl-L-valinate (SAAUV), and 11-acrylamidoundecanoyl-L-phenyl-alaninate (SAAUP)) were synthesized. The acid form of the five acryloyl amide surfactants derived from leucine, valine and phenylalanine head groups were thermally polymerized with ethylene glycol dimethacrylate (EDMA) to form five anionic polymeric-based chiral monolithic columns. The physical characterizations of the five monolithic columns were performed by scanning electron microscope, nitrogen adsorption, and HPLC flow methods. Enantiomers of (±)-pseudoephedrine was used as model compound to study the influence of mobile phase CEC parameters on chiral separations. Under the optimum mobile phase conditions, the effect of surfactant chain length and head group of chiral CEC columns were optimized and compared. For comparison of chiral CEC to MEKC, the SAAUL surfactant was polymerized in aqueous solution under ^{60}Co radiation to form molecular micelles. MEKC experiments were carried out with the poly-SAAUL micelle to separate ten basic chiral compounds. The result suggests that using same chiral selector (SAAUL/AAUL), the enantioselectivities by CEC and MEKC modes are analyte dependent. To the best of our knowledge this study is the first comparison of chiral CEC and MEKC with same surfactant monomer.

6.1 Introduction

Capillary electrochromatography (CEC), as one of the newest mode of capillary electrophoresis (CE), has been widely used in chiral analysis since the first such application was reported in 1992.[1] Chiral CEC has several advantages over other CE modes such as high enantioselectivity with a wide variety of chiral stationary phases (CSPs), ability to separate both neutral and charged analytes, and easy to couple to mass spectrometer (MS).[2] However, not all chiral selectors used in CEC are mass spectrometry compatible. Based on the method used to immobilize the CSPs, chiral CEC can be divided into three major types: open-tubular CEC,[3-5] packed-column CEC,[6-8]and monolithic CEC.[9-11] Among the three modes, monolithic CEC is the newest and hottest CEC mode used in chiral separation in recent years.

In monolithic CEC, the CSP is a continuous, porous structure polymerized inside the capillary.[12] There are two major types of chiral monolithic materials, silica based monolith[13, 14] and organic polymer based monolith.[10, 15] Siliceous monolith is usually fabricated by sol-gel chemistry,[16] while organic polymer based monolith is prepared by the in-situ polymerization of small organic molecules such as acrylates or acrylamides.[11] The major advantage of monolithic capillary vs. packed capillary is the absence of frit, which usually causes air bubbles during the CEC runs. In addition, polymer based monolithic columns are stable over a wider pH range as compared to normal silica based packed columns. For chiral monolithic CEC, chiral selectors are either directly added in the polymerization mixture as monomer or bound/coated onto the monolith after polymerization. Almost all popular chiral selectors have been used to prepare CSPs for chiral monolithic CEC,[17] such as macrocyclic antibiotics,[18, 19] polysaccharide derivatives,[10, 20] cyclodextrins,[9, 21] and ligand exchangers.[15, 22] Recently, several good reviews have been published on chiral CEC using monolithic columns.[2, 17, 23]

In this paper, we propose the development of a new class of polymeric monolithic CSP derived from amino acid based surfactants as chiral selectors for CEC. Amino acid or small peptide based surfactant is one of the most popular chiral surfactants used in chiral micellar

electrokinetic chromatography (CMEKC) in recent years. The structure of the chiral surfactant used in CEMEKC includes a long hydrophobic alkyl chain and a hydrophilic amino acid or dipeptide head group. The chiral surfactants when polymerized into molecular micelles have been successfully used to separate a wide variety of chiral compounds in CMEKC and CMEKC-MS.[24-29] However, as an acknowledged chiral selector in CMEKC, the amino acid based surfactants have never been used as chiral selectors in CEC.

In this paper, three polymerizable acrylamido alkanolyl-L-leucine based chiral surfactants with 8, 11, and 12 carbon alkyl chain [i.e. sodium 8-acrylamidooctanoyl-L-leucinate (SAAOL), sodium 11-acrylamidoundecanoyl-L-leucinate (SAAUL), and sodium12-acrylamidododecanoyl-L-leucinate (SAADoL)] and two polymerizable acrylamido undecanoyl-L-amino acid surfactants with valine and phenylalanine head groups and 11 carbon chains [i.e., sodium 11-acrylamidoundecanoyl-L-valinate (SAAUV) and sodium 11-acrylamidoundecanoyl-L-phenylalaninate (SAAUP)] were synthesized and characterized. With the polymerizable acrylamide tail, all five aforementioned salt forms of the surfactants were converted to acid forms before copolymerization with ethylene glycol dimethacrylate (EDMA) to form chiral monoliths (poly-(AAOL-*co*-EDMA), poly-(AAUL-*co*-EDMA), poly-(AADoL-*co*-EDMA), poly-(AAUV-*co*-EDMA), and poly-(AAUP-*co*-EDMA). The obtained monolithic columns were characterized and evaluated for enantioseparation of (±)-pseudoephedrine (PEP) as a model chiral drug in CEC. First, the mobile phase conditions were optimized. Next, under the optimum mobile phase, the effects of alkyl chain length as well as the head groups on the chiral separation were explored. Finally, using the chiral monolith and chiral molecular micelles, (derived from the same chiral surfactant, Scheme 6.1) enantio-separations of ten basic racemic drugs in CEC and MEKC modes were compared. To our knowledge, this is the first time such a comparison between CEC and MEKC for chiral separations is reported.

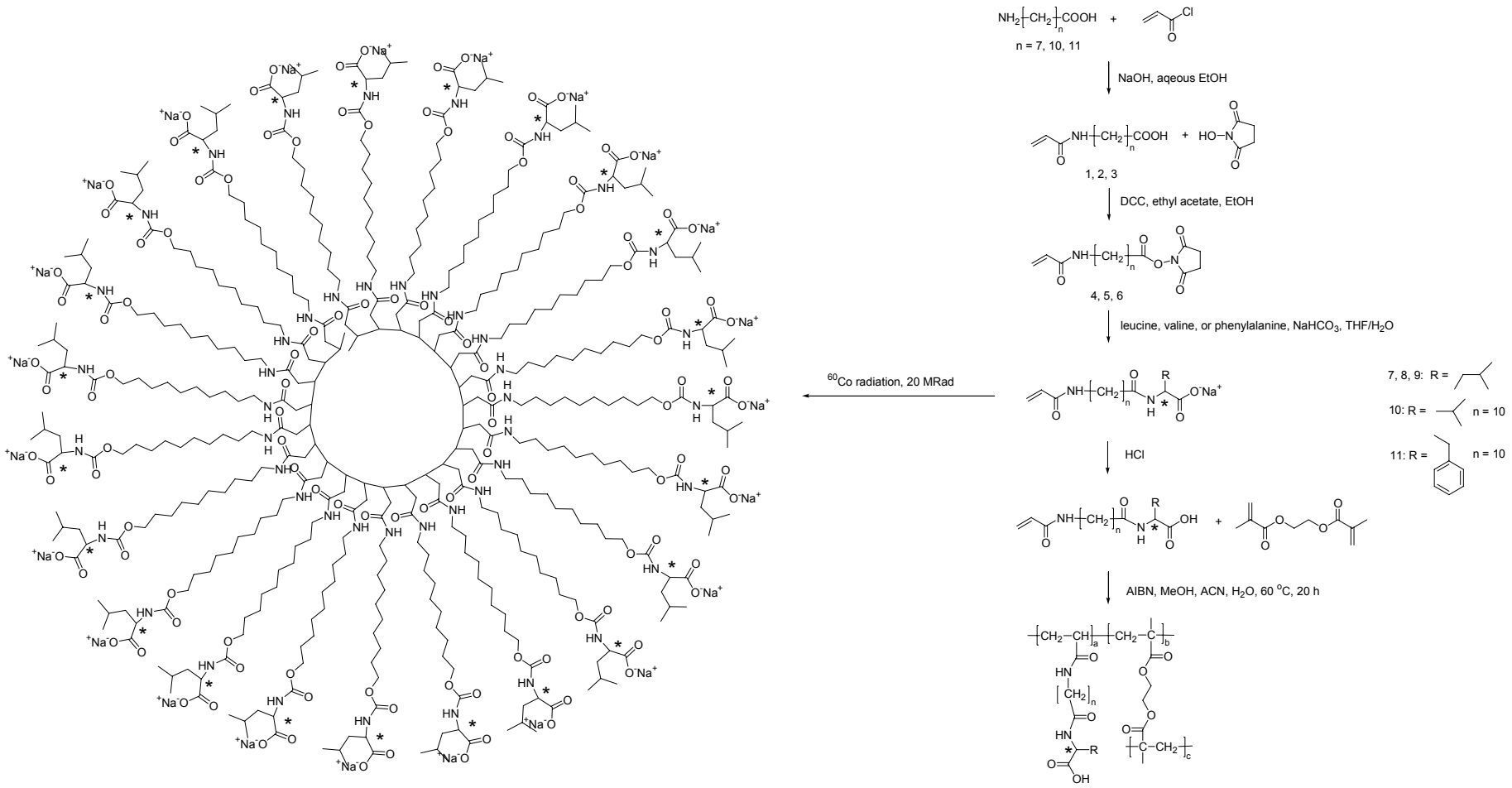

Scheme 6.1. Generalized scheme for the preparation of (A) molecular micelle (polymeric surfactant) prepared from salt form of surfactant irradiating with cobalt-60 gamma radiation and (B) monolithic polymer prepared from copolymerizing the acid form of the surfactant with crosslinker (EDMA) and initiator (AIBN) under heat.

6.2 Experimental Section

6.2.1 Chemicals and Materials.

2,2′-azobis(2-methylpropionitrile) (AIBN), 3-(trimethoxy-silyl)propyl methacrylate (γ-MAPS), acryloyl chloride, 8-aminooctanoic acid, 11-amino-undecanoic acid and 12-aminododecanoic acid were purchased from Sigma-Aldrich (St. Louis, MO). The HPLC grade acetonitrile (ACN), methanol (MeOH), triethylamine (TEA), 7.5 M ammonium acetate (NH_4OAc) aqueous solution, dimethyl sulfoxide (DMSO), (±) propranolol, (±) atenolol, (±) metoprolol, (±) alprenolol, (±) pindolol, (±) pseudoephedrine, (±) ephedrine, (±) synephrine, (±) norephedrine, (±) nor-epinephrine, (±) norphenylephrine, (±) 1,1′-binaphthyl-2,2′-diyl hydrogen phosphate (BNP) and (±) *N*-methyl ephedrine were also purchased from Sigma-Aldrich (St. Louis, MO). Ethylene glycol dimethacrylate (EDMA) obtained from Sigma-Aldrich was distilled to remove inhibitor before its use. Ethanol (HPLC grade) was purchased from Fisher Scientific (Fair Lawn, NJ). Other chemicals used for the synthesis of surfactant monomer, such as *N*-hydroxysuccinimide (NHS), *N,N*′-dicyclohexyl-carbodiimide (DCC), anhydrous Na_2SO_4, L-leucine, L-valine, L-phenylalanine, dichloromethane, sodium bicarbonate, sodium hydroxide, hydrochloric acid, and ethyl acetate were also obtained from Sigma-Aldrich. Triply deionized water (18.2 MΩcm) was generated in the laboratory using Barnstead Nanopure II Water System (Dubuque, IA). All the chemicals have the purity of 98% or higher and were used as received without further purification unless otherwise noted.

6.2.2 Synthesis of Surfactants

The sequence for the synthesis of the acid form of the five surfactant monomers (Table 6.1, column 1, name the surfactant monomers synthesized with abbreviation) is shown in Scheme 6.1. The derivatives (**1-3**, step 1, Scheme 6.1) were synthesized with some modifications according to the procedure described in reference.[23-25] Briefly, 4.8 g, 6.0 g or 6.5 g (0.03 mol) each of 8-aminooctanoic acid, 11-aminoundecanoic acid or 12-aminododecanoic acid was dissolved in 125 mL of neat ethanol and 35 mL of triply deionized water. Next, 6 g (0.075 mol)

of 50% (wt/wt) NaOH solution was added and stirred (see appendix for example calculation). To this stirring solution, 3 mL of neat acryloyl chloride (0.035 mol) was added dropwise. Each of the above reaction mixture was stirred for 3 h at 10 ^{o}C. Next, the solution was filtered and the filtrate was acidified by 6 M HCl to pH ~1. Next, 4 L of H_2O was added to the filtrate and the white precipitate was collected and recrystallized by dissolving in ~20 mL hot ethanol and ~5 mL of triply deionized water. The clear solution was then stored at 4^{o}C overnight. The crystals of 8-acrylamidooctanoic acid (**1**, AAOA), 11-acrylamido-undecanoic acid (**2**, AAUA), or 12-acrylamidododecanoic acid (**3**, AADoA) was then washed with ~20 mL of triply deionized water under vacuum, and lyophilized to yield the pure product of **1-3** (~75% yield). About 3.1 g, 3.8 g, or 4.0 g (0.015 mol) of derivatives **1-3** were dissolved in a mixture of 200 mL ethyl acetate and 200 mL neat ethanol along with 1.7 g *N*-hydroxysuccinimide (0.015 mol) and 3.1 g DCC (0.015 mol). The reaction mixture was stirred at room temperature for 20 h, after which it was filtered with a vacuum flask. The filtrate was then evaporated under vacuum to yield waxy solid, which was then recrystallized with neat isopropanol. The recrystallized white solid was washed with ~10 mL of cold isopropanol and ~20 mL H_2O to yield 4.0 g, 4.5 g, or 4.8 g of the product **4-6** (NHS ester of AAOA, AAUA or AADoA, 0.013 mol, ~87% yield). The product **4-6** was then reacted with equal molar of L-leucine, whereas **5** was reacted with equimolar of L-valine or L-phenylalanine as well as $NaHCO_3$ in 500 mL THF/H_2O mixture (50/50, v/v) for 20 h. The reaction mixture was then acidified by 6 M HCl and binary solvent (H_2O and THF) was evaporated under vacuum. The white solid product i.e., acid form AAOL, AAUL, AADoL, AAUV, or AAUP (**11-15**, Scheme 6.1) was washed with ~50 mL triply deionized water under vacuum and dried by lyophilization. The acid product was then mixed with equimolar of $NaHCO_3$ in 500 mL of triply deionized water and stirred at room temperature overnight. Finally, the resulting solution was extracted once with 500 mL aliquot of ethyl acetate. The bottom aqueous layer was collected and lyophilized to obtain 3.5 g, 3.9 g, 4.0 g, 3.8 g, or 4.2 g

(~0.01mol, ~77% yield) of the salt form SAAOL, SAAUL, SAADoL, SAAUV, or SAAUP (**7-11**), respectively.

Table 6.1. Composition of the reaction mixtures used in the preparation of the optimized surfactant-bound monolithic columns

Column	Monomers (wt%)		Porogen (wt%)			Initiator (wt%)
	Surfactant	EDMA	ACN	MeOH	H_2O	AIBN
AAUL	15	15	45	20	5	0.5
AAUV	15	15	45	20	5	0.5
AAUP	15	15	45	20	5	0.5
AAOL	15	15	45	20	5	0.5
AADoL	15	15	45	20	5	0.5

The acid form of the surfactant which was used in the preparation of monolithic columns was obtained by acidification of the salt form of surfactant. The salt form product (**7-11**) was first dissolved in ~50 mL of H_2O, to this solution, 6 M HCl was added to adjust the pH to ~1. The aqueous surfactant solution was then extracted three times with ~100 mL aliquot of CH_2Cl_2. The bottom CH_2Cl_2 layer was collected each time, dried with anhydrous Na_2SO_4, and rotoevaporated to yield the acid form of the surfactants. The yield of the acidification reaction is about 50%.

The sodium salts of the five surfactants were characterized with ^{1}H-NMR and electrospray mass spectrometry (ESI-MS). The acid form of the surfactants was tested by elemental analysis. The NMR spectra were recorded on a Bruker 400 MHz instrument. All NMR samples were dissolved in D_2O. The ESI-MS analysis was performed on an Agilent 1100 series single quadrupole mass spectrometer. For ESI-MS analysis, each of the surfactant was dissolved in 50/50 (v/v) H_2O/MeOH and direct infusion was performed using a CE nebulizer. The elemental analysis (Table C1 with representative calculation), mass spectra (Figure C1-C10), and ^{1}H NMR spectra (Figure C11-C15) for each surfactant with assignments are attached in appendix.

6.2.3 Preparation of Monolithic Columns

A 40 cm long fused silica capillary (360 μm o.d., 100 μm i.d., Polymicro Technologies, Phoenix, AZ) was flushed under vacuum with acetone and 1 M NaOH for 15 min each. The

capillary was then filled with 1 M NaOH and both ends were sealed with rubber septums and heated at 100 ^{o}C for 2 h in a GC oven. Next, the capillary was flushed with triply deionized water, 1 M HCl, triply deionized H_2O, and acetone for 15 min each under vacuum. A solution of γ-MAPS (30%, v/v in acetone) was then filled through the capillary under vacuum. The filled capillary was once again sealed with rubber septums and kept at 50 ^{o}C for 14 h in a GC oven. Next, the unreacted γ-MAPS solution was removed by flushing the capillary under vacuum using acetone for 5 min. The vinylized capillary was eventually dried by nitrogen for 3 h at 70 ^{o}C in a GC oven.

The polymerization process of monolithic columns is similar to that described in our previous publication.[26] A typical procedure for making AAOL, AAUL, AADoL, AAUV, or AAUP monolithic columns is described as follows. First, 15 mg (15%, wt/wt) of the acid form of each surfactant monomer and 0.5 mg of AIBN were dissolved in a mixture containing various compositions of porogens (% wt/wt) of ACN, MeOH, and H_2O, Table 6.1). To each of the porogen mixture, 14.3 μL (15%, wt/wt) of EDMA was added. The final polymerization solution was then ultrasonicated for 30 min before filling the solution to the pretreated capillary with a handheld syringe. Typically, in the preparation of CEC-UV column, 30 cm out of 40 cm of the pretreated capillary was filled. The column was then sealed with rubber septums and was kept at 60 ^{o}C in a GC oven to polymerize. After 20 h of polymerization, the column was flushed with ACN for 2 h to remove the unreacted monomers. The on-column detection window was then burned in the empty section of the column adjacent to the packed monolithic bed, 8.5 cm to the outlet end of the capillary for CEC-UV experiment. The column was eventually cut to obtain a total length of 33.5 cm with a monolithic portion of 25 cm (from the inlet end). The monolithic capillary was conditioned for 24 h with mobile phase before use.

6.2.4 Preparation of Molecular Micelle

The poly-SAAUL molecular micelle was prepared similar to that described in literature.[27] Briefly, SAAUL was made into 100 mM aqueous solution and left under ^{60}Co γ-radiation

(Phoenix Memorial Laboratory, University of Michigan, Ann Arbor, MI) for a total dose of 20 MRad. The solution was then dialyzed with cellulose ester membrane (1000 MW cut-off, Spectra/Por, Rancho Dominguez, CA, USA) to remove any un-polymerized monomer and followed by lyophilization to obtain the solid poly-SAAUL.

6.2.5 Morphology, Surface Area, Porosity, and Permeability Measurements

A Hitachi X-650 (Hitachi, Japan) scanning electron microscope (SEM) was used to characterize the microscopic morphology of the monolithic columns. The SEM was operated at 7.5 kV; the filament current was set at 40 mA. Monolithic columns samples were cut to 2 mm in length and stuck on an aluminum stub by double-sided carbon tape. The samples were then sputter-coated with gold/palladium alloy with a SPI sputter (SPI supplies Division of Structure Probe, West Chester, PA) for 1 min.

The surface area of the monolithic samples was obtained by nitrogen adsorption experiments. The surface area was calculated via a multi-point BET method applied to nitrogen physisorption data obtained on a Micromeritics Tristar 3020 (Micromeritics Instrument, Norcross, GA). All samples were first heated under vacuum at 70 ^{o}C for 24 hours to remove physisorbed water before being analyzed. The 59 point adsorption/desorption isotherm was then obtained at liquid nitrogen temperatures. Samples for the nitrogen adsorption experiments were prepared in 1.5 mL plastic centrifuge tubes in parallel with the monolithic columns. The monolith was crushed into powder; further cleaned with Soxhlet extraction (MeOH as solvent) for 24 h and dried at 70 ^{o}C for 24 h under vacuum. An Ultra-Plus II micro-HPLC system (Micro-Tech Scientific Inc., Fontana, CA) was used for the measurement of porosity and permeability of monolithic columns.

6.2.6 CEC and MEKC Instrumentation

An Agilent CE system (Agilent Technologies, Palo Alto, CA) equipped with an auto sampler, 0-30 kV power supply, and a diode-array UV detector was used to carry out all the CEC and MEKC experiments. Agilent 3D-CE ChemStation software (Rev. A. 08.04) was used for data

acquisition and analysis. A series III isocratic HPLC pump (Lab Alliance, State College, PA) was used to flush and condition the CEC columns.

6.2.7 CEC and MEKC conditions

Various parameters were used to optimize the CEC conditions for the monolithic surfactant-bound columns as following: voltage was varied in the range of 5-20 kV; high pressure of 6 bar was applied at both ends of the column; column temperature was 20 ^{o}C. The mobile phase, containing a mixture of 30% – 85% ACN and 70%-15% aqueous buffer containing 5 mM NH_4OAc, 0.15% -0.5% TEA (pH 4.0-5.0); UV detection wavelength, 200 nm for all the analytes. A typical aqueous buffer with 5 mM NH_4OAc and 0.3% TEA (pH 5.0) was made by dissolving 66.7 μL of 7.5 M NH_4OAc solution into ~80 mL triply deionized water. To this solution, 0.3 mL of TEA was added. The solution was adjusted to pH 5.0 with acetic acid and transferred to a 100 mL volumetric flask to be diluted with triply deionized water to make up the final volume to 100 mL. The final mobile phase was prepared by mixing the aqueous solution and ACN to the desired ratio. For example, in the final mobile phase of a typical mixture of 70% (v/v) ACN and 30% (v/v) aqueous buffer (containing 5 mM NH_4OAc and 0.3% TEA), the final concentration of NH_4OAc is 1.5 mM; the final concentration of TEA is 0.09% (v/v). Before a monolithic column was used in CEC runs, voltage conditioning was performed to equilibrate the column at an increment of +5 kV, +7 kV, +10 kV, +15 kV and +20 kV. Analyte stock solutions were prepared at 8 mg/mL by dissolving solid analyte into pure ACN. Working analyte solutions were prepared at 1 mg/mL by diluting the analyte stock solution into 50/50 ACN/H_2O (v/v). Injections were performed electrokinetically at +3 kV, 2 sec.

The MEKC separation was performed on a 64.5 cm long fused silica capillary (50 μm i.d., 360 μm o.d., Polymicro Technologies, Phoenix, AZ). At 56.0 cm from the injection end of the capillary, a 3 mm section of polyimide coating was burned off with a home-made electronic burner to create a UV detection window. New capillary was sequentially flushed with 1 M

NaOH and triply deionized water for 40 minutes and 20 minutes, respectively before use. The capillary was flushed with the running buffer for 5 minutes as pre-conditioning before each run. After each run, the capillary was flushed with water for 2 minutes, 1 M NaOH for 2 minutes, and water for another 2 minutes as post-conditioning. The capillary temperature was set at 20 ^{o}C; positive voltage of 20 kV (anode at the inlet end and cathode at the outlet end) was applied for all the experiments. The MEKC running buffer is 25 mM NH_4OAc aqueous buffer, pH 8.8. The buffer was prepared by first diluting 333 μL of 7.5 M concentrate NH_4OAc aqueous solution to ~80 mL in a beaker. Next, the pH of the buffer was adjusted to 8.8 with 1 M NH_4OH. The buffer was then transferred to a 100 mL volumetric flask and made up the volume to 100 mL. Next, poly-SAAUL was dissolved in the NH_4OAc buffer to 25 mM equivalent molar concentration, which is defined as the concentration of the polymeric surfactant that has the same weight as the monomer. The surfactant containing buffer was then vortexed, filtered by 0.45 μm PTFE syringe filter (Fisher Scientific, Pittsburgh, PA), and ultrasonicated for 15-20 min before use. The analytes were prepared at 2 mg/mL in 50/50 (v/v) MeOH/H_2O and injected hydrodynamically at the pressure of 5 mbar for 5 sec.

6.2.8 Calculations

The chromatographic parameters were calculated by the Chemstation software. Resolution (*Rs*) was calculated using the following equation:

$$Rs = \frac{1.18 \times (t_{R2} - t_{R1})}{W_{(1/2)1} + W_{(1/2)2}} \qquad (1)$$

where t_{R1} and t_{R2} are the retention times of the first and second eluting peaks. $W_{(1/2)1}$ *and* $W_{(1/2)2}$ are the peak widths at half height for first and second eluting enantiomer. Capacity factor (*k'*) was calculated by the following equation:

$$k' = \frac{t_R - t_m}{t_m} \qquad (2)$$

where t_R and t_m are the retention times of the analyte and the dead time marker (DMSO), respectively.

The efficiency of a peak was calculated by:

$$N = 5.54\left(\frac{t_R}{W_{1/2}}\right)^2 \quad (3)$$

The mobility of a peak was calculated by the following equation:

$$\mu = \frac{lL}{t_R V} \quad (4)$$

where L is the total length of the column; l is the effective length of the column (i.e. length from the inlet end to the detection window); V is the voltage.

The porosity of the CEC monolithic columns was calculated by the flow method.[12, 26] The porosity experiment was carried out on a micro-HPLC system, in which the volumetric flow rate V (m^3/s) was measured by weighing the mobile phase (pure ACN) eluted out of the column in a certain amount of time. The linear velocity of the mobile phase u (m/s) was measured by taking a ratio of column length with an untrained dead time marker. The porosity was calculated by the following equation:

$$\varepsilon_T = \frac{V}{\pi r^2 u} \times 100\% \quad (5)$$

where ε_T is the total porosity of the column; r (m) is the inner radius of the column.

The specific permeability of the monolithic column was calculated by:

$$K^0 = \frac{u\eta L\varepsilon_T}{\Delta p} \quad (6)$$

where η (Pa s) is the dynamic viscosity of the mobile phase; L (m) is the effective length of the column; Δp (Pa) is the pressure drop along the column.

6.3 Results and Discussion

6.3.1 Optimization of the Polymerization Mixture

It is well established that the composition of the polymerization mixture is essential in the formation of the monolithic column as well as its physical and chromatographic character. The polymerization conditions were optimized using AAUL monomer. The weight ratio of AAUL monomer, crosslinker, and ternary porogen in the polymerization mixture was optimized by several combinations of % wt/wt. The results of the optimization are listed in Table C2. Several trends observed are worth mentioning. For example, using ACN alone as the porogen, the AAUL monomer is not soluble (rows 1-7). To improve the solubility of the monomer, MeOH needs to be added to ACN. However, when using too much MeOH (≥ 40% wt/wt), the column tends to be too dense to have any significant flow (rows 10-13). However, too much crosslinker i.e., 25 and 30% wt/wt of EDMA, also causes flow problem even when MeOH was ≥ 30% wt/wt (rows 8-9). On the other hand, if more AAUL surfactant monomer and less EDMA crosslinker are used i.e., >18% wt/wt and ≤ 10% wt/wt, respectively, the columns tends to be non-homogeneous (row17). On the other hand, if more EDMA (≥ 18% wt/wt) was used than AAUL monomer (≤ 12% wt/wt), the columns were not homogeneous either (rows 15 and 16). In addition, too much water (≥ 10% wt/wt) in the porogen also causes non-homogeneous monolith (row 14). The composition of polymerization mixture that gives good flow of monolithic column was found to be: monomer + crosslinker = 30% (with roughly equal amount of monomer and crosslinker), a ternary porogen system of ACN (20-45% wt/wt), MeOH (20-50% wt/wt), and H_2O (up to 5% wt/wt). Chiral CEC experiments with aforementioned good AAUL columns (rows 18-22) revealed that the optimum combination is 15% wt/wt monomer, 15% wt/wt EDMA, 45% wt/wt ACN, 20% wt/wt MeOH, 5% wt/wt H_2O, and 0.5% wt/wt AIBN (row 21). Other columns (rows 18-20 and row 22) have slightly lower enantioselectivity than the optimum column (row

21). This optimum combination was used to make all five different types of monolithic columns with different head groups and chain lengths (Table 6.1).

6.3.2 Characterization of the Monolithic Columns

(1) Morphology of the Monolithic Columns

The SEM photographs of the five monolithic CEC columns under the optimum polymerization conditions are shown in Figure C17. From the SEM micrographs, it can be concluded that the monolithic material was successfully formed in the CEC capillary. The material is homogeneous and micropores are evenly distributed within a 100 μm i.d capillary. However, for the five different monolithic columns, no significant difference in SEM morphology was observed.

(2) Porosity, Permeability, and Surface Area of the Monolithic Columns

The porosity (ε_T) and specific permeability (K^o) values are tabulated in Table 6.2. It appears that at fixed chain length as the head group becomes bulkier the porosity increases AAUP~AAUL>AAUV. Although varying the chain length of monoliths at fixed (leucine) head group does not seem to follow any definite trend, AADoL column with dodecyl chain has the lowest porosity of 0.78. The K^o of the five monolithic columns follows the decreasing order of AAUP>AAUL>-AAOL> AADoL> AAUV. Again, the least bulky head group monolith (i.e., AAUV column was least permeable), whereas varying chain length on K^o is not obvious.

The overlaid plots of the back pressure vs. the volumetric flow rate observed on the three monolithic columns are shown in Figure 6.1. Consistent with the lowest values of ε_T and K^o, the AAUV column provided the highest back pressure, i.e., the slope of pressure vs. flow rate is the steepest. The plots of AADoL and AAOL columns have relatively less steeper slope but similar back pressure as compared to AAUV column. On the other hand, AAUP and AAUL columns have significantly lower back pressure, consequently much shallower slope. Nevertheless, it is

obvious that the linearity of all five plots is very good, which means the mechanical stability of all five monolithic columns is excellent under the pressure of even 25 MPa.

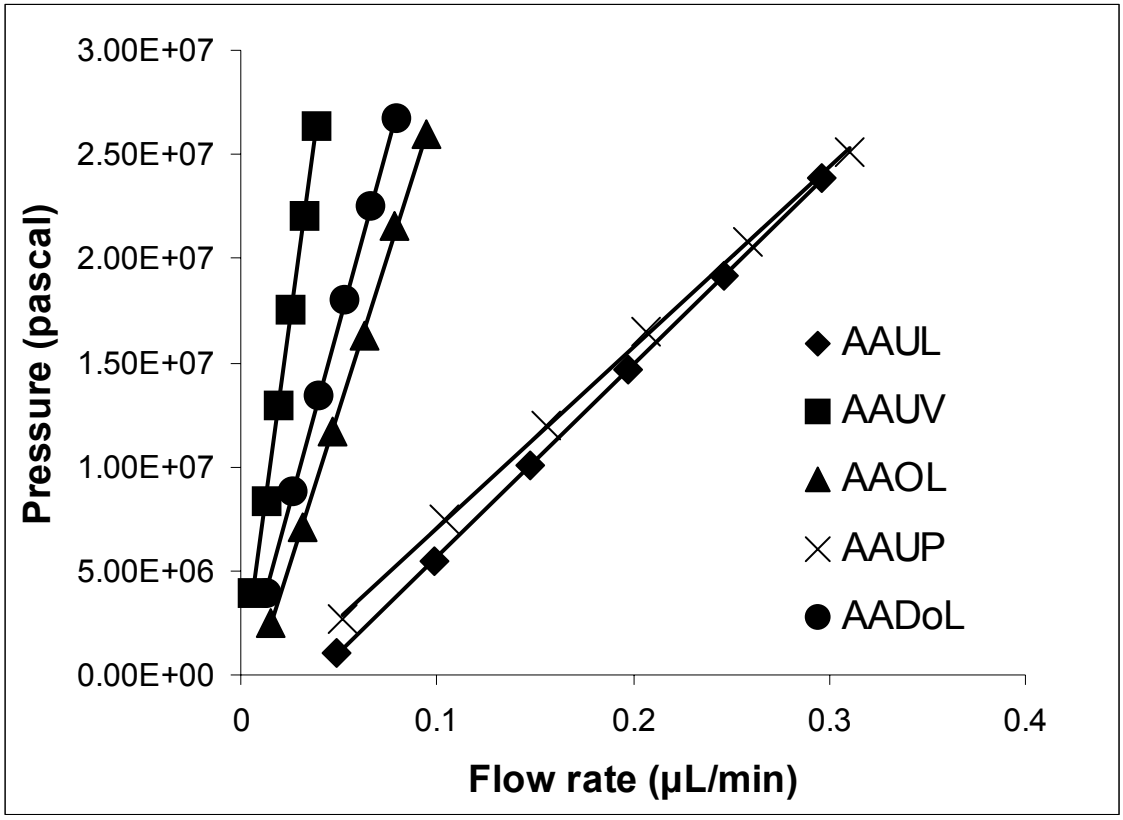

Figure 6.1. Plots of the applied pressure against the volumetric flow rate of ACN in micro-HPLC experiment. Mobile phase: pure ACN.

The surface area data of the monolithic columns measured by BET experiments are also shown in Table 6.2. It is found that AAUP. column has the smallest surface area (15.3 m^2/g), followed by AAUL column ((16.3 m^2/g). AAOL and AADoL columns have similar surface area (19.5 and 19.3 m^2/g, respectively). AAUV column has an exceptional highest surface area of 56.7 m^2/g, which might have resulted in lowest ε_T and K^o.

Table 6.2. Physical characteristics of monolithic columns: ε_T total porosity, K^o specific permeabililty, r surface area

Monolithic columns	Determined with flow method		Determined with BET
	ε_T	K^o (m^2)	r (m^2/g)
AAUL	0.926	1.89×10^{-15}	16
AAUV	0.484	3.06×10^{-16}	57
AAUP	0.960	2.16×10^{-15}	15
AAOL	0.930	7.06×10^{-16}	20
AADoL	0.781	6.18×10^{-16}	19

6.3.3 Mobile Phase Optimization

(1) Effect of Percent Acetonitirle

The optimization of volume fraction of ACN in the mobile phase was performed with CEC experiments using an AAUL column. First, achiral separations of a test mixture of five alkylbenzenes (benzene, toluene, ethylbenzene, propylbenzene, and butylbenzene) were carried out. Three representative overlaid electrochromatograms upon changing % (v/v) ACN from 50% -85% are shown in Figure 6.2. Upon increasing the % (v/v) ACN, the retention time of the five alkylbenzenes dropped significantly. Meanwhile, the methylene selectivity also decreased significantly from 50% ACN to 85% ACN. This is not too surprising considering the C_{11}-hydrocarbon chain of AAUL monolithic column provides the strongest hydrophobic interaction between the stationary phase and the neutral alkylbenzenes.

Next, chiral separation of (±)-PEP was performed with the same AAUL column. Representative overlaid electrochromatograms are shown in Figure 6.3. From the chromatograms it is obvious that initial increase in %(v/v) ACN from 30% to 70% in the mobile phase displays slow but gradual increase in retention time from 3-8 min. Further increase in ACN from 70-85% shows a significant increase in the retention time of (±)-PEP to ~21 min but only a slight increase in chiral selectivity. This increase of retention is probably due to the solubility change of (±)-PEP. Because (±)-PEP is much more soluble in H_2O than in ACN, when the % (v/v) ACN increases in the mobile phase, (±)-PEP tends to retain longer in the stationary phase. Thus causes longer

retention time. In addition to the solubility change of (±)-PEP, the electrostatic ion-pairing interaction between the analyte and CSP may increase in the presence of ACN. This effect may also contribute to the longer retention time at higher % (v/v) ACN. To provide enough retention allowing chiral interaction between CSP and the analyte, 70% was chosen as the optimum percentage of ACN in the mobile phase.

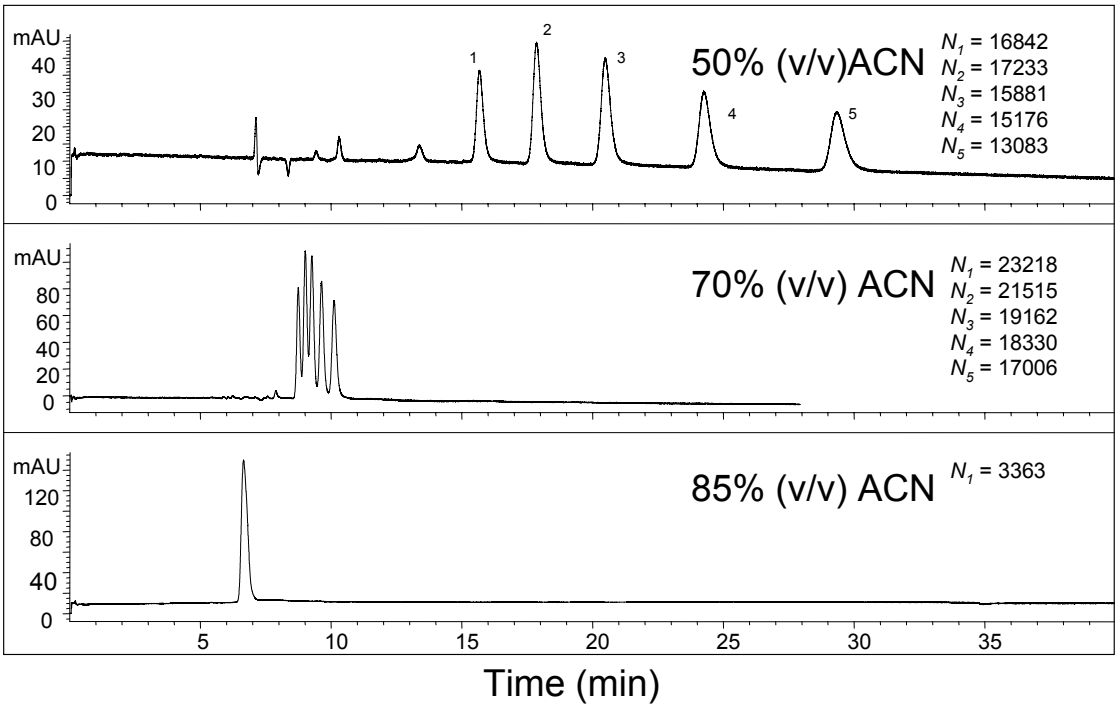

Figure 6.2. CEC separation of 5 alkylbenzenes (benzene, toluene, ethylbenzene, propylbenzene, and butylbenzene) at different % (v/v) ACN. CEC conditions: AAUL column, 33.5 cm total length, 25.0 cm monolithic bed length (8.5 cm from detection window to the outlet end). Applied voltage, +20 kV; high pressure, 6 bar applied at both ends of the column; column temperature, 20 ^{o}C. The mobile phase is a mixture of ACN and an aqueous buffer containing 5 mM NH_4OAc at different ratios using 0.3% (v/v) TEA (pH 4.5). UV detection wavelength, 200 nm. Analyte concentration, 1 mg/mL dissolved in ACN; injection, 3 kV for 3 sec.

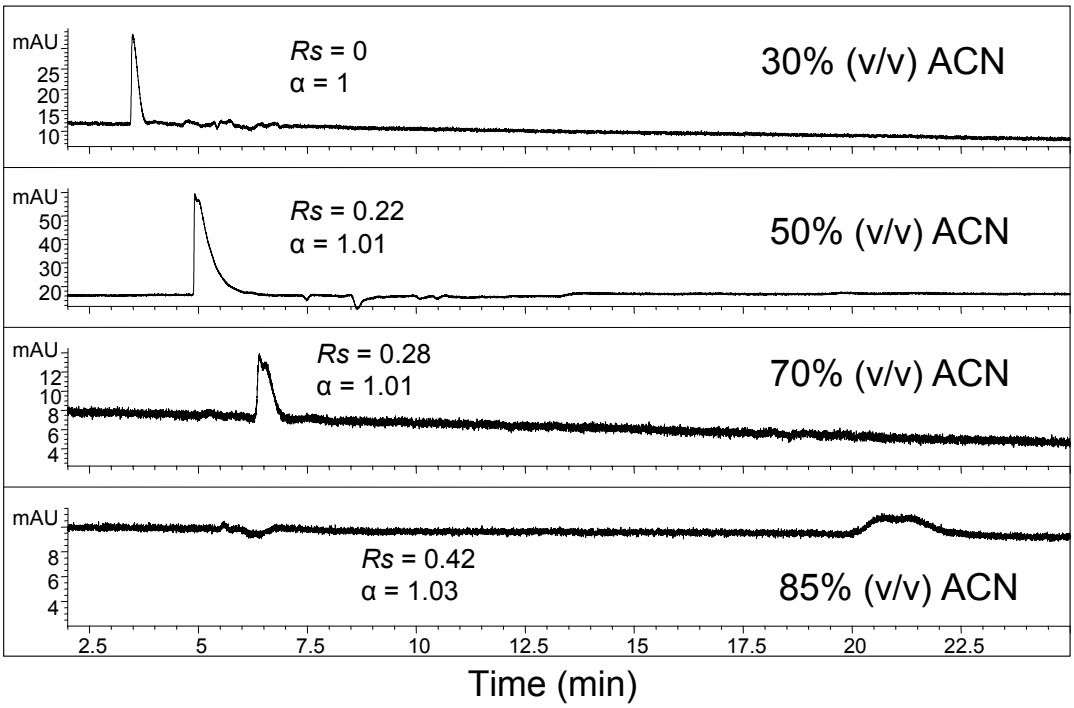

Figure 6.3. CEC separation of (±)-pseudoephedrine (PEP) at different % (v/v) of ACN. CEC conditions are the same as Figure 6.2 except for the mobile phase pH of 4.0. Analyte concentration, 1 mg/mL dissolved in 50/50 (v/v) ACN/H_2O.

(2) Effect of Mobile Phase pH

The pH of the mobile phase is a very important parameter that influences AAUL column performance and its chiral resolution. It is found in our preliminary experiment (data not shown) that when the mobile phase pH < 4.0, the retention of (±)-PEP was too short to provide any chiral resolution. On the other hand, when pH > 5.0, the retention time was too long. To investigate the effect of mobile phase pH on the separation performance a pH range of 4.0-5.0 was tested. In additioin, when pH of the mobile phase ≥ 5.5, the CEC current tends to be unstable, and no reproducible separations can be obtained. As a compromise between retention time and chiral selectivity, the effect of mobile phase pH on chiral CEC separation of (±)-PEP with AAUL column was studied at pH 4.0, 4.5, and 5.0 (Figure 6.4). Insets of each electrochromatogram summarize the retention factor, selectivity, peak efficiency and resolution. In the selected pH values, when increasing the mobile phase pH from 4.0 to 5.0, the retention time as well as chiral resolution both increase with only slight change in α. The k' and N values also increase as pH

increases. At pH 4.0, the *k'* is -0.14, which means (±)-PEP eluted faster than the neutral unretained compound (DMSO). Therefore, at lower mobile phase pH, the carboxyl group on the CSP surface is protonated, minimizing the ion-exchange interaction between CSP and the analytes, causesing shorter retention. On the other hand, upon increasing pH, the anionic carboxyl groups on the CSP tend to be more deprotonated and the ion-exchange effect becomes stronger, which causes longer retention of the cationic analyte. In addition, under all pH conditions, fixed amount of TEA was added. Because TEA is a fairly strong base, significant amount of acetic acid needs to added to the mobile phase to adjust the pH to 4.0 as compared to 4.5 and 5.0 mobile phases. Thus, the total mobile phase ionic strength at pH 4.0 is much stronger, which leads to faster elution due to the competition of TEA cation with the (±)-PEP for the cation-exchange sites on the CSP. Therefore, pH 5.0 mobile phase was optimum due to higher resolution.

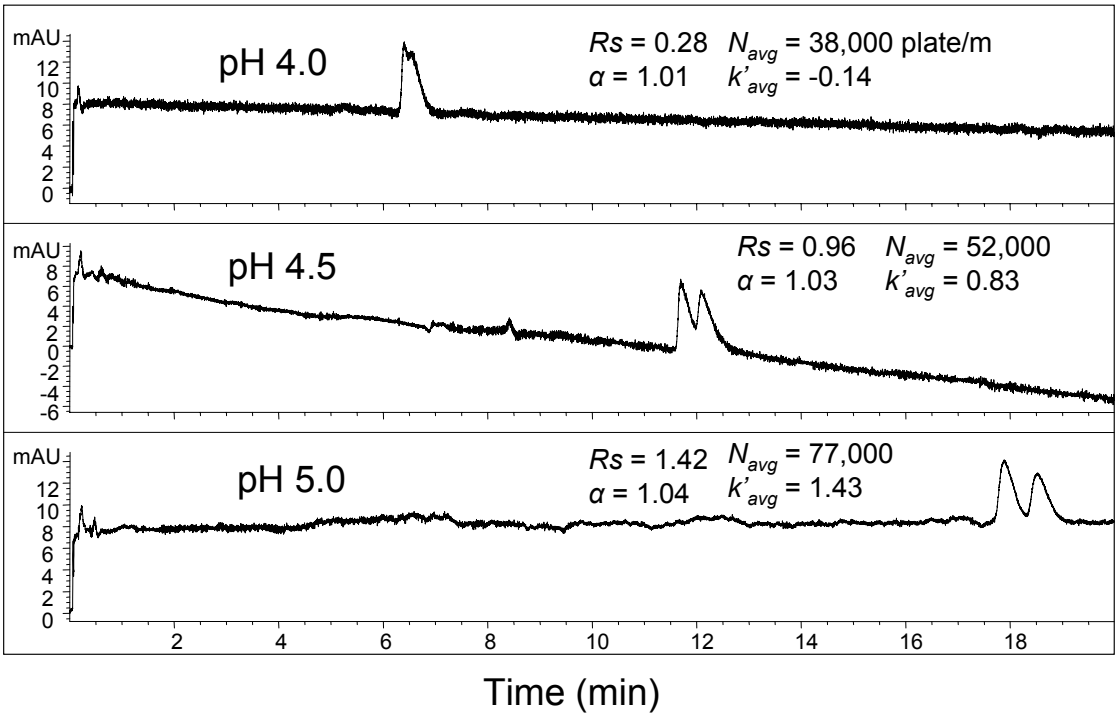

Figure 6.4. CEC separation of (±)-PEP at different mobile phase pH. The CEC conditions are same as Figure 6.2 except for the mobile phase pH was varied at 70% (v/v) ACN and 0.3% (v/v) TEA. Analyte concentration, 1 mg/mL dissolved in 50% (v/v) ACN/H_2O (50/50, v/v).

(3) Effect of Percent Triethylamine

The use of triethylamine as mobile phase additive is an important parameter to control peak asymmetry. On one hand, the concentration of TEA prevents peak tailing of the chiral enantiomer, while on the other hand, it can affect the ion-exchange equilibria altering retention on mixed-mode cation exchange/reversed phase monolithic column. Chiral CEC separations of (±)-PEP with AAUL column at different percent TEA were performed to examine the effect of TEA in the mobile phase. Figure 4 shows three representative enantioseparations with 0.15% (v/v), 0.30% (v/v), and 0.40% (v/v) TEA, respectively. Clearly, upon increasing the % (v/v) TEA, the retention time dropped significantly from 25 min to 15 min. This is probably due to the increasing competition between TEA ions and (±)-PEP ions for the ion-exchange sites on the CSP. This experiment demonstrated that surfactant bound AAUL column not only have hydrophobic interactions but cation exchange interactions are also important. In addition, note that the chiral *Rs* first improves at 0.3% (v/v) TEA and then drops at 0.4% (v/v) TEA. This suggests that a suitable ionic strength in the mobile phase is necessary for the cation exchange mechanism to work effectively, which may influence the chiral *Rs*. However, too much TEA (i.e.,0.4% v/v) may cause excess Joule heating resulting in peak broadening, thus deteriorating chiral separation. The optimum %TEA was eventually chosen to be 0.3% v/v.

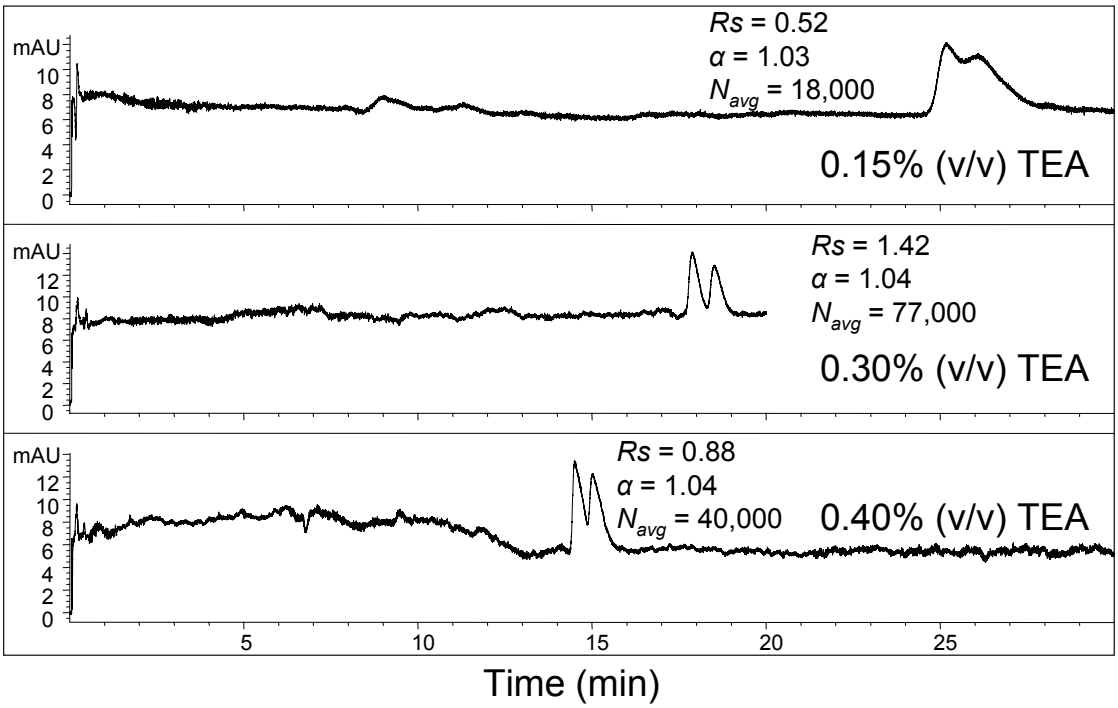

Figure 6.5. CEC separation of (±)-PEP at different % (v/v) of TEA. The CEC conditions are same as Figure 6.2 except % (v/v) TEA was varied at 70% (v/v) ACN and pH 5.0. Analyte concentration, 1 mg/mL dissolved in ACN/H_2O (50/50, v/v); injection, 3 kV for 2 sec.

(4) Effect the Chain Length and Head Group of the Chiral Surfactants

AAOL, AAUL, and AADoL CSP with leucine head group and C_8-, C_{11}- and C_{12}-hydrocarbon chain were tested for chiral separations of (±)-PEP to examine the effect of the surfactant chain length. Figure 6.6 (the top three electrochromatograms) shows the comparison of three overlaid separations. The AAOL monolithic column has the shortest retention, hence lowest *k'* (*k'* = 0.58, see Table 6.3 row #1) with worst chiral resolution and chiral selectivity. On the other hand, the AAUL column showed overall best chiral resolution and selectivity. AADoL column provides similar retention as compare to AAUL column. However, AADoL column provides comparable chiral selectivity and lower resolution than AAUL column. This trend suggests that even though (±)-PEP is a cationic chiral compound, which is retained by ion-exchange mechanism, hydrophobic partitioning between the surfactant monomer chains of the CSP also plays an important role in the chiral recognition mechanism.

The enantioseparations of (±)-PEP were compared with AAUL, AAUV, and AAUP monolithic columns to examine the effect of the surfactant head groups on the enantioselectivity (bottom three overlaid electrochromatograms, Figure 6.6). The elution time and *k'* increases with increasing hydrophobicity of the chiral head group (AAUP>AAUL>AAUV). It was observed that AAUL column provides an overall best chiral resolution, followed by AAUV column and AAUP column. It is not surprising to see that AAUL and AAUV column have similar chiral selectivity because the former differ from the later by the presence of only one extra methylene unit in the amino acid side chain. The enantiomers of (±)-PEP was retained most on the AAUP, through additional π- π interactions. However, this interaction did not provide any guarantee for improved enantioselectivity. Perhaps, the bulky phenyl group on the AAUP head group causes steric hindrance preventing selector-selectand interaction, weakening the diastereomeric complex formation needed for chiral recognition.

Besides (±)-PEP, ten more cationic chiral compounds were separated in CEC with all five surfactant-bound columns. The results are tabulated in Table 6.3. AAUP provided partial resolution of 4 out of 10 tested compounds, whereas AAOL provided no chiral *Rs* for any of ten compounds. The two AAUL and AAUV columns showed better but similar chiral *a* and *Rs*, whereas *Rs* and *a* of AADoL column are slightly worse.

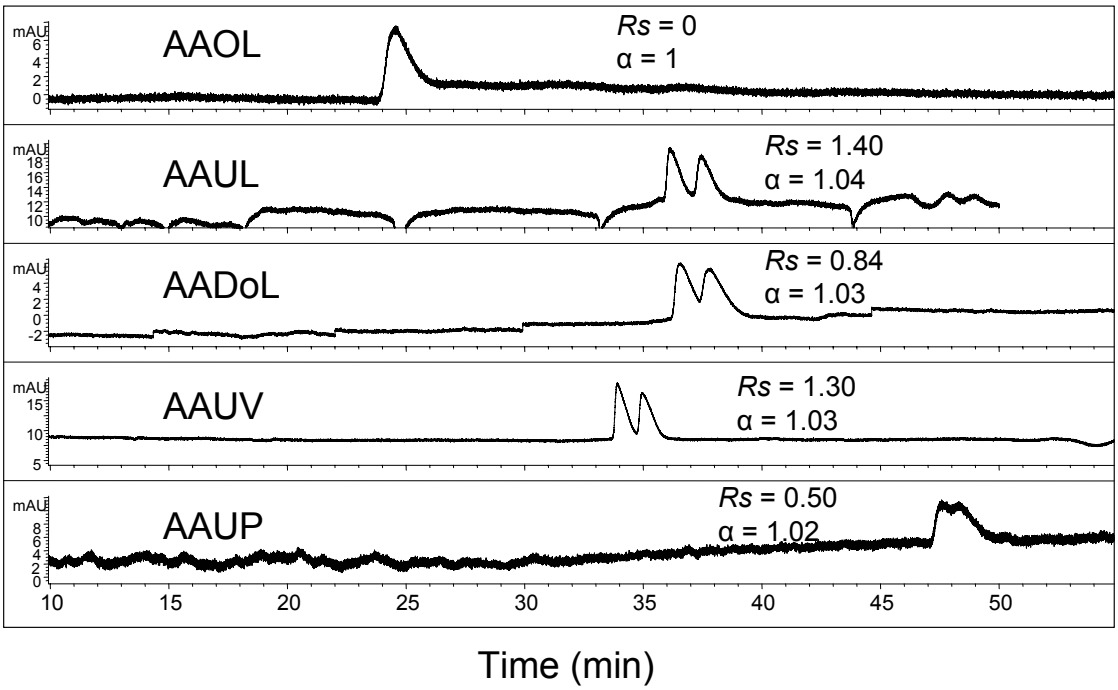

Figure 6.6. Effect of surfactant chain length and head groups of monolithic columns on chiral CEC separation of (±)-PEP. CEC conditions: AAOL, AAUL, AADoL, AAUV, and AAUP columns. Columns dimensions are same as Figure 6.2. Voltage, +10 kV; high pressure, 6 bar applied at both ends of the column; column temperature, 20 ^{o}C; mobile phase, a mixture of 70% ACN and 30% aqueous buffer containing 5 mM NH_4OAc, 0.5% TEA (pH 5.0); UV detection wavelength, 200 nm. Analyte concentration, 1 mg/mL dissolved in ACN/H_2O (50/50, v/v); injection, 3 kV for 2 sec.

Table 6.3. Capacity factor *k'* (average of the two enantiomers), chiral resolution *Rs*, and selectivity *α* for the test compounds on the five monolithic columns*

Analytes	AAOL			AAUL			AADoL			AAUV			AAUP		
	k'_{avg}	*Rs*	*α*	k'_{avg}	*Rs*	*α*	k'_{avg}	*Rs*	*α*	k'_{avg}	*Rs*	*α*	k'_{avg}	*Rs*	*α*
Pseudoephedrine	0.58	0	1	1.76	1.13	1.036	1.80	0.83	1.034	1.46	1.10	1.031	1.77	0.53	1.016
Ephedrine	0.85	0	1	1.92	0.81	1.034	1.88	0.74	1.034	1.93	0.73	1.026	1.88	0	1
N-methylephedrine	0.32	0	1	0.98	0.83	1.031	1.65	0.70	1.029	1.66	0.57	1.021	1.11	0.39	1.016
Norepinephrine	0.83	0	1	1.25	0.50	1.022	1.90	0.09	1.003	1.66	0.58	1.016	1.29	0.27	1.011
Synephrine	0.49	0	1	1.27	0.64	1.026	1.40	0.45	1.007	1.39	0.35	1.013	1.34	0	1
Norphenylephrine	0.63	0	1	1.49	0.58	1.031	1.50	0.51	1.024	1.54	0.45	1.017	1.66	0.55	1.022
Alprenolol	0.76	0	1	2.29	0.35	1.031	2.93	0.66	1.021	2.91	0.26	1.010	2.68	0	1
Atenolol	0.82	0	1	0.94	0.25	1.008	1.07	0.24	1.006	1.35	0.21	1.005	1.57	0	1
Metoprolol	0.37	0	1	1.32	0.31	1.013	1.88	0.37	1.013	2.55	0.17	1.004	1.40	0	1
Oxprenolol	0.06	0	1	1.31	0.42	1.014	1.63	0.45	1.014	1.95	0.25	1.009	1.44	0	1
Pindolol	0.97	0	1	2.37	0.34	1.016	2.74	0.28	1.011	2.74	0.22	1.011	3.24	0	1

* CEC condition: 33.5 cm long monolithic column, 25 cm monolithic bed, 8.5 cm from UV window to the outlet end. M.P.: 70% ACN, 30% aqueous buffer containing 5 mM NH_4OAc, 0.5% TEA, pH 5.0. Voltage: +10 kV, 20 ^{o}C. Analytes: 1 mg/mL in 50/50 ACN/H_2O, Injection: 3 kV, 2 sec.

(5) Comparison of Chiral CEC and CMEKC with Same Surfactant Monomer

Chiral CEC experiments with AAUL monolithic column and CMEKC experiments with poly-SAAUL molecular micelle were compared for a series of chiral compounds to explore the difference between chiral interaction on the surface vs. solution phase in CEC and MEKC, respectively using the same chiral selector derived from the same surfactant. The CEC mobile phase conditions were optimized by the experiments discussed above. The CMEKC conditions (NH_4OAc concentration, molecular micelle concentration, buffer pH, organic modifier) were also optimized (data not shown). Table 6.4 compares the separations achieved on the 11 cationic compounds on the optimized CEC and MEKC mobile phase conditions. Several trends are evident. First, note that the retention time for all the test compounds by MEKC is much shorter compared to CEC. Thus the mobility of the analytes is almost two-fold higher compared to CEC. Second, efficiency of the peaks in CMEKC is an order of magnitude higher. This means CMEKC usually has sharper peaks, but sharper peaks not always generate higher *Rs*. Third, several cationic compounds (±)-PEP, (±)-ephedrine, and (±)-norephedrine were better resolved with CEC. On the other hand, MEKC provides better separation on (±)-atenolol, (±)-metoprolol, (±)-pindolol, and (±)-norphenylephrine. For (±)-alprenolol and (±)-*N*-methylephedrine, both CE modes provide similar enantioselectivity. In CEC, negative analyte such as (±)-BNP does not elute. However, in CMEKC, it is well separated. Therefore, it can be concluded from this experiment that the enantioselectivities for chiral compounds between CEC versus CMEKC are complementary and analyte dependent. Figure 6.7 shows a representative overlaid electropherogram of the chiral separation of (±)-PEP with CEC and CMEKC, respectively. Clearly, the run time is shorter, but *Rs* and α is lower for the same analyte using CMEKC.

Table 6.4. Comparison of CEC using poly-AAUL-co-EDMA monolith as stationary phase and MEKC using poly-SAAUL as pseudostationary phase. t_{R1} and t_{R2} are retention times of the first and second eluting peaks; N_1 and N_2 are efficiencies of the first and second eluting peaks; S_1 and S_2 are symmetry of the first and second eluting peaks; μ_1 and μ_2 are mobility of the first and second eluting peaks; α is the selectivity; Rs is the resolution.

compound	t_{R1} (min)	t_{R2} (min)	N_1 (m^{-1})	N_2 (m^{-1})	μ_1 ($cm^2V^{-1}S^{-1}$)	μ_2 ($cm^2V^{-1}S^{-1}$)	α	Rs
[a)]CEC								
pseudoephedrine	18.0	18.6	6.98×10^4	8.73×10^4	3.89×10^{-5}	3.75×10^{-5}	1.04	1.28
ephedrine	16.2	16.8	9.58×10^4	6.71×10^4	4.30×10^{-5}	4.16×10^{-5}	1.03	1.20
N-methylephedrine	15.9	16.4	5.96×10^4	3.48×10^3	4.39×10^{-5}	4.26×10^{-5}	1.03	0.75
norephedrine	20.6	21.4	5.58×10^4	2.84×10^4	3.39×10^{-5}	3.26×10^{-5}	1.04	0.93
norphenylephrine	20.9	21.4	4.46×10^4	1.53×10^4	3.34×10^{-5}	3.26×10^{-5}	1.02	0.45
metoprolol	16.7	16.9	1.46×10^5	5.57×10^4	4.18×10^{-5}	4.13×10^{-5}	1.01	0.51
pindolol	28.0	28.5	8.62×10^4	2.09×10^4	2.50×10^{-5}	2.45×10^{-5}	1.02	0.47
alprenolol	25.1	25.6	1.09×10^5	3.50×10^4	2.78×10^{-5}	2.73×10^{-5}	1.02	0.47
atenolol	14.7	14.8	2.87×10^5	2.36×10^4	4.76×10^{-5}	4.72×10^{-5}	1.01	0.29
[b)]MEKC								
pseudoephedrine	7.80	7.84	9.18×10^5	1.58×10^5	8.95×10^{-5}	8.90×10^{-5}	1.01	0.38
ephedrine	8.17	8.21	7.97×10^5	9.63×10^4	8.55×10^{-5}	8.50×10^{-5}	1.01	0.29
N-methylephedrine	7.73	7.84	3.53×10^5	1.02×10^5	9.03×10^{-5}	8.90×10^{-5}	1.01	0.75
norephedrine	8.56	8.58	4.62×10^6	2.80×10^5	8.15×10^{-5}	8.14×10^{-5}	1.01	0.20
norphenylephrine	9.43	9.53	2.82×10^5	8.23×10^4	7.40×10^{-5}	7.32×10^{-5}	1.01	0.53
metoprolol	10.63	10.75	7.05×10^5	2.91×10^5	6.57×10^{-5}	6.49×10^{-5}	1.01	0.92
pindolol	12.95	13.06	7.87×10^5	3.91×10^5	5.39×10^{-5}	5.35×10^{-5}	1.01	0.72
alprenolol	14.97	15.02	2.40×10^6	4.76×10^5	4.66×10^{-5}	4.65×10^{-5}	1.01	0.45
atenolol	7.51	7.55	1.32×10^6	3.67×10^5	9.29×10^{-5}	9.24×10^{-5}	1.01	0.51
BNP	13.88	14.10	4.20×10^5	3.70×10^5	5.03×10^{-5}	4.95×10^{-5}	1.02	1.21

a)CEC condition: 33.5 cm long monolithic column, 25 cm packed bed, 8.5 cm from UV window to the outlet end. M.P.: 70% ACN, 30% aqueous buffer containing 5 mM NH_4OAc, 0.3% TEA, pH 5.0. Voltage: +20 kV, 20 ^oC. Analytes: 1 mg/mL in 50/50 ACN/H_2O. Injection: 3 kV, 2 sec.

b)MEKC condition: 64.5 cm capillary, M.P.: 25 mM NH_4OAc, pH 8.8, 25 mM poly-SAAUL, +20 kV, 20 ^oC. Analytes: 2 mg/mL in 50/50 MeOH/H_2O. Injection: 3 kV, 2 sec 5 mbar, 5 sec.

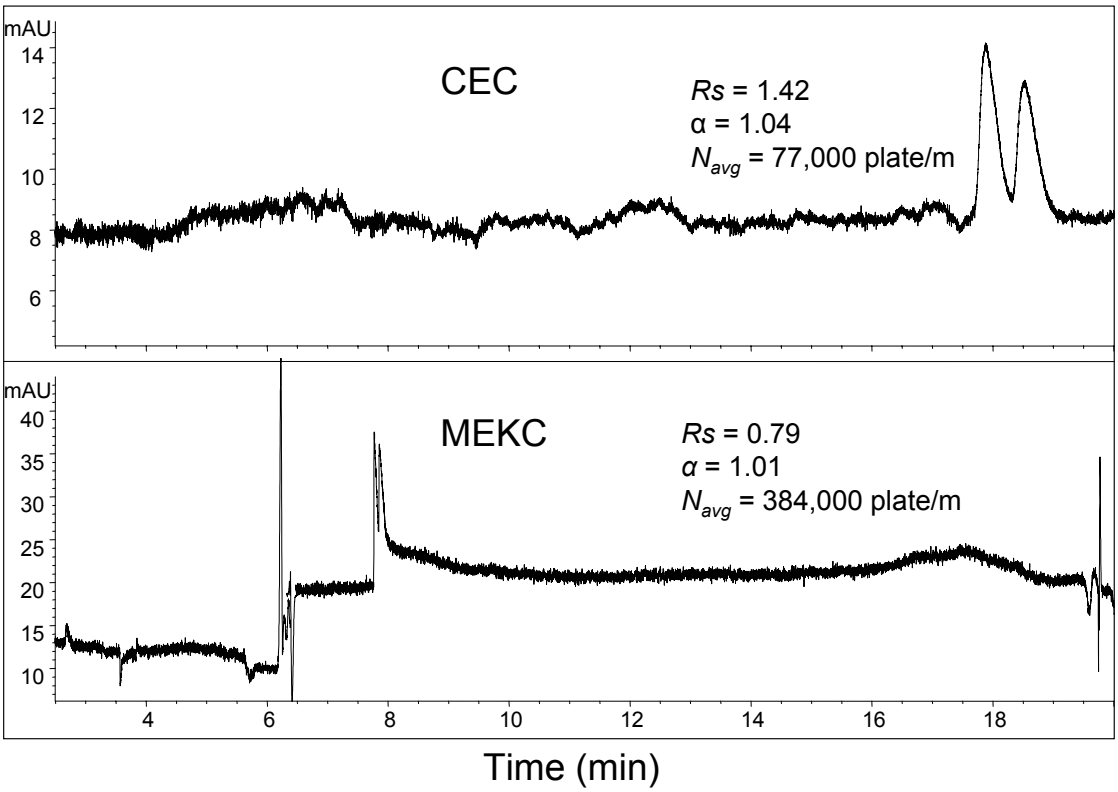

Figure 6.7. Comparison of CEC (with poly-(AAUL-*co*-EDMA) monolithic column, top) and CMEKC (with poly-SAAUL surfactant) on the chiral separation of (±)-PEP. CEC column dimensions are the same as Figure 6.2 and mobile phase conditions are same as optimized in Figure 6.5. MEKC conditions: 50 μm i.d. capillary, total capillary length = 64.5 cm, effective length= 56.0 cm (detention windows made at 8.5 cm from the outlet end). Running MEKC buffer: 25 mM NH_4OAc, pH 8.8, 25 mM poly-SAAUL, +20 kV, 20 ^oC. Analytes: 2 mg/mL in 50/50 MeOH/H_2O; injection, 5 mbar, 5 sec.

6.4 Conclusions

In this study, five chiral surfactant-bound monolithic columns (poly-(AAOL-*co*-EDMA), poly-(AAUL-*co*-EDMA), poly-(AADoL-*co*-EDMA), poly-(AAUV-*co*-EDMA), and poly-(AAUP-*co*-EDMA) monoliths) were successfully synthesized and characterized. After optimizing the polymerization conditions, the application of these columns for chiral separation is demonstrated for the first time in literature. The mobile phase conditions were optimized using AAUL monolithic column for enantioseparation of (±)-PEP. The result indicates that volume fraction of both ACN and TEA influence retention and enantioselectivity, suggesting a mixed-mode hydrophobic and cation exchange mechanism is operative. Under the optimized mobile

phase, the effects of surfactant chain length and head groups on their enantioseparation capability were compared. The result indicates that if the surfactant alkyl chain is too short (i.e. ≤ 8 carbons), the surfactant-bound CSP loses its chiral selectivity. On the other hand, surfactant-bound columns with bulky head group such as AAUP are inferior to monolithic columns with leucine or valine head group (i.e., AAUL and AAUV). Overall, the C_{11} surfactant with leucine head group (i.e., AAUL column) provided the best chiral selectivity.

The sodium salt of surfactant monomer (i.e., SAAUL) was also polymerized in aqueous solution to form molecular micelle (i.e., poly-SAAUL). The poly-SAAUL molecular micelle was then used as a chiral pesudostationary phase in CMEKC separation of several cationic and anionic compounds. The results from the CMEKC were compared with CEC using poly-(AAUL-*co*-EDMA) column. Thus, even using the same chiral selector (SAAUL in CMEKC, AAUL in CEC), the enantioselectivities of the two CE modes are analyte dependent. For example, (±)-PEP, (±)-ephedrine, and (±)-norephedrine were better resolved with CEC; while MEKC provides better enantio-separation for (±)-atenolol, (±)-metoprolol, (±)-pindolol, and (±)-norphenylephrine. In addition, the CMEKC mode has an additional advantage of being able to separate both chiral cationic (e.g., β-blockers, phenylethylamines) and anionic [e.g., (±)-BNP] compounds. Future work will involve detailed study on comparison of chiral MEKC and CEC modes. For example, we plan to compare the effect of chain lengths and head groups for several classes of chiral compounds in both CEC and MEKC modes. Such studies may provide better insights on the structural features that are important in improving the enantioselectivities in these two modes of chiral CEC.

References

[1] Mayer, S.; Schurig, V. *J. High Resolut. Chromatogr.* **1992,** *15* (2), 129-131.

[2] Zheng, J.; Shamsi, S. A., Chiral Analysis in Capillary Electrochromatography (CEC) and CEC couped to Mass Spectrometry. In *Chiral Separation Techniques: A Practical Approach, 3rd, Completely Revised and Updated Edition*, Subramanian, G., Ed. WILEY-VCH: Weinheim, 2007; pp 441-504.

[3] Kapnissi-Christodoulou, C. P.; Zhu, X.; Warner, I. M. *Electrophoresis* **2003,** *24* (22-23), 3917-3934.

[4] Kamande, M. W.; Fletcher, K. A.; Lowry, M.; Warner, I. M. *J. Sep. Sci.* **2005,** *28* (8), 710-718.

[5] Wang, Y.; Zeng, Z.; Guan, N.; Cheng, J. *Electrophoresis* **2001,** *22* (11), 2167-2172.

[6] Kawamura, K.; Otsuka, K.; Terabe, S. *J. Chromatogr. A* **2001,** *924* (1-2), 251-257.

[7] Mayer, S.; Briand, X.; Francotte, E. *J. Chromatogr. A* **2000,** *875* (1-2), 331-339.

[8] Zheng, J.; Shamsi, S. A. *Anal. Chem.* **2006,** *78* (19), 6921-6927.

[9] Tian, Y.; Zhong, C.; Fu, E.; Zeng, Z. *J. Chromatogr. A* **2009,** *1216* (6), 1000-1007.

[10] Dong, X.; Wu, R.; Dong, J.; Wu, M.; Zhu, Y.; Zou, H. *Electrophoresis* **2008,** *29* (4), 919-927.

[11] Lammerhofer, M.; Svec, F.; Frechet, J. M. J.; Lindner, W. *Anal. Chem.* **2000,** *72* (19), 4623-4628.

[12] Gusev, I.; Huang, X.; Horváth, C. *J. Chromatogr. A* **1999,** *855* (1), 273-290.

[13] Liu, Z.; Otsuka, K.; Terabe, S.; Motokawa, M.; Tanaka, N. *Electrophoresis* **2002,** *23* (17), 2973-2981.

[14] Chen, Z.; Hobo, T. *Anal. Chem.* **2001,** *73* (14), 3348-3357.

[15] Schmid, M. G.; Grobuschek, N.; Tuscher, C.; Gübitz, G.; Végvári, Á.; Machtejevas, E.; Maruška, A.; Hjertén, S. *Electrophoresis* **2000,** *21* (15), 3141-3144.

[16] Hayes, J. D.; Malik, A. *Anal. Chem.* **2000,** *72* (17), 4090-4099.

[17] Zhang, Z.; Wu, R. a.; Wu, M.; Zou, H. *Electrophoresis* **2010,** *31* (9), 1457-1466.

[18] Kornyšova, O.; Jarmalavičienė, R.; Maruška, A. *Electrophoresis* **2004,** *25* (16), 2825-2829.

[19] Dong, X.; Dong, J.; Ou, J.; Zhu, Y.; Zou, H. *Electrophoresis* **2007,** *28* (15), 2606-2612.

[20] Dong, X.; Wu, R. a.; Dong, J.; Wu, M.; Zhu, Y.; Zou, H. *J. Chromatogr. B* **2008,** *875* (1), 317-322.

[21] Guerrouache, M.; Millot, M.-C.; Carbonnier, B. *Macromol. Rapid Commun.* **2009,** *30* (2), 109-113.

[22] Mizrahi, S.; Rizkov, D.; Shames, A. I.; Lev, O. *Electrophoresis* **2008,** *29* (18), 3941-3948.

[23] Roy, S.; Dey, J. *Langmuir* **2005,** *21* (23), 10362-10369.

[24] Lapidot, Y.; Rappoport, S.; Wolman, Y. *J. Lipid Res.* **1967,** *8* (2), 142-5.

[25] Yeoh, K. W.; Chew, C. H.; Can, L. M.; Koh, L. L.; Teo, H. H. *Journal of Macromolecular Science: Part A - Chemistry* **1989,** *26* (4), 663-680.

[26] Gu, C.; He, J.; Jia, J.; Fang, N.; Shamsi, S. A. *Electrophoresis* **2009,** *30* (22), 3814-3827.

[27] Hou, J.; Zheng, J.; Shamsi, S. A. *J. Chromatogr. A* **2007,** *1159* (1-2), 208-216.

Appendix A

Supporting Material for Chapter 4

Table A1. Level of factors in the CCD experiment for the optimization of separation parameters

Level	F_1 Voltage (kV)	F_2 pH	F_3 [Surf.] (mM)	F_4 [NH_4OAc] (mM)
-1	15	8	50	20
0	20	9	60	30
+1	25	10	70	40

Table A2. Resolution and total run time data gathered from the CCD experiment for the optimization of separation

	F_1 Voltage	F_2 pH	F_3 [Surf.]	F_4 [NH_4OAc]	Resolution/retention time (Rs/t_R)				t_R
Exp. #	(kV)		(mM)	(mM)	HBNZ	BNZ	BME	BEE	(min)
1	25.0	8.0	70.0	20.0	0.023	0.046	0.037	0.020	33.2
2	20.0	9.0	60.0	50.0	0.023	0.047	0.030	0.015	52.4
3	25.0	10.0	70.0	20.0	0.025	0.061	0.039	0.020	35.7
4	20.0	9.0	60.0	30.0	0.014	0.052	0.032	0.018	43.9
5	20.0	9.0	40.0	30.0	0.018	0.048	0.032	0.019	37.5
6	15.0	10.0	70.0	20.0	0.017	0.032	0.027	0.011	62.7
7	15.0	8.0	50.0	20.0	0.015	0.036	0.021	0.015	50.8
8	25.0	10.0	50.0	40.0	0.021	0.054	0.040	0.017	35.5
9	15.0	10.0	50.0	20.0	0.016	0.040	0.024	0.012	57.7
10	25.0	10.0	50.0	20.0	0.025	0.060	0.044	0.020	34.1
11	20.0	9.0	60.0	30.0	0.017	0.047	0.036	0.015	44.2
12	15.0	8.0	70.0	20.0	0.014	0.033	0.023	0.009	60.7
13	20.0	9.0	80.0	30.0	0.020	0.042	0.028	0.015	51.6
14	20.0	9.0	60.0	30.0	0.019	0.045	0.038	0.016	44.9
15	10.0	9.0	60.0	30.0	0.011	0.024	0.014	0.009	91.4
16	15.0	8.0	50.0	40.0	0.014	0.033	0.024	0.011	64.5
17	20.0	9.0	60.0	30.0	0.018	0.050	0.038	0.016	44.8
18	25.0	8.0	50.0	20.0	0.014	0.049	0.037	0.021	30.7
19	15.0	10.0	70.0	40.0	0.015	0.033	0.022	0.012	85.1
20	15.0	10.0	50.0	40.0	0.014	0.035	0.024	0.012	63.3
21	30.0	9.0	60.0	30.0	0.025	0.063	0.046	0.024	29.4
22	20.0	7.0	60.0	30.0	0.017	0.053	0.035	0.014	47.1
23	20.0	9.0	60.0	30.0	0.017	0.049	0.032	0.016	45.1
24	20.0	9.0	60.0	30.0	0.018	0.049	0.031	0.016	45.0
25	25.0	8.0	70.0	40.0	0.021	0.059	0.041	0.024	42.1
26	15.0	8.0	70.0	40.0	0.016	0.032	0.028	0.012	71.8
27	20.0	9.0	60.0	10.0	0.018	0.047	0.037	0.023	42.8
28	25.0	8.0	50.0	40.0	0.021	0.063	0.047	0.022	36.7
29	20.0	11.0	60.0	30.0	0.019	0.056	0.037	0.021	56.3
30	25.0	10.0	70.0	40.0	0.028	0.066	0.040	0.025	47.9

Table A3. ANOVA table for models used in the optimization of MEKC parameters

Responses	Source	Sum of squares	Degree of freedom	Mean square	*F*-ratio	Prob>*F*
Rs/t_R-HBNZ	Model	3.69×10^{-4}	4	9.23×10^{-5}	18.4	<0.0001
	Residual	1.25×10^{-4}	25	5.01×10^{-6}		
	Corrected total	4.94×10^{-4}	29			
Rs/t_R-BNZ	Model	3.30×10^{-3}	14	2.36×10^{-4}	17.9	<0.0001
	Residual	1.98×10^{-4}	15	1.32×10^{-5}		
	Corrected total	3.50×10^{-3}	29			
Rs/t_R-BME	Model	1.60×10^{-3}	4	4.01×10^{-4}	36.5	<0.0001
	Residual	2.74×10^{-4}	25	1.10×10^{-5}		
	Corrected total	1.88×10^{-3}	29			
Rs/t_R-BEE	Model	4.66×10^{-4}	4	1.16×10^{-4}	21.4	<0.0001
	Residual	1.36×10^{-4}	25	5.44×10^{-6}		
	Corrected total	6.02×10^{-4}	29			
Migration time	Model	6.45×10^{3}	14	4.61×10^{2}	60.3	<0.0001
	Residual	1.15×10^{2}	15	7.64		
	Corrected total	6.57×10^{3}	29			

Table A4. Level of factors in the CCD experiment for the optimization of sheath liquid parameters

Level	F_1 MeOH %(v/v)	F_2 [NH_4OAc] (mM)	F_3 Acetone % (v/v)	F_4 Flow rate (μL/min)
-1	50	2.5	0.5	10.0
0	65	5.0	1.0	12.0
+1	80	7.5	1.5	14.0

Table A5. Peak area gathered from the CCD experiment for the optimization of sheath liquid

Exp. #	F_1 MeOH % (v/v)	F_2 [NH_4OAc] (mM)	F_3 Acetone % (v/v)	F_4 Flow rate (μL/min)	Peak area			
					HBNZ	BNZ	BME	BEE
1	50	2.5	0.5	14	11406	71087	189036	204114
2	65	5.0	0.0	12	15375	100261	203094	205348
3	50	2.5	1.5	14	10157	49136	203189	202825
4	65	5.0	1.0	8	16383	90193	219366	234805
5	65	5.0	1.0	12	16040	104770	341911	373883
6	35	5.0	1.0	12	N/A	N/A	N/A	N/A
7	80	7.5	0.5	14	28723	190898	539254	582720
8	80	2.5	0.5	14	35115	213873	604869	613988
9	80	2.5	0.5	10	47427	278152	577652	596163
10	65	5.0	1.0	12	29804	179265	566755	615312
11	50	7.5	0.5	10	38462	214391	570320	632359
12	95	5.0	1.0	12	36579	209634	694972	703318
13	65	0.0	1.0	12	28062	68230	448115	519447
14	65	5.0	1.0	12	39537	208416	654505	693827
15	50	2.5	1.5	10	31496	171669	575136	618985
16	80	7.5	0.5	10	49471	284042	684655	683005
17	50	7.5	1.5	14	22435	134620	615371	668744
18	50	2.5	0.5	10	41657	241607	590344	635407
19	65	5.0	1.0	12	28899	182179	623164	644606
20	65	5.0	1.0	12	36969	196993	611052	686855
21	65	10.0	1.0	12	35478	201678	690384	758709
22	65	5.0	1.0	12	36031	186579	599116	616705
23	80	2.5	1.5	14	26074	128774	571807	597240
24	65	5.0	1.0	16	29534	169848	633704	687858
25	50	7.5	1.5	10	26864	176185	607213	669941
26	50	7.5	0.5	14	18834	116180	542468	527836
27	65	5.0	2.0	12	20004	120115	538049	524272
28	80	7.5	1.5	10	32378	204029	640586	633165
29	80	2.5	1.5	10	37164	208715	697016	623839
30	80	7.5	1.5	14	33656	166529	702247	649286

Table A6. ANOVA table for models used in the optimization of sheath liquid parameters

Responses	Source	Sum of squares	Degree of freedom	Mean square	*F*-ratio	Prob>*F*
Peak area - HBNZ	Model	9.82×10^{8}	4	2.46×10^{8}	3.10	**0.0343**
	Residual	1.90×10^{9}	24	7.92×10^{7}		
	Corrected total	2.88×10^{9}	28			
Peak area - BNZ	Model	4.06×10^{10}	4	1.02×10^{10}	4.06	**0.0118**
	Residual	6.00×10^{10}	24	2.50×10^{9}		
	Corrected total	1.01×10^{11}	28			
Peak area - BME	Model	0.00	0			
	Residual	6.89×10^{11}	28	2.46×10^{10}		
	Corrected total	6.89×10^{11}	28			
Peak area - BEE	Model	0.00	0			
	Residual	7.24×10^{11}	28	2.59×10^{10}		
	Corrected total	7.24×10^{11}	28			

Table A7. Level of factors in the CCD experiment for the optimization of spray chamber parameters

Level	F_1 DGF (L/min)	F_2 DGT (^{o}C)	F_3 VT (^{o}C)
-1	4.0	100	100
0	5.0	150	150
+1	6.0	200	200

Table A8. Resolution and total run time data gathered from the CCD experiment for the optimization of spray chamber parameters

Exp. #	F_1 DGF (L/min)	F_2 DGT (^oC)	F_3 VT (^oC)	Peak area HBNZ	BNZ	BME	BEE
1	3.3	150	150	10633	55435	427069	436585
2	6.7	150	150	13653	128574	305782	332782
3	4.0	200	100	25696	151395	526240	640864
4	5.0	66	150	57121	332381	763018	819166
5	5.0	150	150	52559	312957	676033	726227
6	5.0	150	150	50350	302586	645936	696015
7	6.0	200	100	11715	53788	193967	276900
8	6.0	100	200	110663	165089	323519	387406
9	6.0	200	200	43217	125289	266209	299572
10	5.0	234	150	36138	176585	353147	411303
11	4.0	100	100	20910	117037	441433	603603
12	5.0	150	150	46175	206247	534744	623161
13	5.0	150	234	N/A*	N/A*	N/A*	N/A*
14	5.0	150	150	33480	188423	383790	439183
15	5.0	150	150	36636	203988	431433	487037
16	5.0	150	66	12998	41986	207566	316791
17	4.0	200	200	40588	180211	361956	388578
18	4.0	100	200	45647	195522	397981	443025
19	6.0	100	100	10664	55451	188852	229542
20	5.0	150	150	31640	178390	386368	423541

* Data unavailable due to current break down

Table A9. ANOVA table for models used in the optimization of spray chamber parameters

Responses	Source	Sum of squares	Degree of freedom	Mean square	*F*-ratio	Prob>*F*
Peak area - HBNZ	Model	9.09×10^9	9	2.46×10^8	3.10	**0.0343**
	Residual	9.42×10^8	9	1.05×10^8		
	Corrected total	1.00×10^{10}	18			
Peak area - BNZ	Model	9.73×10^{10}	9	1.08×10^{10}	2.90	0.0645
	Residual	3.36×10^{10}	9	3.73×10^9		
	Corrected total	1.31×10^{11}	18			
Peak area - BME	Model	3.17×10^{11}	9	3.53×10^{10}	2.16	0.134
	Residual	1.47×10^{11}	9	1.63×10^{10}		
	Corrected total	4.64×10^{11}	18			
Peak area - BEE	Model	3.45×10^{11}	9	3.83×10^{10}	2.26	0.121
	Residual	1.53×10^{11}	9	1.70×10^{10}		
	Corrected total	4.98×10^{11}	18			

Appendix B

Supporting Material for Chapter 5

Table B1. Elemental analysis of AAOCL, AADCL, and AADoCL monomers

Surfactant	Elemental analysis		
	Element	Theory	Found
AAOCL	C	60.65	55.84
	H	9.05	8.93
	N	7.86	4.93
	O	22.44	30.45
AADCL	C	62.47	62.11
	H	9.44	9.47
	N	7.29	6.97
	O	20.80	21.57
AADoCL	C	64.05	64.24
	H	9.77	9.80
	N	6.79	6.77
	O	19.39	19.52

The theoretical numbers for each element were calculated based on the formula of the molecule. For example: In AADCL, the formula of the molecule is $C_{20}H_{36}N_2O_5$; molecular weight is 384.51

C% = 12.01*20/384.51 = 0.6247 or 62.47%

H% = 1.008*36/384.51 = 0.0944 or 9.44%

N% = 14.0067*2/384.51 = 0.0729 or 7.29%

O% = 15.9994*5/384.51 = 0.2080 or 20.80%

Table B2. Composition of the polymerization mixtures used in the preparation of the surfactant-bound monolithic columns

Column	Monomers (wt%)			Porogen (wt%)				Initiator (wt%)
	Surfactant	AMPS	EDMA	Dimethyl ether	ACN	MeOH	H_2O	AIBN
AADCL-1	15	0	15	0	45	20	5	0.5
AADCL-2	15	0	15	0	50	20	0	0.5
AADCL-3	15	0.5	15	0	45	20	5	0.5
AADCL-4	15	0	15	35	0	35	0	0.5

Sample calculation for the make of the polymerization mixture:

Total weight of the polymerization mixture is usually 100 mg.

Surfactant monomer: 100 x 15% = 15 mg (weighted with a balance)

AIBN: 100 x 0.5% = 0.5 mg (weighted with a balance)

ACN: 100 x 45% / 0.786 = 57.2 μL (transferred with a pipette, 0.786 is the density of ACN)

MeOH: 100 x 20% / 0.792 = 25.3 μL (transferred with a pipette, 0.792 is the density of MeOH)

EDMA: 100 x 15% / 1.051 = 14.3 μL (transferred with a pipette, 1.051 is the density of EDMA)

H_2O: 100 x 5% = 5 μL (transferred with a pipette)

Sample calculation for the volumetric flow rate used in the measurement of porosity:

For example, if in 60 minutes, the vial that was used to collect the eluting mobile phase gained 0.05 g, the volumetric flow rate would be:

$0.05/0.786/1000000/3600=1.8\times10^{-11}$ m^3/s (where 0.786 g/mL is the density of pure ACN which was used as mobile phase).

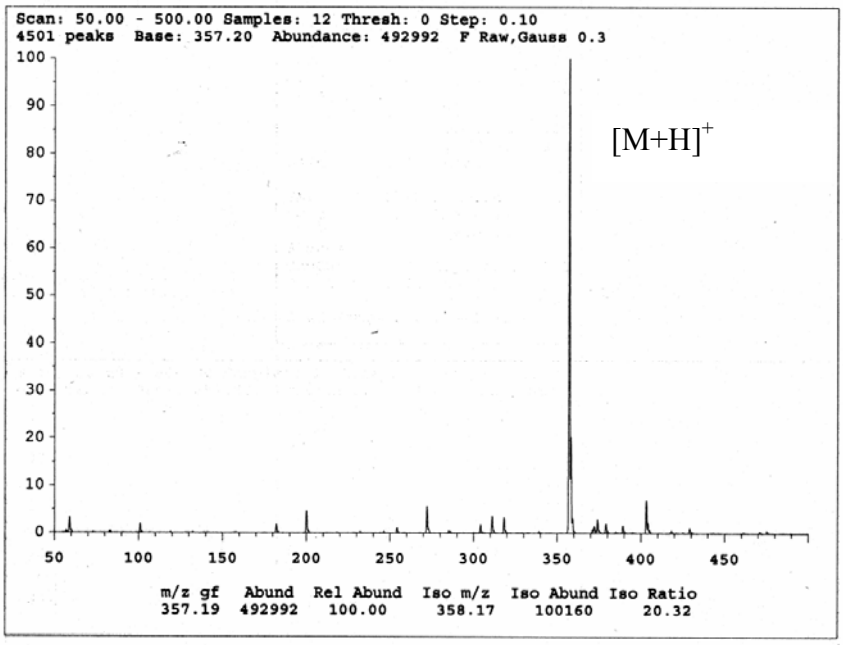

Figure B1. ESI-MS spectrum of SAAOCL in positive ion mode

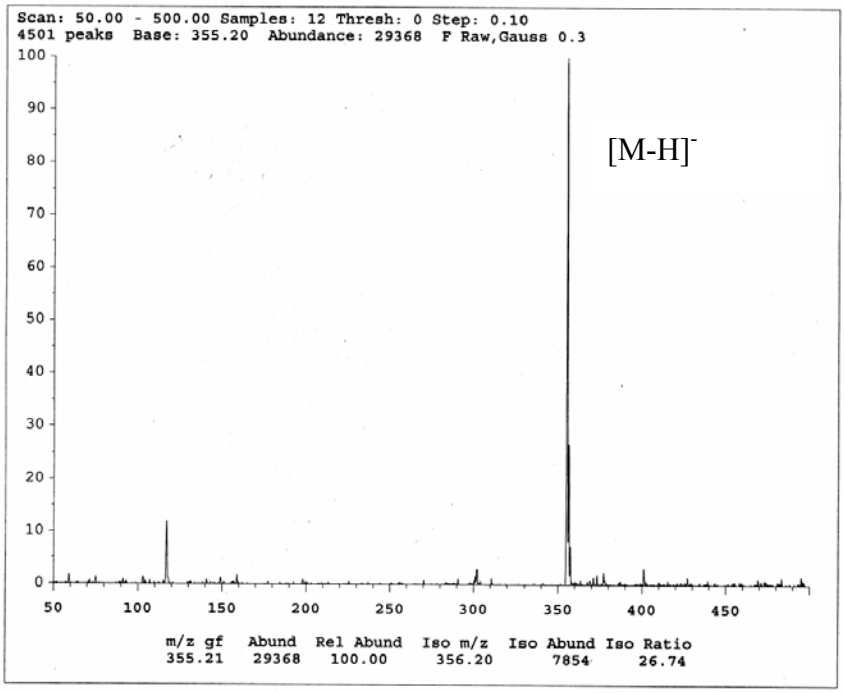

Figure B2. ESI-MS spectrum of SAAOCL in negative ion mode

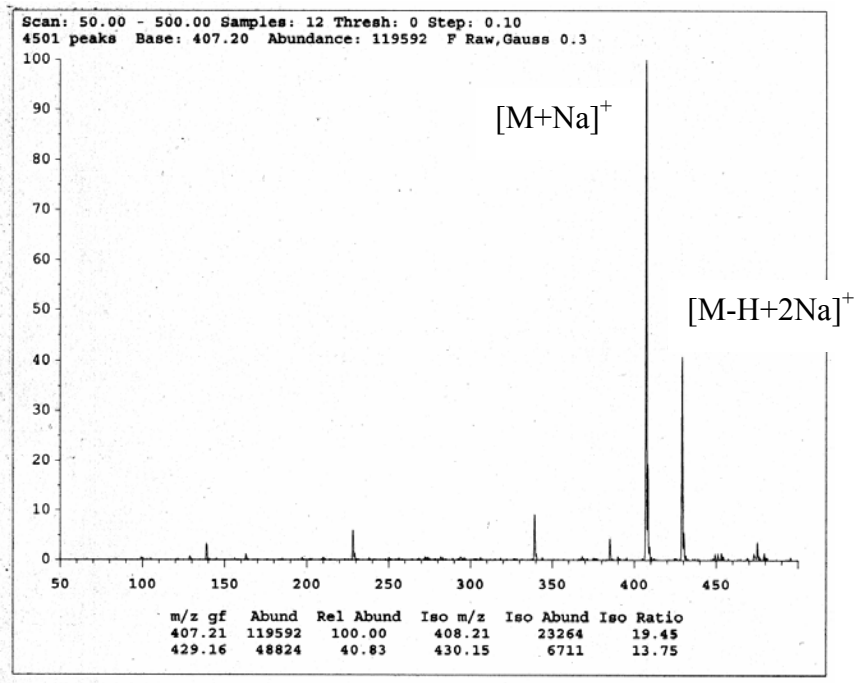

Figure B3. ESI-MS spectrum of SAADCL in positive ion mode

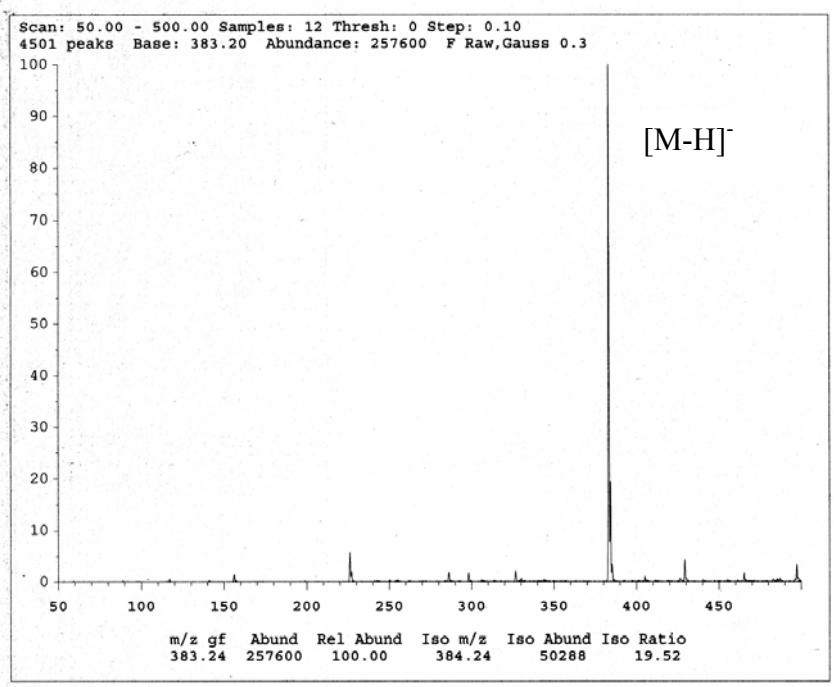

Figure B4. ESI-MS spectrum of SAADCL in negative ion mode

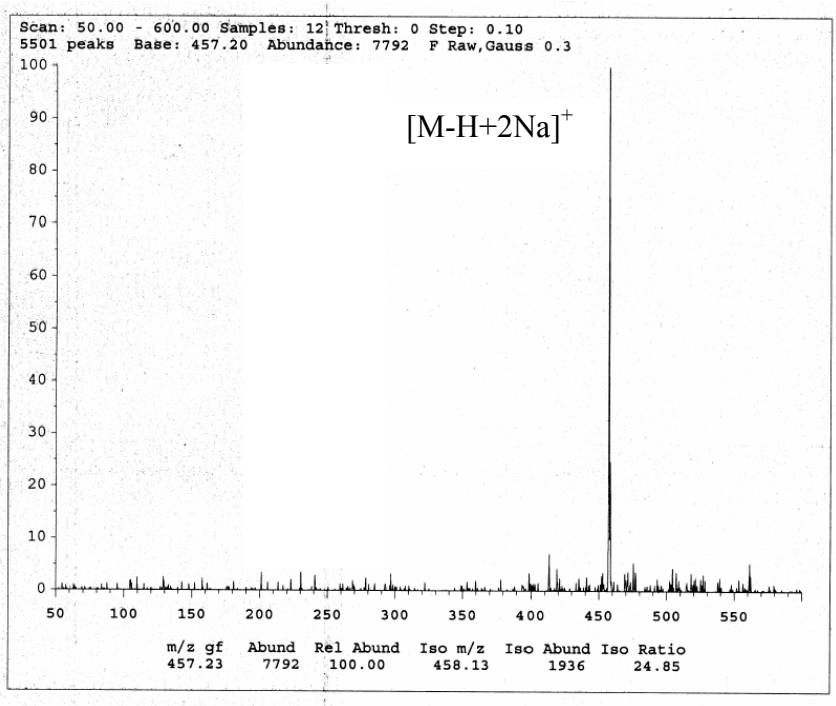

Figure B5. ESI-MS spectrum of SAADoCL in positive ion mode

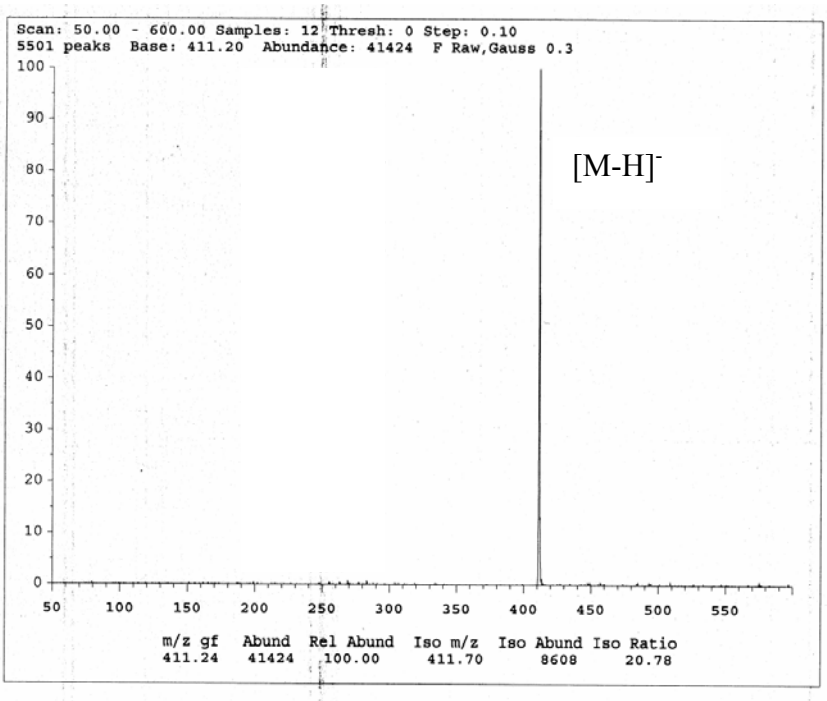

Figure B6. ESI-MS spectrum of SAADoCL in negative ion mode

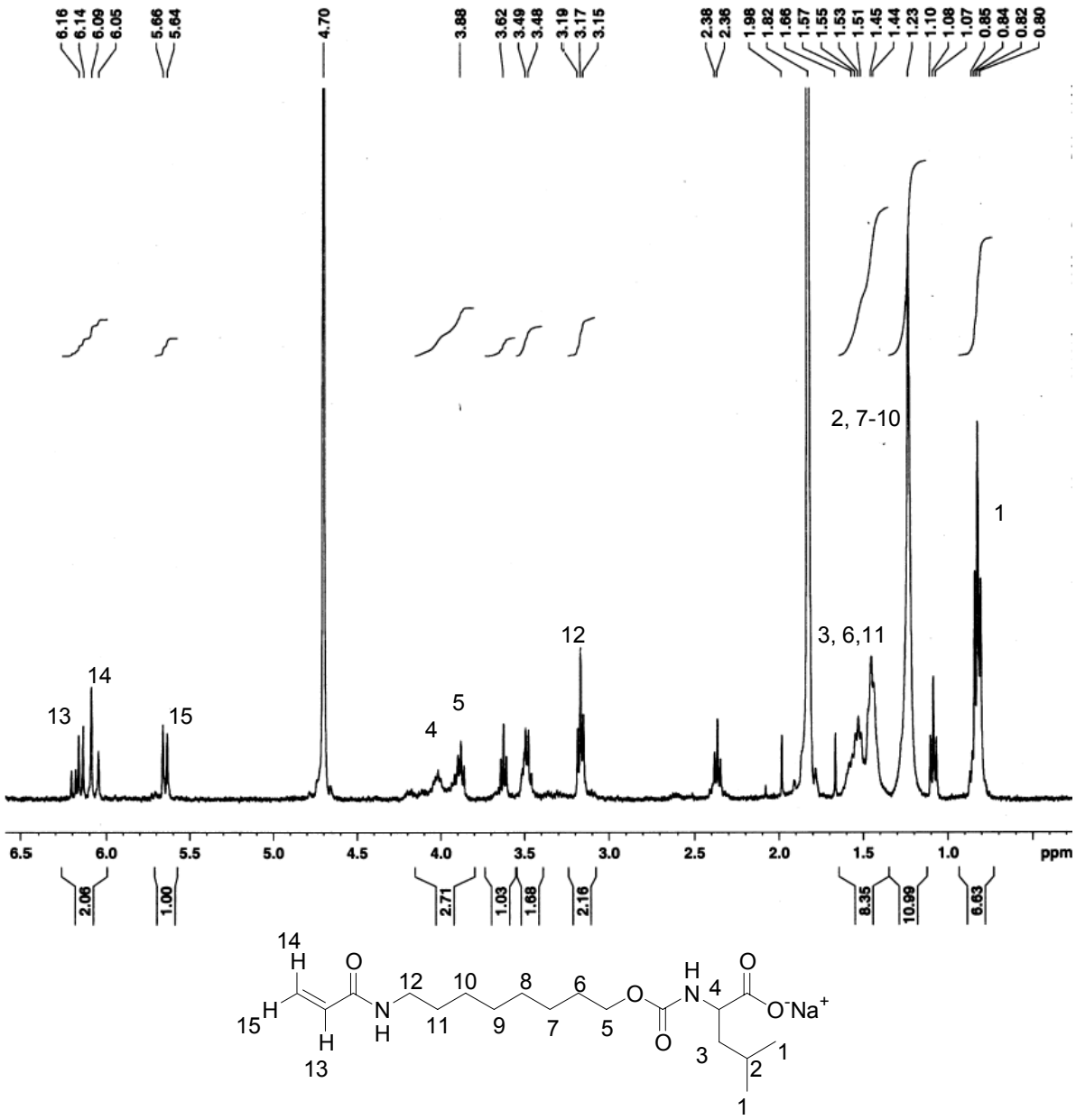

Figure B7. ^{1}H NMR spectrum of SAAOCL

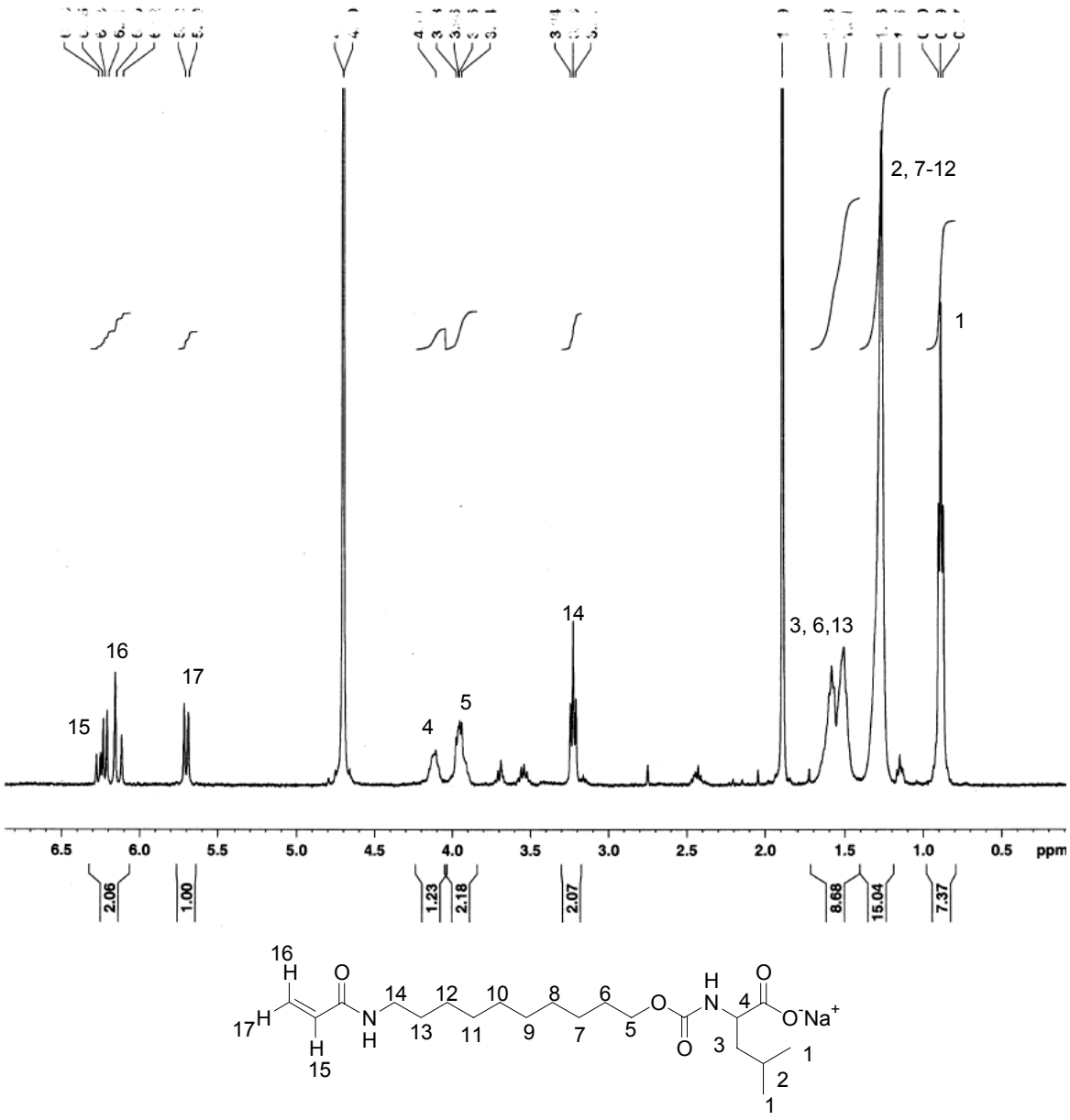

Figure B8. ^{1}H NMR spectrum of SAADCL

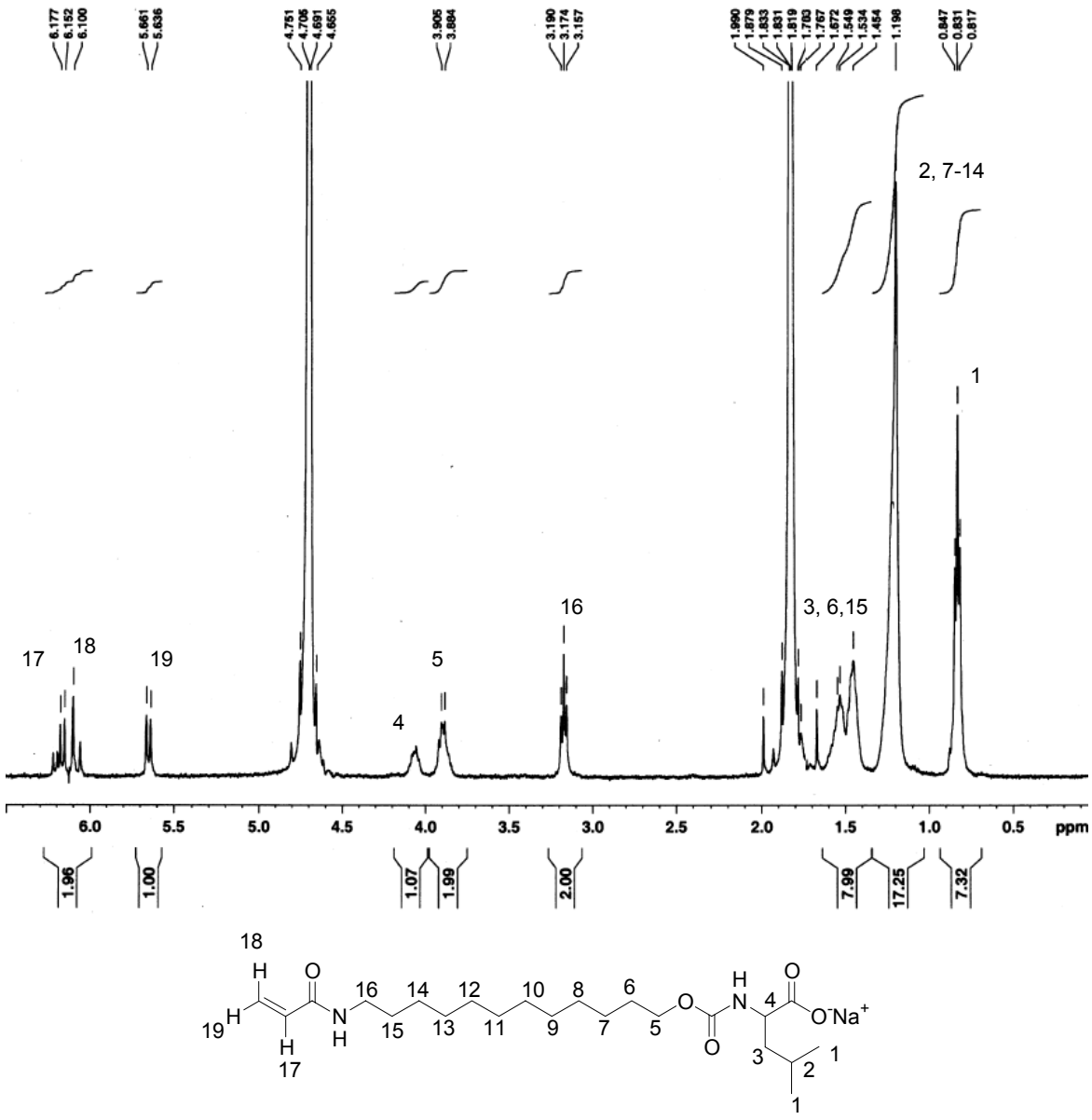

Figure B9. ^{1}H NMR spectrum of SAADoCL

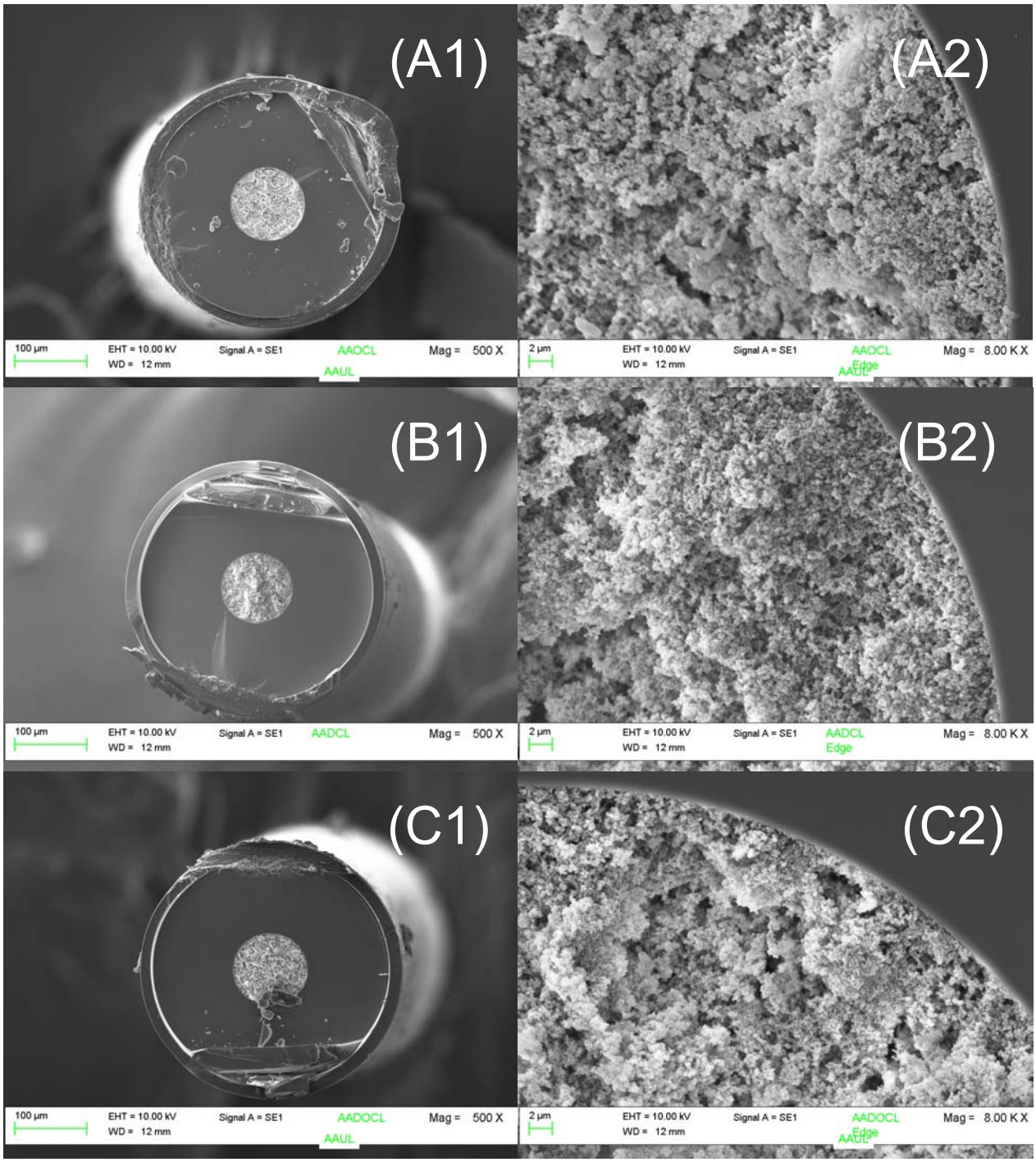

Figure B10. Scanning electron micrographs of monolithic columns. A1, A2: AAOCL column; B1, B2: AADCL column; C1, C2: AADoCL column.

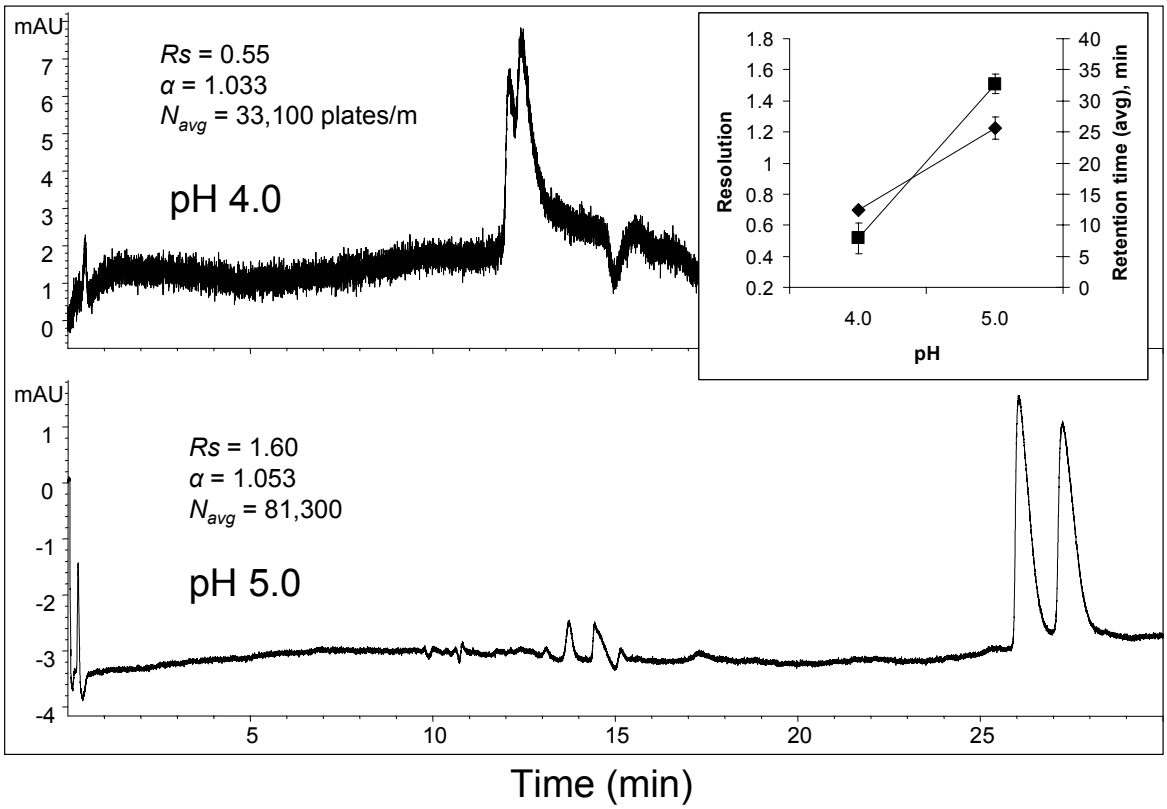

Figure B11. Effect the mobile phase pH on chiral CEC separation of (±)-PEP. The CEC conditions are same as optimized in Figure 2 and 3. The inset of the figure is the plot of retention time (-♦-) and chiral resolution (-■-) as a function of mobile phase pH.

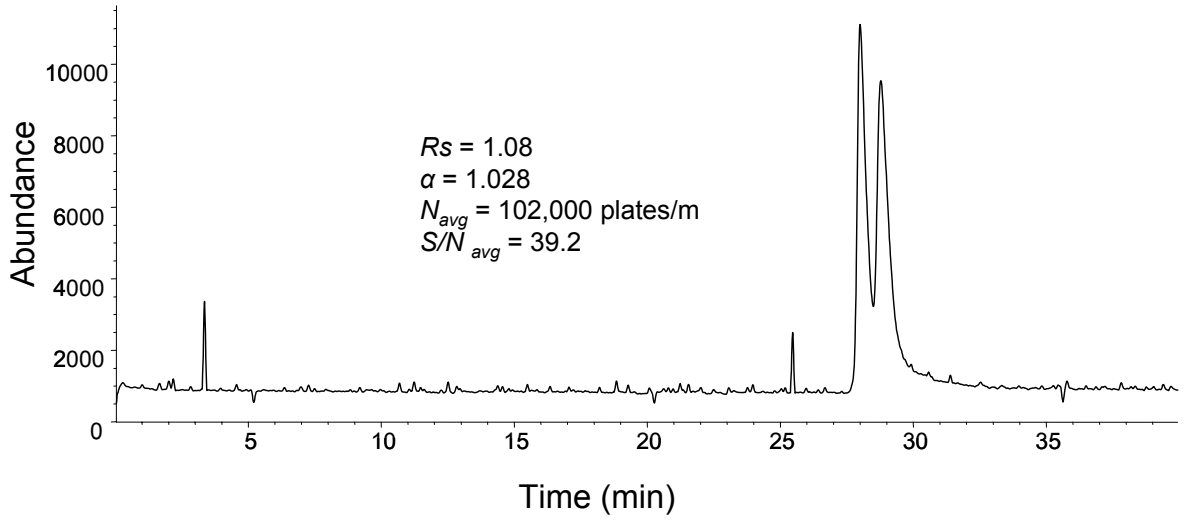

Figure B12. CEC-ESI-MS separation of (±) pseudoephedrine with AADCL column. CEC conditions: 55 cm long column (150 μm i.d.), 30 cm monolithic bed length. Voltage, +10 kV; high pressure, 5 bar applied at inlet end of the column; column temperature, 20 ^{o}C; mobile phase, a mixture of 70% ACN and 30% aqueous buffer containing 5 mM NH_4OAc, 0.5% TEA (pH 5.0); analyte, (±)-PEP (1 mg/mL) dissolved in mobile phase; injection, 3 kV for 3 s. MS condition: positive m/z = 166 was used in selected ion monitoring mode; nebulizer pressure, 7 psi; drying gas flow rate, 5 L/min; drying gas temperature, 150 ^{o}C; capillary voltage, 3000 V; fragmentor voltage, 90 V. Sheath liquid: 80/20 MeOH/H_2O (v/v) with 5 mM NH_4OAc. Sheath liquid flow rate: 8 μL/min.

Appendix C

Supporting Material for Chapter 6

Table C1. Elemental analysis of AAUV, AAUP, AAUL, AAOL, and AADoL monomer

Surfactant	Elemental analysis		
	Element	Theory	Found
AAUV	C	64.38	64.32
	H	9.67	9.73
	N	7.90	7.76
	O	18.05	18.16
AAUP	C	68.63	67.91
	H	8.51	8.65
	N	6.96	6.74
	O	15.90	16.99
AAUL	C	65.19	64.10
	H	9.85	10.09
	N	7.60	7.39
	O	17.37	18.66
AAOL	C	62.55	61.07
	H	9.26	9.12
	N	8.58	8.29
	O	19.61	21.08
AADoL	C	65.93	65.41
	H	10.01	10.13
	N	7.32	7.24
	O	16.73	17.25

Table C2. Composition of the reaction mixtures used in the preparation of the optimized surfactant-bound monolithic columns

Column	Monomer (wt%)		Porogen (wt%)			Initiator (wt%)	Comment
	surfactant	EDMA	ACN	MeOH	H_2O	AIBN	
AAUL-1	11	29	60	0	0	0.5	Monomer insoluble
AAUL-2	8.2	21.8	70	0	0	0.5	
AAUL-3	13.7	36.3	50	0	0	0.5	
AAUL-4	8	32	60	0	0	0.5	
AAUL-5	6	34	60	0	0	0.5	
AAUL-6	8	12	80	0	0	0.5	
AAUL-7	5	15	80	0	0	0.5	
AAUL-8	15	25	30	30	0	0.5	Column has no flow
AAUL-9	10	30	30	30	0	0.5	
AAUL-13	20	15	20	45	0	0.5	
AAUL-14	25	15	20	40	0	0.5	
AAUL-15	20	15	25	40	0	0.5	
AAUL-16	20	15	0	65	0	0.5	
AAUL-23	15	15	40	20	10	0.5	Packing bed not homogenous
AAUL-24	12	18	35	35	0	0.5	
AAUL-25	10	20	35	35	0	0.5	
AAUL-30	20	10	45	20	5	0.5	
AAUL-10	15	15	35	35	0	0.5	Good separation
AAUL-11	15	15	20	50	0	0.5	
AAUL-12	15	15	50	20	0	0.5	
AAUL-22	15	15	45	20	5	0.5	
AAUL-29	18	12	45	20	5	0.5	

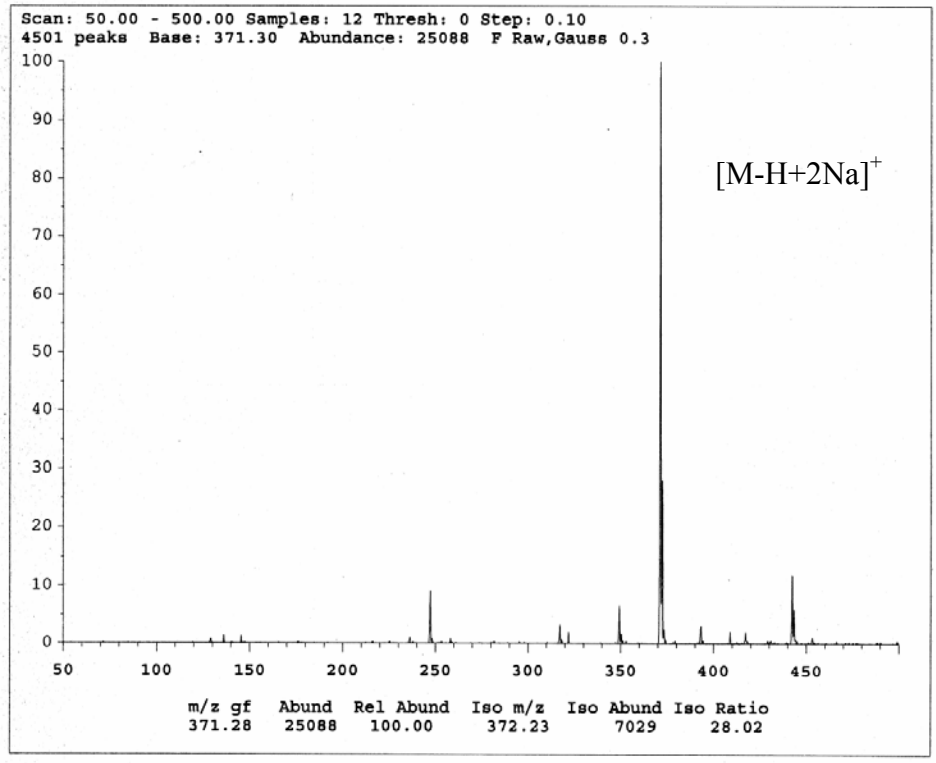

Figure C1. ESI-MS spectrum of SAAOL in positive ion mode

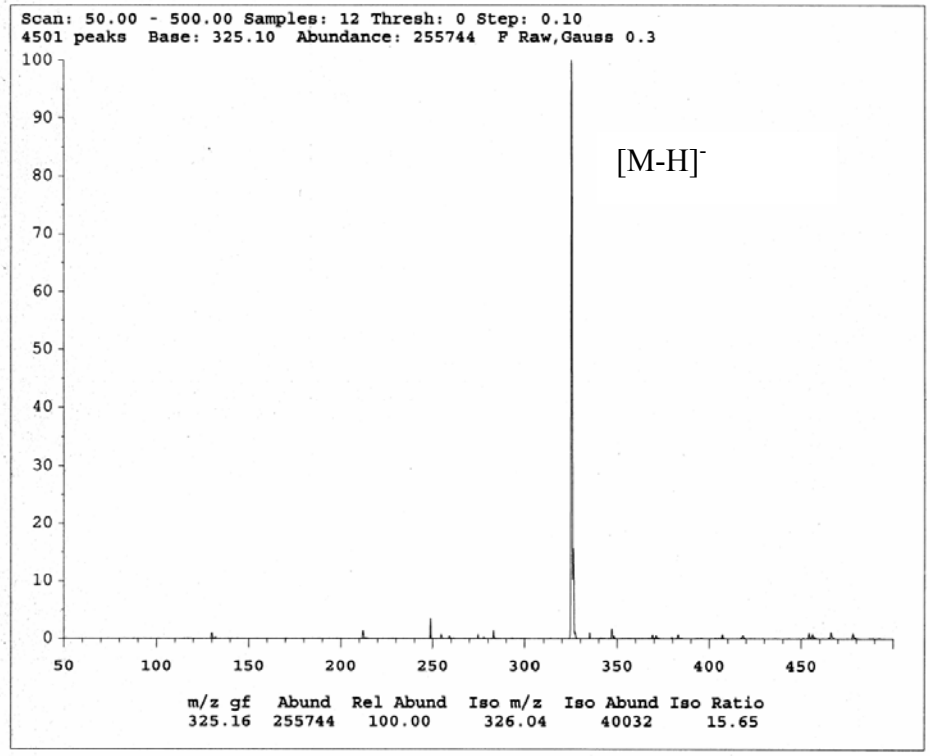

Figure C2. ESI-MS spectrum of SAAOL in negative ion mode

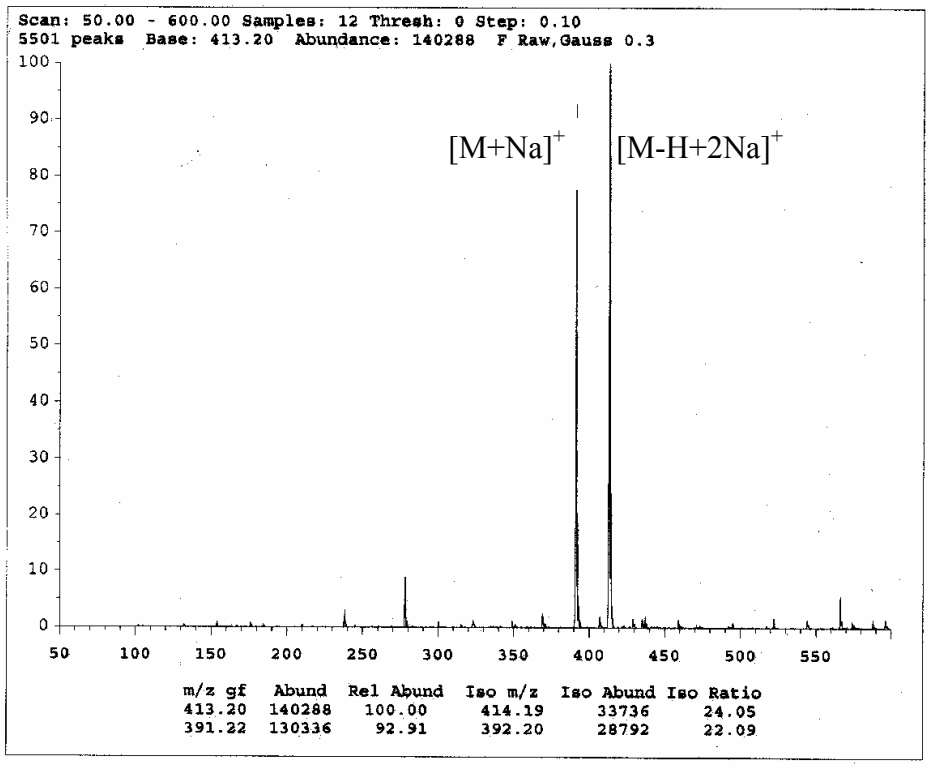

Figure C3. ESI-MS spectrum of SAAUL in positive ion mode

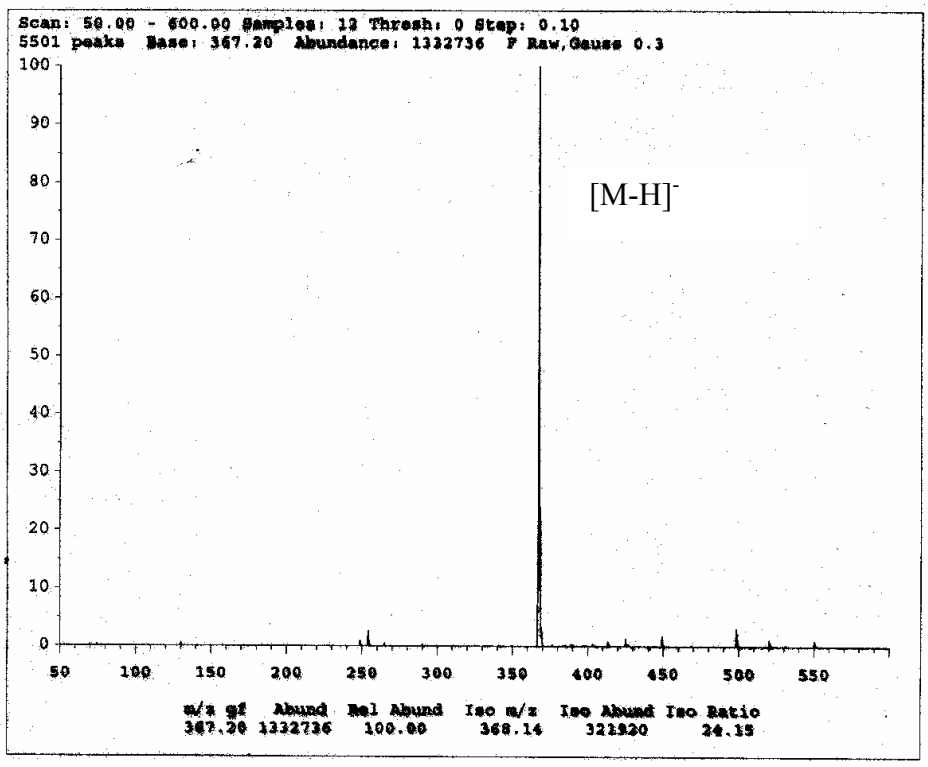

Figure C4. ESI-MS spectrum of SAAUL in negative ion mode

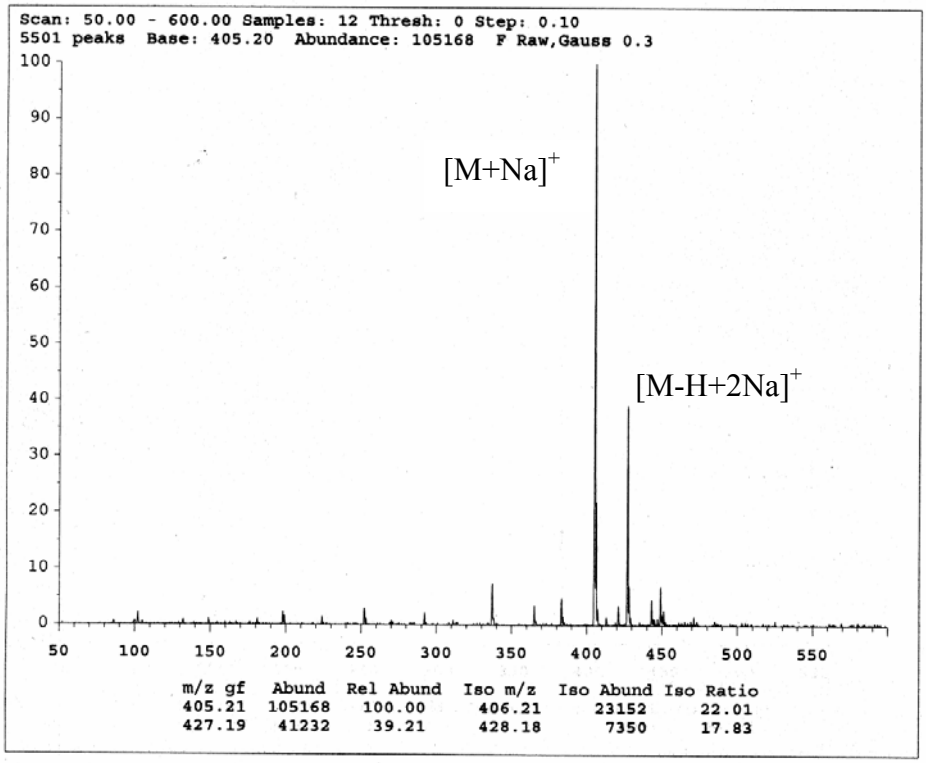

Figure C5. ESI-MS spectrum of SAADoL in positive ion mode

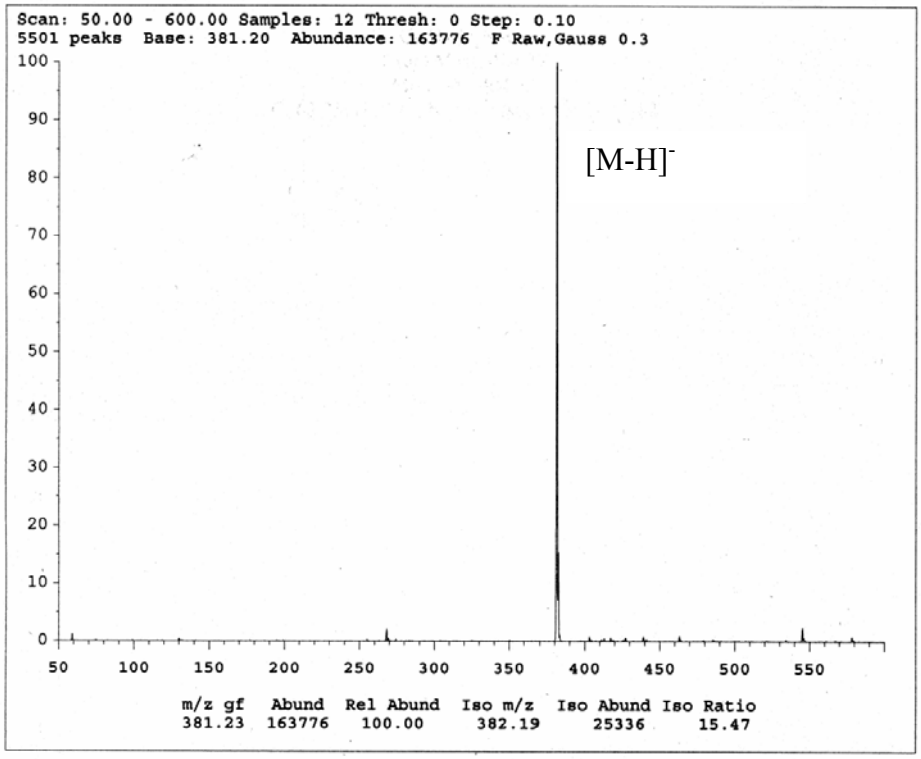

Figure C6. ESI-MS spectrum of SAADoL in negative ion mode

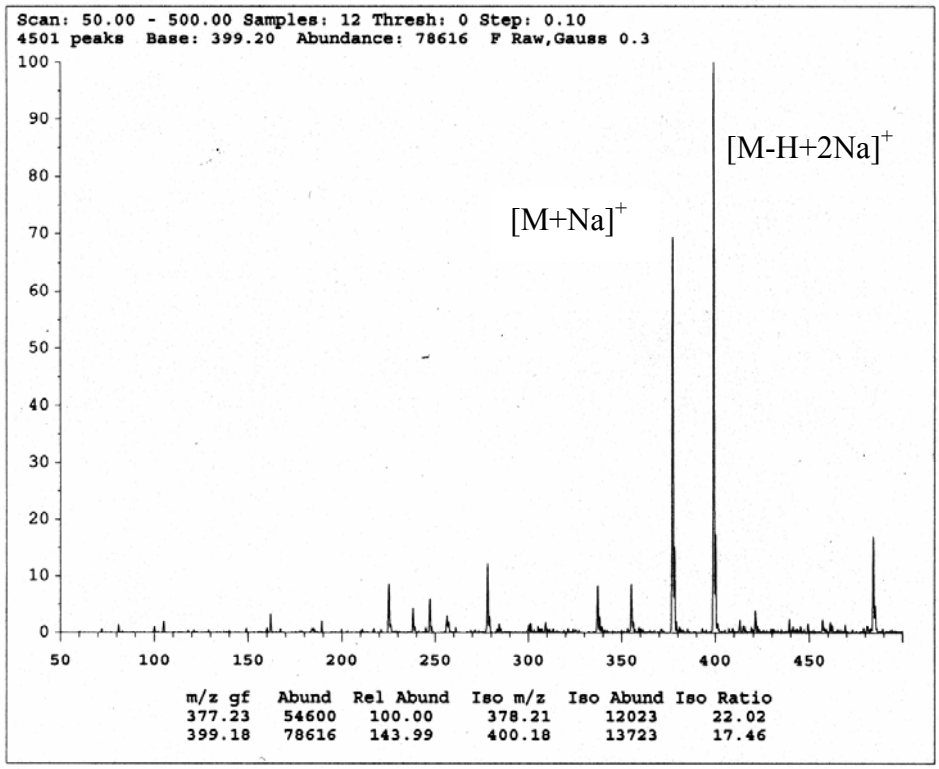

Figure C7. ESI-MS spectrum of SAAUV in positive ion mode

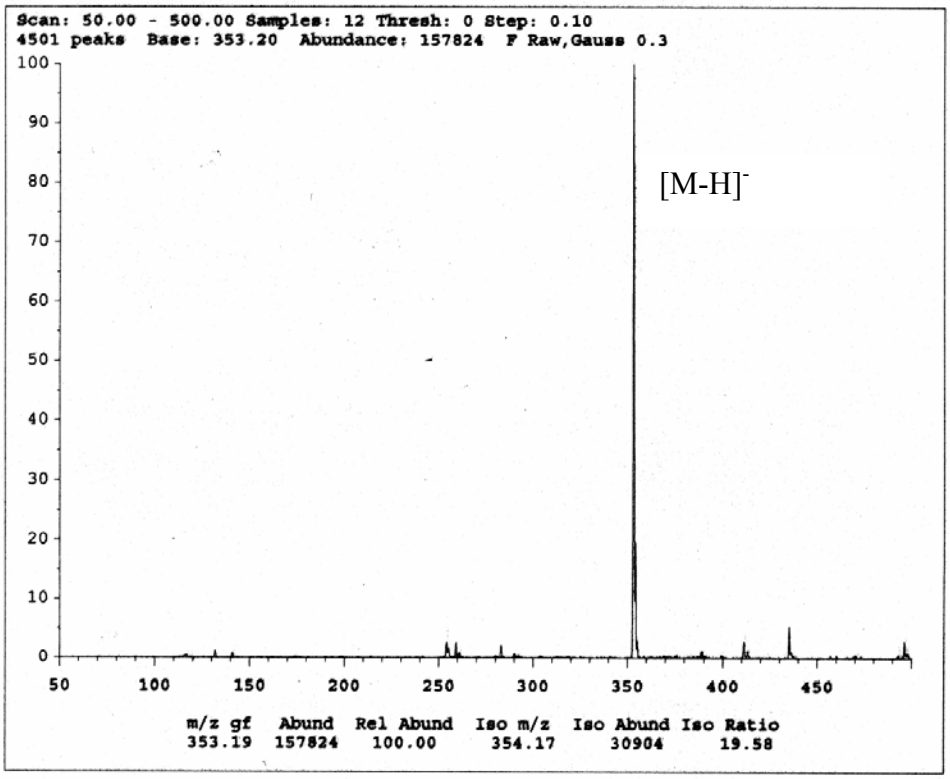

Figure C8. ESI-MS spectrum of SAAUV in negative ion mode

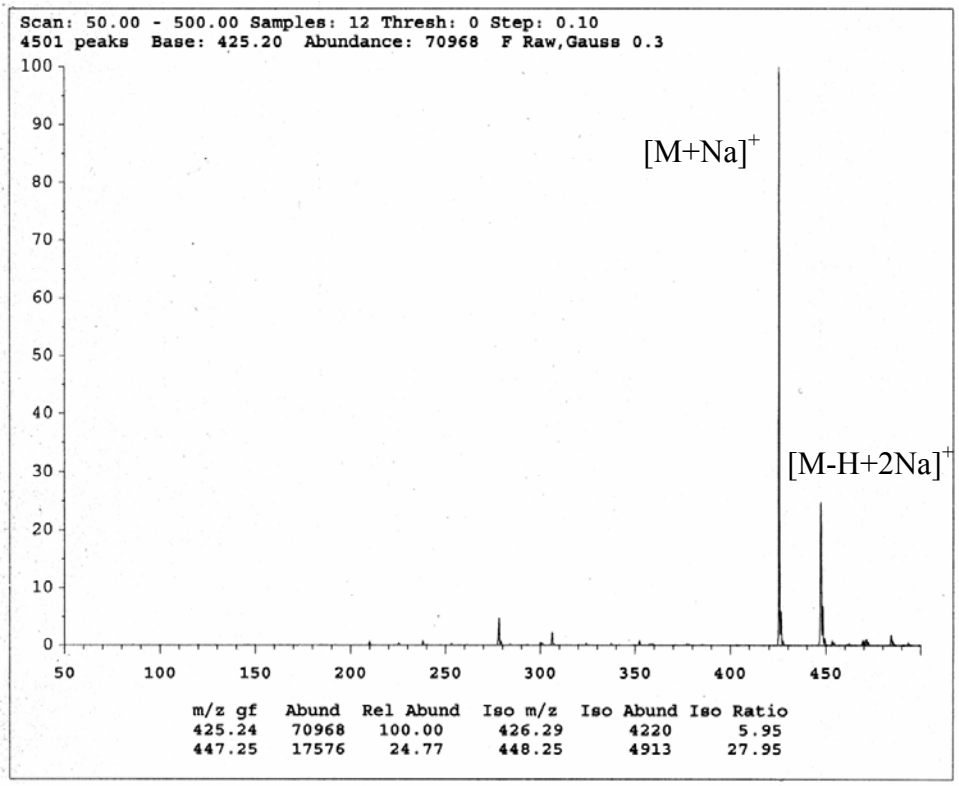

Figure C9. ESI-MS spectrum of SAAUP in positive ion mode

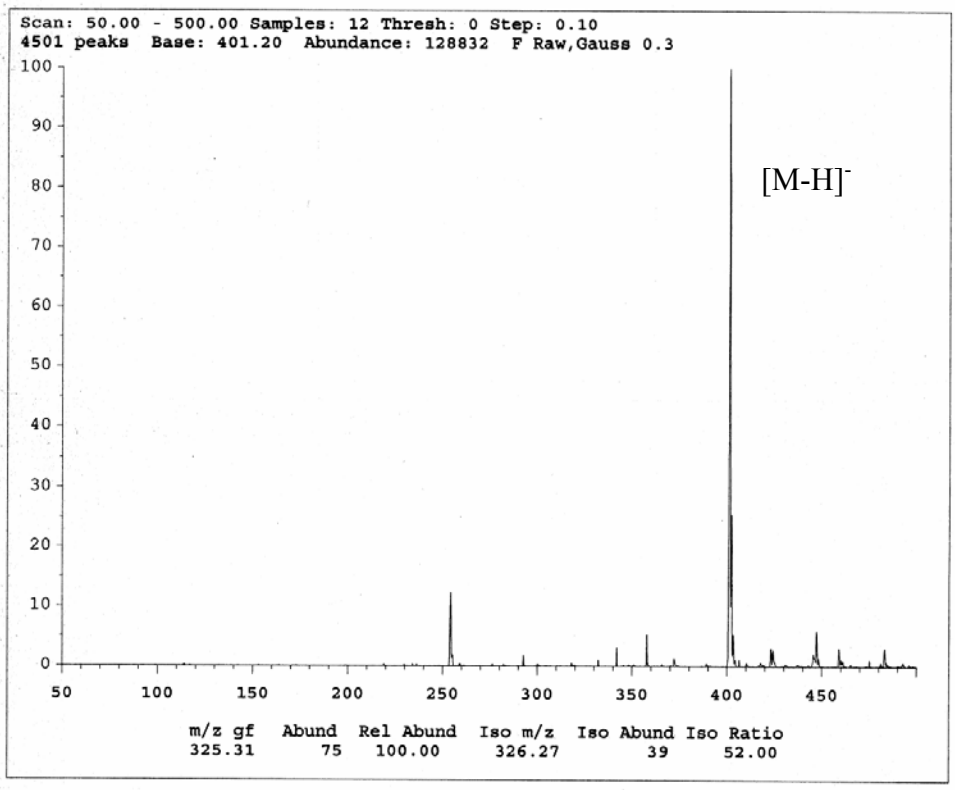

Figure C10. ESI-MS spectrum of SAAUP in negative ion mode

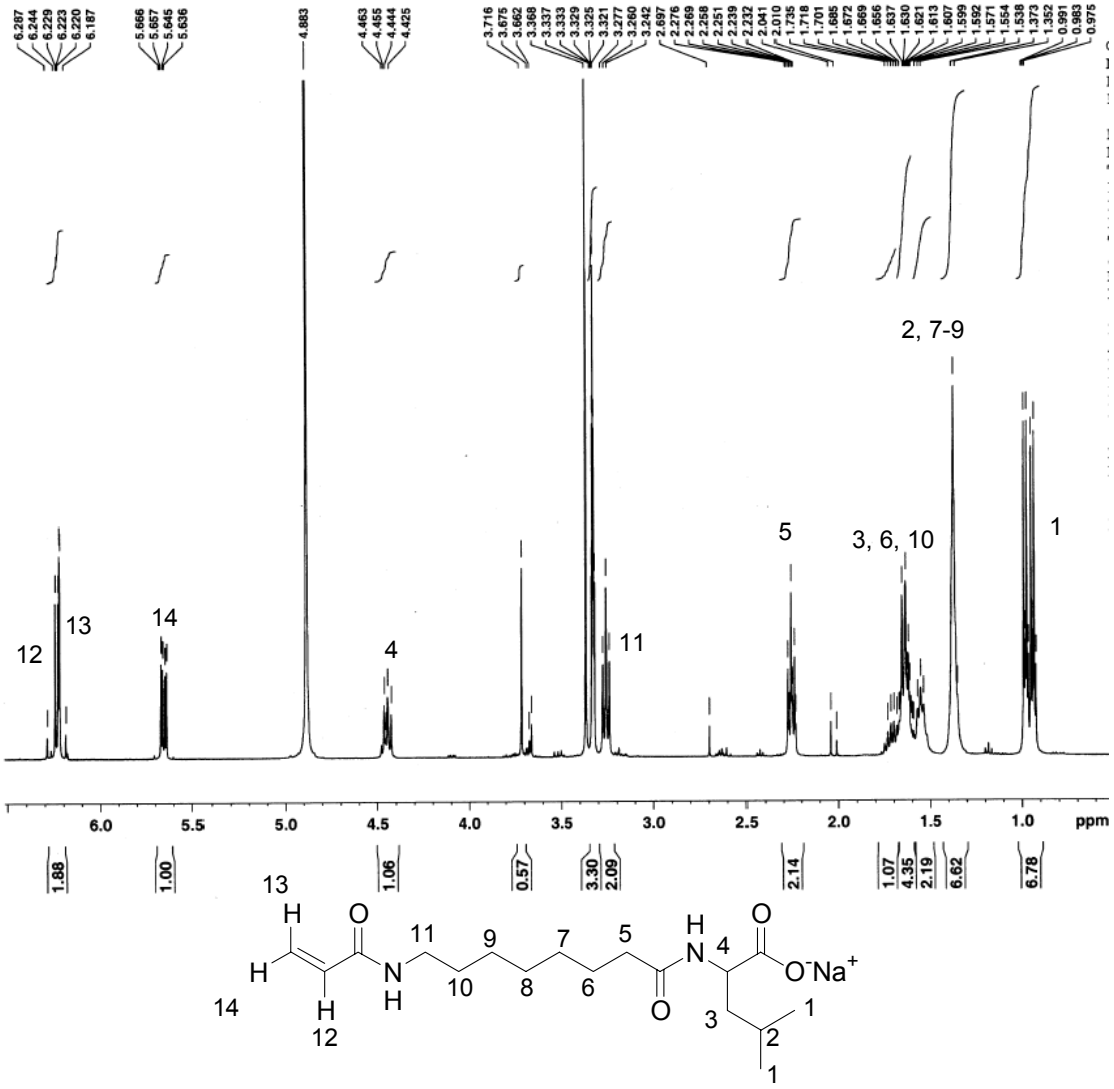

Figure C11. ^{1}H NMR spectrum of SAAOL

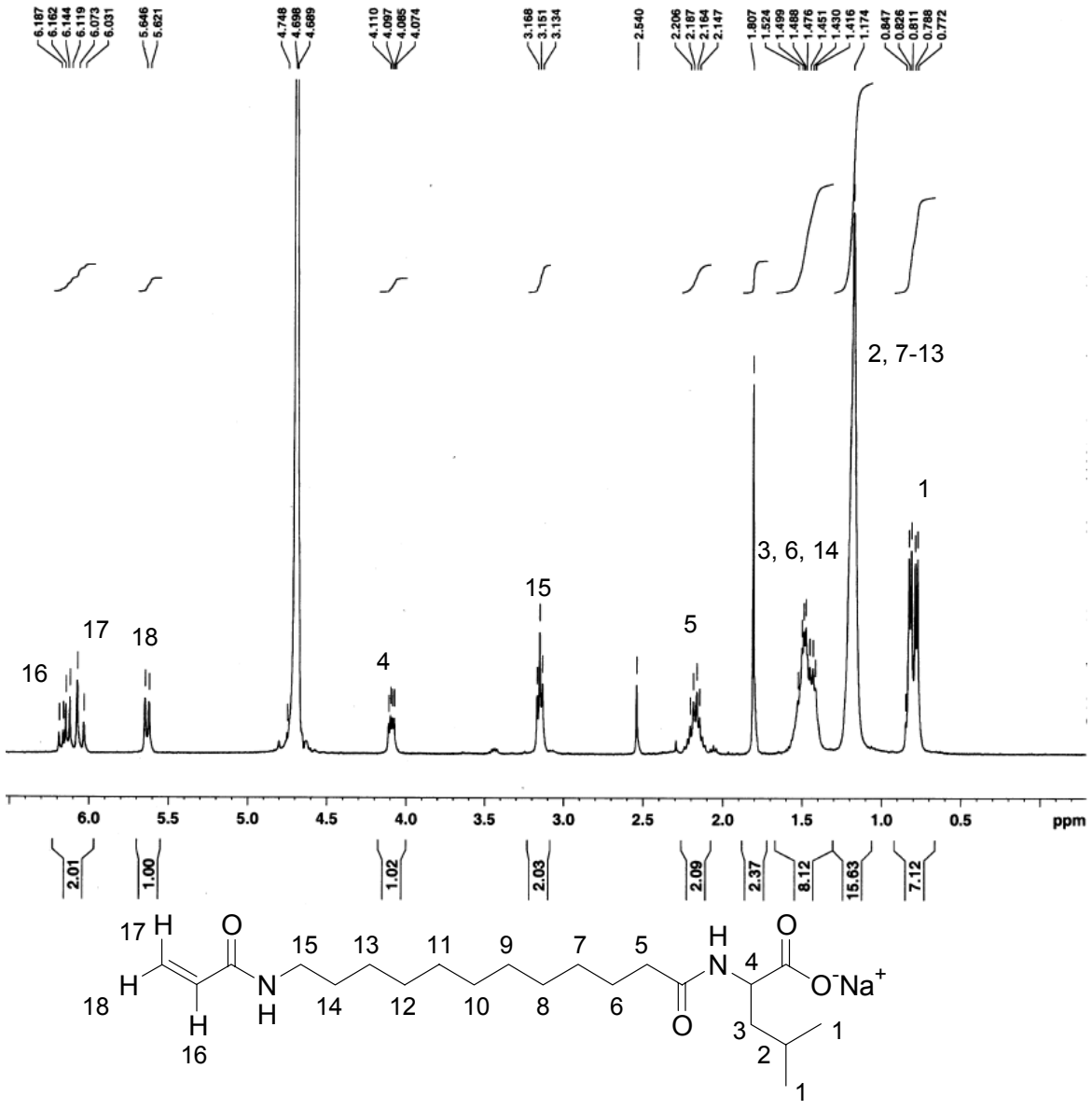

Figure C12. ^{1}H NMR spectrum of SAADoL

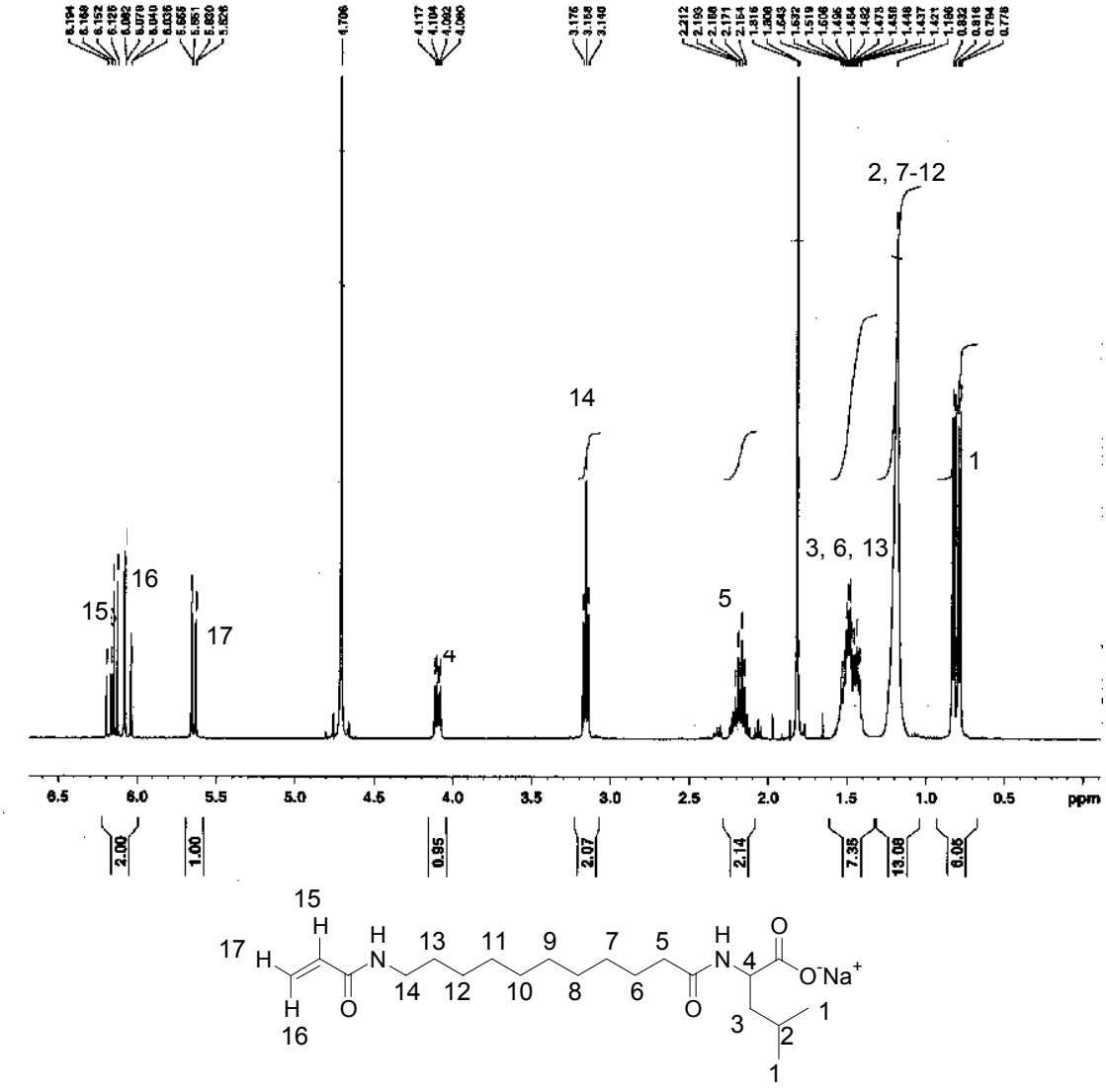

Figure C13. ^{1}H NMR spectrum of SAAUL

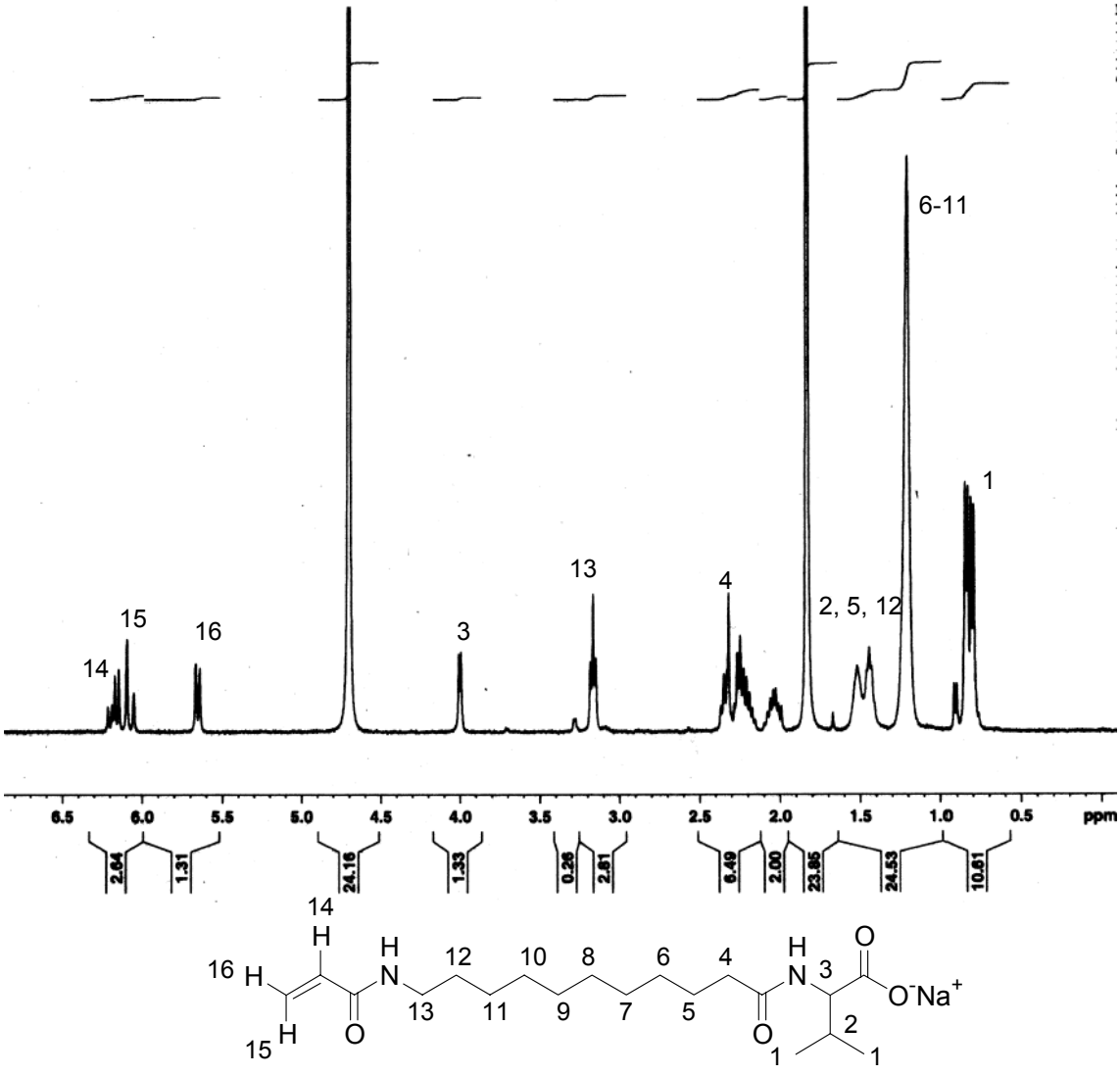

Figure C14. ^{1}H NMR spectrum of SAAUV

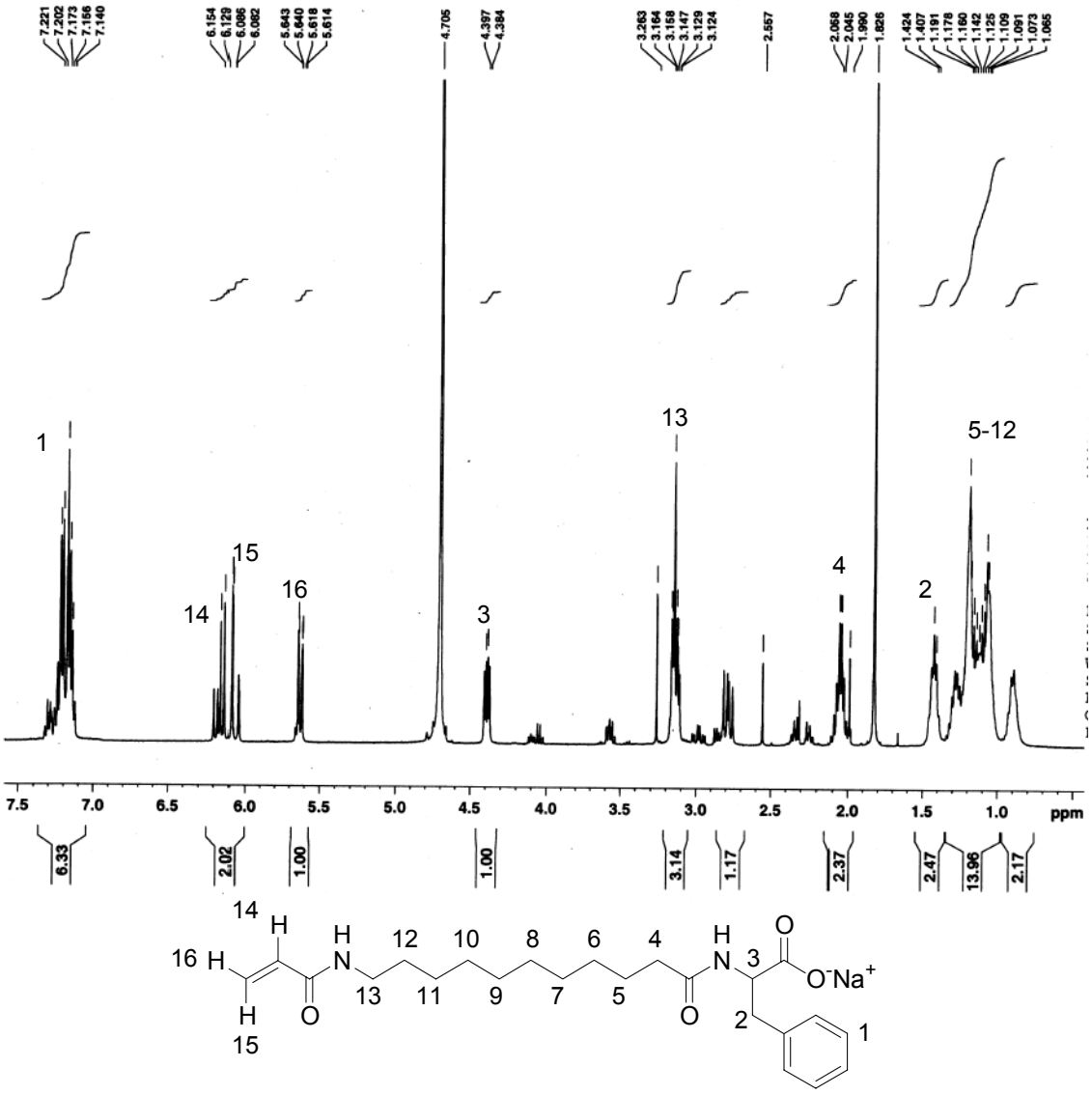

Figure C15. ^{1}H NMR spectrum of SAAUP

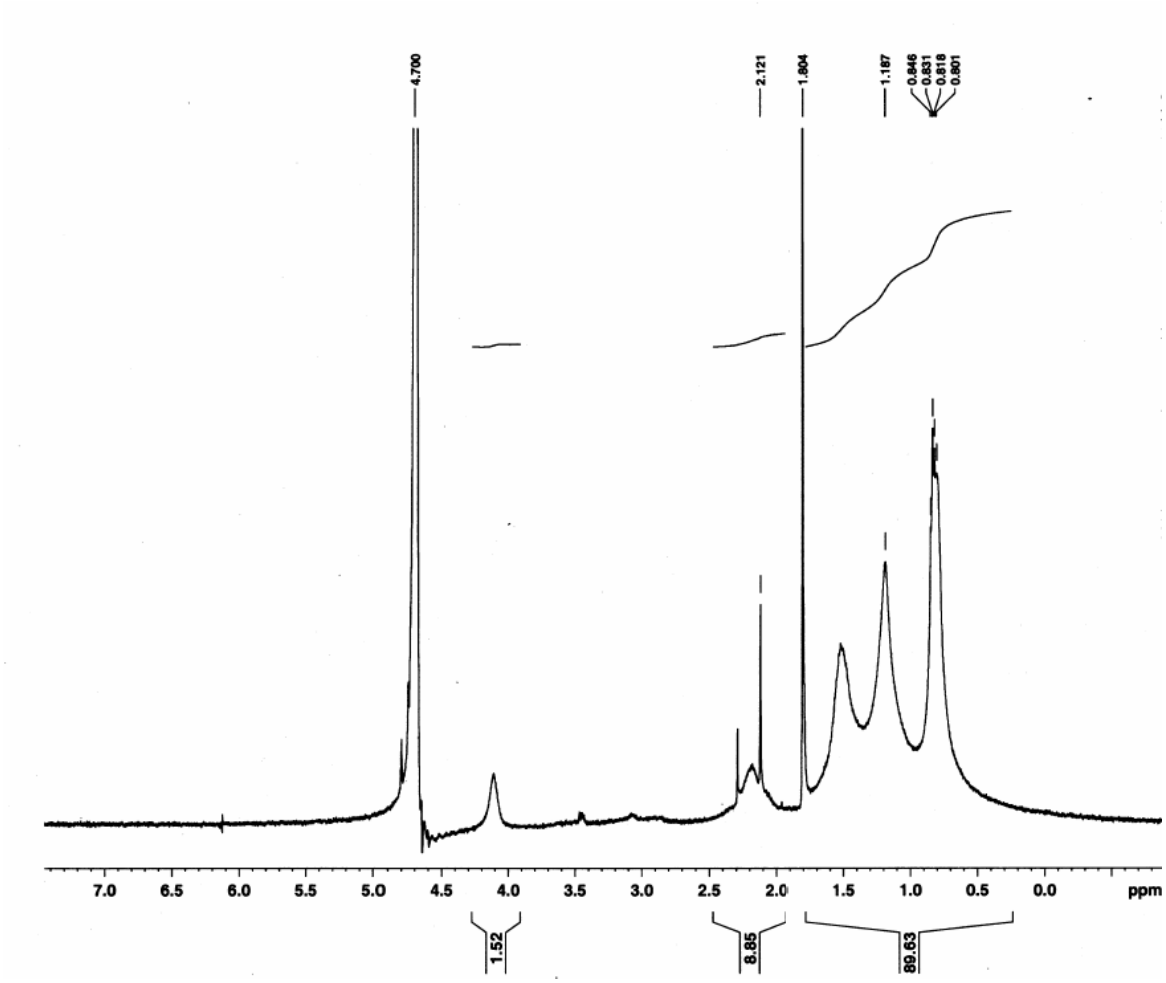

Figure C16. ^{1}H NMR spectrum of poly-SAAUL

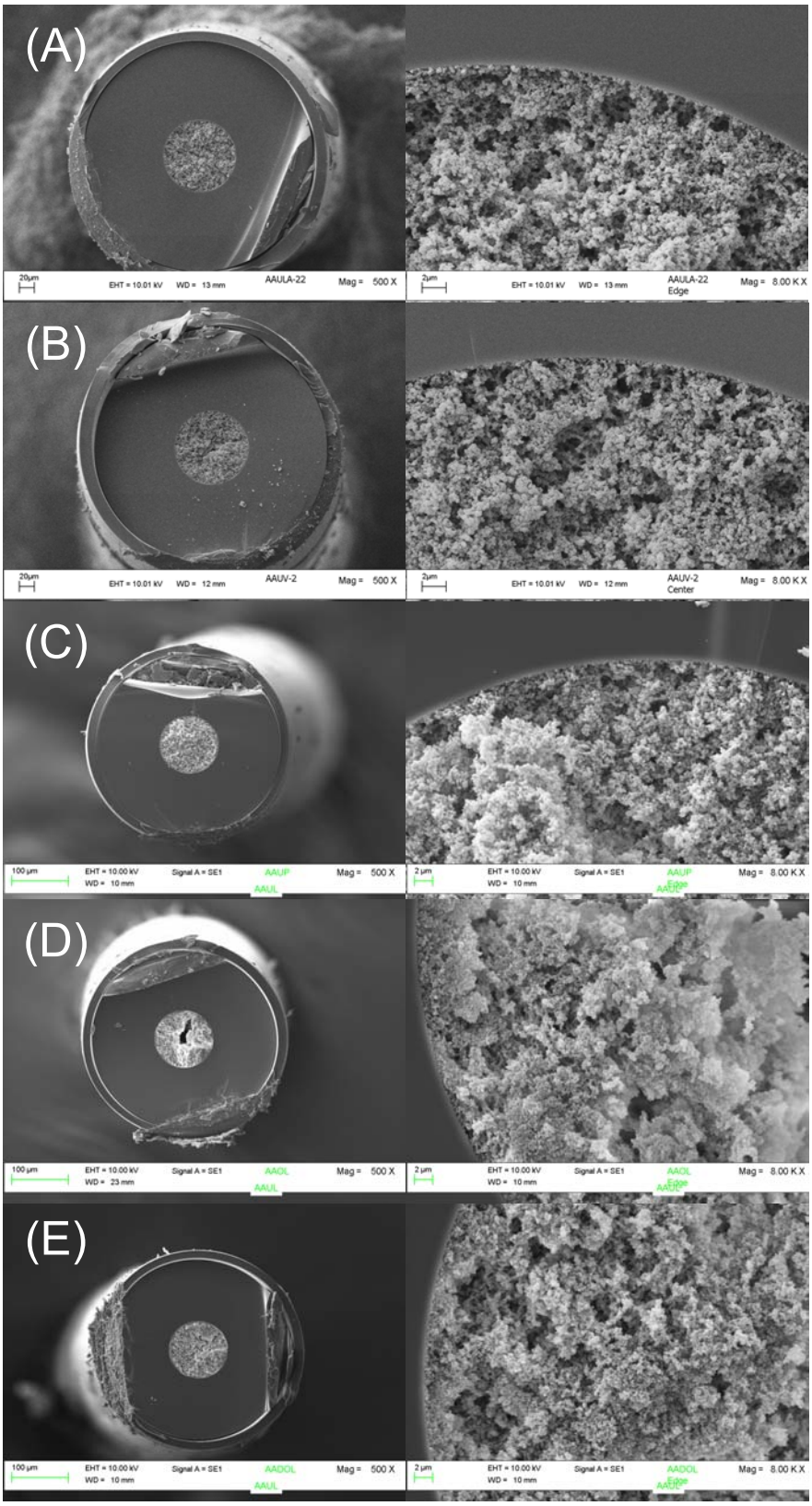

Figure C17. Scanning electron micrographs of monolithic columns. AAUL column (A), AAUV column (B), AAUP column (C), AAOL column (D), and AADoL column (E).

Appendix D

Future Prospectus

Proposal 1: Synthesis of sulfated acrylamido alkenoxy amino alcohol based surfactant-bound monolith and its application in chiral CEC

Similar to the synthesis of carbamate and amide linked acrylamido alkyl amino acid surfactants, surfactants with sulfated amino alcohol head groups can be also synthesized and used as monomers in the one-pot preparation of chiral monoliths. The proposed reaction scheme of monolith with surfactant of sulfated-leucinol head group is shown in Scheme D1. Briefly, amino alcohol (**1**) is first reacted with acryloyl chloride to form acrylamido alcohol (**2**). Compound **2** is then reacted with triphosgene to yield the chloroformate of acrylamido alcohol (**3**). This chloroformate is then reacted with *R* or *S* leucinol to form acrylamido alkenoxy carbonyl leucinol (**4**). Compound **4** reacts with chlorosulfonic acid to yield the acid form of surfactant, acrylamido alkoxy carbonyl leucinate sulfonic acid (AACLSA) (**5**). Compound **5** is then used as chiral monomer in the preparation of the monolithic stationary phase. EDMA is used as crosslinker in this case. The same porogen as described in Chapter 5 and 6 can be used as well. The ratio of different components in the polymerization mixture might need to be adjusted to obtain the best chiral CEC separation.

This proposed sulfated surfactant-bound monolithic stationary phase has stronger acid head group as monomer as compared to the carboxylic acid based monolithic stationary phase described in Chapter 5 and 6. The stronger acid will provide much higher electroosmotic flow (EOF) in CEC as well as more stable current. Strong acid head group also provides stronger ion-exchange sites on the stationary phase, which might help the chiral recognition mechanism between the cationic analyte and the chiral stationary phase. The other advantage of the sulfated surfactant-bound monolith is that it could be used with mobile phase of very low pH in CEC and still has acceptable EOF.

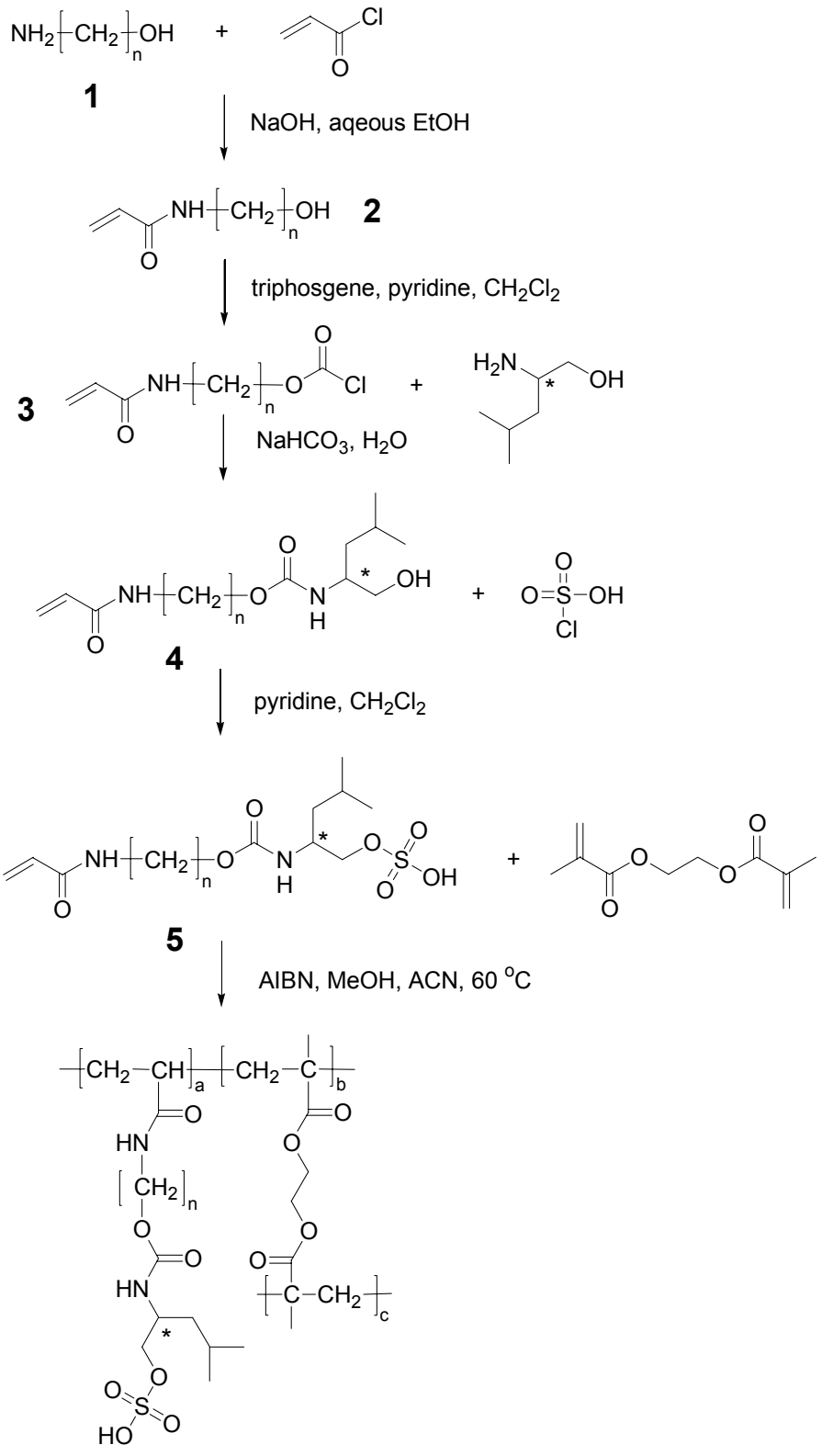

Scheme D1. Proposed reaction scheme of monolith with surfactant of sulfated-leucinol head group. n = 8, 10, or 12. a, b, and c are numbers of subunit in the monolith.

Proposal 2: Preparation of vinyl terminated amino acid based surfactant-bound monolith and its application in chiral CEC

Besides the acrylamido terminated chiral surfactants described in Chapter 5 and 6, traditional vinyl terminated amino acid based surfactants can also be used as monomer to prepare the surfactant-bound chiral monolithic stationary phase. Preliminary experiments in our lab showed that sodium *N*-undecenoyl L-valinate (SUV) can be polymerized with EDMA to form homogenous monolith and give partial chiral separation of (±)-pseudoephedrine in CEC. Similarly, surfactants with better chiral selectivity such as sodium *N*-undecenoyl-L,L-leucylvalinate (SULV) and sodium *N*-undecenoxy carbonyl-L-leucinate (SUCL) can be utilized to form chiral monolithic stationary phase as well. Additionally, cationic polymeric surfactants such as undecenoxy carbonyl-L-leucinol bromide (L-UCLB) (ionic liquid) can also be used as monomer. Scheme D2 is the proposed synthesis scheme of the ionic liquid-bound monolithic stationary phase. With the cationic head group of the ionic liquid, the stationary phase will be able to achieve enantioseparations of anionic compounds.

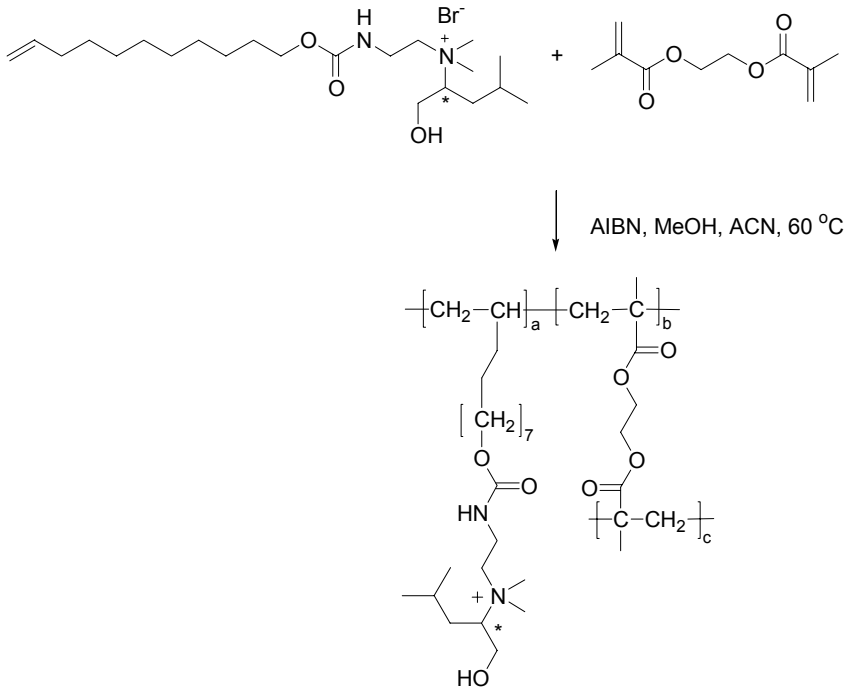

Scheme D2. Proposed synthesis scheme of the ionic liquid-bound monolithic stationary phase.